FINITE ELEMENT AND EXPERIMENTAL EVALUATION OF INJECTION FORGING FOR THE FORMING OF AUTOMOTIVE FASTENERS

Senyong Chen

This Thesis is submitted to the Department of Design, Manufacture and Engineering Management, University of Strathclyde, for the degree of Doctor of Philosophy

This thesis is the result of the author's original research. It has been composed by the author and has not been previously submitted for examination which has led to the award of a degree.

Singed:

Date:

DEDICATION

The author wishes to dedicate the thesis to his father, mother, sister and his wife without whose support and sacrifice, the thesis would have not been completed.

ACKNOWLEDGEMENT

First of all, I would like to thank my supervisor, Professor Yi Qin, for his phenomenal supervision of the research and constant encouragement through the study. He shared his knowledge and taught me how to conduct research which lighted me up towards the right direction.

I also would like to thank my friend, and colleagues at the Department of Design, Manufacture and Engineering Management, the University of Strathclyde, especially Dr Quanren Zeng, Jie Zhao, Yihui Zhao, Yankang Tian, Hao Wu, Gerald Anyasodor, Song Yang, Xinyu Yang, and so on, for their kindly help which made me enjoy the study and life in Glasgow.

A grateful thanks is to Dr Chee Mun Choy for his trust and guidance. He helped me to start the study at the University of Strathclyde and tutored me in tool design and material selection with his valuable expertise.

Last but not least, I would like to thank Ritai (Shanghai) Auto Standard Component Co. LTD. for permitting me to carry out the experiments in the lab and workshop. I would like to thank Mr Qiang Lv, Mr Xiufeng Shang and Mr Ying Pang, for their technical assistance in tool manufacturing and device installation.

ABSTRACT

With the increasing global competition, it is important for the automotive fasteners industries to reduce the cost and improve the production efficiency against other competitors. To achieve it, the author intends to introduce injection forging as an alternative method to conventional forming for automotive fastener production. This study investigates the characteristics of injection forging by finite element (FE) analysis and physical experiment. For the comparison of the conventional forming process with injection forging, ABAQUS and DEFORM were used to conduct FE simulations of the forming of a wheel bolt. Axisymmetric models were developed with both FE codes to analyse forging force, forging energy, forming form-error, tool stress, etc. of conventional multistep forging and injection forging (single step forging). A ring test was also conducted to determine the coefficient of friction between the workpiece and the tools in order to define the contact conditions in the FE models.

Subsequently, tests on injection forging were carried out in Ritai Auto Standard Component Co. Ltd. The trials included forging force measurement, evaluation of lubricants, critical dimension measurement, macroetch testing micro-hardness tests and a manufacturing try-out. FE simulation results and experimental results were then compared. Behaviour of the lubricants was also examined for injection forging. Through the comparison, FE models were verified. Some improvements, regarding the influence of forging speed, thermal issues, meshing plan and the limitation of axis-symmetric model, were proposed.

By using improved FE models, effects of critical aspects such as process parameters (forging speed and coefficient of friction), tool parameters (tool structure, tool geometry and tool materials), and workpiece parameters (workpiece material and workpiece geometry), were investigated in detail. With the improved FE models, influences of these parameters on fatigue life of the die, die wear, form-errors, and grain flow-lines, were examined.

Based on the sensitivity analysis of forging parameters, optimisation was carried out on the tool parameters, and a new tool structure has been proposed for injection forging of the fastener. The tool design was assessed through FE simulations.

As results of FE simulations and experiments, the main findings included the merits and drawbacks of injection forging compared with traditional forging process, the precision of FE models, the optimal lubricant for injection forging, the behaviour of injection forging in manufacture trials, the influence of process factors on tool life, forming accuracy and grain flow line. These findings supported the further tool optimization. After optimization, the tool life and forming accuracy had an increase. Based on the research work, the contributions were defined and recommendations of the further work were proposed.

PUBLICATIONS

1. Senyong Chen and Yi Qin, Comparison study of multistep forging and injection forging of automobile fasteners. *MATEC Web of Conferences*. Vol.21. EDP Sciences, 2015.

2. Senyong Chen, Yi Qin, Chee-Mun Choy, et al. Testing an injection forging process for the production of automotive fasteners. Proceeding of International Conference on the Technology of Plasticity (Submitting).

3. Senyong Chen, Yi Qin, Chee-Mun Choy, et al. Analysis of injection forging in automotive fasteners production (being reviewed by an external reviewer).

CONTENTS

LIST OF FIGURES

LIST OF TABLES

Chapter 1

Introduction

1.1 Background of the Research

Cold forging and extrusion are important manufacturing processes which are widely used in many industries such as automotive, aircraft, military, shipbuilding, etc. Providing great accuracy, good surface finish, low consumption of materials and enhancement of mechanical properties [1], cold forging and extrusion become more and more established for manufacturers. To date, most automotive fasteners are fabricated by cold forging or extrusion, such as heading and forward extrusion. By using these processes, efficiency, cost and quality, which always take the first place in production, are kept within an acceptable range.

However, with the increasing global competition, these conventional metal forming processes are facing challenges. The primary factor is from customers who require the components in a high-precision and stable quality using high strength-to-weight ratio materials. On the other hand, the industries also want to reduce the cost and improve the efficiency against other competitors. To meet these requirements, injection forging is being researched as a new option which can obtain complex components in a minimum of forging steps.

The use of injection forging raises some issues of tool life and component accuracy. Because of shortening the forging chain, the tool experiences more severe stresses than conventional process. The increased tool stress promotes crack growth which deteriorates the tool life. Since the tools occupy nearly 5% to 30 % of manufacturing cost [2], it is vital to have a satisfactory tool life. On the other hand, the high tool stress also increases the tool deflection which influences the component accuracy. Thus, it demands a tool with great stiffness to reduce the tool deflection.

Considering these issues, the research aim and objectives are defined and will be discussed in the following section.

1.2 Research Aim and Objectives

Against this background, the overall aim of this study is to evaluate the feasibility of injection forging for volume production of automotive fasteners based on finite element simulations and physical experiments. It also aims to establish a systematic approach to analyse the parameters which influence tool life and component quality.

The following objectives are defined:

1) To establish FE models for comparing the fastener forming by conventional forging and injection forging.
2) To conduct an experimental study and a manufacturing try-out of the injection forging process to validate and develop the FE model.
3) To investigate component quality with regard to forming errors, grain flow line and hardness distribution.
4) To assess the influences of forming parameters on component quality and tool life through FE simulations.
5) To optimise the tool design of injection forging and verify the new tool design by FE simulations.

1.3 Methodology

To achieve the aim and objectives, the following methodology was used:

1) Literature review on the cold forging process especially on injection forging process, including an understanding of tool designs, tool manufacturing, tool failures, tool service-life prediction and the approaches for analysing and reducing component form-errors.
2) FE simulations of multistep forging and injection forging in automotive fastener production to compare the forging force, forging energy, forming errors, tool stresses, etc.
3) Experimental investigations of injection forging in a commercial fastener manufacturer with different lubricants, and validation of FE models by

comparing the results from experiments and FE simulations.

4) Conducting the FE simulations of injection forging in the improved model to evaluate the influence of some critical parameters in the control of forming errors and tool service life.

5) Optimisation of tool-design for injection forging, and verifying the tool-design through FE simulations.

6) Drawing conclusions from the research and making recommendations for future work.

1.4 Structure of the Thesis

This thesis consists of seven chapters which are organised as follows:

Chapter 1 introduces the background, aim, objectives and structure of the research.

Chapter 2 presents the development of injection forging, including the process principles and forming limits. In addition to this, it covers some common tool failures, tool life prediction and approaches to improve the tool life. Also, the forming errors and errors-reduction methods are discussed. Finally the FE software, ABAQUS and DEFORM, are reviewed.

Chapter 3 presents the comparison of injection forging and multistep forging in bolt forming based on FE simulations. It aims to analyse the differences of forging force, forming errors and tool stresses for both processes. It begins with FE model development and procedures. Finally, the results of simulations are discussed.

Chapter 4 shows the physical experiments of injection forging with three lubricants. A series of tools are prepared for use in a hydraulic press machine and a high speed forging machine. Through the experiment, the forging force, component accuracy, hardness distribution and grain flow lines are obtained. The feasibility of injection forging is also tested by the manufacturing try-out. Lastly, the experimental results are compared with FE simulations. Based on the comparison, the FE models are validated and developed.

In Chapter 5, a comprehensive analysis model with regard to forging speed, the

coefficient of friction, tool structure, tool materials, workpiece materials and workpiece geometry, is developed. Each parameter is evaluated with regards to tool life and component quality.

Chapter 6 presents an optimisation of the tool design for injection forging. The new tool design is assessed by using FE analysis and based on the results suggestions for industrial applications are proposed.

Chapter 7 draws conclusions from the study, summarises the main contributions to knowledge and makes recommendations for future work.

Chapter 2

Literature Review

2.1 Cold Forging and Automobile Component Production

Over the past several decades, the growing automobile industries have increased the demand for automobile components. In order to meet these large requirements, various techniques such as forging, machining and casting, were applied to produce components of different sizes and shapes in an economical way [3]. Among them, cold forging as, an efficient process, plays an important role in automobile components production. With the help of cold forging, the material mechanical properties are considerably improved [1]. Cold forging strengthens some metals which are treated as unacceptable if warm forged, machined or hot forged, for use in vehicles. A good example is the austenitic stainless steel, which the tensile properties increase with cold work. However, in warm or hot forged, it will not happen because of the "self-annealing" [4]. Therefore, cold forging becomes a priority choice for manufacturers when it is feasible for practical production.

To date, there are many types of metal forming processes, including extrusion, heading, rotary forging, closed-die forging, etc.

Cold Extrusion

Cold extrusion is a traditional forging process which manufactures the components by a compressive forming force. Depending on the die configuration and material flow, cold extrusion is classified into forward extrusion, backwards extrusion, and lateral extrusion. The material flow direction is the same as punch movement for forward extrusion, while it is the opposite for backwards extrusion. As for lateral extrusion, the material flow direction is vertical to the direction of punch displacement [5].

In order to produce complex components, these basic extrusion processes can be combined with each other or other forging processes like upsetting, heading, and coining [1]. With the help of these processes, some parts such as universal joints, spur gears, and shafts can be produced with high volumes. Cold extrusion can achieve an excellent forming accuracy (IT7 to IT8) and surface finish (R_a 0.2 μm - 1.6 μm) [6]. Meanwhile, due to lower material consumption, the material use ratio is more than 80% in most situations [6]. This merit is especially useful when the workpiece material is expensive.

Currently, cold extrusion is widely used in automobile industries, e.g. most automotive fasteners are formed to intermediate products or final products by extrusion. Other components, such as shock absorber cylinders, piston pins, starter gear, etc. all involve the cold extrusion processes.

Cold Heading

Cold heading is defined as a change of the dimensional cross-section area of a workpiece at room temperature. The outstanding advantage of cold heading is the high production rate. Depending on the part size, the production rate reaches around 2000 to 50,000 pieces per hour [5]. Combining with extrusion, coining, trimming, and thread rolling, it is often used to produce small sized or medium sized products in high volume. Some typical examples are screws, bolts, nuts and other fasteners.

Usually, the cold heading is carried out in a horizontal forging machine which is called a header. Because of the high-automation of the heading machine, the cost of labour is relatively low. Meanwhile, due to good accuracy and surface finish, the components produced by cold heading seldom require post machining.

Rotary Forging

Rotary forging is a kind of incremental forging, which means forging the workpiece under the continually pulsed forging press. Since the contact surface between tools

and workpiece is small, the friction force is relatively low. With the reducing of friction force, the forging force decreases. This makes the tool life higher than that in conventional forging processes. Moreover, it reduces noise and vibration during the process because there is no impact force used [5], [7], [8]. However, it also has some limitations, e.g. the production geometry is limited to symmetrical parts like hubs and bearing rings [9], [10]. In addition to this, the design of rotary forging machines is difficult as a result of the big die motion required [5].

Closed-Die Forging

In closed-die forging, the initial workpiece is placed within the walls or cavities of the die. Through closing the die, the material is deformed to a defined shape [5]. Depending on the flash, closed-die forging can be classified into flash allowance and without flash [1]. For the forging with flash, the tool stress is relieved via the flash channel. Meanwhile, the forging pressure has a drop which can be controlled by the volume of flash, however post-machining is required for the produced component. Fig. 2-1 shows a typical closed-die forging with flash.

For the forging without flash, there is little or no machining required after forging. However due to the absence of a relief channel, the tool works in a severe environment. Therefore, the requirements of tool making becomes stringent and it increases the risk of tool failure. On the other hand, it is also important to calculate the workpiece volume precisely. Any unintended extra material will adversely impact the tools because of the increased unexpected forging pressure [5].

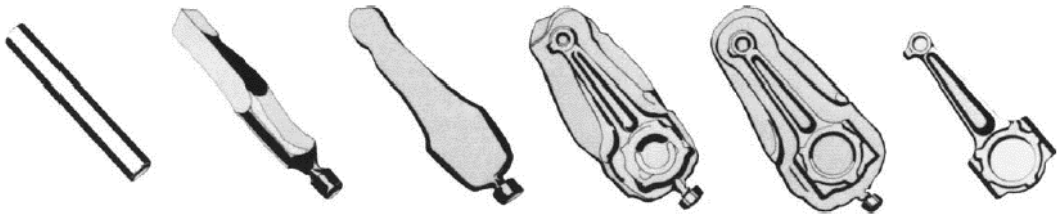

Fig. 2-1: Manufacturing of connecting rod by closed-die forging with flash [5].

In automotive industries, closed-die forging is used to produce many complex parts, such as the steering knuckle, crankshaft, connecting rod, etc. [1], [5]. Usually, closed-die forging is shaping material which may be heated to a high temperature. In this way it can reduce the flow strength of material. For some soft materials closed-die forging also can be carried out at room temperatures.

Besides involving various manufacturing processes, the cold forging can fabricate components with diverse materials. Steel as a traditional metal was and still is popular in automobile industries because of its good ductility, accepted properties and low cost. A large number of car parts such as roof, fasteners, chassis and wheels, consist of steel. However, with increasing demands of lightweight design in automotive industries, traditional steel is unable to meet them. Some light metals and advanced high strength steel, therefore, gradually replace traditional steel in some parts of vehicles. Two benefits are introduced concerning car weight reduction. Firstly, in the same body structure, using light metals can reduce the car weight [11]. Secondly, with using high strength steel, the body structure can be optimised to get same component behaviour [12]. As results, the fuel consumption is correspondingly decreased [13].

Some research has been conducted to investigate the cold forging of light materials, including aluminium alloys [14], [15], [16], [17], [18], titanium alloys [19], [20], [21] and metal matrix composites [22], [23], [24]. Meanwhile, a combination of cold forging and warm/hot forging was applied to overcome problems with some light metals with low formability at room temperature. One example was forming a composite material (containing Al alloy 2124, Al-Li 8090 and particulate SiC) successfully by hot forming, heat treatment and precision cold forging [25]. In terms of high strength steel, the cold forging can process some high strength low alloy steel (alloy content < 6%), such as AISI 4340 and SCM 435. However, for the high strength high alloy steel, the hot and warm stamping (press hardening) are mainly used in sheet forming area [26].

2.2 Injection Forging

Injection forging is a plastic deformation approach which deforms the workpiece by injecting the material into the die chamber. This method can be used for bulk and tubular material. Since it is treated as a variant of extrusion, there are several names for this technology, such as radial extrusion, side extrusion, lateral extrusion and transverse extrusion [27]. In this study, the term injection forging is used.

2.2.1 Development of the Technology

In 1963, to mass produce flanges, injection forging as a new extrusion configuration was introduced by the National Engineering Laboratory, UK [28]. Compared with other forging processes such as heading or flange forging, this new method showed as being more stable and efficient. After two years, pioneering research on injection forging was conducted by Alexander [27] who investigated the effect of hydrostatic constraining pressure on the forging of flanges. By applying this pressure, the forming limitation of injection forging was extended.

Because of lacking useful theoretical analyses for injection forging, in the 1970s, Parsons et al. [29] employed the upper band analysis to study forging of thin flanges. It was argued that this method could describe the process accurately when materials were treated as ideal plastic materials. Another attempt on injection forging was to forge axisymmetric tubular materials. Some remarkable studies in this area were carried out by Dieterle [30] and Hendry et al. [31]. They analysed different defect types in injection forging of tubes by physical models and experiments.

From the 1980s to 2000, finite element analysis gradually became a popular tool to analyse the forging process. With the help of it, Balendra and Qin published many studies about injection forging [32], [33], [34]. Within these studies, they comprehensively defined the forming limits and summarised the failure-forms of products. Meanwhile, they introduced a pressure-assisted forging process for thick-walled tubes. With the assistance of media, the hollow parts were able to be

successfully obtained [35], [36]. On the other hand, they analysed the pressure losses in the injection chamber. It was reported that the pressure could drop 40%-60% in the injection chamber because of the great friction force [37]. Therefore, some lubricants were evaluated in [37] to improve the pressure transmission efficiency. Ma et al. [38] continued previous works of Qin to examine media materials, rubber and polyethene, in pressure-assisted injection forging. It was found that the rubber showed a better behaviour than the polyethene.

In the past ten years, injection forging was used to produce solid and hollow flanged parts [27], universal joints [39], gears [40], [41], hollow gear shafts [38], etc. (refer to Fig. 2-2). With using injection forging, some limitations were exposed e.g. great die stresses. The divide flow method [40] was introduced to release the die stress. As well as the die stress, the production efficiency was also a problem. For most injection forging parts, the forging speed was quite slow such as 18 mm/min [40] or 100 mm/min [39]. Therefore, the low efficiency prevented its use in volume production.

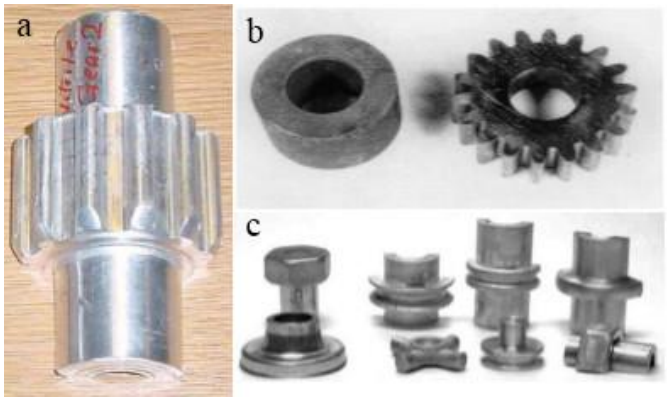

Fig. 2-2: Injection forging components: (a) gear shaft [38]*, (b) gear* [41]*, (c) flanged parts and universal joints* [27].

2.2.2 Process Principle

Based on tool configurations, injection forging can be divided into bulk, tube and

pressure-assisted injection forging. Fig. 2-3 (a) shows a typical bulk forging. Initially, a workpiece is placed into the die chamber. With the movement of the punch, the workpiece material begins to flow in the radial direction until the final geometry is obtained. In different tool configurations, the counter punch can be moveable or stable. In this way, it is possible to manufacture some specimens which are impossible or difficult to be produced by conventional operations.

In tube forging (as shown in Fig. 2-3 (b)), the mandrel is used to support the workpiece or prevent inward material flow. This method is useful for thin-walled components. For thick-walled parts, however, the die stress is so high that it is beyond industrial limit [27]. Moreover, due to the limitations of mandrel geometry, it is unable to fabricate some components, e.g. the gear shaft. Therefore, the pressure-assisted approach is applied to produce this kind of part. The tube is filled up with media material, as shown in Fig. 2-3 (c). After this, the tube ends are sealed by a punch and counter punch. With pressures from punches and media material, the tube bulges to the final shape.

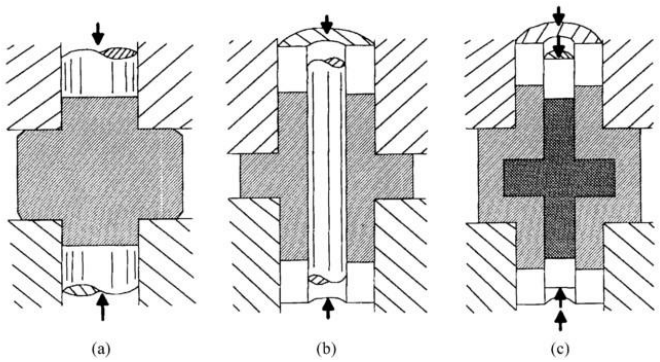

Fig. 2-3: Illustration of three injection forging configurations [27]*: (a) bulk forging, (b) tube forging, (c) pressure-assisted forging.*

2.2.3 Forming Defects and Forming Limitations

2.2.3.1 Forming of Bulk Materials

In injection forging of solid materials, the forming defects are defined as the

following five forms (refer to Fig. 2-4) [33], [34]:

- *Buckling/asymmetrical deformation*. Instability of the billet results in this defect. The work-hardening exponent affects the risk of buckling. It is argued that the smaller the work hardening, the larger the buckling effect.
- *Fracture.* It appears on the core or on the rim of components and is caused by the tensile stress on the material.
- *Folding.* It is caused by the rotation of material and the radial material flow at the bottom of the workpiece.
- *Underfilling/notch.* Due to the pressure losses during the injection forging, the material cannot fill up the die chamber. Therefore, small corner radii are not recommended for injection forging.
- *Unevenness/thinning.* Unevenness is defined as the unevenly distribution of material on the workpiece. It is caused by some factors, such as the initial workpiece geometry, tool assembly and tool quality, etc. By increasing the forming force at the final forming stage, this can be adjusted.

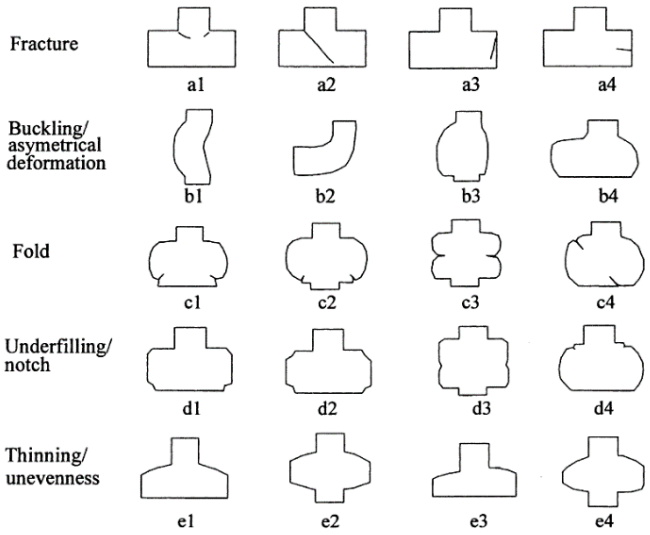

Fig. 2-4: Classification of failure forms on injection forging of bulk materials [33].

In order to prevent these forming defects, some parameters were analysed to discover forming limitations. The most important parameters are the aspect ratio of primary deformation zone $\boldsymbol{T}$ and diameter ratio $\boldsymbol{D}$ [33]:

$$T = t/d_0 \quad (1)$$

$$D = d_1/d_0 \quad (2)$$

where $\boldsymbol{t}$, $\boldsymbol{d_0}$ and $\boldsymbol{d_1}$ are unsupported billet length, billet diameter and flange diameter, respectively. These parameters are explained in Fig. 2-5. According to [33], the parameter $\boldsymbol{D}$, which depends on the materials, affects the incident of fracture considerably. When it increases from 2.0 to 3.0 for injection forging of aluminium E1CM, the fracture can be prevented. Besides $\boldsymbol{D}$, the exit-radii and friction conditions also influence the occurrence of fracture. For example, with a small exit-radii and high friction force fractures can be observed at the exit from the injection chamber [33], [42].

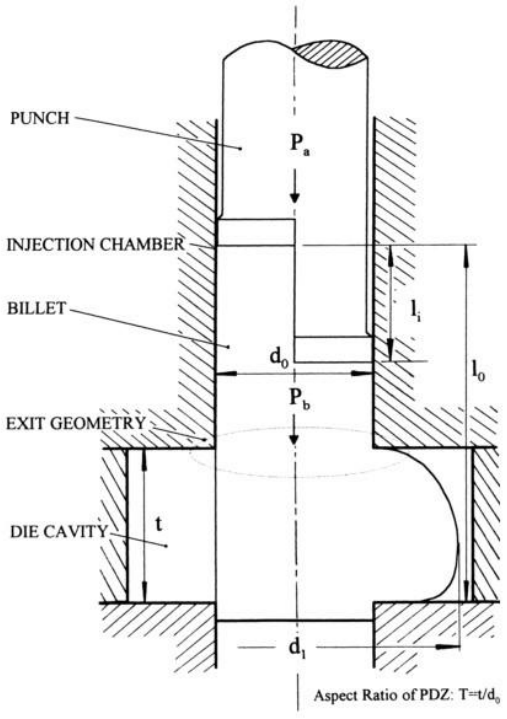

Fig. 2-5: The illustration of injection forging process and critical parameters [27].

As for parameter $\boldsymbol{T}$, it has significant influences on forming defects. It was argued that the buckling could take place on the workpiece when $\boldsymbol{T}$ was higher than 1.64 [43]. In other words, in a range of 0 – 1.64, the buckling can be prevented. However, this range is obtained when the billet cannot side slip. In other conditions, an upper limit of 1.4 - 1.64 is recommended [32]. On the other hand, $\boldsymbol{T}$ cannot be too small as results of the unevenness which often occurs in small values of $\boldsymbol{T}$ <0.5 [33]. When the fold is taken into consideration, this range needs to be recalculated. It was suggested that $\boldsymbol{T}$ should be smaller than 1.3 [32] for a single acting injection forging [44]. In order to extend the forming range, the preform design was employed on the injection forging [45]. It can reduce the ratio of radial expansion to prevent the folding. As results show, the upper limit can be improved to 1.4-1.5 by pre-shaping and 1.5-1.64 by preforming for flanged components [45].

2.2.3.2 Forming of Tubular Materials

Compared to bulk materials, fewer researchers paid attention to the injection forging of tubular materials [46]. Based on experiments, some researchers attempted to find the reasons which caused defects on tubular materials [46], [47], [48], [49]. According to [46], it showed that some major process parameters, such as $\boldsymbol{d_i/d_o}$ ($\boldsymbol{d_i}$: inner diameter; $\boldsymbol{d_o}$: outer diameter), $\boldsymbol{w/t}$ ($\boldsymbol{w}$: wall thickness, $\boldsymbol{t}$: gap height) and die chamber geometry (refer to Fig. 2-6), can impact the final component. When the $\boldsymbol{w/t}$ is less than 0.5, the folding risk on the workpiece materials stays at a high level. When $\boldsymbol{w}$ is much less than $\boldsymbol{t}$, the local reduction and fracture will happen on the outer edge of the flange [47], [50]. Moreover, $\boldsymbol{w}$ cannot be very small. Otherwise, it increases the risk of an uneven flange thickness, irregular plane surface and irregular peripheral surface [27], [51].

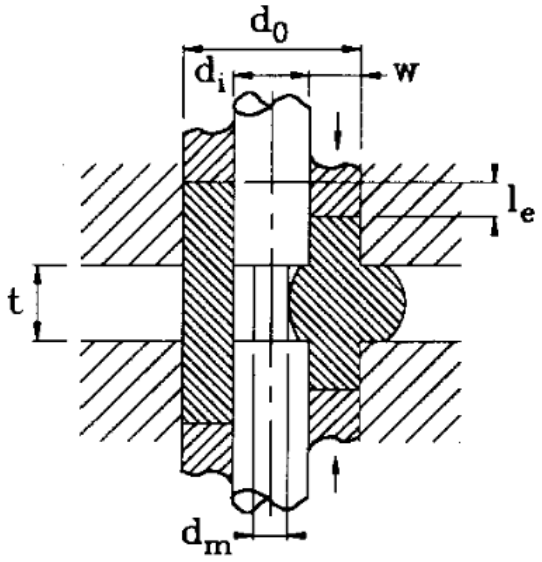

Fig. 2-6: Die configuration of double-sided injection forging of tubes [52].

2.3 Tool Failures and Tool Life Improvements

2.3.1 Types of Tool Failures in Cold Forging

There are three main modes of tool failures, i.e. fracture, plastic deformation and wear [53], [54]. Fig. 2-7 shows an example of different failure-forms in the forward extrusion die. Depending on different forming processes, the major tool failure is different. Usually, in the cold forging of complex components, fracture is the main failure reason for tool failure and 80% of these fractures occur when producing complex components [55]. However, when in volume production of simple components, the tool always fails because of tool wear. In this section, the common tool failures in cold forging are reviewed.

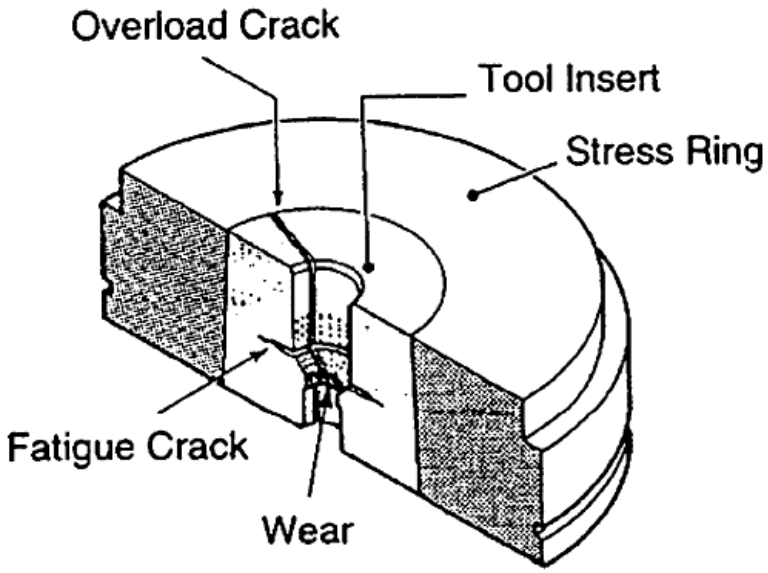

Fig. 2-7: Tool Failure in Cold Extrusion die [55].

Wear. Wear is one of common tool failures in cold forging [54]. It is classified into adhesive wear and abrasive wear. In general, the adhesive wear is the predominant wear mechanism in cold forging [5]. This is because of the considerable deformation and contact of the tool with deformed metal, especially in the process of press-cutting, resulting in cold welds and adhesive joints. However, in some particular regions of the tooling, such as the front surface of punches and die edges, the abrasive wear becomes the main failure factor [56].

Plastic deformation. During the forging process, if the pressure exceeds the yield stress of tool material, plastic deformation can grow as a localised effect or a widespread condition. An example of a localised effect is rolling the corner of a punch or the initial yielding in a stress concentration position before a fatigue failure [53]. This results in the formed parts unable to keep an acceptable dimensional tolerance.

Fracture. There are two common modes of die fracture failure which are overload fracture and fatigue fracture [57]. The overload fracture is caused by the high applied stresses that exceed the ultimate strength of the die material [53]. It may be caused

by the poor tool design, improper pre-stressing or lacking of control of forging load and energy [5]. Usually, this fracture takes place within a few forging cycles. It creates a safety hazard for the operator as a result of releasing enormous amounts of energy from the die. Fatigue fracture is defined as a tool failure after the tool undergoes repeated or cyclic stress reversals [54], [58]. This kind of loading condition contributes to the micro-crack initiation and growth in the forming process [57]. Because there is no prior warning, it is a dangerous failure in factory production.

2.3.2 Fatigue Analysis

According to [59], the tool life of cold forging is limited by fatigue in most situations. Therefore, many researchers developed methods to analyse and predict the fatigue life. To date, there are two main approaches to evaluate the fatigue life, including a stress approach (S-N curve) and strain approach. The stress approach is more suitable for high cycles fatigue analysis with low-stress level (in the elastic range) and a plenty of test cycles (more than one million in some cases). In low cycles fatigue analysis, in practice the tool experiences plastic deformation, the stress approach cannot provide an accurate result. In this condition, strain approach becomes the first choice.

2.3.2.1 Stress Approach

Wohler developed the basis of this approach in 1860, known as an S-N curve. In 1910, Basquin quantified the S-N curve which expressed the relationship between forging cycles $\boldsymbol{N_f}$ and admissible stress amplitude $\boldsymbol{\sigma_{ar}}$:

$$\sigma_{ar} = \sigma_f'(2N_f)^b \tag{3}$$

In this model, $\boldsymbol{\sigma_f'}$ and $\boldsymbol{b}$ are fatigue strength coefficient and fatigue strength exponent. The $\boldsymbol{\sigma_f'}$ is close to the tensile strength of material and $\boldsymbol{b}$ is within 0.05 to 0.12 for

steels and bronzes [60]. This model fits the practice well when the mean stress is zero. However, when the mean stress is positive, the tool damages before the predicted life [60]. In order to address this problem, many correction models are put forward such as the Goodman model, Gerber model, Soderberg model and Morrow model:

$$\text{Goodman [61]: } \frac{\sigma_a}{\sigma_{ar}} + \frac{\sigma_m}{\sigma_u} = 1 \quad (4)$$

$$\text{Soderberg [62]: } \frac{\sigma_a}{\sigma_{ar}} + \frac{\sigma_m}{\sigma_y} = 1 \quad (5)$$

$$\text{Gerber [63]: } \frac{\sigma_a}{\sigma_{ar}} + \left(\frac{\sigma_m}{\sigma_u}\right)^2 = 1 \quad (6)$$

$$\text{Morrow [64]: } \frac{\sigma_a}{\sigma_{ar}} + \frac{\sigma_m}{\sigma_f'} = 1 \quad (7)$$

These models take account the effect of mean stress $\boldsymbol{\sigma_m}$ on the stress amplitude $\boldsymbol{\sigma_a}$ related to yield stress $\boldsymbol{\sigma_y}$, tensile strength $\boldsymbol{\sigma_u}$ and endurance limit $\boldsymbol{\sigma_{ar}}$ at $\boldsymbol{\sigma_m} = 0$ [65]. Each model has its merits. Goodman model is suitable for brittle metal, while people apply Gerber model for ductile metal. For most metals, the Soderberg model gives a conservative result [60]. Morrow equation shows the favourable ability for various metals, except aluminium alloys [65]. Combining Basquin and Morrow equations, the stress approach can be modified as [66]:

$$\sigma_a = (\sigma_f' - \sigma_m)(2N_f)^b \quad (8)$$

Currently, this equation has already become a popular criterion for evaluating fatigue life. Dehghani and Jafri judged the different tool designs by the stress approach [67]. Two equations, as shown in Table 2-1, were employed to decide the material constant $\boldsymbol{b}$ and $\boldsymbol{\sigma_f'}$. These equations are effective when the material test is difficult to carry out.

Saroosh et al. developed a new model (refer to Table 2-1) based on Basquin and Morrow's approach [68]. This model was useful when the tool and workpiece

materials were tungsten carbide and S45C or SCM435, respectively [68]. Meanwhile, they analysed the influence of mean stresses on the fatigue life. The result showed that the prediction from the Basquin model with mean stress was more realistic than it without mean stress. Akhtar and Arif [66] compared the stress approach and strain approach in extrusion. With the help of FE simulation, they showed that the stress approach was accurate, while the result from a strain approach was higher than the reality of tool life.

Table 2-1: Stress-life approach models.

Authors'	Model
Dehghani and Jafri [67]	$b = -\frac{1}{3}\log\left(\frac{f\sigma_u}{\sigma_{ar}}\right)$ (9) $\sigma_f' = \frac{(f\sigma_{ar})^2}{\sigma_u}$ (10) $\boldsymbol{f}$ is a constant (0.8 – 0.95)
Saroosh et al. [68]	$N_f = 0.5\,(\frac{2.5K+Kn-1482.8}{\sigma_f'+499.3-2.3K-0.9Kn})^{\frac{1}{b}}$ (11) **K, n, $\boldsymbol{\sigma_f'}$** and **b** are the strength coefficient (MPa), strain-hardening exponent, fatigue strength coefficient (MPa) and fatigue strength exponent, respectively.

2.3.2.2 Strain Approach

In 1954, Coffin and Manson found a relationship between fatigue life and plastic strain which addressed the tool life prediction in high strain forging [69]. The model is listed below:

$$\frac{\Delta\varepsilon_p}{2} = \varepsilon_f'(2N_f)^c \quad (12)$$

In this equation, the plastic strain amplitude $\boldsymbol{\Delta\varepsilon_p}$ is expressed by fatigue life $\boldsymbol{N_f}$, fatigue ductility coefficient $\boldsymbol{\varepsilon_f'}$ and fatigue ductility exponent $\boldsymbol{c}$. Because the total

strain amplitude $\Delta\boldsymbol{\varepsilon_{tot}}$ equals elastic strain amplitude $\Delta\boldsymbol{\varepsilon_e}$ plus plastic strain amplitude $\Delta\boldsymbol{\varepsilon_p}$, the Coffin and Manson equation can be written as [70]:

$$\frac{\Delta\varepsilon_e}{2} = \frac{\Delta\sigma}{2E} = \frac{\sigma_f'}{E}(2N_f)^b \tag{13}$$

$$\frac{\Delta\varepsilon_{tot}}{2} = \frac{\sigma_f'}{E}(2N_f)^{\,b} + \varepsilon_f'(2N_f)^c \tag{14}$$

where E is Young's modulus. *Equation 14* is the basis of strain approach for the subsequent fatigue research. Taking mean stress into *Equation 15*, it can be modified as [71]:

$$\frac{\Delta\varepsilon_{tot}}{2} = \frac{\sigma_f'-\sigma_m}{E}(2N_f)^{\,b} + \varepsilon_f'(2N_f)^c \tag{15}$$

The model has two stages, including a low cycle fatigue regime ($N<10^4$) and a high cycle fatigue regime ($N>10^5$). It is inflexible for an application within FE simulation software [72] because it could not predict a whole range of the fatigue life of the tool. M Geiger et al. revised the original model in which the fatigue life depended only on the total strain range. The new model, seen in

Table 2-2, showed accuracy estimation of die life compared with the experimental results.

In other studies, the relationship between the hardness of metal and the fatigue was investigated by Lee and Chen [73]. Usually, the die materials demand both hardness and ductility. In general, the proper heat-treatment can improve the ductility, but the hardness may vary over a wide range. It is therefore simple to only measure the hardness of the die material to estimate the die quality. Following this concept, Lee and Chen [73] developed an equation based on a strain approach, as shown in

Table 2-2. It was reported that this model was a new approach to estimate die life. However, according to the [73], "*this proposed fatigue model is yet to be validated by more experimental data"*. Therefore, it is difficult to ensure its accuracy.

Table 2-2: Strain-life approach models.

Authors'	Model	
M. Geiger et al. [72]	$\log\frac{\Delta\varepsilon_{tot}}{2} = \frac{b-c}{4z}(\log N_f)^2 + c\log N_f + A$	(16)
	$A = \frac{z}{4}(c-b) + \log 2\varepsilon_f'$	(17)
	$Z = \log\left\{\left(\frac{\varepsilon_f' E}{\sigma_f'}\right)^{1/(b-c)}\right\}$	(18)
Lee and Chen [73]	$\Delta\varepsilon_{tot}\left(1 - e^{-\frac{A}{\Delta\epsilon_{tot}}}\right) = \frac{\sigma_f'}{E}(2N_f)^B$	(19)
	$\sigma_f' = \sigma_f$	(20)
	$\sigma_f = 24.4H + 702.9$ (JIS SK4)	(21)
	$\sigma_f = 21.2H + 869$ (JIS SKS3)	(22)
	$\sigma_f = 29.2H + 436.3$ (JIS SDK11)	(23)
	$\sigma_f = 23.3H + 952.6$ (JIS SKH9)	(24)
	A, is a correction factor from experiment and H is a hardness value based on HRC. B is a constant which depends on the hardness of the die material. (SK4 is a carbon tool steel. SKS3 is a cold work too steel. SKD11 is a cold work steel. SKH9 is a high speed steel.)	

2.3.3 Fracture Analysis

Because the traditional stress approach and strain approach cannot describe the fracture process, Paris developed a fracture model in 1963, known as Paris' law [74]:

$$\frac{da}{dN} = C(\Delta K)^m \tag{25}$$

$$\Delta K = \Delta\sigma Y\sqrt{\pi a} \qquad (26)$$

In this criterion, Irwin stress intensity range $\Delta \boldsymbol{K}$ was introduced to decide the length of crack $\boldsymbol{a}$ based on cycle number $\boldsymbol{N}$. Parameter $\boldsymbol{C}$ and $\boldsymbol{m}$ are material constants which can get from experiment. $\Delta \boldsymbol{K}$ is decided by stress amplitude $\Delta \boldsymbol{\sigma}$, geometry factory $\boldsymbol{Y}$ and half-crack length $\boldsymbol{a}$. Based on this equation, the Paris curve was able to describe the crack process, seen in Fig. 2-8. In this figure, the $\boldsymbol{K_{max}}$ is maximum stress intensity factor and $\boldsymbol{K_c}$ is critical stress-intensity factor for fracture. According to the curve, the fracture process is divided into three stages: slow growth (threshold region), Paris region and quick growth (unstable region). In the first region, the crack will not arise until the threshold $\Delta \boldsymbol{K_{th}}$. After it, the crack increases slowly [75]. In the Paris region, the crack growth is stable, and the mean stress influences the growth rate. At the last region, the crack growth becomes unstable until the final failure.

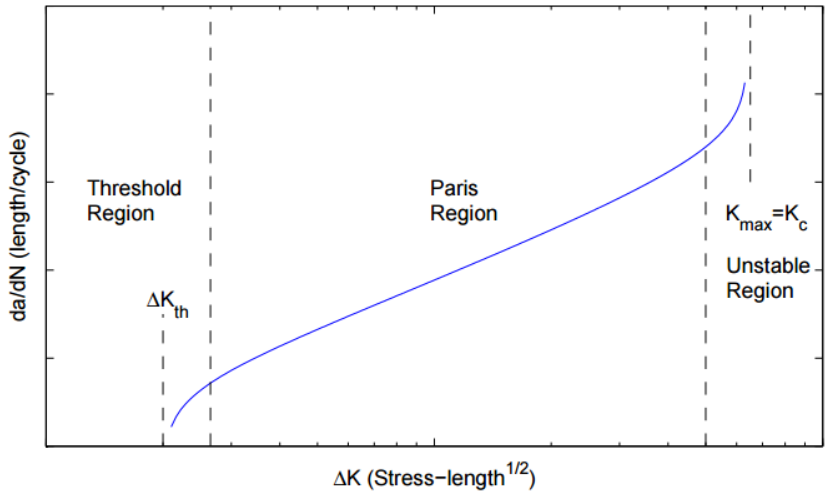

Fig. 2-8: Crack growth curve [76]

However, there are some limitations for this model. Firstly, this equation does not define the effect of stress ratio $\boldsymbol{R}$ on crack propagation [76], while the stress ratio is important for crack growth, especially in threshold region and unstable region. Secondly, in the unstable region, Paris' law cannot predict the crack growth accurately [77]. Therefore in subsequent research work, the stress ratio was

investigated by Walker [78]. It was suggested that the stress ratio $\boldsymbol{R}$ accelerated the growth rate. The modified model is listed below:

$$\frac{da}{dN} = \frac{C}{(1-R)^{m(1-\gamma)}}(\Delta K)^m \tag{27}$$

where $\boldsymbol{\gamma}$ is constant decided by experiment. This equation fits well in the Paris region, whereas it still cannot predict the unstable region. Forman proposed an improved expression which was called as Forman equation [79]:

$$\frac{da}{dN} = \frac{C(\Delta K)^m}{(1-R)(K_c - K_{max})} \tag{28}$$

Through Forman equation, it addressed the crack growth in the unstable region.

2.3.4 Wear Analysis

The tool wear is a complicated process which is influenced by temperature, surface roughness, material, lubricant, relative velocity, etc. Hence, it extremely difficult to formulate the wear process [80], [81]. Currently, the most popular model in the prediction of tool wear is the Archard model. This model was developed in 1953 [82], which defined the wear volume $\boldsymbol{W}$ by normal load $\boldsymbol{P}$, sliding speed $\boldsymbol{V}$, Hardness $\boldsymbol{H}$ (HRC) and wear coefficient $\boldsymbol{K}$.

$$W = K\int \frac{PV}{H}dt \tag{30}$$

In this equation, the hardness is constant during the forging. However, in practical production, the material hardness depends on the working temperature [83]. In other words, the thermal energy is able to soften the hardness. Therefore, the previous model was updated by Kang et al. [83]:

$$\delta d = \frac{KPL}{3H(T,t)} \tag{31}$$

where $\boldsymbol{L}$, $\boldsymbol{t}$, $\boldsymbol{T}$ and $\boldsymbol{d}$ are sliding length, time, temperature and wear depth, respectively. In the following research, Lee and Jou [84] found that the wear coefficient $\boldsymbol{K}$ increased with the temperature as well. Therefore, a new modified

model was proposed [84]:

$$W(T) = K(T)\frac{LF}{H(T)} \tag{32}$$

$$K(T) = (29.29 \ln T - 168.23) \times 10^{-6} \tag{33}$$

$$H(T) = 9216.4T^{-0.505} \tag{34}$$

where T is centigrade temperature, H is Vickers hardness and F is the normal force. This equation can describe the wear process well when the tool material is SKD61 and workpiece material is SCM415. Based on this model, Lee et al. [85] developed empirical equations for a two stage bolt forming process.

$$\mathrm{D_A} = K'(1.30 \times 10^{-5} - 4.14 \times 10^{-4} + 0.00478\mathrm{n}^2 - 0.0232\mathrm{n}^3 + 0.0403\mathrm{n}^4) \tag{35}$$

$$\mathrm{D_B} = K'\left\{50.35\mathrm{e}^{\left(-\frac{\mathrm{n}}{0.0040}\right)} + 3.4 \times 10^{-7}\mathrm{e}^{\left(-\frac{\mathrm{n}}{0.17}\right)} + 6.73 \times 10^{-8}\right\} \tag{36}$$

$\boldsymbol{D_A}$, $\boldsymbol{D_B}$, $\boldsymbol{K'}$, $\boldsymbol{n}$ are wear depth in the top part of die insert, wear depth in the bottom part of die insert, strength coefficient and strain hardening exponent of the material, respectively. According to experimental results, it was argued that the tool with soft materials should take the wear into consideration, while the tool was subjected to high-cycle fatigue from the strong materials.

Although the Archard's model shows good results in some processes, there are also some limitations. In the opinion of Sobis et al. [86], the wear process was so complicated that it cannot be figured out by this "simple" model. It is because the Archard's model only involves sliding length, hardness and the load. Some important parameters, such as friction and lubrication which impact the wear rate, are not covered. Moreover, the lubricant controls the real contact area which affects the contact pressure. Therefore, they believed that this model only could be applied in some simple operations [86].

2.3.5 Tool Design

Tool design is the most critical part in automotive components production. A good design can improve the tool life enormously. There are three rules of thumb in tool design:

- Avoid sharp tool geometry which causes stress concentration [1];
- Reduce the tool stress, especially the damaging tensile stress which deteriorates the fatigue life [59];
- Selection of suitable tool materials [87].

2.3.5.1 Considerations on Tool Geometry

In cold forging, the geometric discontinuities, such as holes, grooves and keyways, cause stress concentration which magnifies the local stress and shortens the fatigue life [88]. Therefore, when doing the tool design, it is necessary to reduce these discontinuities on the tool geometry via optimisation of the tool shape [72]. Some research has been conducted in this area. In the early work performed by K. Lange and his colleagues [1], the maximum principle stress was located in the transition area of die inserts for cold heading during the forming process. Therefore, the transition radius should be as large as possible to reduce the notch effect. J.S. Jin et al. conducted other similar works [89] for bevel gears which showed that the bottom face and vertical wall underwent high stresses. Therefore, they enlarged the bottom hole of the die which reduced the stress level. It resulted in the redesigned tool life increased by ten times.

2.3.5.2 Considerations on Tool Stress

Generally speaking, the high stress could deteriorate the tool life. Some approaches, therefore, were proposed to overcome the high tool stress. The most popular one is called “divided flow” which is an application of the relief-axis and relief-hole in the

tool [90]. With using this design, the required forging force can have a big decrease which in turn reduces the tool stress. In reference [91], Kondo and Ohga combined the conventional closed die forging and "divided flow" concept to fabricate the ring gear. They only used 2.6 times the yield strength of the work material to produce the ring gear. It not only extended the tool life but also improved the forming accuracy.

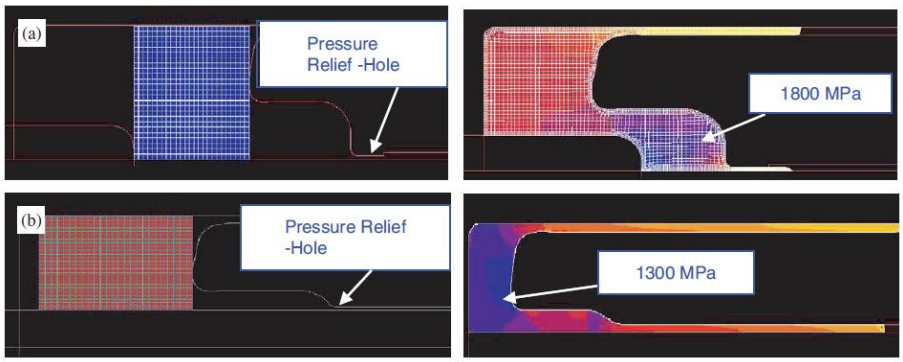

Fig. 2-9: Illustration of divided flow in backwards can-extrusion: (a) solid material (b) tubular material [92].

Other works were done in backwards can-extrusion of cartridge-cases [92]. Results showed that the high stress in the punch-pocket was reduced via the pressure relief channel, seen in Fig. 2-9. However, this technology is not appropriate for volume production of automotive fasteners because of the residual flash on the workpiece which would need machining after forging.

Besides using "divided flow", eliminating the damaging tensile stress can also improve the tool. In tool designs, therefore, pre-stressing is introduced to the die insert by a shrink ring (refer to Fig. 2-10). In this way, it can decrease or counteract the tensile stress concentrations at or near the critical sections [67], [93]. There are some approaches to optimise and reinforce the pre-stressing for cold forging. Firstly, Victor [87] proposed a new pre-stressing design for cold heading. In his work, the external diameter of the die insert was higher at each end and steadily drops toward the middle part. It can cause a "bending" effect that generates a higher compressive stress [87].

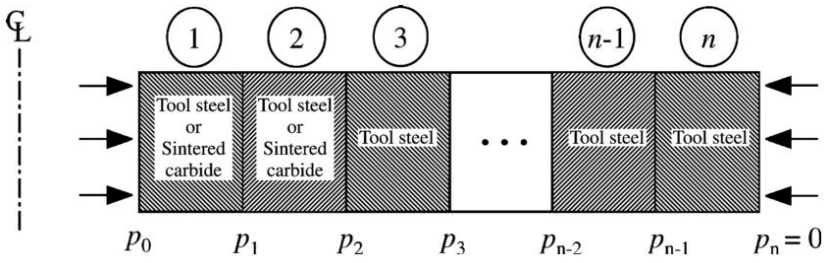

Fig. 2-10: Illustration of shrink ring and die insert [94].

Moreover, to increase the pre-stressing, a double shrink ring may also be used. This is because the pre-stressing cannot reach the ideal level by single shrink ring in some cases. However, it is noticeable that with more than two shrink rings it is difficult to improve the fatigue life further [54]. This is because the pre-stressing in the die insert could exceed its yield stress by increasing shrink rings numbers. In addition to using multiple shrink rings, advancing design e.g. strip-wound die design, can also improve the die life significantly [55], [59], [95]. It is argued that this design extends the tool life by 3-10 times than traditional tools [96].

The last method is splitting the die insert at the position where tensile stress is concentrated. It can reduce the maximum principal stresses at the critical area [53], [67]. Another benefit from the split die is making the pre-stressing design more flexible than the single die insert design. Depending on different requirements, the pre-stressing could be varied at the die inserts. When using the multiple die inserts, it is suggested to employ an angle between interfaces of each die insert. This can achieve a higher contact pressure at the die inserts interface and constrain the movement of the insert. No mark, therefore, is introduced during the forging [87]. Fig. 2-11 shows an example of splitting die inserts.

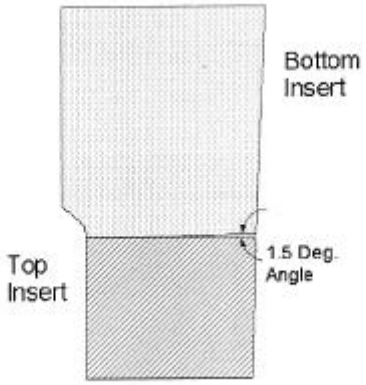

Fig. 2-11: An example of the split die insert [87].

2.3.5.3 Considerations on Tool Materials

For selecting die materials, the paramount considerations are wear resistance, deformation resistance and anti-fatigue behaviour [97]. Hardness plays an important role in the material behaviour of wear resistance [1], [5]. Usually, the higher hardness, the less wear happens. Therefore, the magnitude of hardness becomes the essential characteristic for selection of die materials. Moreover, to withstand the severe stresses in the die insert, the material should have enough compressive strength. At last, since the temperature and stress changes repeatedly during the forging, a tough material can ensure satisfactory fatigue life and forming accuracy [97].

In Table 2-3, some common materials used for cold forging tools are listed. Currently, the most popular die insert material is tungsten carbide which has outstanding hardness and compressive strength. However, this brittle material is easy to break under tensile stress. Therefore, using ductile materials with the hardness close to tungsten carbide can improve the die life. In reference [98], it was suggested that a new tungsten carbide with a nanophase structure could be useful in the future for cold forging. Other materials, such as commercial AISI M4 (high speed steel) and steel bonded carbide, all have better ductile behaviour than tungsten carbide [87].

However, changing the die material also has drawbacks. According to [87], the biggest issue is an increase in the tool deflection because of a reduction of stiffness in the ductile material. Hence, it is better to redesign the tool shape to reduce the tensile stress instead of changing the tool materials.

For the shrink ring materials, AISI H13 (tool steel) is widely used in industry [94], [99]. It provides accepted toughness and wear resistance. In some cases, H13 was replaced by GTi 50 (sintered carbide) to achieve higher stiffness. It was proven by Kwan-Do who analysed the die stiffness with H13 and GTi 50 [94]. The results showed that the stiffness was improved by 14.29% by using this new shrink ring material.

Table 2-3: Chemical composition of tool materials.

Commercial Name	Designation AISI	C (%)	Mn (%)	Si (%)	Cr (%)	V (%)	Mo (%)	W (%)	Co (%)
Macsteel 2379 [100]	D2	1.50 ~ 1.60	0.15 ~ 0.45	0.10 ~0.40	11.00 ~ 12.00	0.80 ~ 1.10	0.60 ~ 0.80	-	-
Macsteel 2080 [100]	D3	1.9 ~ 2.2	0.15 ~ 0.45	0.10 ~ 0.40	11.00 ~ 12.00	-	-	-	-
Macsteel 2542 [100]	S1	0.40 ~ 0.50	0.20 ~ 0.40	0.80 ~ 1.10	0.90 ~ 1.20	0.15 ~ 0.20	-	1.80 ~ 2.10	-
Macsteel 2436 [100]	D6	2.00 ~ 2.25	0.15 ~ 0.45	0.10 ~ 0.40	11.00 ~ 12.00	-	-	0.60 ~ 0.80	-
Macsteel 2344 [100]	H13	0.37 ~ 0.43	0.30 ~ 0.50	0.90 ~ 1.20	4.80 ~ 5.50	0.90 ~ 1.10	1.20 ~ 1.50	-	-
Macsteel 2510 [100]	O1	0.90 ~ 1.05	1.00 ~ 1.20	0.15 ~ 0.35	0.50 ~ 0.70	0.15	-	0.50 ~ 0.70	-
Steel Express A2 [101]	A2	1.00	1.00	-	5.00	0.15-0.5	1.00	-	-
Uddeholm Calmax [102]	-	0.60	0.80	0.35	4.50	0.20	0.50	-	-
ASSAB ASP 23 [103]	M3:2	1.27	-	-	4.20	3.10	5.00	6.40	-
San Alloy Industry G7 [103]	-	-	-	-	-	-	-	75.0	25.0
CB-Ceratizit ST7 [104]	-	-	-	-	-	-	-	80.0	20.0
West Yorkshire Steel M2 [105]	M2	0.85	-	-	4.10	1.80	5.00	6.40	-
West Yorkshire Steel M42 [105]	M42	1.05	-	0.35	3.75	1.15	9.50	1.50	8.00

2.3.6 Tool-Fabrication Techniques

2.3.6.1 Machining Processes

The machining processes can be classified into:

- Traditional machining like turning, milling and grinding, etc.
- Non-traditional machining, for example, electro-discharge machining (EDM).

Traditional machining processes are used for almost all machinable materials. It provides a high machining accuracy and a good surface finish [1], but it cannot deal with some super hard metals, e.g. tungsten carbide. In order to machine these materials, non-traditional machining was developed in tool making. EDM, as a representational technique, became the first choice to cut the super hard materials in tool-making industries [106], [107]. As long as the material has electrical conductivity, EDM can process it regardless of material hardness and strength. Meanwhile, because there is no direct contact between the electrode and workpiece during the process, contact deformation will not happen. Therefore EDM can machine very thin and small components [106].

However, the die surface finish and service life are not as good as traditional machining [108]. It is because the intense heating and cooling induce the resistance stress which introduces micro-cracks on the machined surface [106]. The micro-cracks are the main reason for the reduction of the fatigue life and corrosion resistance [109], especially under tensile loading conditions [110]. Fig. 2-12 shows the micro-cracks on a die surface after EDM processing. Many studies were conducted to analyse the cracks in EDM. According to [111], the amount and depth of surface cracks increase with the discharge energy. Therefore, the pulse current and pulse-on duration are the major factors. This was proved by Lee and Tai [110] who did an experiment to examine the effect of pulse current and pulse-on duration on surface cracks. Results showed that the increasing pulse current and pulse-on duration promoted the crack growth. In the meantime, the surface roughness also became worse. Therefore, selection of suitable pulse current and pulse duration are important for the EDM process.

Fig. 2-12: Surface of dies (H13) after EDM process [112].

2.3.6.2 Heat Treatment

After machining, heat treatment is required to improve the tool properties, i.e. toughness, hardness and ductility. A traditional heat treatment for a die steel includes three steps [113]:

1) Heating the die steel to austenitizing temperature and keeping it for a specified time.

2) Cooling down the dies under air, water or oil. Depending on the cooling rate, the die material has diverse phases. Fig. 2-13 shows the different phases in different cooling rate. For most die steels, the martensite is an ideal structure.

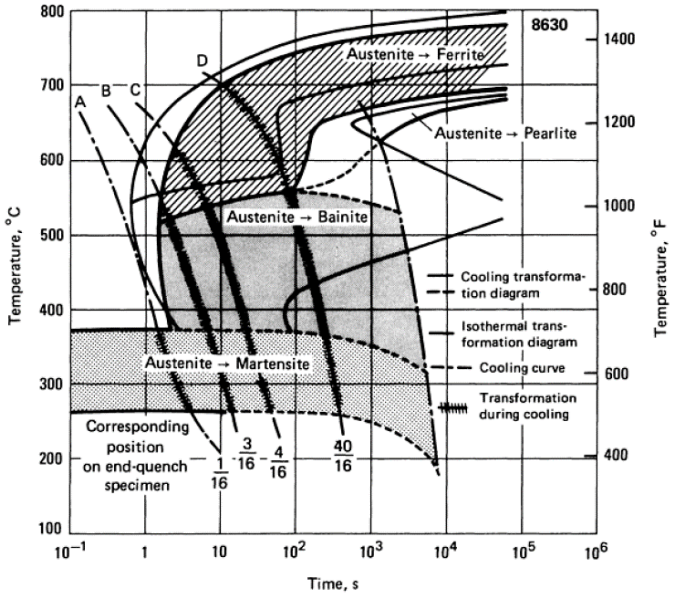

Fig. 2-13: The relationship between cooling rate and transformation diagrams for 8630 steel [114].

3) Heating dies again to make the martensite stable which improves the toughness of materials.

During the heat treatment, precise control of temperature, holding time and cooling rate decide the tool properties [115]. To date, the temperature and holding time are standardised for die manufacture, while the ideal cooling rate is subject to dispute. In most cases, the traditional heat treatment avoids a high cooling rate which causes distortion or even cracking [116]. However, according to Nikolai [117], an extremely high cooling rate can optimise the performance of tooling. The effect of cooling rate in low alloy steel was studied in [118]. As shown in Fig. 2-14, after the cooling rate increases to a threshold value, the crack formation probability decreased rapidly. It was reported that the service life of a punch made of AISI S5 steel increased by two times after high cooling rate treatment.

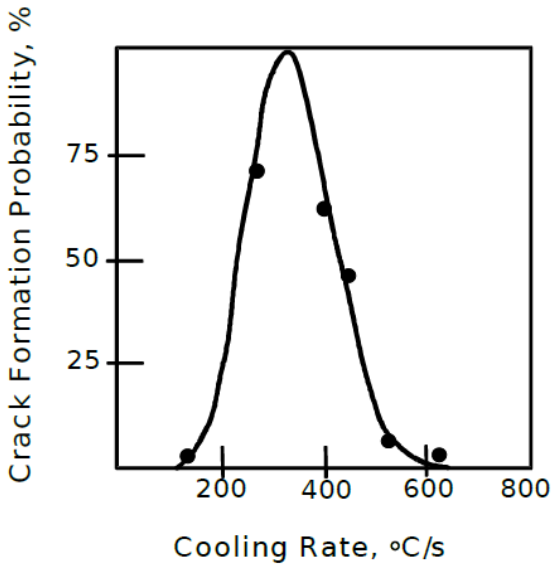

Fig. 2-14: Effect of cooling rate in low alloy steel [118].

2.3.6.3 Surface Treatment

Surface treatment is applied in cold forging to improve the tool properties. Because wear resistance has a remarkable improvement after the treatment, this technique shows prospect for wide application in tool making. In past decades, many researchers studied the influence of surface treatment on the tool life. These results are listed in Table 2-4. Based on suitable surface treatment, the tool properties can

have various enhancements.

Surface hardness. There are some ways to enhance hardness. Firstly, the hardness can be improved by coating. The typical technique is physical vapour deposition (PVD) which utilises the vacuum deposition to coat the tool surface by physical methods [119]. Since PVD works at low temperature, the thermal distortion can be avoided in tooling. The second approach is a thermal diffusion process. It introduces carbides, nitrides or carbonitrids to the tool surface [114]. Through these processes, some hard metallic compounds, such as, Fe-N, Al-N, and Fe-C, are generated on the tool surface. These metallic compounds can prevent the tool from wearing.

Table 2-4: Tool life for different materials under various surface treatments.

Authors	Methods	Tool material	Object	Remarks
Farrahi and Ghadbeigi [120]	Shot peening (standard steel shots S230)	AISI D3 cold work tool steel	Rotating-bending fatigue test Specimen	Fatigue tool life increases by 14%
	Double stage nitriding	AISI D3 cold work tool steel	Rotating-bending fatigue test Specimen	Fatigue tool life decreases by 8%, improvement of surface hardness
	Single stage nitriding	AISI D3 cold work tool steel	Rotating-bending fatigue test Specimen	Fatigue tool life decreases by 50%, improvement of surface hardness
	Nitrocarburizing	AISI D3 cold work tool steel	Rotating-bending fatigue test Specimen	Fatigue tool life decreases by 29%, improvement of surface hardness
Monika Gierzynska-Dolna [56]	Nitriding	WNL die-steel	-	Decrease of fatigue strength
	Al_2O_3, WC, Cr plasma spraying	WNL die - steel	Punch	Tool life increases

Wanger et al. [121]	Hard roller burnishing	-	Cold forging die	Tool life increases by 100-160%
	Laser beam treating	-	Cold forging die	Keep or decrease of tool life
	Surface texturing	-	Punch	Tool life increases by 84-122%
Cassio and Cralos [122]	Plasma nitriding	VF800 AT steel	Die	Average wear rate of tool reduces by 67%
	TiCN - PVD	VF800 AT steel	Die	Average wear rate of tool reduces by 83%
Tohru Arai [123]	Vanadium carbide - TD	AISI D2/AISI M2	Die/Punch	Tool life increases
M. Geiger et al. [124]	Laser surface texturing	High speed steel	Punch	Average tool life increases by 169%

Residual compressive stress. During the forging, the hazardous tensile stress can break the tooling. Residual compressive stress, therefore, is employed to overcome tensile stress by surface treatment. One common approach to generate residual compressive stress in tools is shot peening which uses spherical media to impact the tooling. In this way, the fatigue life is extended [125].

Retaining the lubricant. In cold forging, the tool surface needs to transport a sufficient amount of lubricant into the forming zone [124]. An extremely smooth surface is unable to retain the lubricant. Therefore, an ideal tool surface requires proper micro-geometry to reduce the friction force by retaining the lubricant [126]. This micro-geometry is produced by shot peening or surface texturing. As by decreasing the friction force, the tool life is improved [127].

2.4 Component Form-Errors and Error-Reduction

2.4.1 Component Form-Errors in Cold Forging

Component quality is an important pillar in the cold forging industries as is reflected

by its development [128]. Because component errors decide the quality, understanding of component errors is critical. According to [1], component errors are classified into dimensional error, positional error, form error, surface error and material properties error. The first four errors can be considered as the deviation of final production shape from the targeted value. The last error is material properties not meeting requirements. Usually this is caused by improper heat treatment [1].

Other than the material properties error, the component errors are introduced from three stages in cold forging. The first stage introduces initial errors. Mainly, it is caused by tool quality, set-up of tools, forging machine, deviations in material composition, etc. [129], [130]. Some errors can be reduced by improving the machine stiffness, proper maintenance of forging tools and appropriate operator training [130].

The second stage, forming, can contribute highly to shaping errors. During the forming operation, both workpiece and tools undergo great stresses. Such high stresses result in elastic deformation in tools [131]. An example is the punch which is shortened by 1 mm and thickened by 0.05 mm under 2000 MPa stress in [132]. The dimensional change of tools leads to component errors. On the other hand, after loading, the elastic energy from the tools can change the component shape again which is called as “secondary yielding” [133], [134]. It is obvious for soft workpiece materials [135]. The last issue is springback of the workpiece. Since no tool constrains the workpiece after ejection, the elastic energy of workpiece can be released. In this condition, the dimension will change again.

Moreover, temperature is another important factor which affects component errors. Because most forming energy is transformed into heat energy, it means the temperature in the workpiece can reach around 300°C in some cases of cold forging [113], [132], [136]. This temperature is enough to impact some thermal-sensitive materials such as aluminium and copper. In large volume-production, the forming temperature increases with forging cycles. As results from [137], it shows the component errors fluctuate during the multi-cycle cold forging process. This is because the forging temperature is low in the initial stage. After many steps, the temperature reaches the maximum point and keeps stable.

The last stage is after the forging process. It is caused by inappropriate transport or storage [129]. This phenomenon is especially severe for some components with a weak structure, such as threads and sharp corners. During transport, component collisions could damage their structure.

2.4.2 Measurement of Component Form-Errors

The simplest method to measure component errors is by comparing the final component with the targeted component directly. In this way, the component geometry is measured by a coordinate measuring machine (CMM). However, there are two limitations for this approach. Firstly, the comparison result is affected by support software of CMMs [138]. Secondly, this method is unable to observe component errors in process. Hence, some researchers applied strain transducers at the tools to measure the tool deflection. It can reflect the errors on components indirectly [139], [140]. However, this measurement is costly and cannot show the elastic strain in tools completely because of the limited space for installation of transducers. Therefore, finite element analysis (FEA) is employed to quantify the component errors [141].

In the 1970s, FEA was applied to analyse the forming process [27]. At the beginning, people used a rigid-plastic model to conduct the simulation. In this model, the elastic deformation was neglected. It only could be used when elastic deformation was inconspicuous, and the plasticity was the main deformation. Therefore, it was not suitable for the component errors analysis which involved elastic recovery. Another model, elastic-plastic model, became the first choice for researchers. This model covered both elastic deformation and plastic deformation during the metal forming. Based on it, many studies about component errors were published. Qin and Balendra [142] analysed the influence of die-elasticity on the component dimension in forward extrusion. Lee et al. [143] evaluated the tool elastic deformation behaviour in cold forging of a ball stud. Long [144] investigated the elastic deformation of the die during loading, unloading, ejection and cooling down for backwards extrusion. Most simulation results showed good agreement with experiments. In order to improve the computational efficiency, Lu and Balendra [145] employed a new simulation model, the linear elastic model, to calculate the die-cavity compensation. It indicated that the

linear-elastic model had enough accuracy for simple elastic analysis, this model required the pressure contour on the die before the simulation.

Currently, various FE simulation software is available in the market, such as DEFORM, ABAQUS, ANSYS, QForm, DYTRAN, etc. The FE codes of ABAQUS and DEFORM will be discussed in the subsequent subsection.

2.4.3 Errors-Reduction Approaches

2.4.3.1 Process and Tool Design

In cold forging, the material flow status depends on the tool geometry. Therefore, a proper tool geometry design benefits component quality [96]. Several studies describe the relationship between tool shapes with component errors [142], [146], [147], [148], [149], [150]. Some suggestions are drawn from their results for common tool designs, as following:

- Transition radii at die corners (refer to Fig. 2-15). Because the stress focuses on the corners, it can cause large elastic deformation. Therefore, it is necessary to design transition radii to release the stress at corners. Qin and Balendra [142] compared the die with/without transition surfaces in cold extrusion. The results showed that form errors were reduced by the die with transition surface design. It was confirmed by Long [148] who analysed the entire cold extrusion cycle.

- Die angle (refer to Fig. 2-15). The die angle are determined by the friction condition and maximum workpiece strain [1]. The component distortion increases with increasing die angle [146], [147].

- Die land length (refer to Fig. 2-15). It was reported that the die land length affected the component errors significantly [150]. In the research from [150], with increasing die land length from 3 mm to 7 mm, the component errors decreased by 53.58%.

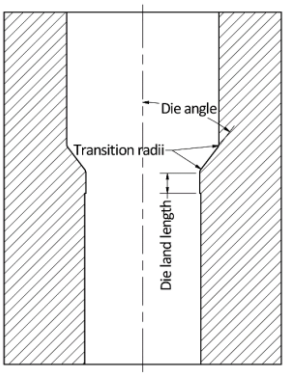

Fig. 2-15: Illustration of the parameters of a die insert.

For die configuration, some approaches were proposed to deal with the form errors. In the early stage of research, the ring-shaped die was analysed by Shiraishi et al. [151]. With the help of this design, the component errors can be reduced in extrusion and drawing. However, this design is only feasible in free extrusion and low-reduction drawing. Additionally, the constant friction condition between die and component is required by this design, but this is impossible in long manufacturing runs [149]. To improve this design, Wanheim et al. [149] proposed a new concept called the truncated-shell die. Fig. 2-16 (a) shows the conventional design and proposed design. In the new design, the rotation of the die in the bearing surface compensates for the component error (refers to Fig. 2-16 (b)). What is important is that the extrusion force could prescribe the rotation of the die rotation. In other words, the influenced factors may be simplified by this die configuration, which improves the accuracy of extrusion [149].

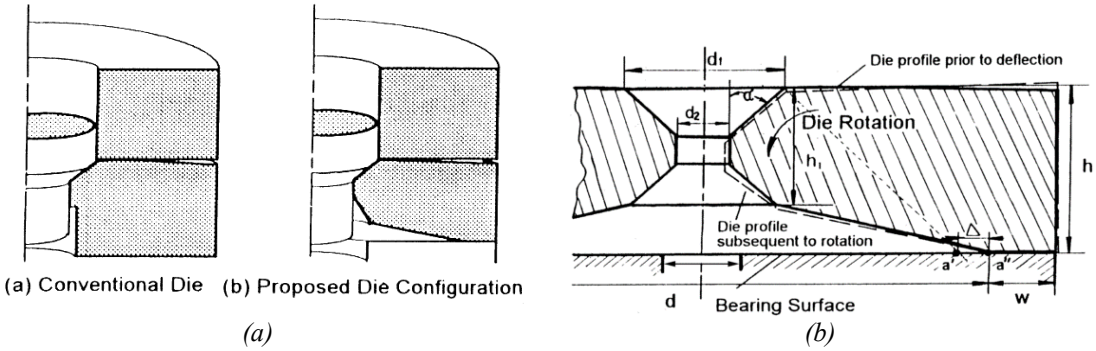

Fig. 2-16: Illustrations of truncated-shell die, (a) the configuration of the conventional die and proposed die configuration, (b) the work principle of the proposed die configuration [149].

Besides approaches mentioned above, some smart tools which can adjust the

dimension in processes, were developed in Europe. In Germany, an active die with additional hydraulic pressure was introduced by Jutte for highly precision gear forging [152]. In the UK, an innovative tool design was proposed by the University of Strathclyde and University of Birmingham [153]. In Fig. 2-17 the basic configuration of this tooling design is shown. As can be seen from the figure, the shape memory alloy (SMA) is the core of this design. The SMA can sense and adjust the variations in the work environment and can give a response to improve the performance characteristics of the structure. Therefore, "in-process" error compensation can be achieved by this design [96].

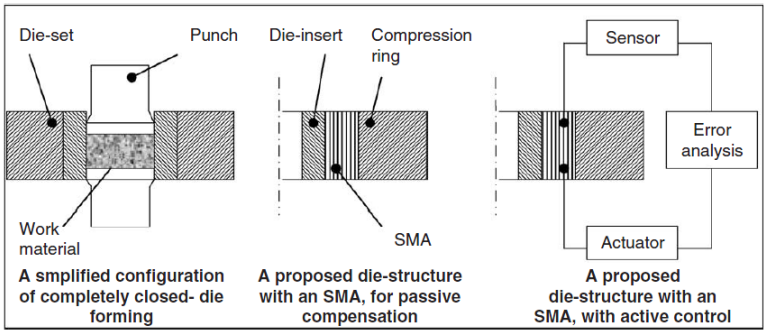

Fig. 2-17: The basic concept of smart forming tooling [153].

2.4.3.2 Forming-Stages and Preforms Design

For some components with complex geometry, modification of die geometry and die configuration are very time-consuming. Therefore, some researchers have attempted to refine the billet geometry. It was reported that the redesigned billet-geometry could reduce the forming pressure which resulted in better forming accuracy [129]. An ideal approach to optimise billet-geometry is preforming which reduces the forging force requirement and springback [129]. In this way, Qin and Balendra [45] employed the preform in the injection forging, which avoided the folding in components and improved the component accuracy.

To obtain a suitable preform design for the workpiece, some approaches are developed. In the early stage of studies, Sheng and Guo [154] proposed the continuous reverse simulation technique to help the preform design. In this method, the simulation begins from the final part and finishes at the original billet. In the following research, Lee et al. [155] used an electric field approach to explore the

preform shape in hot forging. Zhao et al. [156] employed sensitivity analysis to design a preform shape for H-shaped cross-sectional components. Lu et al. [157] applied an evolutionary topological approach for rail wheel forging preform design. Through these approaches, the proper preform design can be obtained for metal forming processes.

2.4.3.3 Friction and Lubrication Control

The friction condition plays an important role in cold forging. It not only relates to the die life but also does impacts the die deflection. Zimerman and Avitur [158] and Pan et al. [159] showed that the increasing of friction force resulted in high tool distortion. Qin and Balendra [142] presented that the larger friction between the die and workpiece could lead to greater radial deflection of the die during extrusion. It caused a large fluctuation in workpiece dimension. This was proved by Balendra et al. [138] and Long [160] in later research. It was argued that a reduction of friction was indeed helpful for the forming accuracy.

In order to refine friction conditions, the lubricant should be considered. A good lubricant can separate die and workpiece surface, causing low friction and less tool wear [1]. Several lubricants such as soap lubricants, oil-base lubricants and solid lubricants are used in metal forming. For severe deformation, the soap lubricants showed better behaviour than other lubricants [136]. In order to improve lubricants behaviour, the workpiece material often needs phosphating before the forming process. This process provides conversion coatings on the metal surface, which can help the lubricants to adhere to the workpiece [136]. However, conventional phosphating brings environment pollution. Recently, it has been gradually substituted by some developing lubricant systems [161]. Electrolytic phosphating is a successful alternative for traditional phosphating. As shown in Fig. 2-18, the coating is much finer after electrolytic phosphate than that in the old technique. It may suggest that this coating can provide better behaviour of lubricant with lower friction force during the forging process. Also, some lubricants which do not need the conversion coating are introduced. Nakamura et al. [162] examined two types of lubricants which included a mixture of wax and metal soap and a mixture of MoS_2 and graphite. Both of them exhibited good behaviour.

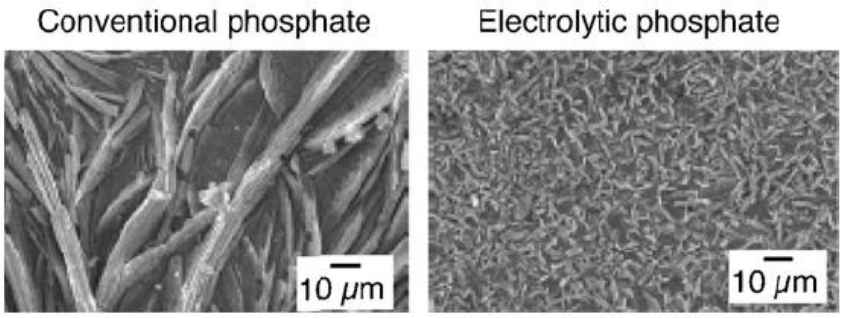

Fig. 2-18: The SEM micrograph of conventional phosphate and electrolytic phosphate [163].

2.5 FE Codes of ABAQUS and DEFORM

Throughout the last decades, DEFORM and ABAQUS, by virtue of their excellent non-linear processing ability and accurate results, were widely used in forming analysis [67], [142], [164], [165], [166], [167]. In ABAQUS, there are three main modules, Standard, Explicit and CFD (computational fluid dynamics), which are designed for different application fields. Among them, the standard module mainly intends to analyse static problems and some dynamic problems by implicit methods. This module is hard to use for metal forming analysis, especially for severe deformation forging. It is because the mesh distortion terminates the analysis. Therefore, the FE simulation for forging is finished by an explicit module instead of the standard module. The explicit module can solve transient dynamic, quasi-static and steady state problems. For most forging processes, it can be regarded as quasi-static problems. Although some noise is introduced by the explicit module during the quasi-static analysis, the results still are acceptable after suitable filtering [168].

In DEFORM similar solution methods to ABAQUS/Standard are used which are based on direct or Newton-Raphson iteration. Therefore, the results from DEFORM can keep stable compared with that from ABAQUS/Explicit. Meanwhile, the DEFORM provides an automatic remeshing system during the simulation. It ensures the simulation can be finished regardless of mesh distortions. However, the mainly used material model in DEFORM is a rigid-plastic model. In other words, the elastic period of the material is ignored during the simulation. It is acceptable for general forging simulation because the elastic period has only a slight influence on metal forging. However, for some simulations focused on tool deflection, this kind of

model must be abandoned. Moreover, compared with DEFORM, the post-processing of ABAQUS is more powerful. Due to these limitations, it makes the ABAQUS more popular than DEFORM in the research area.

However, whether using ABAQUS or DEFORM, some issues which need attention are the same, such as model simplification consideration, schemes for meshing and remeshing. These issues are reviewed below.

Model Simplification Consideration

It is expensive and time-consuming to execute a model which considers all details. For some large models, it may take a couple of weeks. Therefore, simplifying the model before the simulations is an important issue. There are two areas, geometry and process, which need to be considered.

For geometry, using a 2D model instead of a 3D model is the most simple and effective approach. As the simulation in [169], the result from the 2D model and the 3D model can match well under suitable parameter settings. Additionally, some small and unconsidered features in the geometry, such as fillets and chamfers, can be eliminated during the modelling. These features with small elements increase the processing time in modelling and simulations. Therefore, it is better to ignore these features when they are not important. At last, using some connection elements to replace related components also is beneficial for the geometry simplification. In ABAQUS, there are many connection elements. Using beam elements instead of fasteners, using spring elements instead of spring, using CV joint element instead of joints, etc. contributes to the model simplification.

For process consideration, it wastes time to simulate the whole process because a large proportion is unimportant for the result. Getting rid of these unnecessary aspects improves the simulation efficiency. A good example is a drop test simulation of a ball from a defined height in the ABAQUS manual [168]. Another suggestion is using a rigid body rather than the deformable body for running. As well known, simulation of a rigid body requires less time than a deformable body. Therefore, setting some parts, which do not experience deformation during the simulation, can simplify the model.

Schemes for Meshing and Remeshing Functions

Mesh schemes are another important issue for FE simulation. Excessively fine mesh does not improve the simulation accuracy yet incurs more computation time. In ABAQUS/Explicit, the stable increment time $\Delta \boldsymbol{t}$ depends on the following equations:

$$\Delta t = \frac{L_e}{c_d} \tag{37}$$

$$c_d = \sqrt{\frac{E}{\rho}} \tag{38}$$

where $\boldsymbol{L_e}$ is the element length, and $\boldsymbol{c_d}$ is the dilatational wave speed which is decided by Young's Modulus $\boldsymbol{E}$ and the material density $\boldsymbol{\rho}$. Therefore, when the material properties are given, the increment time is determined by the element length. More fine mesh, more computation time is taken. On the other hand, the coarse mesh brings distorted predictions. Therefore, arranging the mesh properly is important for FE simulations. A good suggestion is focusing mesh in regions of interest and using a coarser mesh elsewhere. Specifically, in large stress gradients, the mesh should be increased to prevent important details from being lost in simulations. When the model involves contact with a rigid body, especially a rigid body with a transition curve, a fine mesh density is recommended. It is because the rigid body plays as a master body in simulation, the deformable body is a slave body. When the mesh in a deformable body is coarse, the element of the slave body invades the master body which is called "element penetration" and introduces unpredictable errors.

After obtaining a reasonable mesh, maintenance of mesh quality during severe deformation is a problem. DEFORM provides an automatic remeshing function which is based on a remeshing criterion. In ABAQUS, there are two approaches. One is used in the standard module which is called "Map-Solution (MP)", and another is commonly used in the explicit module which is named as "ALE adaptive mesh (ALE)". For MP, the mesh quality for the deformed part is determined manually by the researcher. Therefore, this method is very complicated and time-consuming. It is unrealistic to use it in a large simulation because the number of remeshings could be more than thousands.

Therefore, most simulations involving severe deformation use the ALE approach. ALE refers to Arbitrary Lagrangian-Eulerian analysis. This approach combines the features of Lagrangian analysis and Eulerian analysis. Both standard and explicit modules can apply this function. However, the designed purposes of ALE for two modules are different. For the standard module, ALE mainly solves the analysis about structural acoustic, while it cannot handle large deformation problems. For the explicit module, it is particularly effective for metal forming simulation with robust controlling [168].

2.6 Summary

Cold forging is one of the most important techniques widely used in the automotive industries. It provides high production efficiency and stable component quality in volume production. Injection forging as a branch of cold forging is being developed in research and industry to shorten the forging process. Despite various studies being finished in injection forging on the forming limitation, modelling, lubricant, etc. There are still opportunities for improvement in this subject. One area is the component quality. The influence of process parameters on forming errors and mechanical behaviour is not systematically analysed.

Moreover, the tool life also is a challenge for injection forging. Although some approaches were proposed to release the tool stress, they could not be suitable for the industrial production because of extra post-machining or high tool-making costs. Therefore, it is necessary to provide a practicable and reliable method to extend the lifecycle of tools. In addition to this, the main use of injection forging is on a low forging speed. The area of volume production with high forging speed is unexplored. Therefore, more effort should be made for this area regarding the balance of tool life, component accuracy and production efficiency.

To achieve these demands, finite element analysis is applied to analyse and optimise the forging process and tool design. Regarding the economy and accuracy, a proper analysis model will be employed. Some parameters like friction condition will be adopted depending on practical production conditions in industry. After this, the theoretical results will be validated by experiments involving the forging of fasteners.

Chapter 3

Comparison of Multistep Forging and Injection Forging

3.1 Introduction

In this chapter, two forging processes, multistep forging and injection forging, were compared for forming an automotive fastener. A series of finite element simulations were carried out to analyse the capability of injection forging by forging force, dimension errors, tool stress and grain flow. Through observing the forging force, some parameters such as load amplitude and forming energy were discussed. The dimension errors were another important issue for this comparison. Due to the requirement task of shortening the forging process chain, controlling the component accuracy is a challenge for injection forging. Poor accuracy adversely affects the practical application of the component. It increases the potential risk of failure and makes the fastener unable to be fixed in the right position. In terms of tool stress, it reflects some areas of concern, including tool life, critical positions for cracking and tool deflection. Finally, the mechanical behaviour of the component was compared by the simulation of grain flow lines in DEFORM. According to comparisons, the behaviour of injection forging in auto fasteners production was demonstrated.

3.2 Process and Geometry Models

Fig. 3-1 presents a conventional multistep forging process in hexagon bolt forming. To secure the final forged hexagon bolt, the initial billet experiences five steps. In the first operation, the round bar is extruded forwards to reduce the diameter in the bottom part. Then, it is upset in the second operation. After this, the head is compressed by the punch to form a cavity. Before the final operation, the hexagon head begins to take a shape. The last operation is heading to get the final component.

To shorten the process chain, a concept of injection forging is introduced. As can be seen from Fig. 3-1, it intends to combine the first three operations into one operation. The process concept is shown in Fig. 3-2, which uses a floating die design. In this design, the die inserts move with the punch, together at the same velocity. The

ejection pin remains stable during the metal forming. It can, therefore, support the billet until the final dimension. In this way, the initial billet is formed directly into the intermediate product with a cavity by radial and backwards metal flow.

The initial geometries of the workpiece for two forging processes are illustrated in Fig. 3-3. To get the full size of the final product, the volume of the initial workpiece must equal that of targeted components. The volume is calculated by CAD/Inventor, which is 7789.161 mm^3.

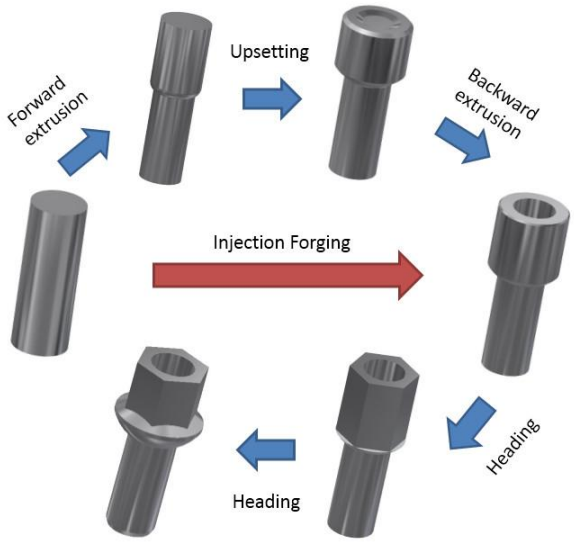

Fig. 3-1: Illustration of the traditional forging process and the injection forging process.

The geometry models of multistep forging tools relate to the design used in practice. As for injection forging, the key parameters of the tools correspond to the shape of a targeted component. To prevent detrimental tensile stresses, the die insert of the injection forging is split at the positions where the tensile stresses stay at the highest level. Meanwhile, with using an interference fit between the shrink ring and die inserts, pre-stressing is employed in order to withstand the tensile stress. Both the split die process and the interference fit design are stated in Appendix A. The geometry models of two forging processes are showed in Fig. 3-4.

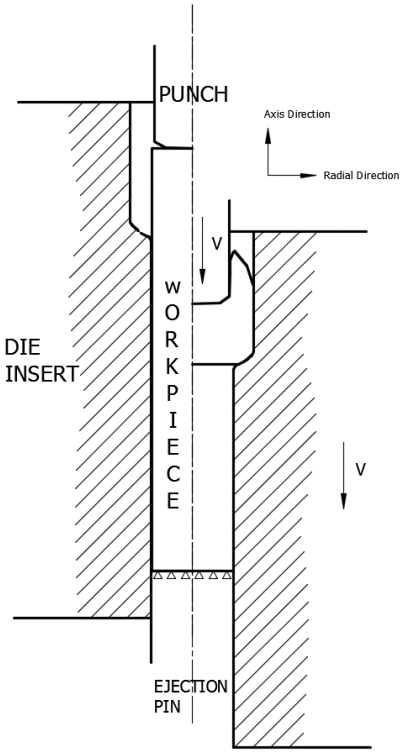

Fig. 3-2: Illustration of injection forging process in forming bolt.

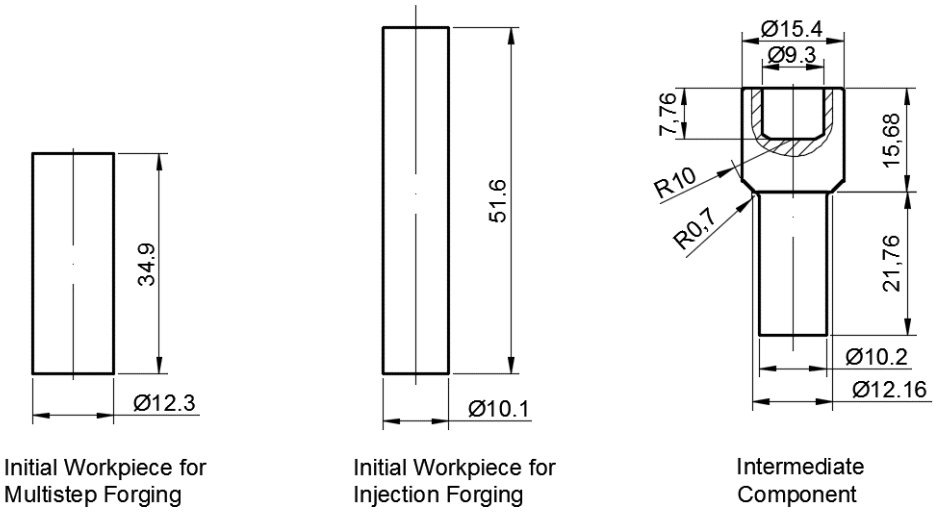

Fig. 3-3: The targeted component dimension and initial workpiece dimension for multistep forging and injection forging.

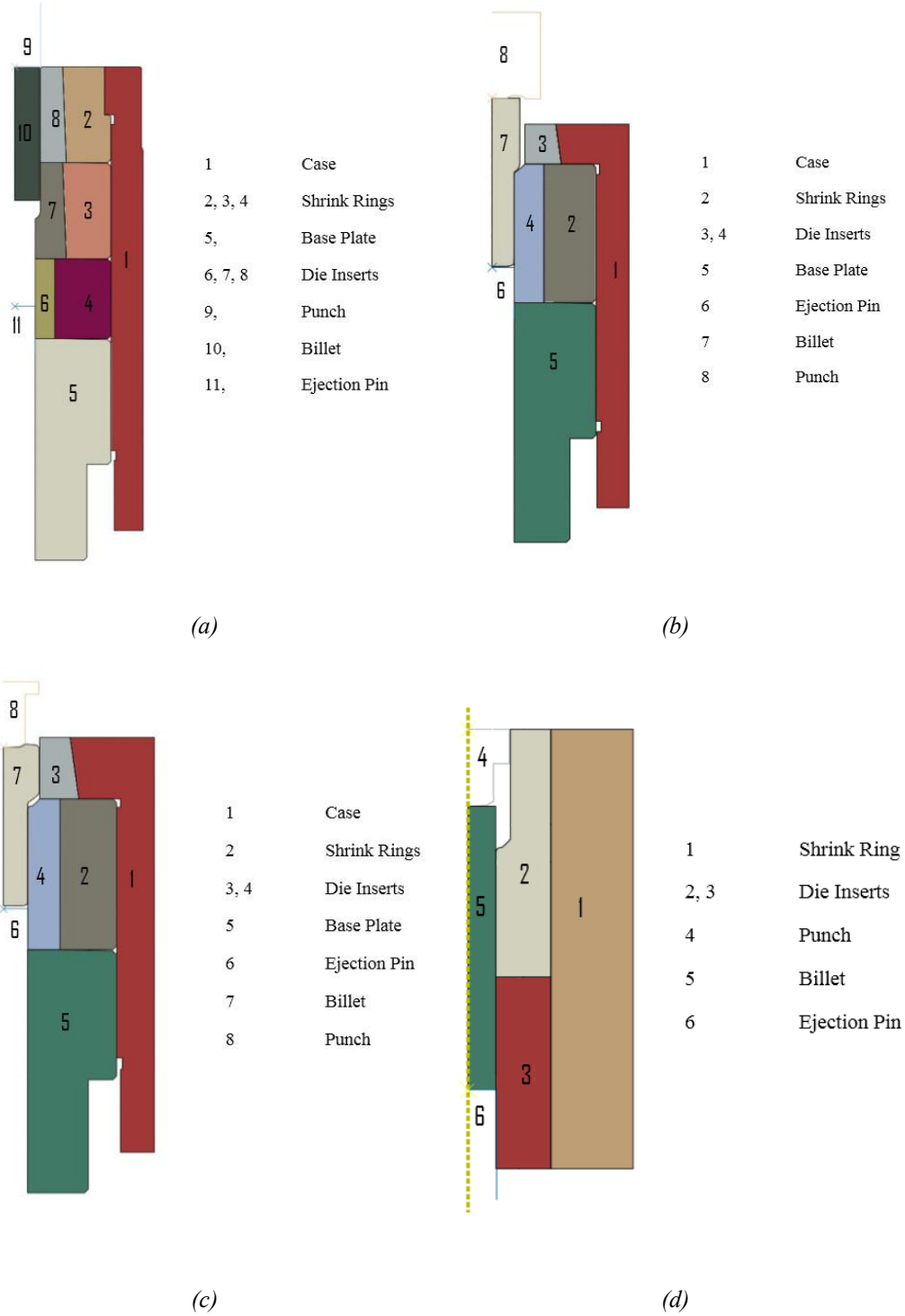

Fig. 3-4: Geometry model in ABAQUS: (a) first step of multistep forging, (b) second step of multistep forging, (c) third step of multistep forging, (d) injection forging.

3.3 FE Simulations

DEFORM and ABAQUS were used to perform FE simulations. The forging force for each process was compared in both software systems. The dimension errors and tool stresses were discussed according to the results obtained from ABAQUS.

3.3.1 Material Properties

AISI 1010 was selected as the workpiece material in FE simulations. The material of the die inserts was WC (tungsten carbide), other tools were made of AISI H13 (tool steel). The stress-strain relationship of AISI 1010 (low carbon steel) stated from [143] is shown below:

$$\sigma = 759\varepsilon^{0.24}$$

where $\boldsymbol{\sigma}$ is stress (MPa) and the $\boldsymbol{\varepsilon}$ is the plastic strain. Table 3-1 and Table 3-2 presents the mechanical properties of these materials and their chemical composition.

Table 3-1: Material mechanical properties.

Material	Density *(Kg/m^3)*	Young's modulus *(MPa)*	Yield stress *(MPa)*	Poisson's ratio
WC [170]	1.525×10^4	640000	6000	0.22
AISI H13 [99]	7.69×10^3	212000	1300	0.3
AISI 1010 [99]	7.87×10^3	205000	305	0.29

Table 3-2: Chemical composition for materials used [171].

AISI 1010	Element	Fe	C	Si	P	S	Mn
	Content (%)	99.2	0.114	0.068	0.008	0.0045	0.378
AISI H13	Element	Fe	C	Si	Cr	Mo	V
	Content (%)	90.95	0.32 – 0.40	1.0	5.13 - 5.25	1.33 – 1.4	1.0
WC	Element	W	C	-	-	-	-
	Content (%)	80	20	-	-	-	-

3.3.2 FE Models

Table 3-3 shows some parameters of boundary conditions in ABAQUS and DEFORM. For both models, the simulation progress was controlled by a constant velocity. It was decided by the average velocity of practical production (around 120 pieces per minute). The coefficient of friction depends on the ring test which is shown in Appendix B.

Table 3-3: Boundary conditions for ABAQUS and DEFORM.

Software	Velocity (mm/s)	Coefficient of friction	Friction model
ABAQUS/DEOFRM	45	0.055	Coulomb law of friction model

3.3.2.1 FE Models in ABAQUS

Because the tools and workpiece were symmetric in this study, the axis-symmetric model was used in ABAQUS/Explicit to save computation time. In simulations, the punch and ejection pin were set as analytical rigid bodies, while other parts were treated as elastic-plastic bodies. The FE models used in ABAQUS are shown in Fig. 3-4. Before executing simulations, some issues such as mesh penetration, mesh distortion, computational efficiency and data processing deserve attention.

In ABAQUS, the mesh penetration is a common trouble. It occurs as the slave surface invades the master surface which results in inaccurate results. In order to eliminate this, choosing a suitable contact model is important for simulations. The “hard” kinematic contact was applied in the contact model of FE simulations for deformable parts. When the contact condition involved two rigid parts, the “hard” penalty contact was the only choice in ABAQUS. Additionally, large mass mismatch between master/slave parts can cause contact penetration. In this regard, balancing the master/slave mass is a direct and effective approach.

Another issue is mesh distortion because of large deformation gradient during the simulation. To cope with mesh distortion, ABAQUS provides Arbitrary Lagrangian-Eulerian (ALE) adaptive mesh. It maintains a high-quality mesh of the billet in

computation. Depending on the degree of mesh distortion, the frequency of re-mesh is different. In both forging processes, the mesh was recreated after five increments to retain the mesh quality. Each re-mesh was carried out 15 times to obtain a more fine mesh in injection forging whereas it was 10 times in multistep forging.

However, using ALE also brings an obvious drawback, a significant increase of the computation time. Regarding the computational efficiency in ABAQUS, mass scaling was applied to the simulations to reduce the time consumed. The basic idea of this function is to artificially increase the model density to achieve an economical solution. With the help of this function, the model density was magnified until the minimum time increment could meet the set value 1e-7.

The last issue is data processing. In the simulations, the forging process is treated as a quasi-static process. When the ABAQUS/Explicit simulates a quasi-static response, some noise in results is unavoidable according to [168]. It expresses as a fluctuation in the outputs of results, particularly in force prediction. To eliminate the influence of the noise on results, two approaches were used. The first method was using double precision instead of single precision in job execution. Another was employing an anti-aliasing filter during the simulation, which obtained smooth curves for the results.

In Table 3-4, the mesh type and mesh number used for each simulation are listed. Because the ejection pin and punch were analytical rigid bodies, it was unnecessary to mesh them in ABAQUS.

3.3.2.2 FE Models in DEFORM

Fig. 3-5 presents the FE model in DEFORM. In DEFORM, most parts were set as a rigid body, except the workpiece was a rigid-plastic body. It brings two influences in simulations. Firstly, since the characteristic is of the rigid body, die inserts were created as a single die insert instead of multiple die inserts. It prevents the unnecessary contact between two rigid bodies and simplifies the model. Secondly, the elastic period of the workpiece was ignored in DEFORM because of using a rigid-plastic body. Compared with the plastic period, the elastic period only occupied a small portion of the deformation process. Therefore, the elastic period influenced

the whole forging force slightly.

An axis-symmetric model was created for all forging processes. For each process, 5000 elements were generated on the workpiece. Thanks to the automatic re-meshing system in DEFORM, the mesh in the component was recreated when it became unstable or met the remeshing criteria. However, it introduced a side-effect which was volume lost. Therefore, volume control was used to maintain a constant volume of the workpiece. During the simulations, only the punch is moveable and other tool parts are fixed in multistep forging. In injection forging, the punch moves with die insert together with the same velocity, and the ejection pin keeps stable.

In this study, DEFORM carried the simulation of grain flow during the forging process. With observation of flow line distribution, some mechanical properties, such as tensile strength and shear strength, can be evaluated. Specifically, it shows high tensile strength and low shear strength in the parallel direction of the grain flow line. Instead, in the vertical direction, it presents low tensile strength and high shear strength.

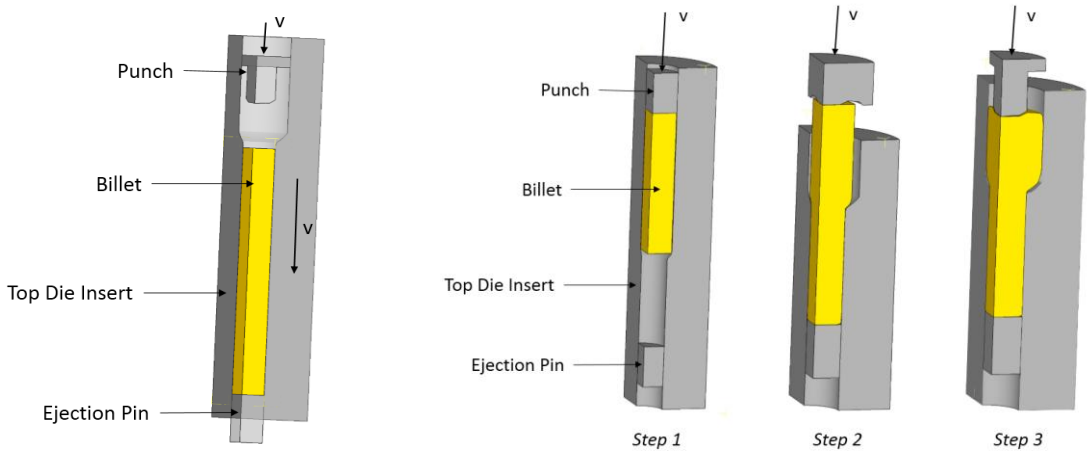

Fig. 3-5: FE model in DEFORM: (a) injection forging, (b) multistep forging.

Table 3-4: Mesh types and number of elements for each part in ABAQUS.

Multistep Forging (Step 1)										
Description	Billet	Base Plate	Case	First Die Insert	First Shrink Ring	Second Die Insert	Second Shrink Ring	Third Die Insert	Third Shrink Ring	Die Case
Mesh Type	CAX4R	CAX4R	CAX4R	CAX4R	CAX4R	CAX4R	CAX4R	CAX4R	CAX4R	CAX4R
Number of Elements	32186	356	700	279	179	647	220	410	221	700

Multistep Forging (Step 2)						
Description	Billet	Base Plate	First Die Insert	Second Die Insert	Die Case	Shrink Ring
Mesh Type	CAX4R	CAX4R	CAX4R	CAX4R	CAX4R	CAX4R
Number of elements	32186	356	165	472	311	585

Multistep Forging (Step 3)						
Description	Billet	Base Plate	First Die Insert	Second Die Insert	Die Case	Shrink Ring
Mesh Type	CAX4R	CAX4R	CAX4R	CAX4R	CAX4R	CAX4R
Number of elements	32186	442	224	707	350	198

Injection Forging				
Description	Billet	Die Insert 1	Die Insert 2	Shrink Ring
Mesh Type	CAX4R	CAX4R	CAX4R	CAX4R
Number of elements	12660	1704	1160	1900

3.3.3 Analysis Procedures

Because there were three forging stages in multistep forging, transferring results of a workpiece such as stress/strain distribution and component dimension from step to step were important for simulation accuracy. ABAQUS provided a function called "predefined field" which introduced the data from the previous model to the next model as an initial condition. Meanwhile, it was used to define pre-stressing in tools in ABAQUS/Explicit based on results from ABAQUS/Standard. The process of transferring in ABAQUS is shown in Fig. 3-6. In DEFORM, the data transfer was finished by the software automatically.

To compare the forging forces, the results of the forging forces were extracted from ABAQUS and DEFORM to OriginPro to do the post analysis. Based on the maximum forming force, the punch deflection in axial direction was estimated. In this study, the tool stresses focused on die inserts which were core parts of forging tools. Some important parameters, such as axis stress S22, hoop stress S33, mean stress, etc. were compared to evaluate the stress condition. To make the tool stress computation more accurate, a "submodel" was used in simulations. The "submodelling" involves use of a global model and a submodel or multi-submodels. In this study, the global model included the whole model of the forming process based on which the forming simulation was conducted. However, the submodel only contained the forging tools with a finer mesh in this study. In the submodel, the boundary conditon was same with that in the global model. Through extracting the loads and conditions at the boundary on the tools (submodel) from the global model, a more accurate calculation of the tool stresses and strains could be carried out.

In comparison of component accuracy, the forging process was divided into two phases, as shown below:

- At the end of loading, in this stage, the component was constrained by tools. Therefore, the tool deflection could be reflected by the component dimension errors.
- After loading and removing the contact between tools and workpiece, it is intended to analyse the springback of components.

In ABAQUS/Explicit, it was difficult to simulate the springback because of the dynamic effect. In other words, the existence of inertia energy makes the component unstable during the springback simulation. It brings distortive simulation results. Even though using viscous pressure can damp out the dynamic effect in the explicit module, selecting a suitable pressure is tricky. Therefore, the springback analysis was finished in the standard module via results transferring. In standard module, the initial out of balance dynamic effect was removed by software. The result of component accuracy was analysed on the 2D profile. The dimension errors, $\boldsymbol{e_d}$ (refers to Fig. 3-7) represented the forging accuracy for the forging processes. The dimension errors concentrated on the radial dimensions of components, which were bolt head diameter ***D*** and rod diameter ***d***.

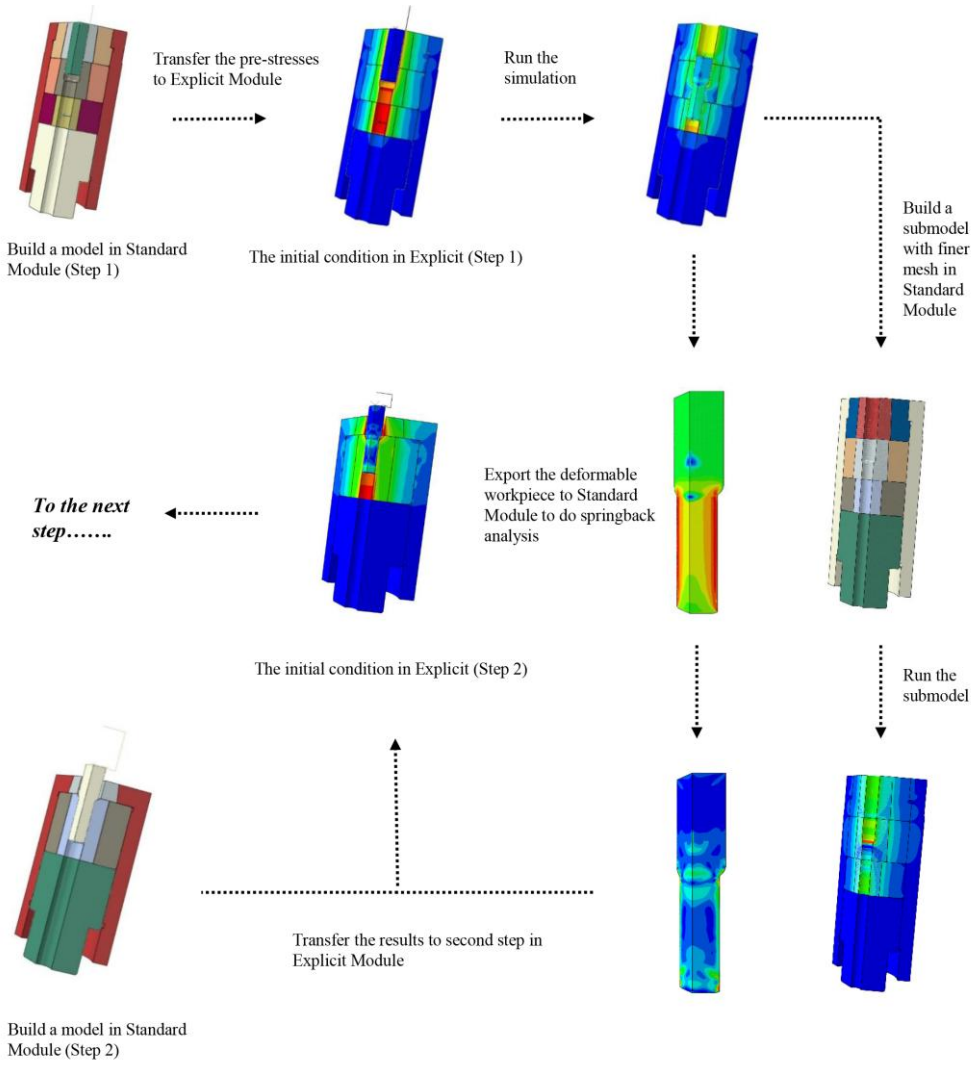

Fig. 3-6: Schematic illustration of the simulation process in ABAQUS.

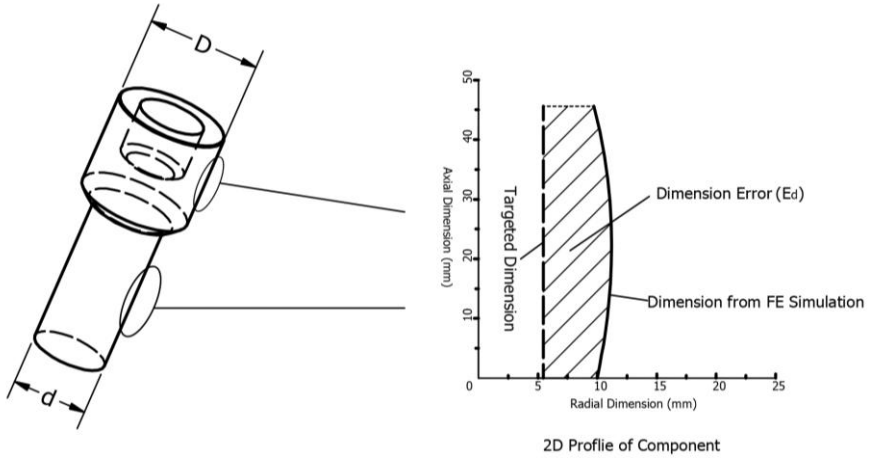

Fig. 3-7: Two critical parameters, D and d, for forging accurate and the dimension errors e_d.

3.4 Results and Discussion

3.4.1 Comparison on the Forging Force

Some FE simulations results are shown in Table 3-5. Fig. 3-8, Fig. 3-9, Fig. 3-10 and Fig. 3-11 indicate the force prediction for multistep forging step 1, step 2, step 3 and injection forging, respectively. From the comparison of the force-stroke curves, both simulations software shows a good agreement, except the following two differences:

- The initial stage of force growth in step 2 and step 3. In ABAQUS, due to the springback of components, the diameter of component is larger than the size of die chamber. The force, therefore, is introduced when the workpiece begins to enter into the die chamber. However, the workpiece in DEFORM is unable to perform the process of springback due to limitations of the FE codes. In this situation, the rod part of the workpiece will not touch with the die surface until it contacts with the ejection pin to deform. Thus, the force remains zero in the initial stage of step 2 and step 3.

- More stroke is required to fill up the die chamber in ABAQUS as results of tool deflection. It takes place in simulating of injection forging and multistep forging. The amount of extra stroke may reflect the magnitude of tool stress and tool deflection indirectly. It may suggest that the tool experiences high stresses and deflection in the process with highly extra stroke. However, in step 3, the stroke in ABAQUS is less than that in DEFORM. It casued by several reasons. Firstly,

the tool stresses in this step are small which is shown in the following subsection about tool stress. It makes the tool deflection in step 3 small. Secondly, as mentioned before, due to springback, the initial diameter of components in section ***d*** is larger than that of the die insert. In other words, the metal forming starts at the beginning of the stroke, whereas it does not happen in DEFORM. The combination of two factors makes the process finish earlier in ABAQUS than DEFORM.

In view of the maximum forging force, there is no doubt that the injection forging, as one step forging, requires the highest force. It may bring the high-stress amplitude and tool deflection in the tools, resulting in a potential issue of forming accuracy. Besides the highest load, the force changes more frequently in the injection forging than that in the multistep forging. It adversely influences the lifespan of the tools, and it could be an issue for injection forging in high volume production. In the view of tool deflection in axial direction, the punch is shorten around 1 mm, while the maximum value in multistep forging is 0.8 mm in step 3. The injection forging shows advantages over traditional forging process when comparing forging energy. When considering some extra energy, e.g. transferring the workpiece between forging stages, this advantage becomes more obvious. Thus it appears that the injection forging can help industry to save the energy cost during forging.

Table 3-5: The comparison of forging force, forging energy and extra stroke for multistep forging and injection forging.

Process	Multistep Forging (stage 1)	Multistep Forging (stage 2)	Multistep Forging (stage 3)	Injection Forging
ABAQUS Max. Force (kN)	205.322	231.754	185.837	240.346
DEFORM Max. Force (kN)	207.916	229.920	182.928	270.864
Forging Energy (kJ)	1290	517	748	2280
	Total Energy = 2555			
Extra Stroke (mm)	0.440	0.255	-	0.515
Punch Deflection in Axial Direction (mm)	0.439	0.015	0.847	1.110

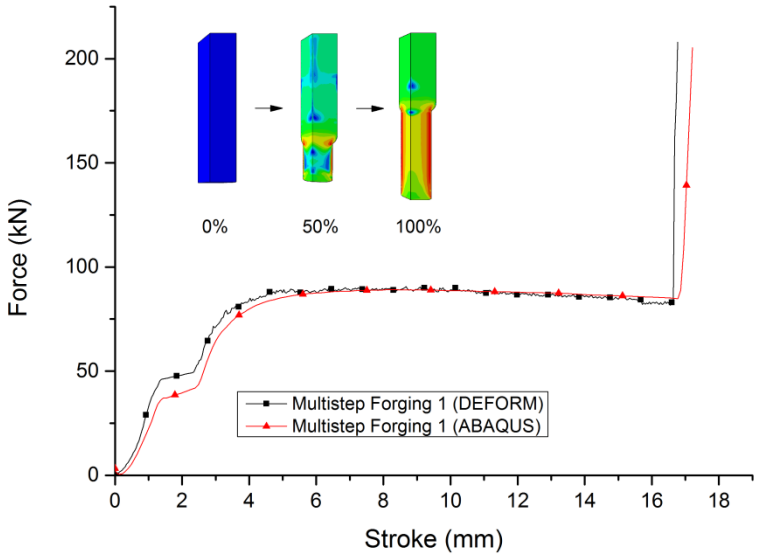

Fig. 3-8: The force-stroke curve obtained from DEFORM and ABAQUS simulations for multistep forging step 1.

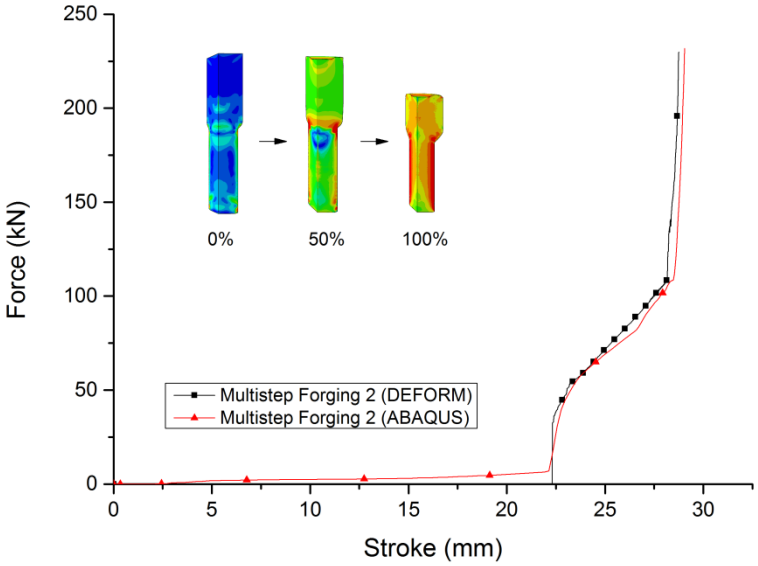

Fig. 3-9: The force-stroke curve obtained from DEFORM and ABAQUS simulations for multistep forging step 2.

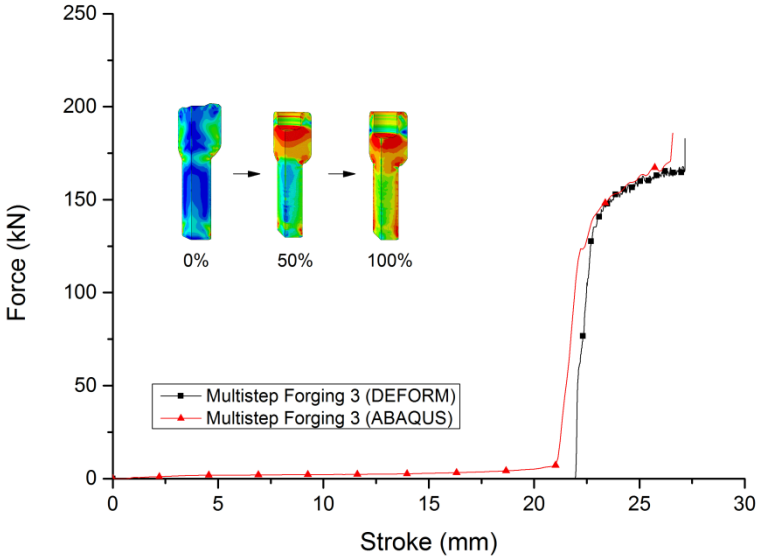

Fig. 3-10: The force-stroke curve obtained from DEFORM and ABAQUS simulations for multistep forging step 3.

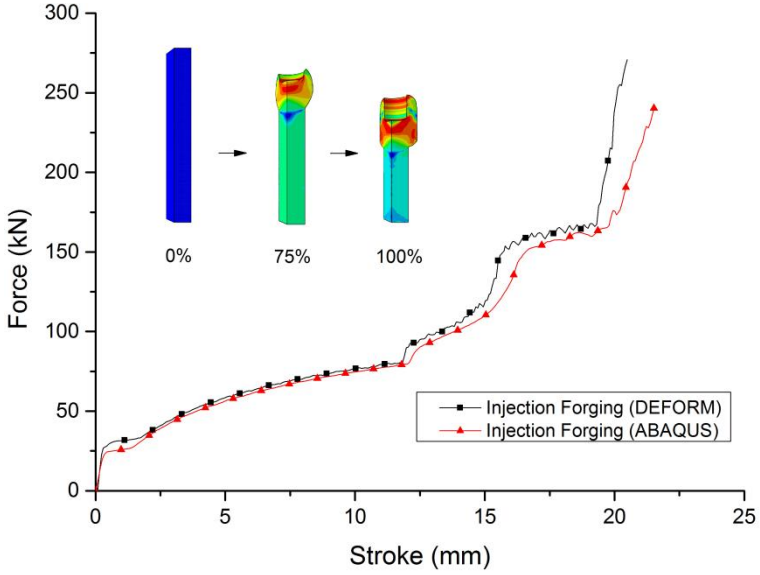

Fig. 3-11: The force-stroke curve obtained from DEFORM and ABAQUS simulations for injection forging.

3.4.2 Comparison of the Tool Stresses

Fig. 3-12 to Fig. 3-15 show the different kinds of the maximum stress for forging processes. In the multistep forging, step 2 has the maximum forging force (refers to Table 3-5). However, the maximum effective stress in step 2 is small which is close to the level of pre-stressing. It is because the main forming method is upsetting in step 2. In this way, the main deformation is almost completed before the workpiece touches the die insert. Therefore, the die insert sustains a small forming pressure. The same situation happens in step 3. In contrast, in step 1, the workpiece contacts with the die insert at the beginning of forging. It introduces extremely high stresses to the die insert, especially in the second die insert. It may indicate that step 1 is the most critical step in multistep forging. It is not only in the effective stress but also in the mean stress, hoop stress and axial stress. These stresses express as high level of tensile stresses instead of compressive stress. With increasing of forging cycling, it is believed that the fatigue crack may grow in step 1 before the other two steps.

Compared with the multistep forging, the die insert experiences the highest effective stress in injection forging, and the position of stress concentration is different. The stress only focuses on the bottom part of the die insert instead of other positions. This is because the different material flow approaches. In injection forging, the material in the bottom part of workpiece does not attend the severe forming in the axial direction. Only a small amount of radial material flow takes place in this area. After the workpiece contacts the die insert surface, the “dead” material has no space to flow. With the continuous forming process, the increasing force applies on the die insert which creates the stress concentration area. Besides the effective stress, the positive hoop stress and axial stress also reflect potential issues about tool stresses in injection forging. Because the pre-stressing has a significant influence on the stress, it suggests that injection forging requires more stiffness in die design.

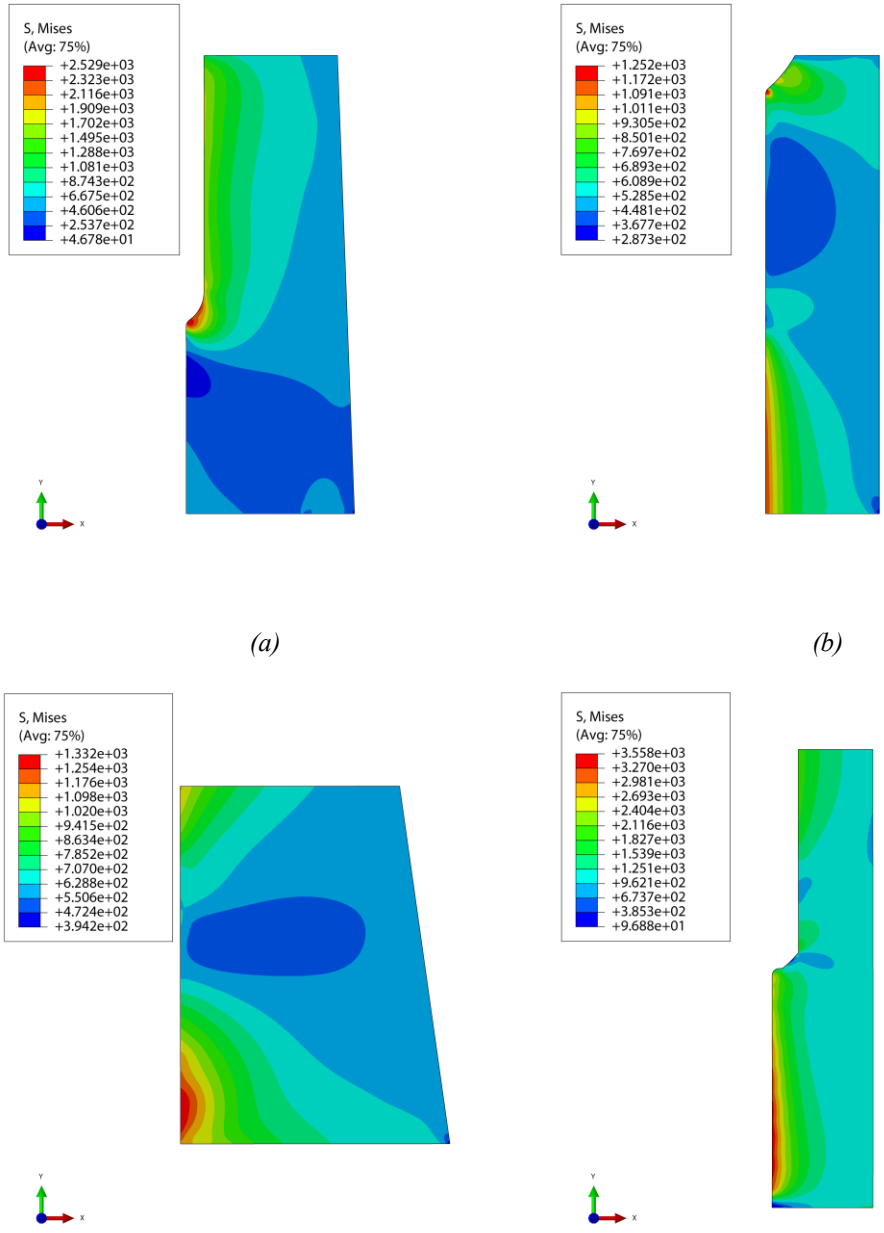

Fig. 3-12: Effective stress (MPa) distribution in die inserts: (a) step 1, (b) step 2, (c) step 3, (d) injection forging.

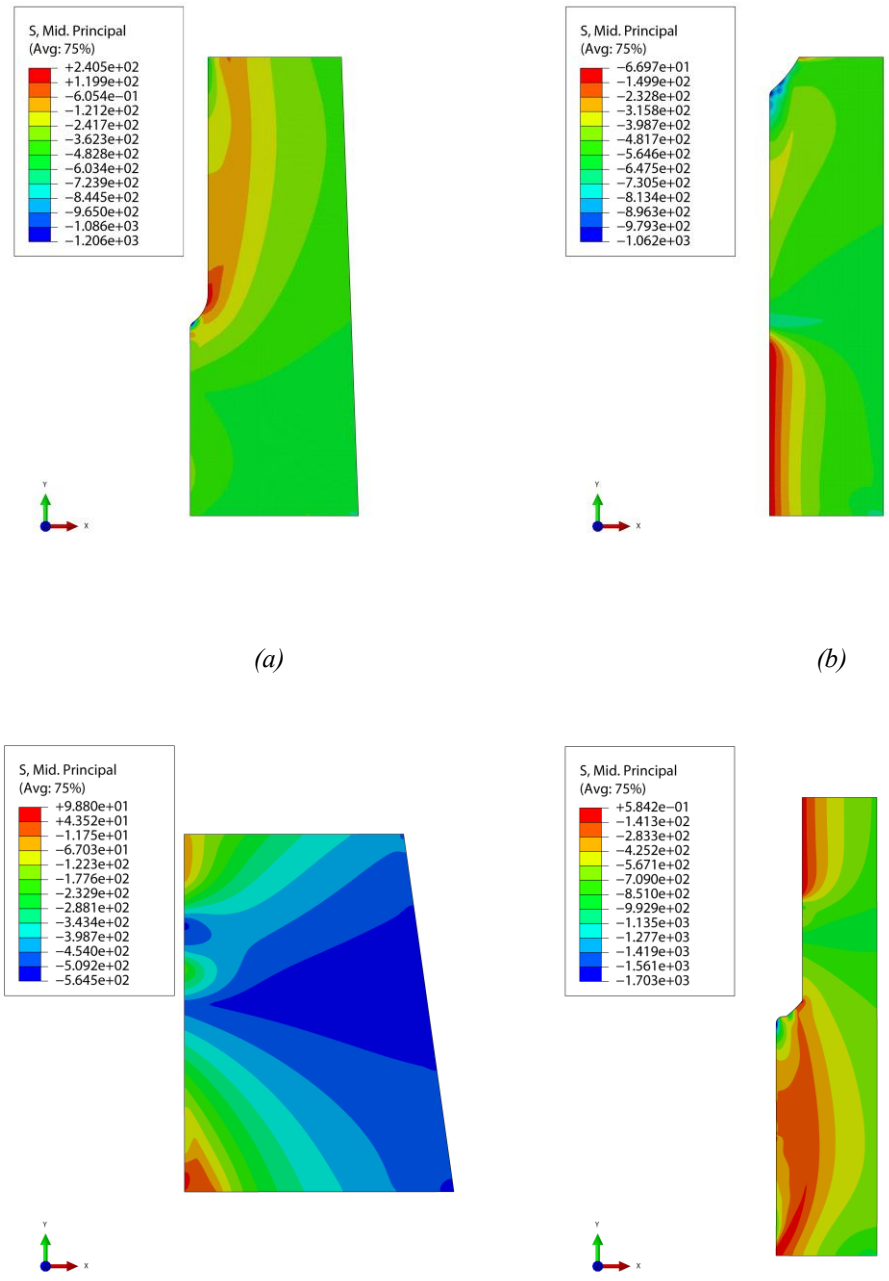

(a) *(b)*

(c) *(d)*

Fig. 3-13: Mean stress (unit) distribution in die inset: (a) step 1, (b) step 2, (c) step 3, (d) injection forging.

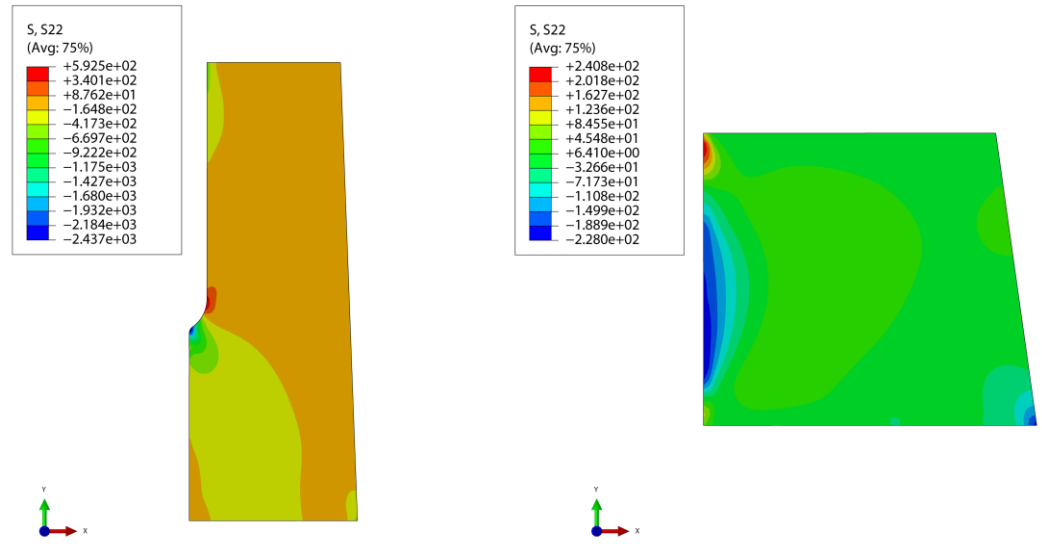

(a) *(b)*

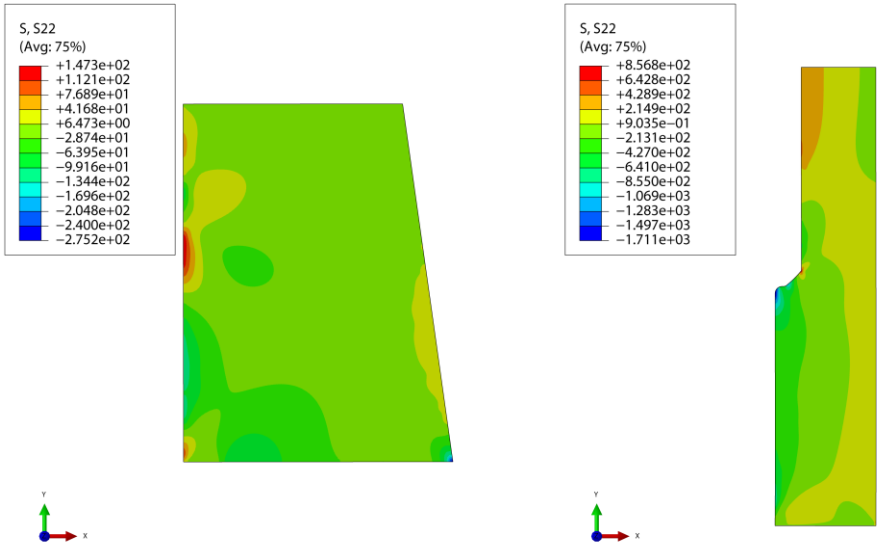

(c) *(d)*

Fig. 3-14: Maximum axial stress (MPa) distribution in die inserts: (a) step 1, (b) step 2, (c) step 3, (d) injection forging.

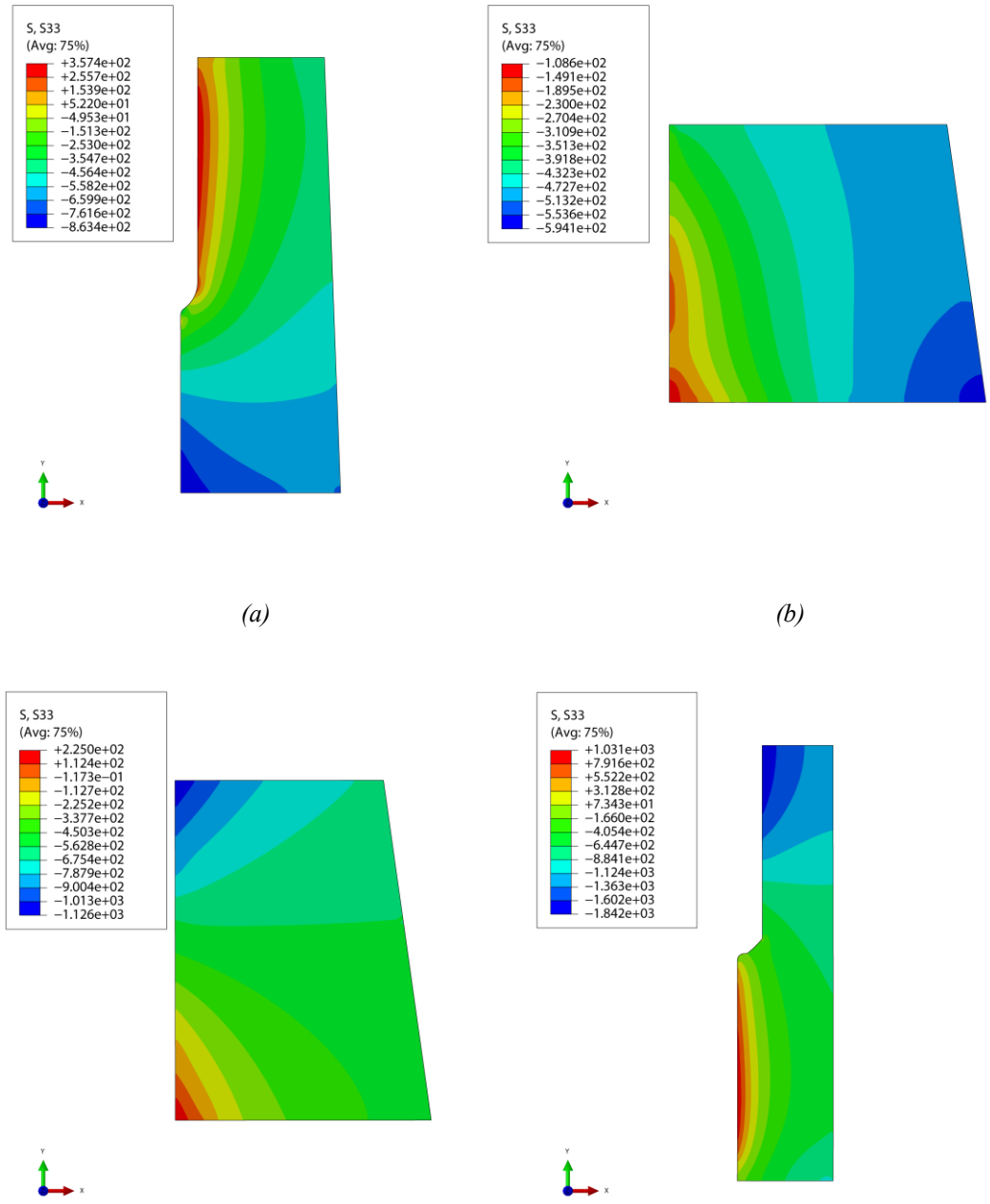

Fig. 3-15: Maximum hoop stress (MPa) distribution in die inserts: (a) step 1, (b) step 2, (c) step 3, (d) injection forging.

3.4.3 Comparison of the Component Dimensional Accuracy

The component dimensions in section ***D,*** and ***d*** for multistep forging are presented from Fig. 3-16 to Fig. 3-21. The same parameters are analysed in injection forging, are shown in Fig. 3-22 and Fig. 3-23. Some critical positions for folding are highlighted in these figures. The comparison of injection forging and multistep forging in component accuracy are shown in Fig. 3-24 and Fig. 3-25.

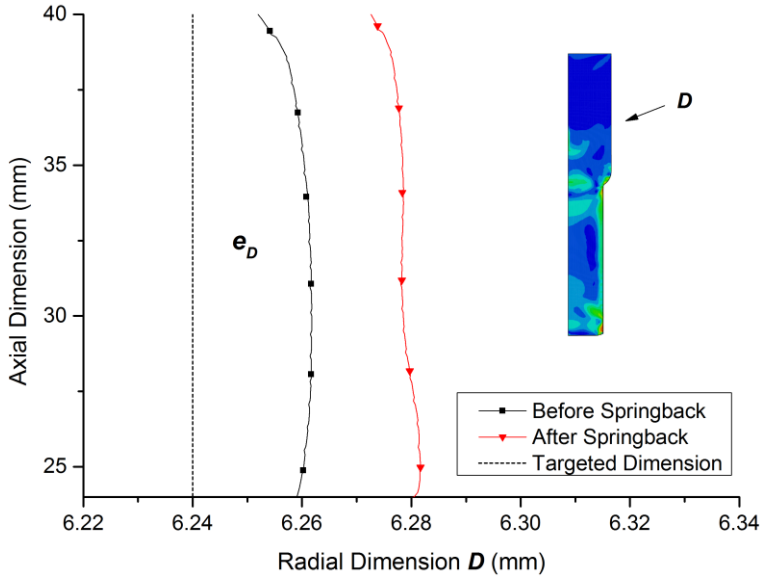

Fig. 3-16: 2D profile before and after springback in section D for forging step 1.

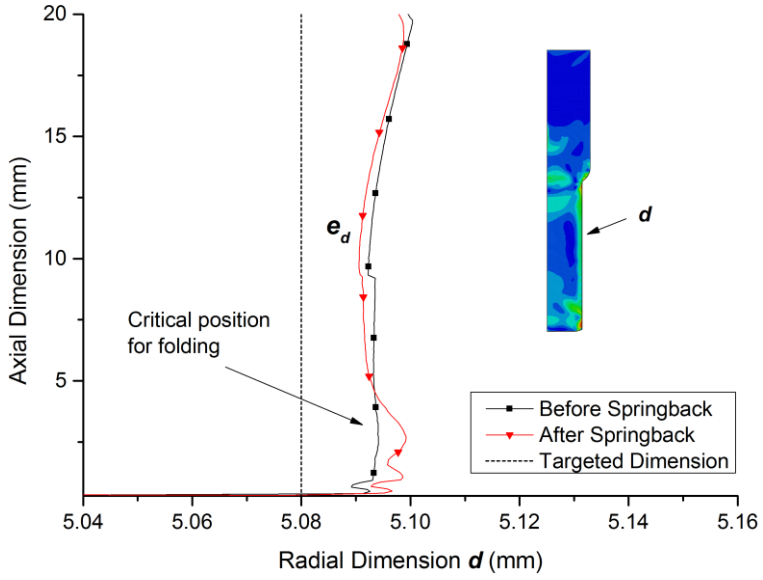

Fig. 3-17: 2D profile before and after springback in section d for forging step 1.

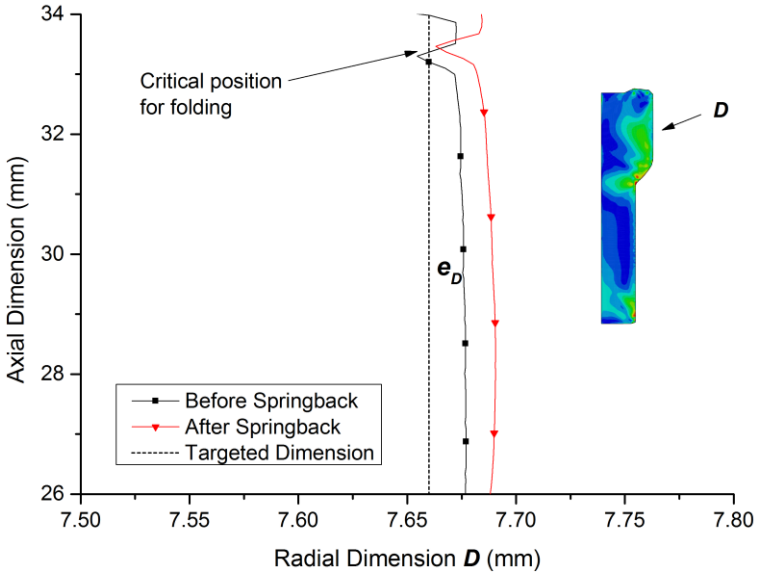

Fig. 3-18: 2D profile before and after springback in section D for forging step 2.

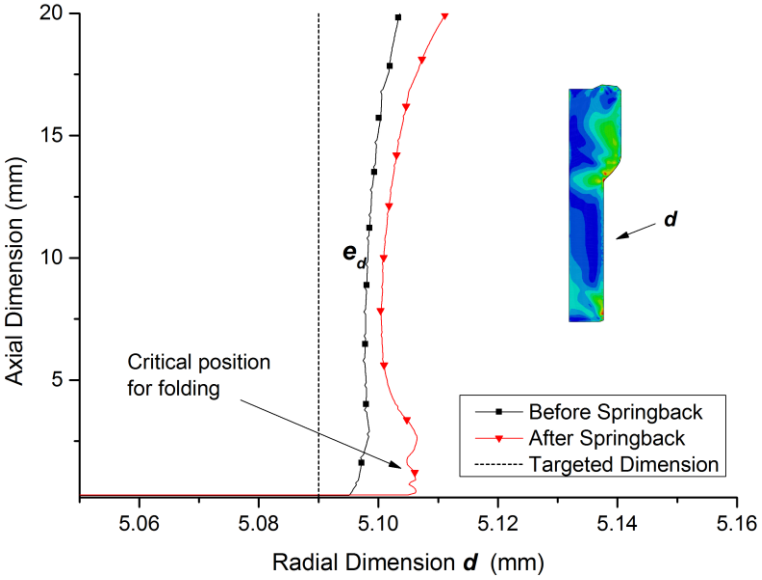

Fig. 3- 19: 2D profile before and after springback in section d for forging step 2.

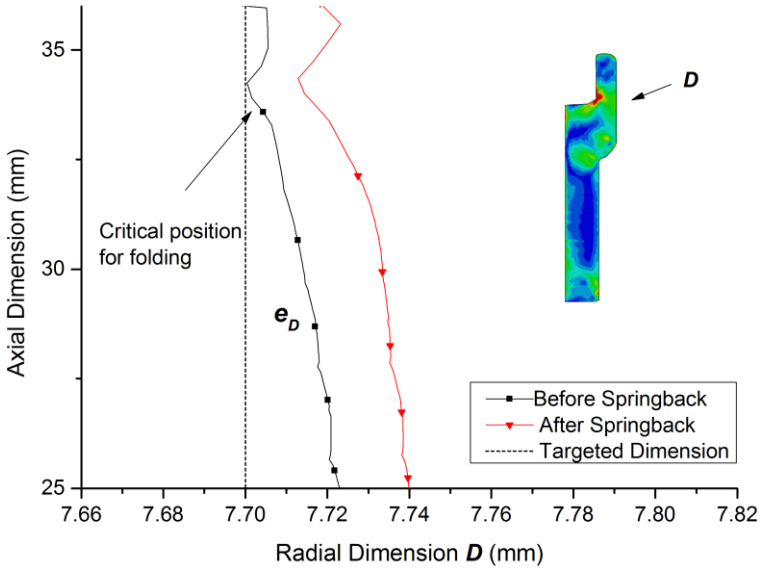

Fig. 3-20: 2D profile before and after springback in section D for forging step 3.

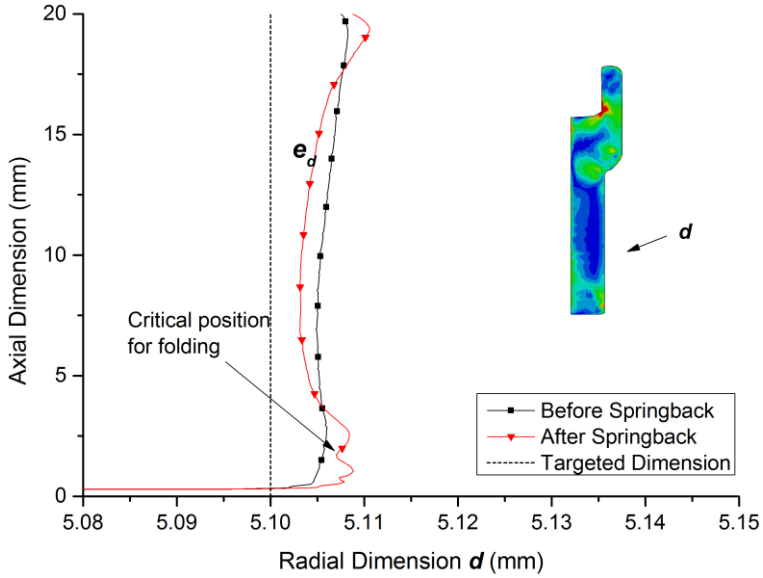

Fig. 3-21: 2D profile before and after springback in section d for forging step 3.

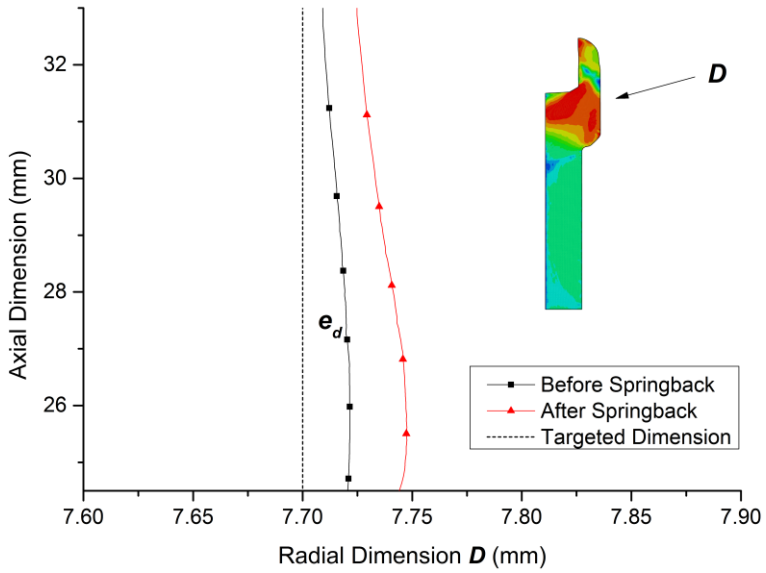

Fig. 3-22: 2D profile before and after springback in section D for injection forging.

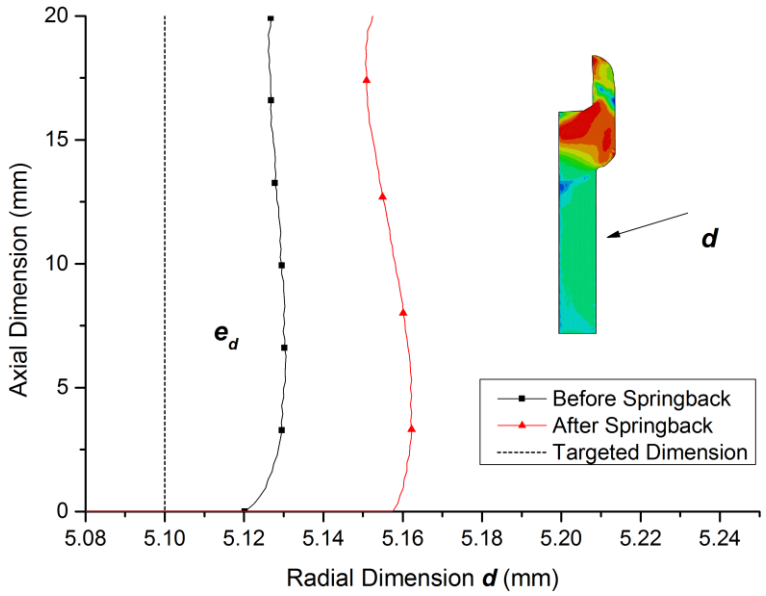

Fig. 3-23: 2D profile before and after springback in section d for injection forging.

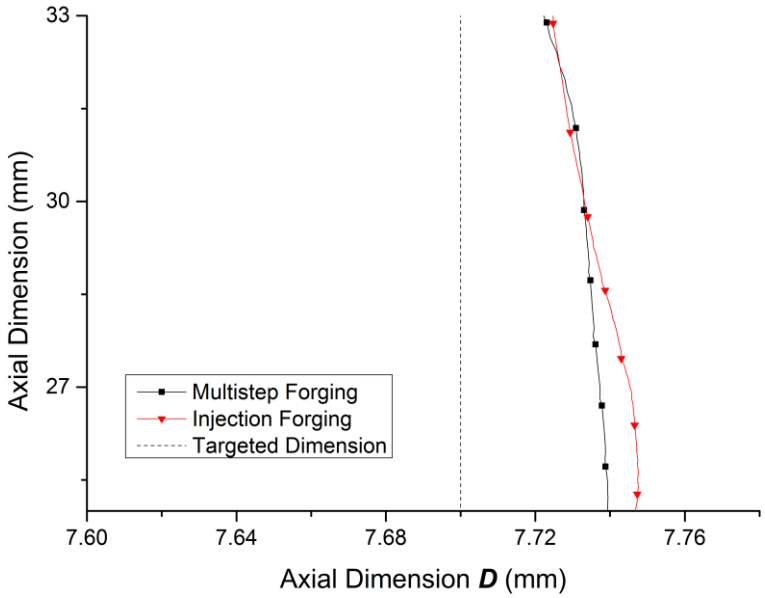

Fig. 3-24: 2D profile after springback in section D for injection forging and multistep forging.

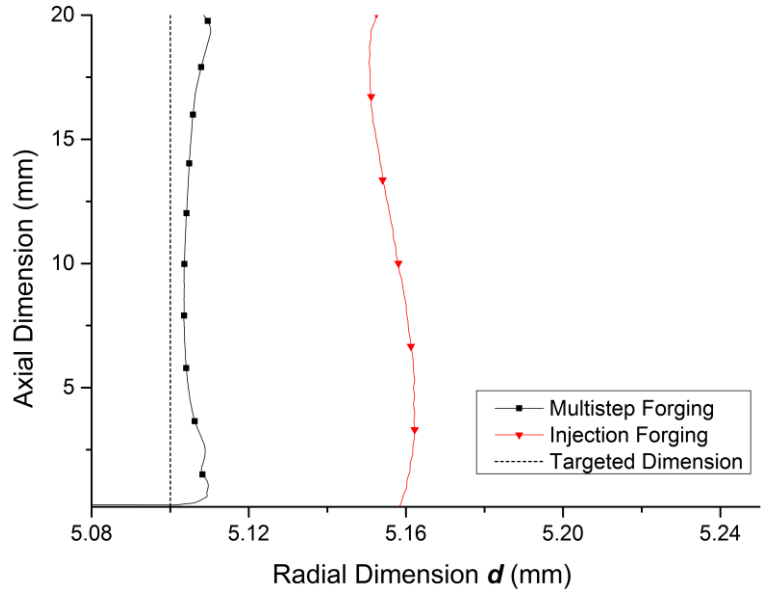

Fig. 3-25: 2D profile after springback in section d for injection forging and multistep forging.

As can be seen from these figures, the final dimensions in section ***d*** and ***D*** exceed the targeted value for multistep forging and injection forging. After removing contact between tools and workpiece, the springback contributes to increase of dimension errors for most components, except the rod diameter in step 1. This is caused by the die insert design in the forging process. Referring to Fig. 3-26, in order to reduce the friction force, a die land ***L*** is employed at the exit of extrusion. After the material passed the ***L***, the springback has already begun to take place in section ***d***. Therefore, when the component is not constrained by tools, the mean diameter error $\bar{\boldsymbol{d}}$ is unable to increase further but is reduced slightly.

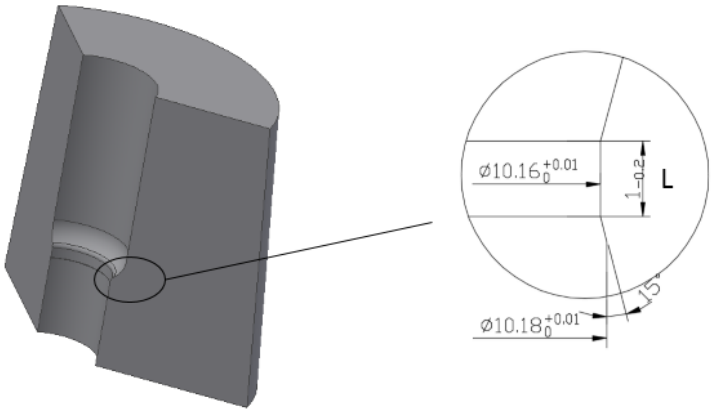

Fig. 3-26: Die insert design in forging step 1.

On the other hand, due to the different degrees of springback, it intensifies underlying folding risk for the subsequent forging process which is shown in the figures as critical positions. A typical example is presented in step 1 which the bottom dimension in section ***d*** has a big change after springback. Due to the maximum dimension of the component being larger than the chamber diameter in step 2, the protruding part is easy to cover other places during the extrusion in the following step. In addition to springback, some critical positions grow in-process, e.g. the critical part in section ***D*** of step 2. It suggests that some optimisation works should be conducted in step 2 to prevent this defect. It is noticeable that these problems are not obvious for injection forging in section ***D*** and ***d***. It is because of different approaches of material flow.

Based on the magnitude of errors shown in the figures, the mean errors $\bar{\boldsymbol{e}}_{\boldsymbol{D}}$ and $\bar{\boldsymbol{e}}_{\boldsymbol{d}}$

are used in the Table 3-6 to evaluate component accuracy. Step 1 introduces the maximum errors in multistep forging to the component. Subsequently, the dimension errors reduce gradually from step 1 to step 3, especially in section ***d***. It may suggest that using multistep forging can improve the forging accuracy from step to step. In comparison with injection forging, the multistep forging shows an advantage over the injection forging. Due to the deformation being finished in one step for injection forging, it cannot be avoided that tool stresses stay at a high level. The high tool stresses turn into increasing dimension errors. Hence, depending on the requirement of dimension accuracy, it should be carefully considered in injection forgings.

Table 3-6: Comparison of the component accuracy for multistep forging and injection forging.

	Process	Multistep forging (step 1)	Multistep forging (step 2)	Multistep forging (step 3)	Injection Forging
Mean Error $\bar{e}_D$ (mm)	Before Springback	0.020	0.014	0.014	0.017
	After Springback	0.039	0.027	0.032	0.038
Mean Error $\bar{e}_d$ (mm)	Before Springback	0.014	0.009	0.006	0.028
	After Springback	0.013	0.013	0.006	0.057

3.4.4 Comparison of the Grain Flow Lines

Fig. 3-27 shows the prediction of grain flow line in two kinds of process. In practice, the bolt mainly resists the force in two directions. One is in the axial direction which is tensile stress, and another is shear stress in the horizontal direction. According to the results, the component from injection forging and multistep forging show the same flow lines in the rod part. Therefore, the mechanical behaviour in the rod part for the two processes is comparable. Considering the head part of the bolt, the component from multistep forging shows better tensile strength but lower shear strength. Additional, due to the metal flow approach in injection forging, the flow line in position A of the component is horizontal (refer to Fig. 3-27 (b)). Therefore, it may suggest that A is a critical position to break if the tensile stress exists.

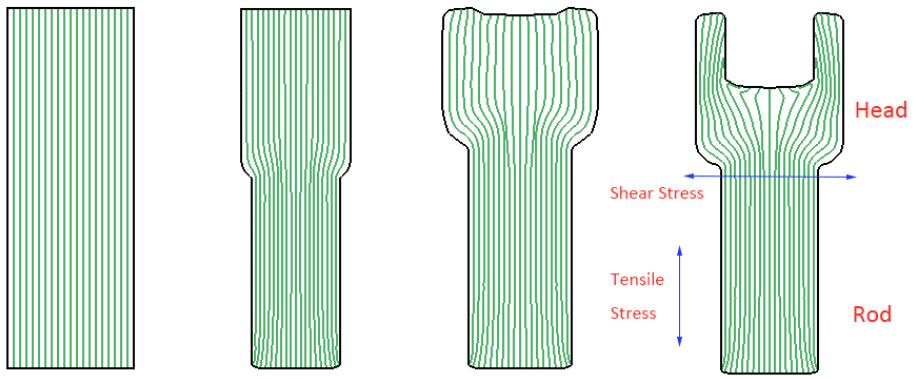

(a)

(b)

Fig. 3-27: Grain flow line prediction: (a) multistep forging, (b) injection forging.

3.5 Summary

In order to compare injection forging with multistep forging in automotive fasteners production, axis-symmetrical models were applied in ABAQUS and DEFORM. The forging behaviours, including forging force, component accuracy, tool stresses and grain flow line were analysed. Some results from the simulations can be concluded as:

1) Because the large deformation ratio in injection forging, it shows the highest forging force in forging processes. It may bring some issues for the tool life and forming accuracy. However, it is noticeable that the energy requirement of injection forging is less than the traditional process. Especially when other energy consumption such as transferring work and tool-making is taken into consideration, this advantage becomes more evident.

2) In the comparison of forming errors, the multistep forging shows better behaviour than injection forging. With increasing of forging steps, the dimension errors reduce gradually. As for injection forging, the large force brings high deflection and severe stresses. It causes the higher dimensional errors in injection forging than that in multistep forging. Therefore, when the dimensional clearance is very small for components, the multistep forging is a good option. Additionally, more stiffness in the tool design should be applied to overcome high tool stresses in the axial direction and hoop direction for injection forging.

3) Due to the metal flow and springback, the underlying fold is an issue for multistep forging. Most fold risks are introduced after component springback, while some fold risk grows in-process. The position of folding could be a critical part for cracking when fasteners are used in practice. However, the folding risk is not evident for injection forging in section ***D*** and ***d***, according to the simulation results.

4) In view of multistep forging, forging step 1 is the most critical step. It generates positive axial stress, mean stress and hoop stress which increases the risk of tool failure. Therefore, some optimisation works should be carried out for this step.

5) As for the grain flow, the multistep forging brings better flow line distribution. It shows as a mild flow line with less bending which is beneficial to component properties. It may suggest that the multistep forging introduces tougher tensile strength and shear strength to components than injection forging does.

Chapter 4

Experiment, Manufacturing Trials and Model Validation

4.1 Introduction

The forging force, tool stress, forming accuracy and grain flow line of injection forging process have already been analysed with ABAQUS and DEFORM in chapter 3. In this chapter, the forging experiment was conducted on a hydraulic press machine. ISO 100 forging oil, ISO 68 forging oil and $MoS2_2$ grease, were tested in the experiment to find the optimal lubricant for injection forging process. The forging force was monitored by a load cell during the process. Three important parameters such as component accuracy, hardness distribution and grain flow line, were examined to evaluate the fasteners behaviours.

Moreover, a manufacturing testing was carried out in industry to examine the feasibility of injection forging in the industrial environment. Trials were undertaken in a high-speed forging machine, based on which the issues relating to the practical deployment of injection forging were identified. Finally, the results from experiments and FE simulations were compared. Depending on the experimental and manufacturing trials, the accuracy of the FE model was assessed and improvements to the model was considered.

4.2 Tool, Materials and Equipment for Experiments

4.2.1 Tool Design

As shown in Fig. 4-1, the forging experimental setup consists of three main parts which are the force-measurement device (part 1), top die (part 2) and bottom die (part 3).

Fig. 4-2 shows the exploded view of part 1, including ten components. The load cell is the core component in this design, which is secured by two clamp plates with a bearing surface. Double-screw bolts connect the two clamp plates. To prevent the

load cell slipping off the bearing surface, an inner ring (hollow cylinder) is used to constrain its radial motion. On the interface between load cell and plates, two insulating washers block the interference from the plates. Meanwhile, this avoids the electrochemical reaction as a result of the long-term contact between the load cell case and plates. It ensures that the load cell works in a stable environment.

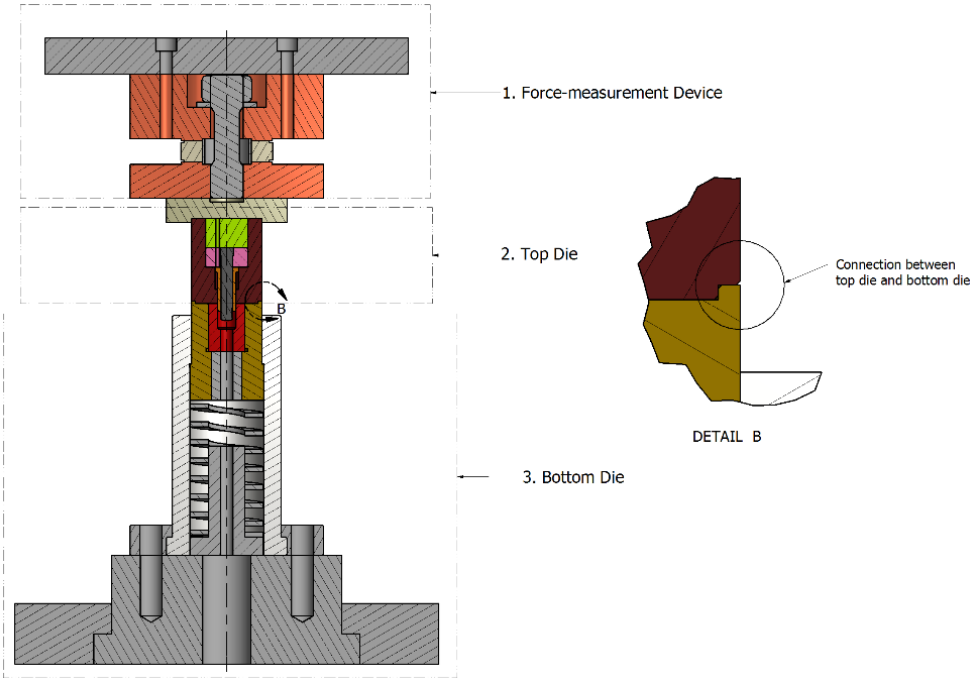

Fig. 4-1: The illustration of experimental setup.

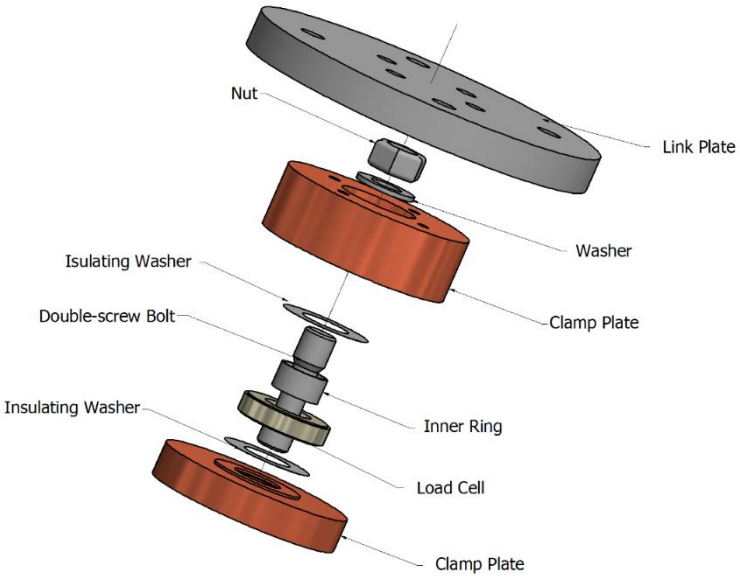

Fig. 4-2: The exploded drawing of force-measurement device.

Refer to Fig. 4-3, an adaptor is used in the top die design. This prevents the forging force concentrating on the double-screw bolt (in part 1) which causes measurement errors. Two cushion blocks secure the punch in the right position. In order to take the final production out from the top die after forging, three small ejection pins are put into the corresponding holes which are located on two blocks. Through pushing these pins, the sleeve can move along the channel in the top die case. In this way, the component can be ejected by the sleeve.

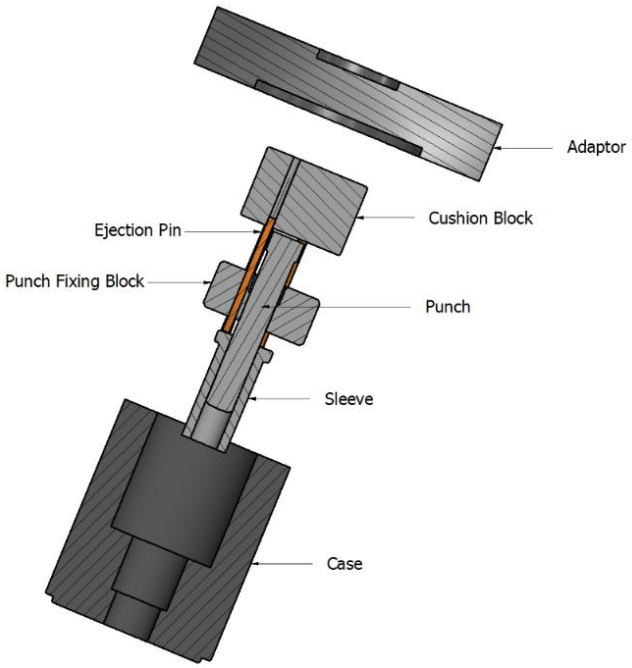

Fig. 4-3: The exploded drawing of top die.

Part 3 plays an important role in the experiment, seen in Fig. 4-4. The position of die splitting and the interference design refers to the approach in Chapter 3. A floating die design is adopted to realise the injection forging in experiments. The die spring acts as an absorber with a good stiffness. With the help of a spring, the bottom die insert and shrink ring are able to move with the top die together to form the workpiece and return to the initial position by the spring force. For the ejection pin, it provides two functions. Besides ejecting the component out of the bottom die after forging, it supports the billet during forging. Finally regarding material cost and replacement, the fixture for the bottom die is divided into several parts, including clamp plate, base plate and fixing cylinder.

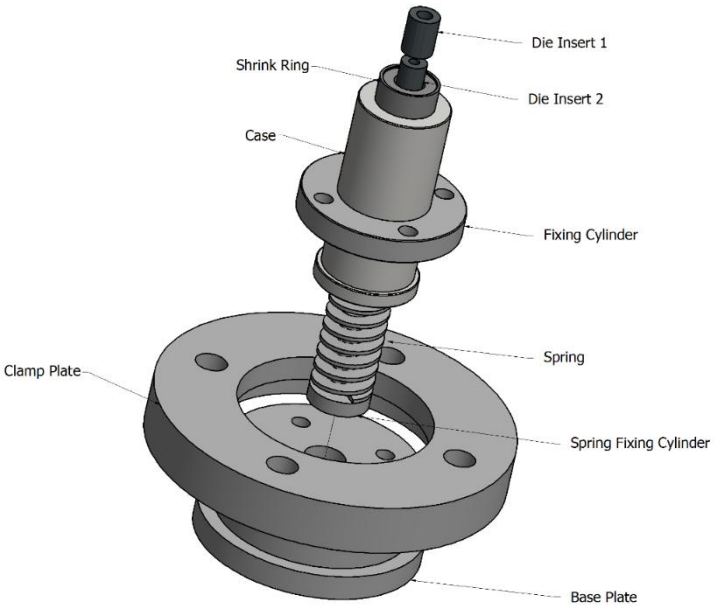

Fig. 4-4: The exploded drawing of the bottom die.

In this setup, the part 1 and part 3 are fixed on the top work platform and bottom work platform by bolts, respectively. Part 2 is mounted on part 3 via a connection between the shrink ring and top die case, seen in Fig. 4-1. The whole experimental setup in the hydraulic press machine is shown in Fig. 4-5. The detail dimensions of some important tools can be found in Appendix C.

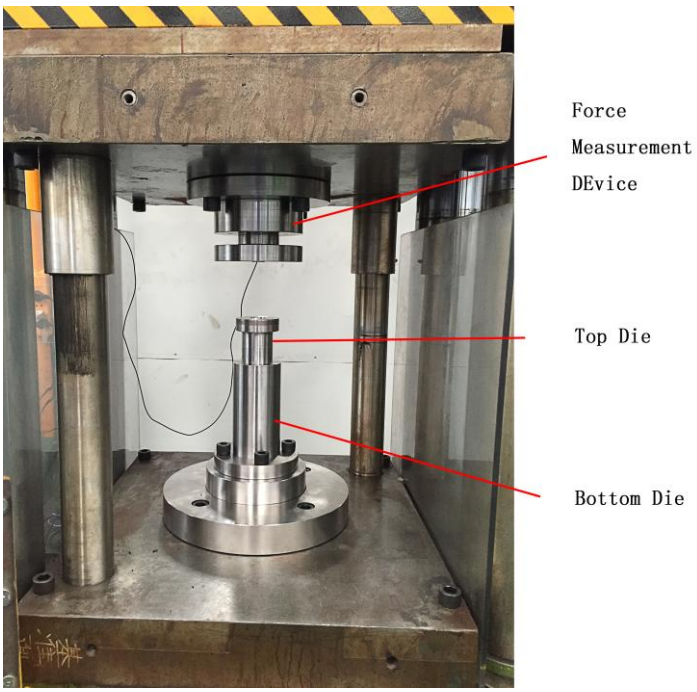

Fig. 4-5: The experimental setup in a hydraulic press machine.

4.2.2 Specimen/Material Preparation

In this experiment, the specimen was cut from a branch of wire rod which was made of AISI 1010. Before machining, it was necessary to carry out some pre-treatments such as wire drawing and phosphating on the raw material. It was intended to modify the rod diameter and improve the behaviour of holding lubricant. Usually, the initial radius of wire rod could not reach the requirement. Hence, a rough drawing was carried out which made the wire radius close to the designed value.

After this, a conversion coating was introduced to the material surface by the phosphating process. In this process, the material was put into a pickling bath to remove the oxide film on the material surface firstly. The second stage was rinsing which washed away the residual particles, sundries or grease on the surface. After acid pickling, the metal surface became rough which weakened the effect of phosphate coating. Surface adjustment therefore, was employed to refine the surface condition. It also brought another benefit which could reduce the process temperature of phosphating. Then the phosphate film was coated on the material surface. This kind of film enhanced the material flow during forging process and improved the friction condition between workpiece and tools. The last step was saponification that strengthened phosphate film further.

When phosphating was finished, the finishing drawing was employed to obtain the accurate radius of the metal wire. Meanwhile, it also enhanced the mechanical properties of material to some extent.

After pre-treatments, the metal wire was cut into pieces by trimming tools in the cold header. Because the end surface of the billet was uneven after trimming, it caused uneven metal flow in subsequently forging process. In order to avoid it happening, the last process, preform, was used to flatten the end surfaces of billet. Fig. 4-6 shows the billet before/after preform process. The final dimensions of billet were 10.10 mm × 51.6 mm.

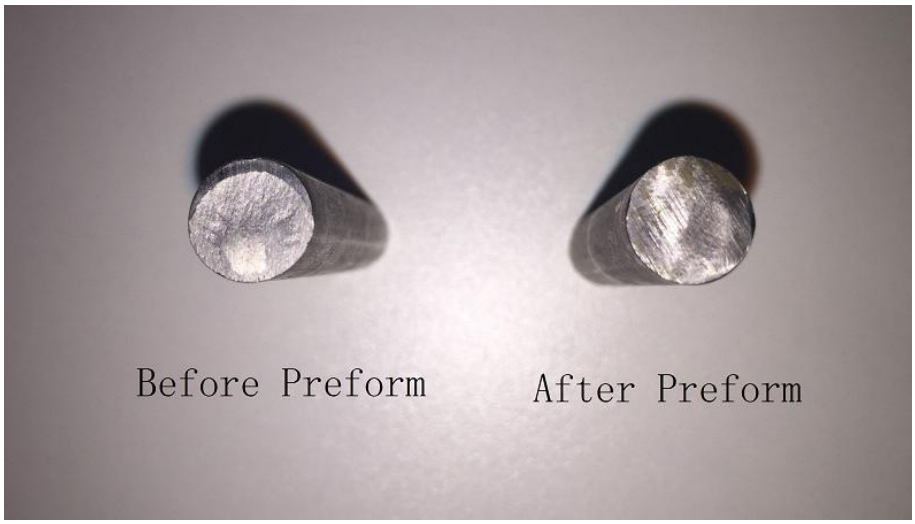

Fig. 4-6: Comparison of workpiece end surface before/after preform process.

4.2.3 Equipment

The detailed information of equipment, containing the forging equipment and measurement equipment, is listed below.

Vertical Hydraulic Press

A 3000 kN vertical hydraulic press carried the whole forging process. Appendix D shows the main technical data of this machine.

Load Cell and Data Acquisition (DAQ) System

A load cell type, Kistler 9107A, with a measuring range of 0 – 700 kN, was employed to monitor the force during the forging. Before using the load cell, a suitable preloading was necessary. In the experiment, approximate 150 kN preloading was used according to the suggestion from Kistler Company. The detail of the preloading process is presented in Appendix E.

An amplifier, Kistler 5073A111, was applied to enhance the output signal. The amplifying sign was fed into a Yanhua PCI-1710U card via connection card PCLD-8710. The PCI card was responsible for collecting the signal and converting the analogue signal to digital. Labview was the terminal of DAQ system to analyse and

record the signal. For the whole measurement system, the sampling frequency was set as 1000 Hz.

Calibration Equipment for Load Cell

Since the load cell 9107A was uncalibrated, it must be calibrated after mounting. Fig. 4-7 indicates the calibration system. In this system, MTS 810 material test machine was the reference machine. The maximum force for this test system was 300 kN. To be safe, the used maximum force was 250 kN which covered the measuring range in forging process. By comparing the reading from MTS 810 and the load cell, the calibration was completed in Labview. The result of calibration is shown in Appendix E.

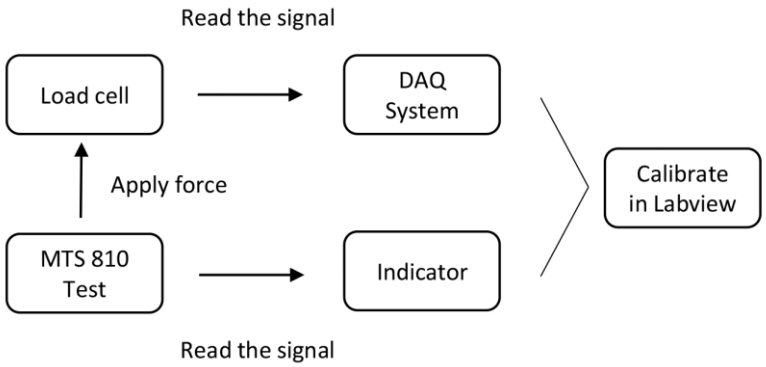

Fig. 4-7: Illustration of the load cell calibration system.

Profilometer and Hardness Testing Machine

Because the size of specimens was small, some minor but important dimensions of the component were difficult to measure. An example is the radii under the head which affects the practical application of bolt. Specifically, too small radii cause a stress concentration which breaks bolts, while too big radii mean that the components cannot be assembled. To measure these dimensions, the MITUTOYO profilometer was used.

In order to find the hardness gradient in the component, the micro-hardness test machine, MITUTOYO HM-101, was used.

4.3 Experimental Procedures

The experimental procedures have three stages, pre-measurement stage, forging stage and post-measurement stage, which are shown in Fig. 4-8. Each stage is described clearly below.

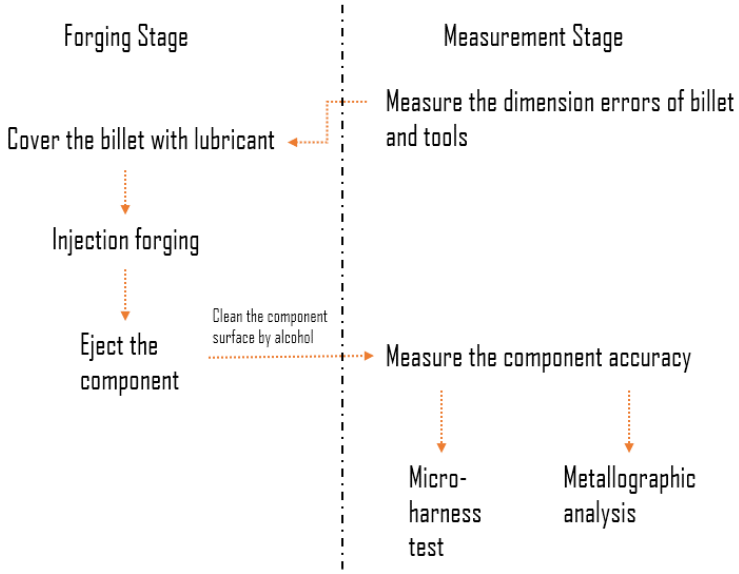

Fig. 4-8: Flow diagram of experimental procedures.

4.3.1 Pre-measurement

In this stage, billets and tools were measured before forging to make sure they can meet the requirements. For the billets, around ten specimens were randomly selected, which occupied around 10% of total billets. Because the dimensions of the initial billet was nearly similar, the billet errors were evaluated by weight to simply the measurement procedures. Based on the same material, the weight for each billet should be the same when the volume was equal. The weight of the billet was scaled by electronic scale one by one. The results were listed in Appendix F.

As for tools, the dimension may have a slight change after assembly, especially for some core parts involved interference fitting. Therefore, it was necessary to measure the tools after assembling. However, it was hard to measure the tools directly when most tools were enclosed in the die case. In this situation, paraffin is commonly used in factories. At room temperature, the paraffin is in a solid state and it turns into the

liquid state at 40 – 50 ℃. Moreover, the adhesion force between the paraffin and metal was small. In other words, it was easy to take the unbroken paraffin out from the die chamber. In this way, the detail size of tools could be obtained via measuring the paraffin. It works well for solid part. For the hollow part, the paraffin is easy to break in the process of taking out. Therefore, it is hard to measure the inner dimension by this method.

4.3.2 Forging

Before doing the forging, the billets and tools were washed by alcohol and dried by a blow gun until the surfaces were clean enough. As shown in Fig. 4-9, the injection forging process was conducted in four steps. At the beginning of forging, the billet, covered uniformly with lubricant, was placed into the die chamber of the bottom die. Secondly, the top die was secured by the "connection" on the bottom die. With the force from the top work platform, the top die pushed the bottom die insert to deform the billet. When the stroke achieved the set value, the top work platform returned to the original position. In the meantime, the spring force supported the bottom die insert back to its initial position. Then the ejection pins on the bottom die knocked the workpiece out from the die chamber, whereas the punch still was embraced by the workpiece. Therefore, the adaptor was taken away from top die, and three ejection pins were placed to get the workpiece.

Three lubricants, ISO VG 100 forging oil, ISO VG 68 forging oil and MoS_2 grease, were employed in the forging process. Among them, ISO VG 100 forging oil is a widely used lubricant in the factory. It is made of relatively highly viscous chlorine, active sulphur additives and refined mineral oil, which show good performance in forming of alloy steel. For ISO VG 68 forging oil, it is based on refined mineral oil with contains fatty and special oiliness additives. MoS_2 grease, which is commonly used in industry, was tested in this experiment. In this experiment, all forging oil was produced by LOCKS OIL and the MoS_2 grease was made by MOLYKOTE. For each group of lubricant, there were six workpieces. After one group test was finished, tools were cleaned by alcohol again. In this way, no previous lubricant existed in tools to affect the following test.

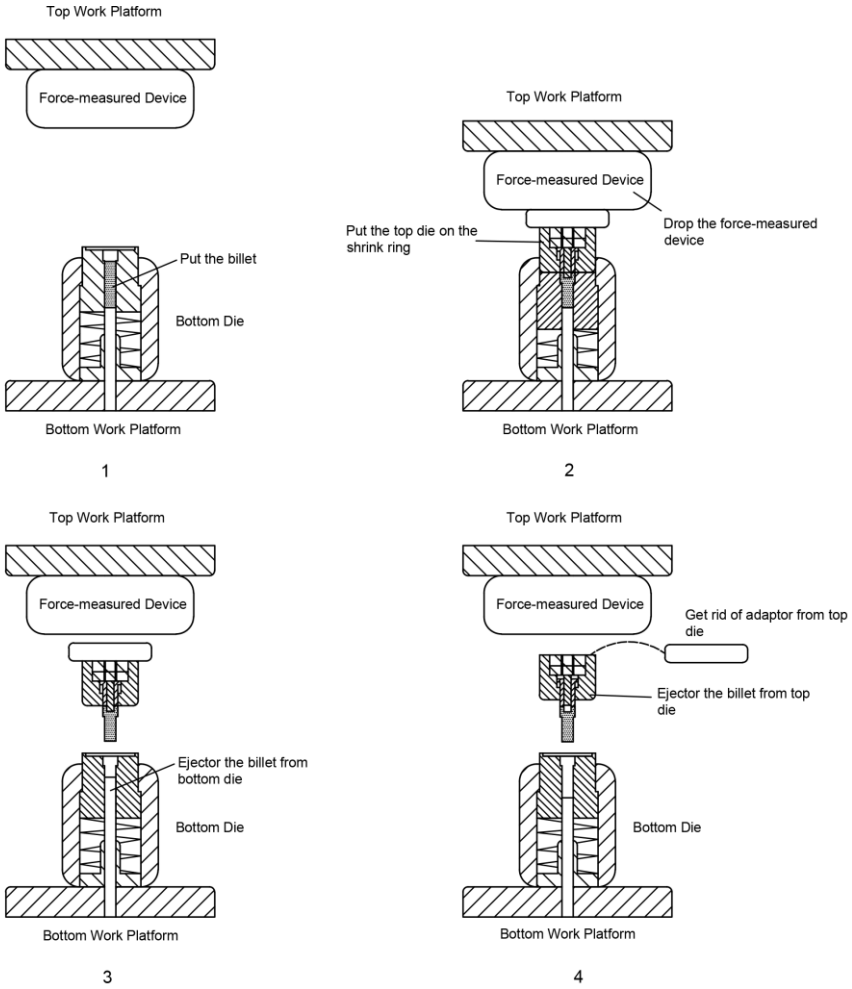

Fig. 4-9: Illustration of injection forging process.

4.3.3 Post-measurement

After forging, three post-measurements were conducted on the components, including component form-accuracy measurement, hardness test and grain flow analysis.

4.3.3.1 Measurement

In this study, 18 pieces of specimens were measured concerning component accuracy. The measurement focused on five key parameters of the component, which covered bolt head diameter $\boldsymbol{D}$, bolt rod diameter $\boldsymbol{d_1}$, bore diameter $\boldsymbol{d_2}$, and transition radius $\boldsymbol{R}$ and radius under the head $\boldsymbol{r}$. In the parameters, $\boldsymbol{D}$ and $\boldsymbol{d_1}$ were measured from position 1 to 4 and 5 to 8 (refer to Fig. 4-10) respectively by a micrometer. Bore diameter $\boldsymbol{d_2}$ was examined from position 9 to 12 by vernier calliper. $\boldsymbol{R}$ and $\boldsymbol{r}$ were

detected by contour graph.

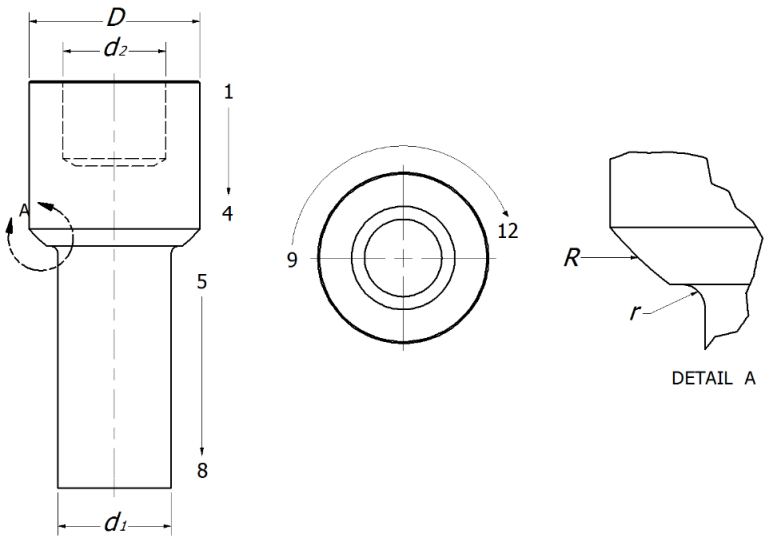

Fig. 4-10: The key parameters in the workpiece and the explanation of measurement positions.

4.3.3.2 Micro-hardness Test

In order to satisfy the demands of specimens for a micro-hardness test, the specimen required some pre-treatments. Firstly, since the original size of the specimen was too big for a micro-hardness test, the redundant rod was removed. Then, the residual part was cut through the middle section. Subsequently, the part with a better cutting surface was used to do the rough grinding. Before doing the fine grinding and polishing, a thermoplastic was employed for mounting the specimen. The last step was surface cleaning. The finished specimen was presented in Fig. 4-11. This process references to ASTM E3-11 2011 [172].

Fig. 4-11: Mounted specimen for hardness test.

To save the test time, the micro-hardness test was conducted on a half of the specimen based on the centre line. As can be seen from Fig. 4-12, the specimen was tested on ten rows from top to bottom. On the first four rows, there were six indentations for each row, and it increased to ten for last six rows. The test force was 2,942 N. The hardness of raw material was approximately 172 HV. Under the force, the mean diagonal of indentation was 0.0568 mm based on [173].

According to [174], each centre of adjacent indentation should keep a safety distance which the minimum value was three times the mean diagonal length of indentation. In addition, to avoid the influence of specimen boundary on the hardness test, the first/last indentation for each row had 2.5 times the mean diagonal length of indentation away from the edge of the test piece. In the practical test, these values were 0.25 mm and 0.15 mm, respectively.

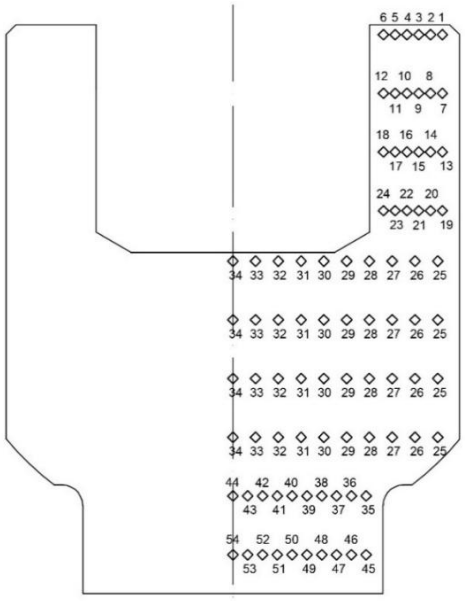

Fig. 4-12: The illustration of indenting positions.

4.3.3.3 Grain Flow Analysis

The specimen for grain flow analysis also needed some preparation. However, unlike doing the hardness test, the specimen did not need mounting, fine grinding and polishing. So after rough grinding, the washed specimen was put into the hot hydrochloric acid solution (50% hydrochloric acid and 50% water) around fifteen

minutes [175]. After the specified time, the corrosive specimen needed to be washed by hot water and cleaned by brush. In this way, the smut, which interfered with the following observation, was able to be removed.

4.4 Manufacturing Trials

To test the injection forging in volume-production, the manufacturing try-out was carried in Ritai Auto Standard Component Co, LTD. In this test, the forging tools were mounted on the FORMAX 2000 cold header, seen in Fig. 4-13. This machine can process wire diameter up to 14.8 mm, and the peak forging force is 1,200 kN.

The workpiece was cut by the trimming tools in the cold header and transferred to the die by the transfer finger. ISO 100 forging oil was used as a lubricant. Three forging speed conditions, 80 strokes per minute (SPM), 100 SPM and 120 SPM, were adopted. The force curve was monitored by the built-in transducers. The transducers could measure the forging force and cam angle in-process.

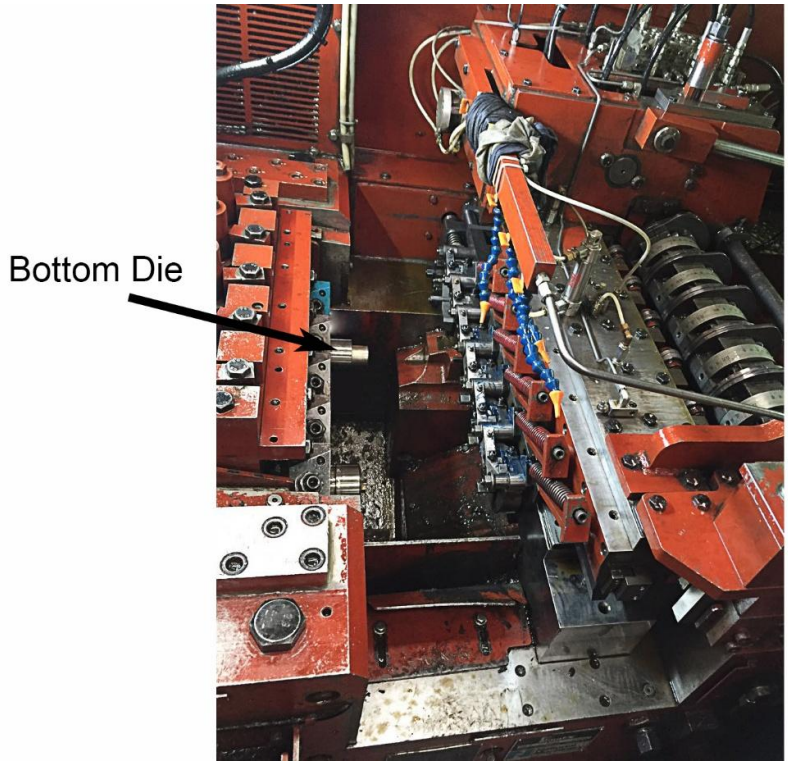

Fig. 4-13: The forging tools in the cold header.

4.5 Results and Discussion

4.5.1 Forging Force

Fig. 4-14 shows the force-time curve for injection forging which is carried out on hydraulic press with ISO 100 forging oil, MoS_2 grease and ISO 68 forging oil. According to results, the whole forging force curve is divided into four stages. In the early stage of period A, the force increases slowly to overcome the spring force from bottom die. When the punch contacts with the workpiece, the force ascends rapidly because of the elastic deformation of workpiece. In period B, this deformation turns into plastic deformation, and the force rises gently because of work hardening of workpiece materials. Subsequently, the flowing material is stopped by the die insert which contributes to the growing force significantly. In the latter stage of period C, the force is sufficient for metal flow so that it remains stable. In the final period, the flowing metal is blocked by a sleeve which brings the force to the peak point.

In the comparison of lubricants, the force curves from ISO 68 and ISO 100 show a similar trend. As for MoS_2, it can be seen that the repeatability of the force from specimen No.1 to No. 6 is not very high. Two reasons could cause it. Firstly, it is hard to keep the amount of grease applied on the workpiece surface to be the same for each workpiece. The workpiece with more lubricant requires relatively low forging force, while the workpiece with less lubricant led to a high forging-force. Secondly, for each specimen, it is difficult to apply the grease onto the surface smoothly, which resulted in an uneven grease distribution. As a consequence, it shows some differences of the forging forces among different samples.

As for force reduction, the ISO 68 shows the best behaviour which means the maximum value keeps below 200 kN. For MoS_2, it is evident that the increased ratio in stage B and C is quicker than ISO 68 does. Finally the peak force exceeds 210 kN for all specimens.

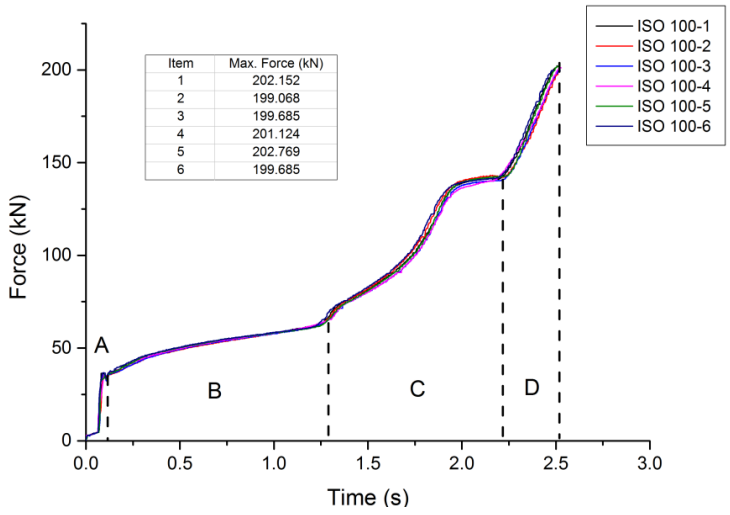

(a)

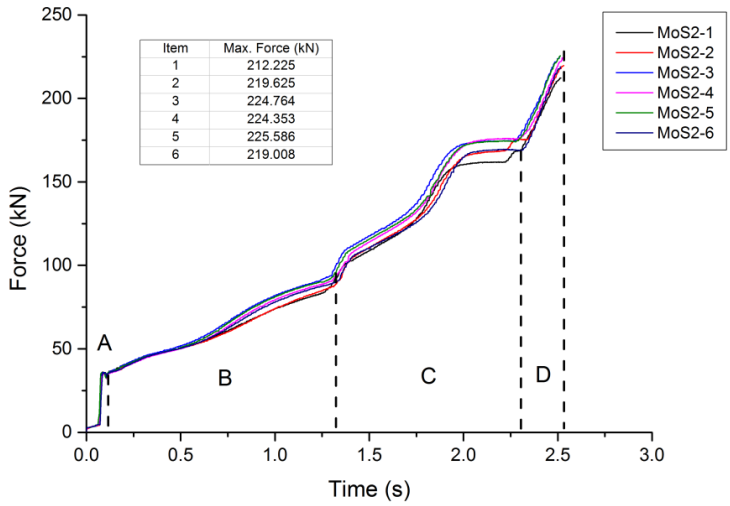

(b)

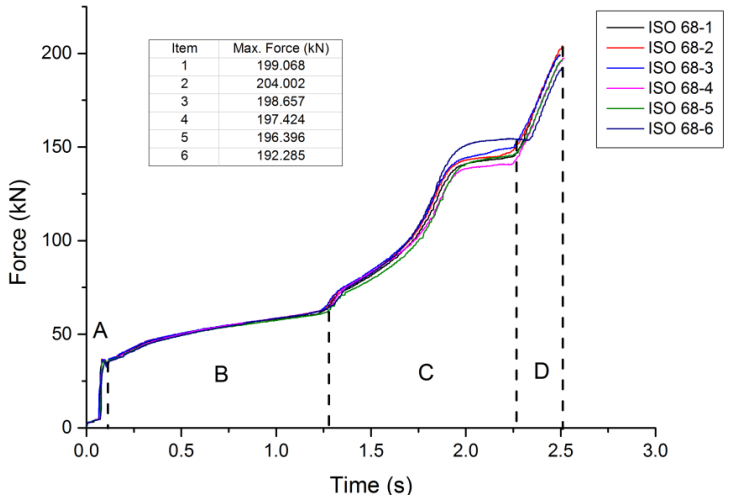

(c)

Fig. 4-14: Force-time curve: (a) ISO 1000 forging oil, (b) MoS_2 grease, (c) ISO 68 forging oil

4.5.2 Component Dimensional Accuracy

In this study, five key parameters were examined for specimens (refer to Fig. 4-15) concerning rod diameter, radii under the head and head dimension.

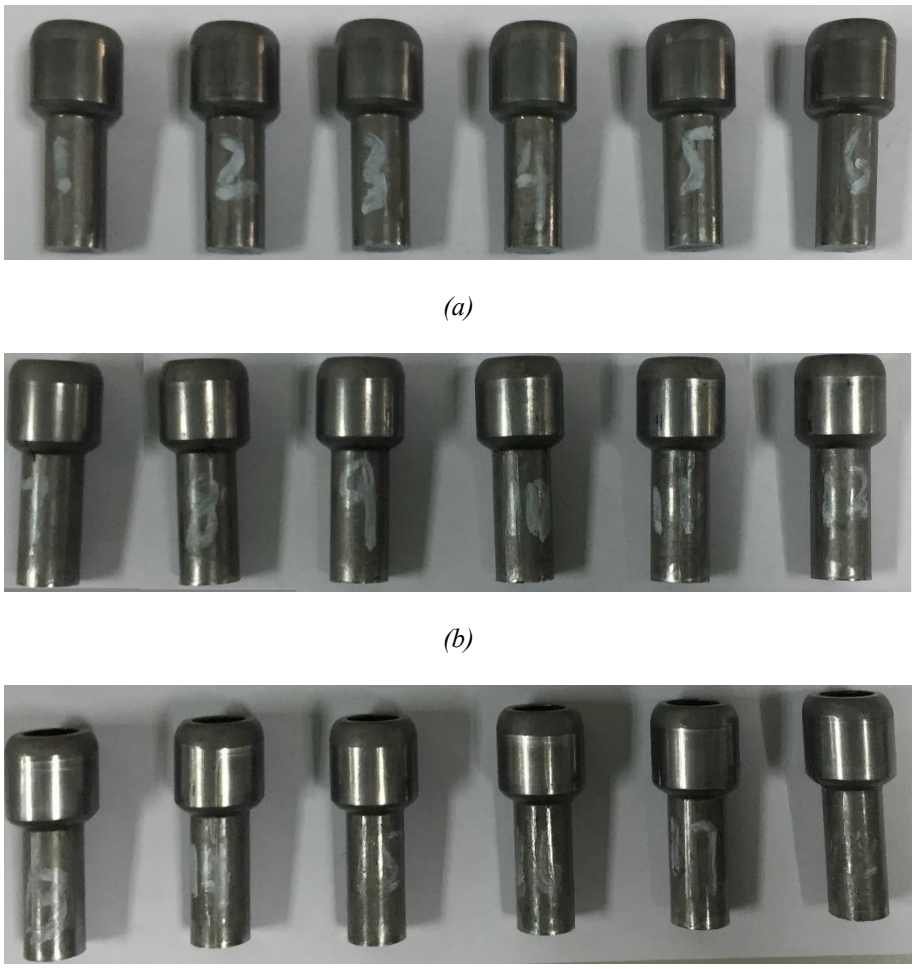

(a)

(b)

(c)

Fig. 4-15: Specimens produced by: (a) ISO 100 forging oil, (b) MoS_2 grease, (c) ISO 68 forging oil.

Rod diameter

Fig. 4-16, Fig. 4-17 and Fig. 4-18 present the profile graph of rod diameter $\boldsymbol{d_1}$ for ISO 100, ISO 68 and MoS_2 respectively. For most specimens, the rod diameter unevenly distributes around the designed dimension (10.2 mm) after forging. The maximum dimension concentrates on the top end of the rod where it is adjacent to the transition area. Then the dimension reduces to the minimum value along the rod. Lastly, the dimension increases again in the bottom of the workpiece. In most positions of the

rod, the diameter is less than the designed value. This may be caused by lack of oil outlet in the die chamber. Due to using a vertical forging process, the lubrication oil is concentrated at the bottom part of the die chamber and it is hard to clear. Therefore, with the increasing forging cycles, this issue could become more severe. It stops the forging process early and means the component dimension cannot reach the targeted one. Nevertheless this issue is addressed at the end section of the rod. The existing clearance between the die chamber and the ejection pin could act as an oil outlet under a high pressure. The extra lubricant can be ejected out through this oil outlet. Therefore, at the end-section of the workpiece, the dimension reaches nearly the targeted dimension. Comparing to the forging oil, the MoS_2 grease shows better lubrication behaviour. This is because the grease will not gather at the bottom part of the die chamber to stop the forming process unexpectedly.

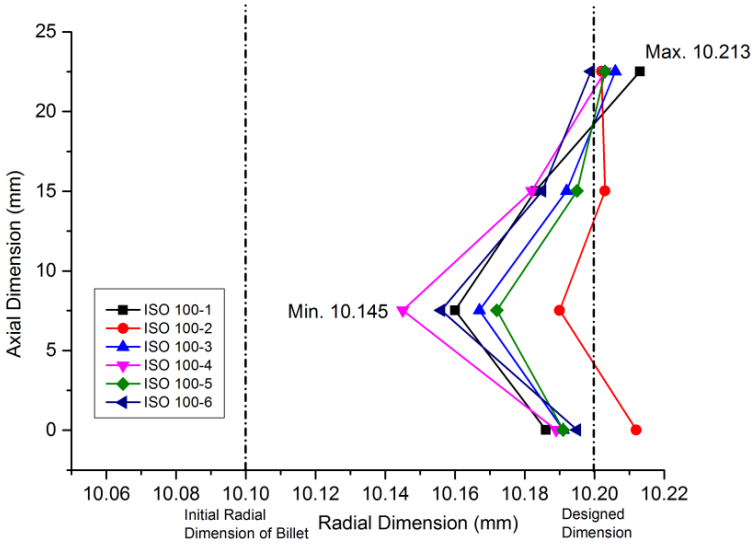

Fig. 4-16: The rod dimension errors with using ISO 100 forging oil.

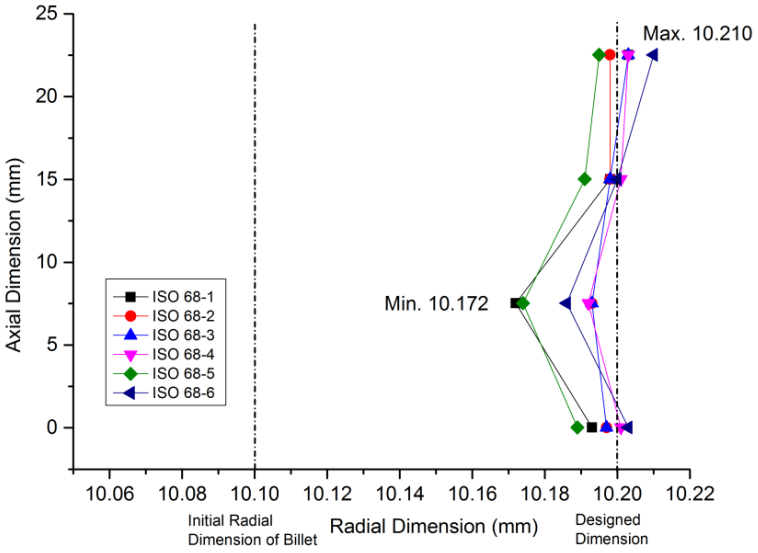

Fig. 4-17: The rod dimension errors with using ISO 68 forging oil.

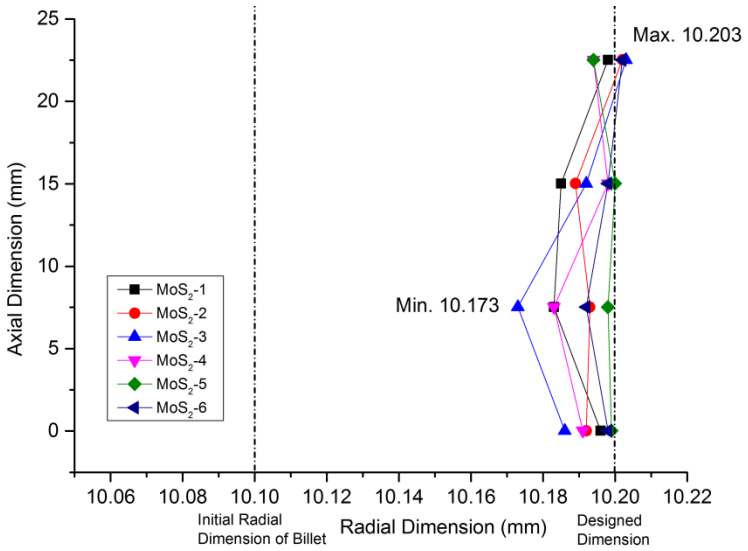

Fig. 4-18: The rod dimension errors with using MoS_2 grease.

Radii under the head

Table 4-1 shows the radii under the head with different lubricants. The detail graphs for these data are presented in Appendix G. As can be seen from the table, for most specimens, ***r*** bulges to more than 0.6 mm after forging, except for a few specimens. However, for ***R***, all specimens are far less than the designed dimension. The unfilled space is known as a dead-metal zone which is caused by a velocity gradient. Because

there is friction existing between billet and tools, the material in peripheral zones is restricted at the billet/die interface. It creates the velocity gradient where the material in the centre flows at a higher speed and a low speed near the billet surface. With increasing of forging cycles from item 1 to item 6, it is found that dead-metal zone is reduced. It is caused the increasing lubricant is introduced into the die chamber with the forging cycles. These extra lubricant can improve the friction condition which reduces the velocity gradient. It makes the dimension $\boldsymbol{R}$ increases with the item number.

Table 4-1: Radii under the head measured from experiments.

Item	ISO 100-1	ISO 100-2	ISO 100-3	ISO 100-4	ISO 100-5	ISO 100-6
R (mm)	3.724	3.972	4.026	4.063	4.314	4.541
r (mm)	0.605	0.605	0.621	0.646	0.603	0.535
Item	MoS_2-1	MoS_2-2	MoS_2-3	MoS_2-4	MoS_2-5	MoS_2-6
R (mm)	3.818	4.518	4.481	5.004	4.436	4.506
r (mm)	0.607	0.696	0.697	0.616	0.696	0.554
Item	ISO 68-1	ISO 68-2	ISO 68-3	ISO 68-4	ISO 68-5	ISO 68-6
R (mm)	3.902	4.122	4.39	4.245	5.781	3.66
r (mm)	0.626	0.605	0.53	0.667	0.694	0.581

Head dimension

In the head of the bolt, it has two key parameters, including the head diameter $\boldsymbol{D}$ and bore diameter $\boldsymbol{d_2}$. Fig. 4-19 to Fig. 4-21 and Fig. 4-22 to Fig. 4-24 present the mean head diameter $\overline{\boldsymbol{D}}$ and mean bore diameter $\overline{\boldsymbol{d_2}}$. As shown in the figures, $\overline{\boldsymbol{D}}$ and $\overline{\boldsymbol{d_2}}$ do not reach the designed dimension. Because the oil prevents the forming in the rod section, more material flows to the top section of the die chamber. It increases the tool deflection at the top-section of die chamber when using forging oil as a lubricant. MoS_2 grease shows slightly better behaviour in terms of achieving forming accuracy than other lubricants in the head diameter. The forming errors for ISO 100 and ISO 68 are similar.

However, the extra material in the top section brings better forming accuracy in bore diameters. With using ISO 68, the mean bore diameters mostly are close to the targeted one. For MoS_2, the errors of bore forming stays at the highest level which is around 0.06 mm.

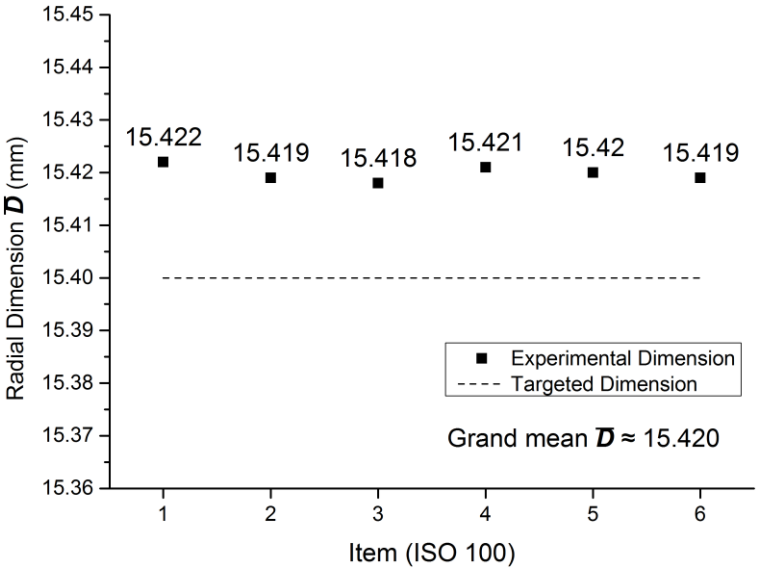

Fig. 4-19: Mean head diameter with using ISO 100 forging oil.

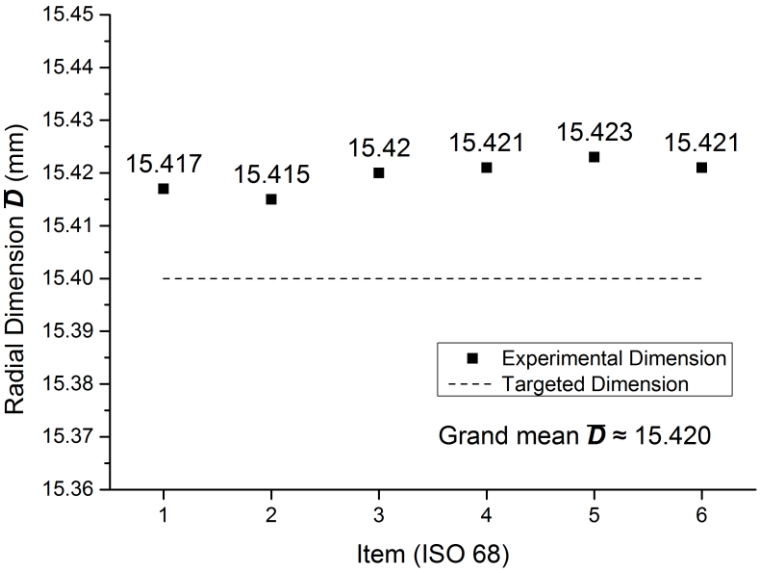

Fig. 4-20: Mean head diameter with using ISO 68 forging oil.

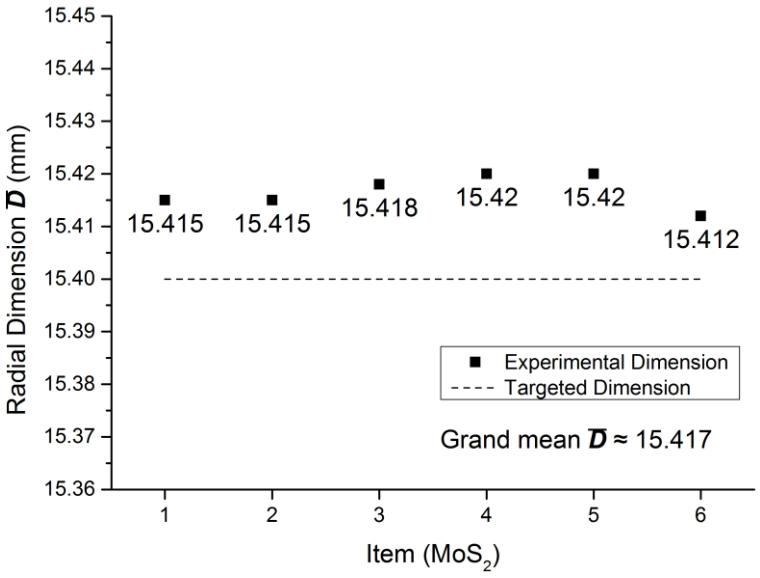

Fig. 4-21: Mean head diameter with using MoS_2 grease.

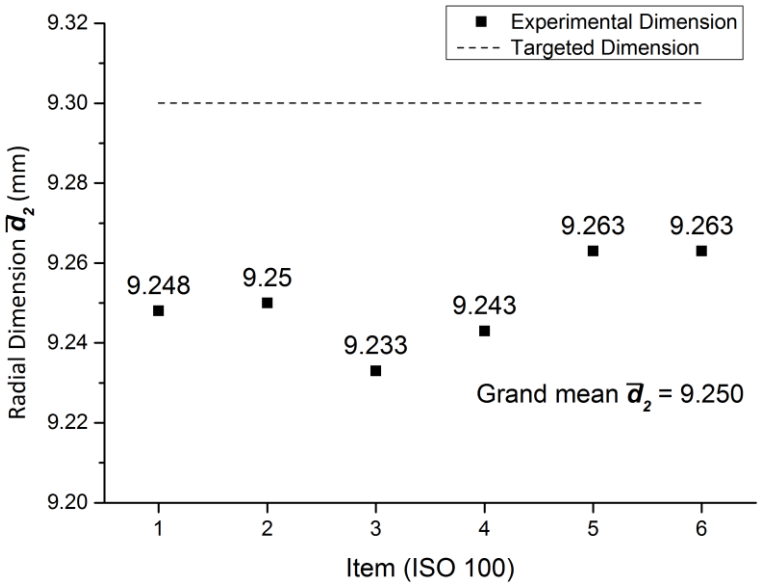

Fig. 4-22: Mean bore diameter with using ISO 100 forging oil.

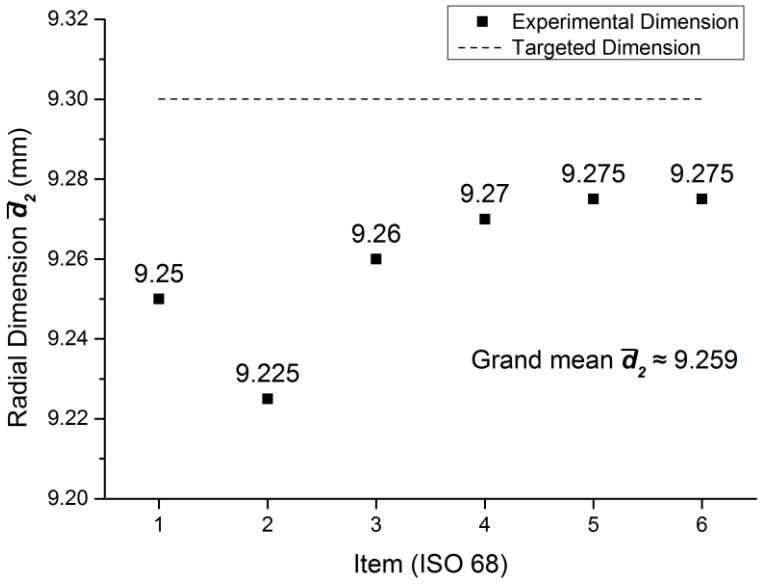

Fig. 4-23: Mean bore diameter with using ISO 68 forging oil.

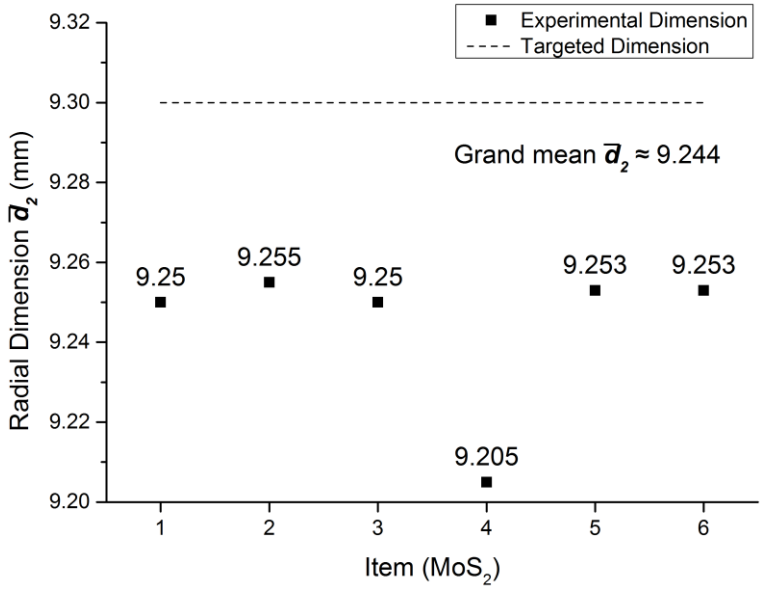

Fig. 4-24: Mean bore diameter with using MoS_2 grease.

4.5.3 Grain Flow Line

During the forging, some brittle inclusions in the material are orientated by the forging force. These inclusions display a flow line along the component forming direction after macro etching. In this test, the grain flow line of AISI 1010 is not very obvious, and only the flow line in the centre of the specimen is visible in Fig. 4-25.

Three groups of specimens A (ISO 68), B (ISO 100), C (MoS_2) were etched by muriatic acid solutions. As results, some components, like specimen 1, 3 and 5, show good grain flow line distribution which is basically symmetrical. In specimen 2, 4 and 6, the flow line is disorganised, especially in specimen six which flow lines in centre present "S" shape. Therefore, it is believed the specimen 6 is easier to break than specimen 1 under the tensile force.

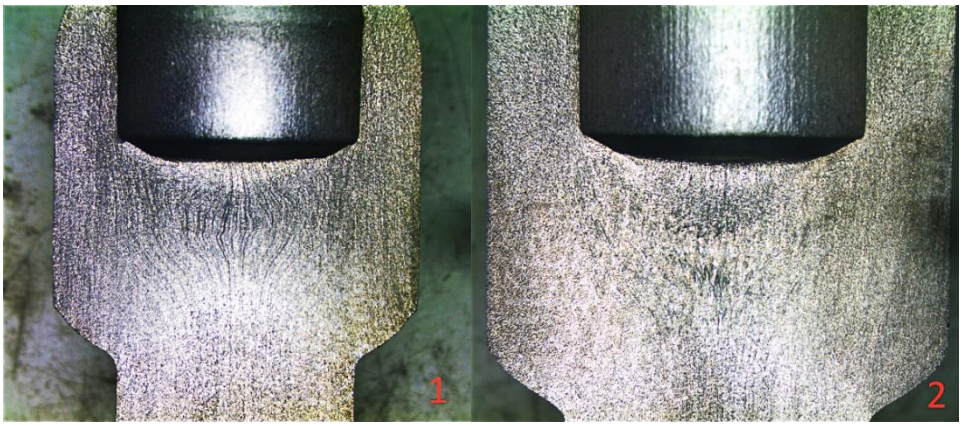

(a)

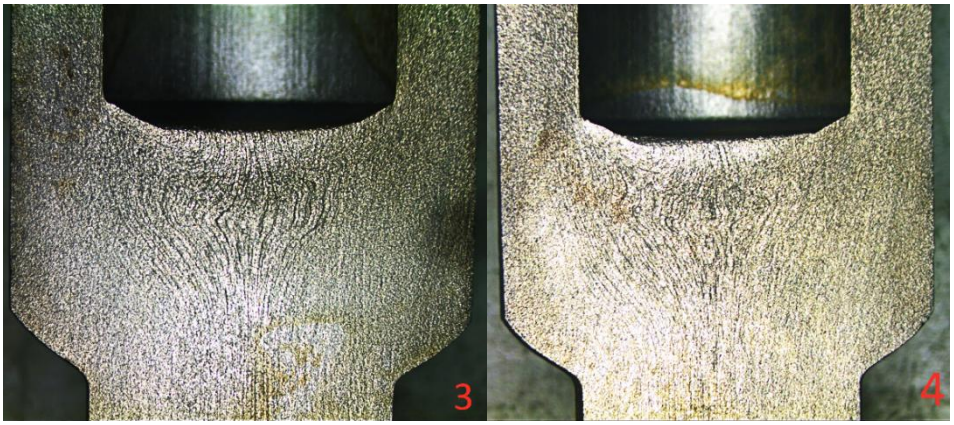

(b)

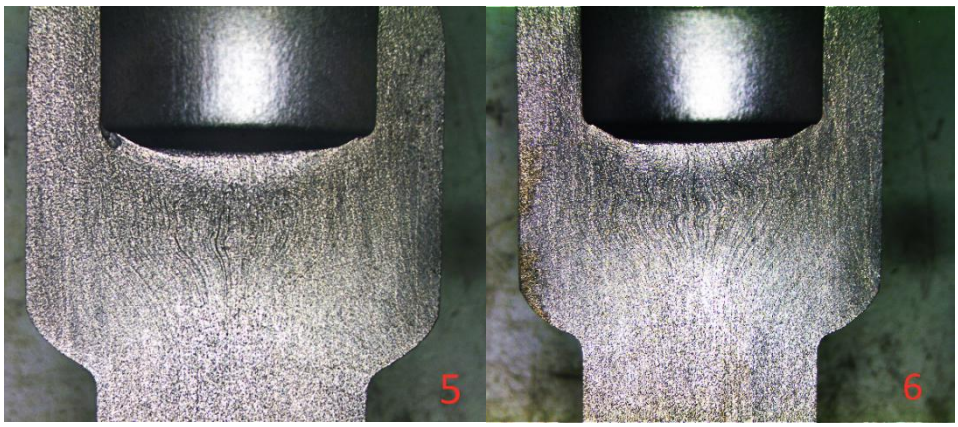

(c)

Fig. 4-25: Grain flow line under microscope: (a) ISO 68, (b) ISO 100, (c) MoS_2.

4.5.4 Hardness Test

Fig. 4-26 shows the hardness distribution at the specimen after forging. The maximum hardness is located on part A which is caused by forming the bore. With part A as a centre, the hardness gradually reduces. In the process of reduction, part B/C keeps relative high level. It implies that the plastic deformation in part B/C is severe. The minimum hardness focuses on the rod part of the component. It is close to the initial material hardness which is 88.5 HRB. It is because the material on the rod part, especially the material in the centre of the rod, does not participate in large plastic deformation. The low plastic deformation brings low work hardening that causes the slight hardness change. Therefore, through observation of hardness change, the strain distribution can be predicted in practice.

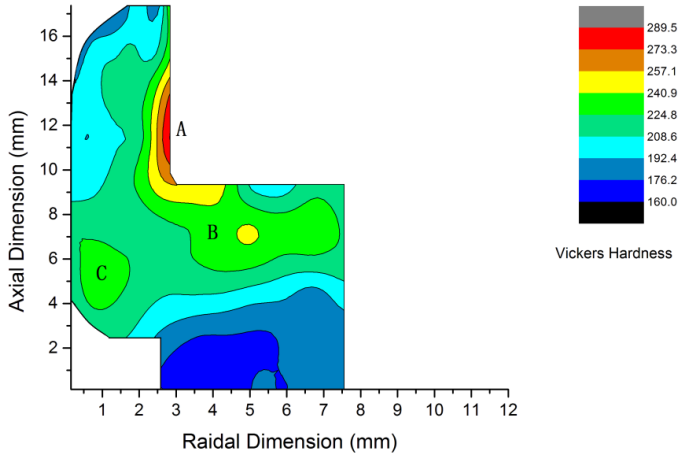

Fig. 4-26: The contour of hardness on the workpiece.

4.5.5 Manufacturing Trials

The manufacturing trials are carried out on cold header. Fig. 4-27 shows the forging force curve in low, medium and high forging speeds. As results show, with increasing forging speed, the force growth has a considerable improvement. In the highest speed, the peak force can reach around 280 kN. This large force creates a high ejection force which breaks the ejection pin in this test (refers to Fig. 4-28). Therefore, in high-speed production, more tough material is suggested for the ejection pin.

In terms of component accuracy, because the forging process is carried out on a horizontal press machine, the lubricant oil is less likely to gather on the die chamber as a result of gravity. Meanwhile, the oil is easier to be ejected in the ejection process. This causes the mean dimension of components in section ***d*** to be more than the targeted dimension 10.2 mm after forging.

Moreover, the high forging speed creates severe scratching on the component surface, seen in Fig. 4-29. Due to the large forging force, the shear stress between workpiece and die inserts stays at a high level. This shear stress breaks the adhesion force between the phosphate coating and the component surface. It is obvious when the forging speed is 120 SPM. The coating on the rod part is removed totally, and the substrate surface is scratched. With reducing the forging speed to 100 SPM, the coating remains on the top of rod part. However, in the bottom part, the coating is still damaged partially. It suggests that the bottom part undergoes more severe contact stress. This issue is solved in the low forging speed which coating covers the component well in the whole part. Compared with the rod part, the coating in the head part of component keeps well regardless of forging speed. It may indicate that the shear stress in this part is not severe.

Because this component is an intermediate product of the process chain, it is better to keep the phosphate coating intact as much as possible in order to improve the friction condition for the following forging step. Therefore, in this coating condition, the forging speed in 120 SPM is not suitable for this forging process. Meanwhile, thicker and stronger phosphate coating is suggested to resist the high shear stress for high speed forging.

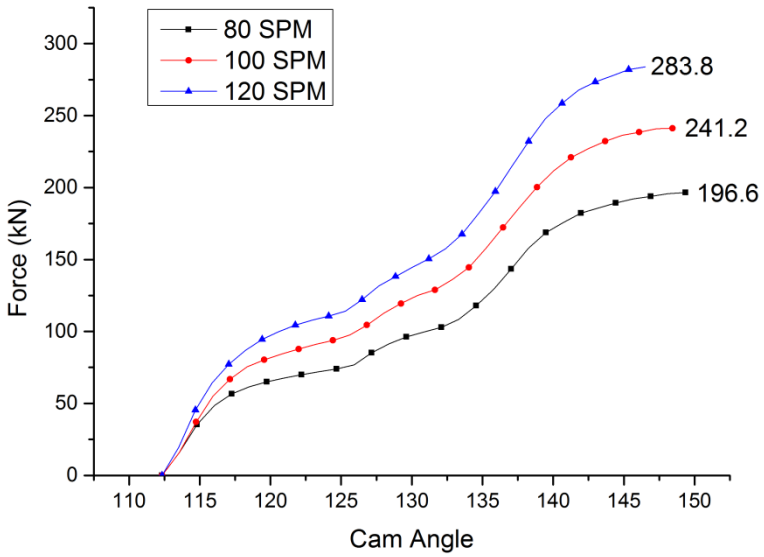

Fig. 4-27: The force-angle curve in different forging speed.

Fig. 4-28: Illustration of the damaged ejection pin in high speed forming.

Fig. 4-29: Illustration of starch on the component surface.

4.6 Comparison of Experimental and FE Simulation Results

Updating FE Models

Based on the experiment tooling, some updates were employed in the FE model which is shown in Fig. 4-30. In the new model, there are some modifications including using some new parts, results output, and a boundary condition.

- New parts. To make the simulation more close to the real production, a spring element is introduced to models. The stiffness of spring is 720N/mm, which references to the spring used in the production. To make the spring force uniformly distributed on the tools, two rigid parts are used in the model.
- Boundary condition. Because the velocity of the hydraulic press cannot reach 45mm/s (refers to Table 3-3), the corresponding value in FE simulation has to be reduced to an average value of 8 mm/s which based on the hydrualic press.
- Result output. Due to the lack of a stroke transducer in the hydraulic press, the forging force curve is recreated which depends on time.

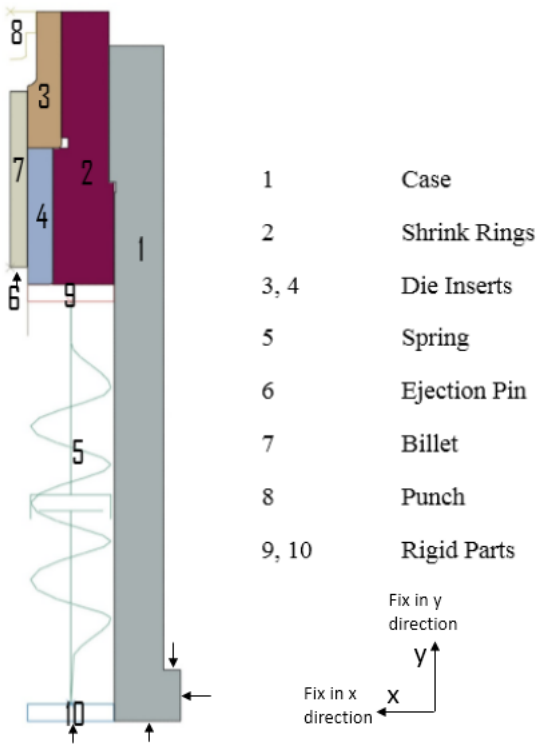

Fig. 4-30: Modification FE models based on the forging experiment.

Because the coefficient of friction used in FE simulation is based on ISO 100 forging oil, the following comparison adopts the experimental results of ISO 100 forging oil.

Comparison of the Forging Force

Based on simulation results, the comparison of force is presented in Fig. 4-31. With comparing the forging force, the simulations and experiments show good agreement in force growth tendency. However, in view of force magnitude, the estimated value of simulation is slightly large. In DEFORM, the maximum force is 257 kN, and it is 238 kN in ABAQUS, which exceeds around 18% to 28 % of the experiment results, respectively. It may be caused by the material model used in FE modelling as well as the meshing scheme and definition of boundary conditions, etc.

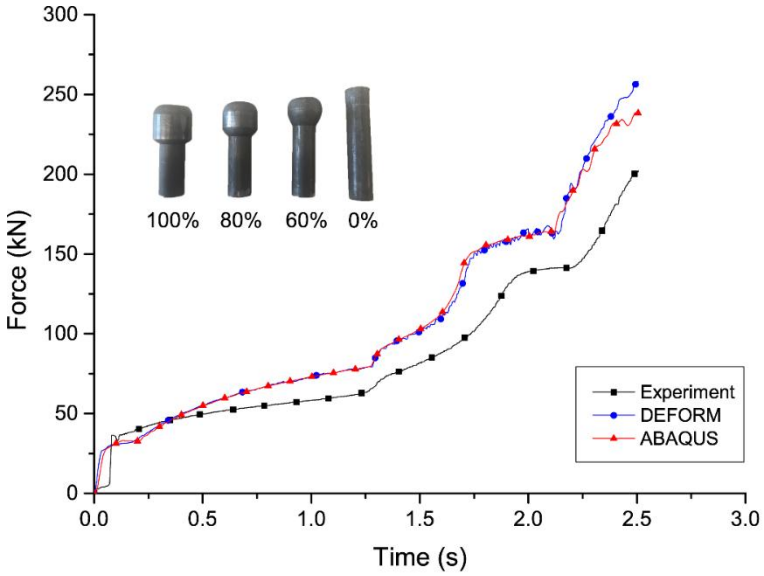

Fig. 4-31: Comparison of forging force between experiment and simulations.

Strain vs. Hardness

Fig. 4-32 (a) shows the effective plastic strain on the specimen in ABAQUS. Comparing the strain with hardness (refers to Fig. 4-26), the distribution is similar. The location of high strain, A_1, B_1 and C_1 corresponds to that of high hardness A, B and C. The same results are presented in DEFORM in Fig. 4-32 (b).

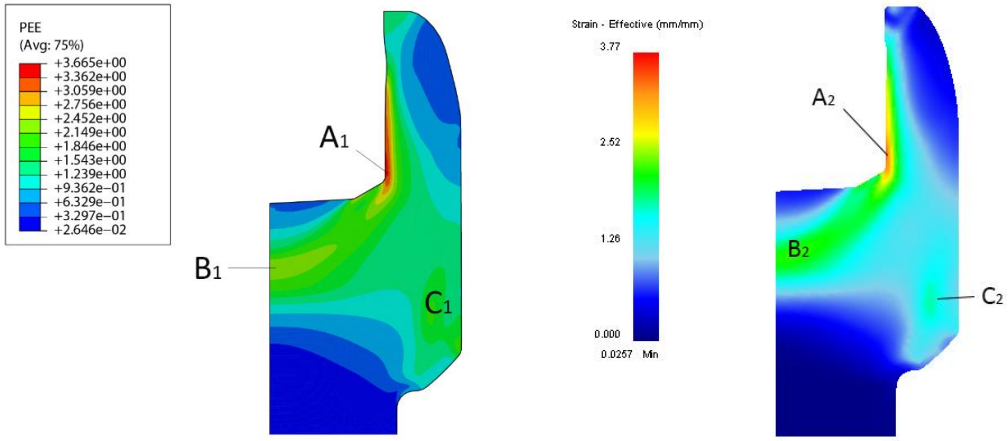

(a) *(b)*

Fig. 4-32: Effective strain distribution on the workpiece: (a) ABAQUS, (b) DEFORM.

Grain Flow line vs. Flow Net Prediction

Fig. 4-33 shows the grain flow line in the component at the end of forging.

According to the results, the centre line is almost straight during the forging process. The flow line on either side of the centre line remains symmetrical, as shown in Fig. 4-33. However, in the experiment, the centre line is bending, and the symmetrical characteristic is unsatisfactory. It may be caused by the uneven end surface of the initial specimen. Although the specimen is preformed, the end surface still cannot achieve an ideal condition. On the other hand, the tool assembly and stiffness possibly are reasons for uneven grain flow.

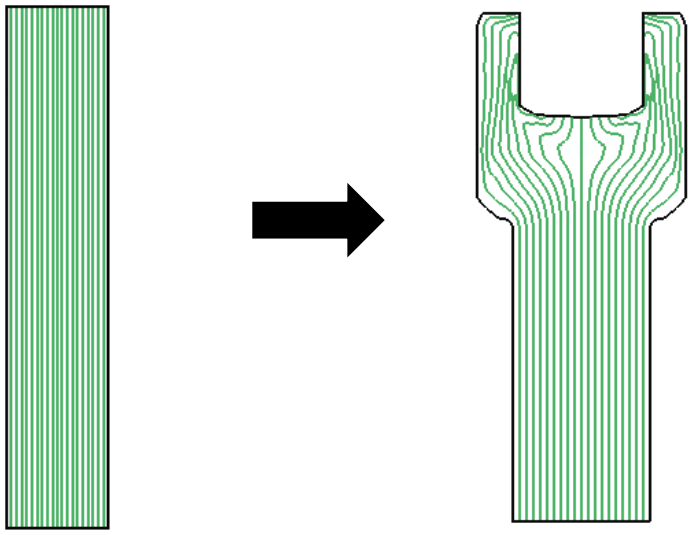

Fig. 4-33: Flow net prediction of the component in DEFORM.

Comparison of the Forming-Errors

Three dimensions are compared in order to evaluate the reliability of the simulation results. As shown in Table 4-2, in the prediction of dimension in section ***D, d1*** and ***d2***, experimental and simulation results show a good agreement. Generally speaking, the dimensions from the FE simulation are slightly larger than experimental results.

Table 4-2: Comparison of the results of component dimensions based on experiments and simulations.

Item	FE simulation	Experiment	Error
Mean Dia. $\overline{\boldsymbol{D}}$ (mm)	15.470	15.420	0.050
Mean Dia.$\overline{\boldsymbol{d_1}}$ (mm)	10.304	10.189	0.115
Mean Dia. $\overline{\boldsymbol{d_2}}$ (mm)	9.32	9.250	0.07

4.6 Improvement of FE Modelling

Based on the comparison with experiments and FE models, the limitations of simulations are found out, and some improvements are proposed.

Issues relating to heat generation during forming

In cold forging process, the temperature of the workpiece can reach a relatively high value because of the heat energy during the forming. Therefore, the temperature is also a critical issue which may affect the forming errors. However, in the current FE model, the thermal problem is not taken into consideration. This will cause some errors in the prediction of component size. Therefore, it is suggested to use the model with thermal module to replace the current one.

Limitations of the Axis-Symmetric Model

Because using an axis-symmetric model, some issues cannot be covered. For example, the geometry of the workpiece in practical forging is not perfect. Usually, some initial billets have an uneven end surface. This uneven end surface will influence the metal flow which in turn changes the final component quality. However, the axis-symmetric model cannot show this influence. Therefore, a 3D model can be used to investigate the influence of initial workpiece geometry in order to overcome this drawback.

Meshing and ALE Adaptive Meshing

In view of the workpiece, the bottom part of mesh does not participate in the severe forming. In other words, the bottom part is not the concerned position compared with other positions. Therefore, the mesh can be coarser than elsewhere. Additionally, as the mesh distortion in the bottom part is slight it can be ignored, it is unnecessary to use ALE adaptive mesh in this part to extend the computation time.

The Material Model

The material model is important when running a FE simulation. The used material model only considered the influence of the strain on the flow stress, while the strain rate was ignored. This issue is not obivous in slow forging process, whereas it is

important in high-speed forging. Therefore, a comprehensive material model should be employed.

4.7 Summary

In this chapter, the injection forging of fasteners was tested in a hydraulic pressure machine and a cold header. Some results like the forging force, dimensional errors, hardness distribution and grain flow line were analysed based on different lubricants. For forging force, the ISO 68 and ISO 100 presents better behaviour of force reduction. It also provides good force repeatability during the multi-cycle forging. It is, however, unstable with using MoS_2 grease because of the uneven covering on the workpiece surface. It may suggest that the MoS_2 grease is a worse choice than forging oil.

However, the forging with MoS_2 shows better forming accuracy in most positions of the component, except the bore diameter. Because there is no oil outlet in the die chamber, the gathering oil blocks the forming progress. It causes the relatively low forming accuracy when using forging oil as lubricants. However, in practice, the forging direction is horizontal which can resolve the problem. It is because the oil will not gather at the bottom part of die chamber because of gravity. Meanwhile, in the ejection process, the oil is easy to push out by the ejection pin. It has already been proved in manufacturing trials. On the other hand, the grain flow line is disorganised with using MoS_2. It makes the fastener easy to fail in application. Considering the behaviour of force reduction and grain flow line, the ISO 68 may be more suitable.

In the manufacturing try-out, three forging speed conditions were tested. It was found that the increasing forging speed enhanced the forming force. The increasing forging force introduces two issues. Firstly, when the forging speed reaches around 120 SPM, the severe stress breaks the ejection pin. Secondly, the high forging force damages the phosphate coating in the component, especially in 120 SPM. Therefore, it may suggest that the ejection pin needs to adopt tougher material. In the meantime, a thicker and stronger coating should be applied to the workpiece surface. Otherwise, this tool configuration may be not suitable at 120 SPM.

Through the experiment, the FE models were updated. Comparing the FE simulation

with experiments, it presents a good agreement in hardness/strain, force growth tendency, component accuracy and grain flow line. It validates not only the FE models but also the experimental methods. In the meantime, it provides the foundation for the following analysis based on the FE models. Lastly, some suggestions are proposed for the FE models which will be used in the following chapter.

Chapter 5

FE Analysis of Forming Quality and Tool Life

5.1 Introduction

According to Chapter 4, the FE model has already been verified by forging experiment. Based on it, an improved FE model is applied in this chapter to evaluate the influence of some parameters, including the forging speed, friction, workpiece material, tool structure, tool materials, etc. The lifecycle of die inserts, forming errors and grain flow line in the component were set as evaluation criteria. In analysing the forging speed the Cowper-Symonds model was used to describe the change of flow stress because of strain rate. Morrow and Basquin's model was used to predict the fatigue life which was based on mean stress and stress amplitude from simulations. The wear amount on the die insert was taken into consideration by Archard's model. The forming errors were analysed by the 2D profile of the component which used the same approach in Chapter 3.

5.2 Analysis Scheme and DoE

During industrial production, many factors affect the tool life and forming errors. Some factors are uncontrollable such as labour skill, forging machine performance, tool assembly, etc. Some controllable variables were examined for injection forging process, as follows:

Forging Speed

The forging speed is the first concerned issue that involves energy and efficiency. The rising forging speed will increase strain rate. It makes the workpiece material become tougher and more forging force is required. Lastly, the increased force introduces higher thermal energy and more severe tool deflection which impacts the tool life and component accuracy.

Friction

Friction is an important factor for metal forming. It not only has an influence on metal flow but also affects some other parameters, such as forging force, tool stresses and thermal energy. Commonly speaking, the high friction force between tool/workpiece adversely affects the tool life and forming accuracy. However, the forming accuracy may benefit from some friction force, e.g. the friction between split die inserts. Therefore, the friction between die/die is also taken into consideration in this study.

Workpiece Geometry and Material

In practice, the end surface of the initial workpiece is uneven which has a 1° to 2° gradient. This small angle leads to asymmetric metal flow which may influence the grain flow line. In addition to workpiece geometry, the workpiece material also is covered as a variable in this study. The workpiece material is not only limited to carbon steel. Other materials, such as aluminium E1CM and alloys metal AISI 4340, are examined to explore the application range of injection forging.

Tool Material, Structure and Geometry

Currently, various tool materials are used in tool-marking. Different material brings different behaviours of die elasticity and service life. Therefore, some popular tool materials, tungsten carbide WC, D2 tool steel and H13 tool steel, are investigated. Table 5-1 shows the suggested combination of tool materials for FE simulations.

Table 5-1: The tested tool materials for injection forging.

Item	Die insert material	Shrink ring material
A	WC	H13
B	D2	H13
C	WC	WC
D	WC	D2

As for tool structure, it mainly involves the pre-stressing in die inserts. Two models are tested in FE simulations to make the influence of pre-stressing clear. One has

introduced pre-stressing to the die inserts, and another is without pre-stressing.

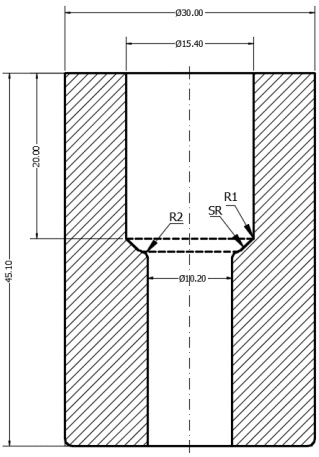

Fig. 5-1: Illustration of the die insert dimension used in injection forging.

The tool connecting geometry affects the metal flow which relates to the component quality. Fig. 5-1 shows the main dimension of die insert. The $\boldsymbol{R_1}$ and $\boldsymbol{R_2}$ are transition radii, and the ***SR*** are the spherical diameter. To find the influence of transition radii and spherical diameter on the grain flow line, some parameters were applied, as shown in Table 5-2.

Table 5-2: The dimension of transition radii and spherical surface in FE models.

Item	R_1 (mm)	R_2 (mm)	SR (mm)
A	0	0.7	10
B	0	1.4	10
C	0	0.7	15
D	0.5	0.7	10

To analyse these parameters, an analysis scheme is developed (refers to Fig. 5-2). A standard FE model, whose parameters depend on industry production, is employed as a reference group. Then the analysis is divided into seven groups. Each group is conducted on one parameter, and the others kept constant. Lastly the influenced parameters include tool life, component accuracy and grain flow line. For all simulations, the forging stroke is set to be 19.0 mm which is about 90% of the full stroke. The detailed parameters are presented in Table 5-3.

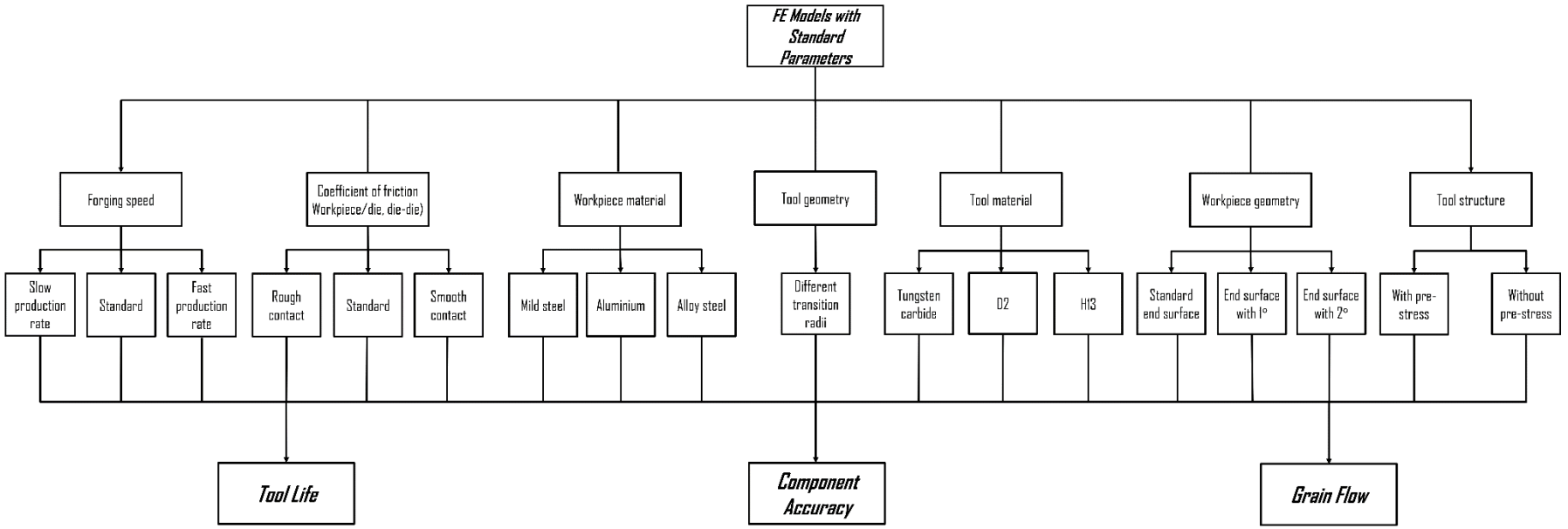

Fig. 5-2: Analysis schemes of injection forging.

Table 5-3: The detail information of parameters used for FE simulations.

Standard parameters in FE simulation		1	2	3	4	5	6	7	8
Velocity (mm/s)	60 (≈120 piece/min)	30 (≈60 piece/min.) 90 (≈180 piece/min.)	-	-	-	-	-	-	-
Coefficient of friction (tool/workpiece)	0.055	-	0.01 0.07	-	-	-	-	-	-
Coefficient of friction (die/die)	0.2	-	-	0.08 0.5	-	-	-	-	-
Workpiece material	Mild steel (AISI 1010)	-	-	-	Aluminium E1CM Alloy Steel AISI 4340	-	-	-	-
Initial geometry of workpiece	Prefect end surface	-	-	-	-	1° 2°	-	-	-
Tool geometry	Standard	-	-	-	-	-	Radii under the head	-	-
Tool structure	With pre-stressing	-	-	-	-	-	-	Without pre-stressing	-
Tool Material	Tungsten carbide and H13	-	-	-	-	-	-	-	D2

5.3 FE Model

5.3.1 ABAQUS

In the FE model, two extra workpiece materials (E1CM and AISI 4340) and one tool material (D2), were tested. The mechanical properties are listed in Table 5-4.

Table 5-4: The mechanical properties of E1CM, AISI 4340 and D2.

Material	Young's modulus *(MPa)*	Poisson ratio	Density *(Kg/m^3)*	Flow strength *(MPa)*
E1CM [176]	70600	0.33	2.705×10^3	$\sigma = 159(0.02+\varepsilon)^{0.27}$
AISI 4340 [99]	192000	0.29	7.85×10^3	$\sigma = 1151.43(\varepsilon)^{0.193}$
D2 [94]	209000	0.30	7.7×10^3	-

Thermal properties of materials were introduced to examine the coupled effect of thermal expansion and springback on component dimensions, seen in Table 5-5. The simulations were consisted of two steps as follows:

Forging. An initial temperature was set as 20 ℃ for tools and workpiece, which was close to the room temperature. The heat transfer coefficient between tools/workpiece was set as 20 kW/m^2K [177]. However, when distances between each part were larger than a specified value, the heat transfer stopped.

Cooling down. The workpiece was taken from the die chamber and placed into room temperature to cool down. The heat transfer coefficient between air and component surface was assumed to be 10 W/m^2K [178]. Subsequently, observation of the workpiece dimension was finished in post analysis software.

During the simulations, the metal deformation was conducted in a closed environment. Therefore, there was no heat transfer between workpiece/tools and air. Also, the cooling effect from the lubricant was not covered therefore the predicted temperature could be higher than practical production. All the transferring work in ABAQUS was as same as that in Chapter 3.

Table 5-5: Thermal properties of tool/workpiece materials [171], [148].

Material	Thermal Conductivity ($mW/mm \cdot ℃$)	Thermal expansion ($mm/m \cdot ℃$)	Inelastic heat Fraction	Specific Heat ($mJ/ton \cdot ℃$)
AISI 1010	49.8	1.22e-5	0.9	448e6
Tungsten Carbide	70	5.8e-6	0.9	235e6
H 13	24.3	1.15e-6	0.9	460e6
Aluminium E1CM	231	2.18e-5	0.9	900e6
AISI 4340	44.5	1.23e-5	0.9	475e6
D2	50	1.38e-5	0.9	460e6

In order to analyse the influence of the forging speed on component-form accuracy, a strain rate sensitively model, Cowper-Symonds model (refers to *equation 39*), was employed for AISI 1010. However, in analysing other parameters, the strain rate sensitivity was not considered.

$$\sigma_{y,1} = \sigma_{y,0}\left[1 + \left(\frac{\dot{\epsilon}}{C}\right)^{1/P}\right] \tag{39}$$

The $\boldsymbol{\sigma_{y,0}}$ is the static stress. The $\boldsymbol{\sigma_{y,1}}$is the dynamic stress after hardening because of strain rate $\dot{\boldsymbol{\epsilon}}$. $\boldsymbol{C}$ and $\boldsymbol{P}$ are constant according to [179], as shown in Table 5-6.

Table 5-6: Material constant for AISI 1010 in Cowper-Symonds model.

C (s^{-1})	*P*
2000	6.6

In ABAQUS, the power law was used to describe strain rate dependent material which is

$$\dot{\varepsilon} = D(R-1)^n \tag{40}$$

Therefore, the *equation 40* was transferred into *equation 41*.

$$C\left(\frac{\sigma_{y,1}}{\sigma_{y,0}} - 1\right)^{P} = \dot{\varepsilon} \tag{41}$$

5.3.2 DEFORM

In DEFORM, a 3D FE model was used to replace the axis-symmetric one, which intended to analyse the workpiece with gradient from 1° to 2° (refer to Fig. 5-3). The workpiece volume kept stable while the shape of the workpiece changes. More than 40000 elements were created in the workpiece, and the thermal issue was not covered in this simulation.

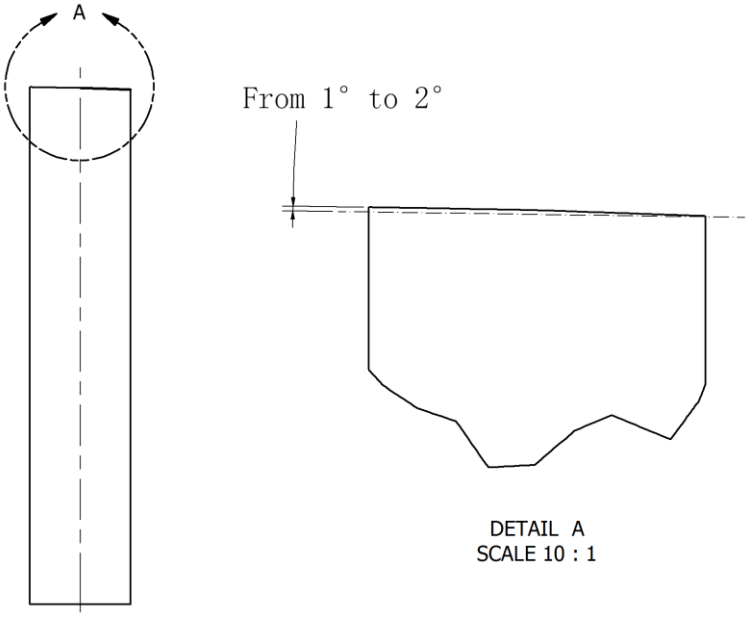

Fig. 5-3: Illustrations of initial workpiece geometry.

After FE simulations, Basquin and Morrow's equation (correspond to equation 8 on page 17) was used to evaluate the fatigue life $\boldsymbol{N_f}$, as follows:

$$\sigma_a = (\sigma_f' - \sigma_m)(2N_f)^b \tag{42}$$

$\boldsymbol{\sigma_a}$ is the stress amplitude and $\boldsymbol{\sigma_m}$ is the mean stress. According to [68], the detail value of fatigue strength coefficient $\boldsymbol{\sigma_f'}$ and fatigue strength exponent $\boldsymbol{b}$ are showed in Table 5-7. As analysing in Chapter 3, the die insert 1 is the most critical part in injection forging tools. Some reference elements (refers to Fig. 5-4) were selected in

die insert 1, which represented the fatigue life.

Table 5-7: Material constant for tungsten carbide in Basquin and Morrow's model.

$\sigma_f^{'}$ *(MPa)*	*b*
-0.289	33,415

Archard's model, as shown in *equation 5*, was applied to evaluate tool wear. In this equation, the wear volume ***W*** is decided by normal load ***P***, velocity ***V***, hardness of material ***H***, the wear coefficient ***K*** and time ***t***. When the tool material is defined, ***K*** and ***H*** were same. Therefore, ***W*** is simplified by ***P*** and sliding length ***L*** in this Archard's model. In this study, the maximum normal load was used to predict the maximum wear amount in the die inserts. Because of a lack of data about wear coefficient ***K***, the wear amount of die insert cannot be estimated by a detailed value. In the following study, a wear ratio between each parameter was given. Through this ratio, the wear resistance of die inserts can be examined.

$$W = K\int \frac{PV}{H}dt = \frac{KPL}{H} \tag{43}$$

The investigation of forming errors references to the method in Chapter 3. The 2D profile of component involves two periods, 1) at the end of forging stroke, 2) after cooling down and spring back.

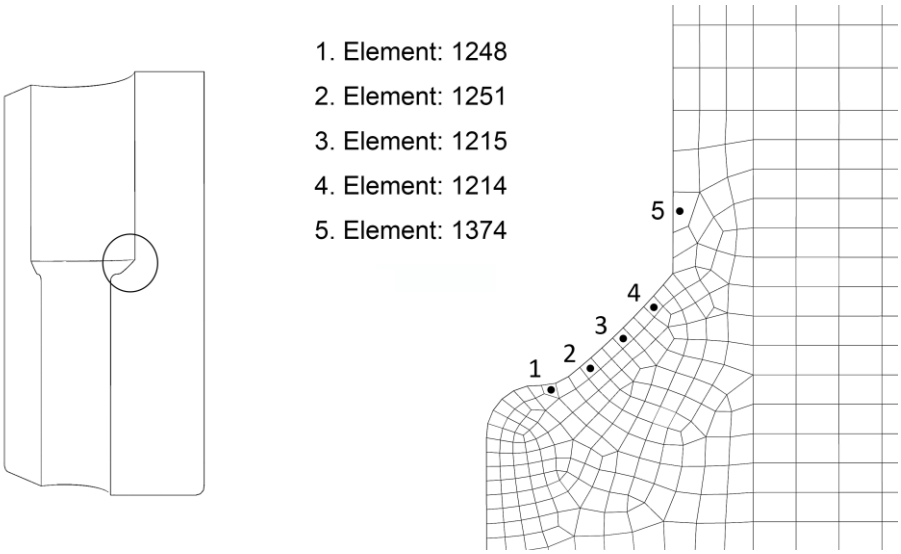

Fig. 5-4: Reference elements for fatigue life prediction.

5.4 Results and Discussions

5.4.1 Forging Speed

Fig. 5-5 shows the force growth curve in three speed conditions. It shows the increased speed turns to extra forging force which is around 5 kN for each model. It also brings higher forming errors to the components. It is obvious in section ***d*** for two 1 low speed brings better forming accuracy at the end of forging. However, after springback, the forming accuracy at higher speeds becomes better (refer to Fig. 5-7). Table 5-8 shows the mean dimension errors.

Table 5-8: Mean dimension errors in section D and d of the component under three speed fields.

Velocity		30 (mm/s)	60 (mm/s)	90 (mm/s)
Mean Error $\bar{e}_D$ (mm)	End of Forging	0.025	0.026	0.026
	Cooling Down	0.031	0.029	0.027
Mean Error $\bar{e}_d$ (mm)	End of Forging	0.044	0.045	0.046
	Cooling Down	0.077	0.078	0.079

Depending on the stress distribution in die inserts, the estimated fatigue life of the reference elements is listed in Table 5-9. The results show that the low forging speed brings slightly improved fatigue resistance in most reference elements. From the life prediction, the elements 1374 and 1248 are the most critical elements. Especially for element 1248, it limits the tool life around 20,000 lifecycles for all models.

As for the tool wear, the maximum normal load are 84.40 kN, 86.73 kN and 88.64 kN for 30 mm/s, 60mm/s and 90 mm/s, respectively. Therefore, according to Archard's model, the maximum wear volume ratio is around 1: 1.03: 1.05 (30 mm/s: 60 mm/s: 90 mm/s). It may suggest that the forging speed influences the maximum tool wear mildly.

Table 5-9: Fatigue life of reference elements in 30 mm/s, 60 mm/s, and 90 mm/s.

Tool Life (cycles) / Speed (mm/s) / Element	90	60	30
1374	36,637	38,706	44,095
1214	112,432	103,285	126,226
1215	74,676	89,742	100,439
1251	53,041	61,817	72,841
1248	19,775	21,906	25,946

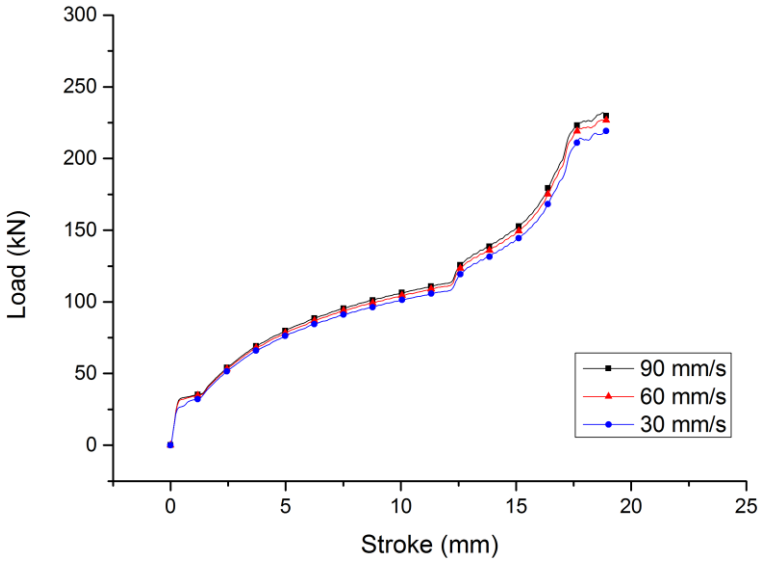

Fig. 5-5: Comparison of forging force under forging speed of 30 mm/s, 60 mm/s and 90 mm/s.

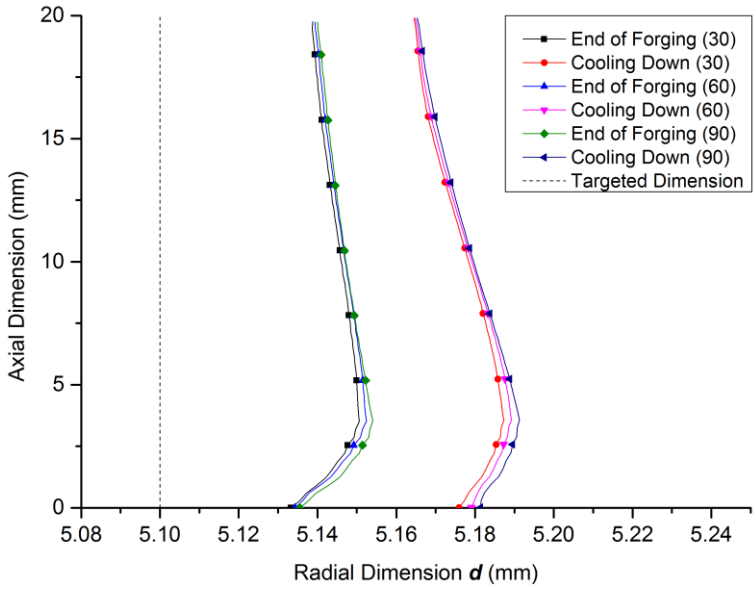

Fig. 5-6: The dimension errors d under forging speed of 30 mm/s, 60 mm/s and 90 mm/s.

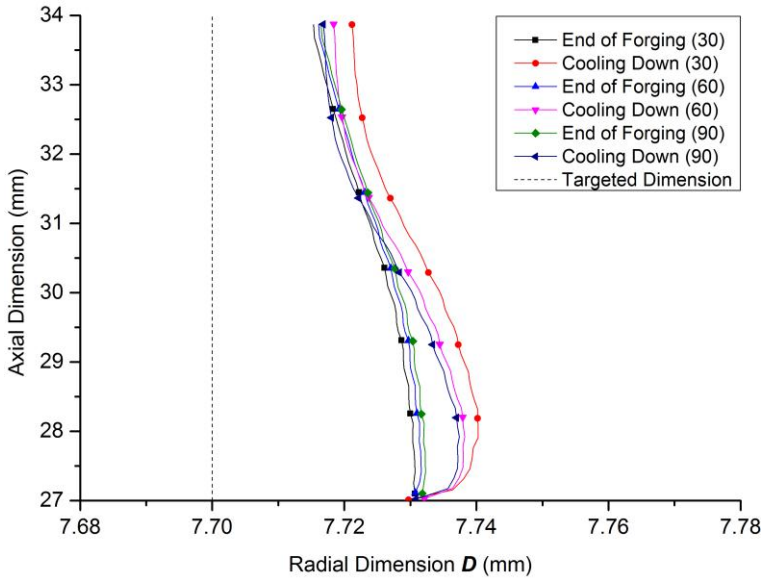

Fig. 5-7: The dimension errors D under forging speed of 30 mm/s, 60 mm/s and 90 mm/s.

5.4.2 Friction at Die-Workpiece and Die-Die Interfaces

5.4.2.1 Friction at Die-Workpiece Interfaces

Fig. 5-8 shows the forging force curve with different coefficient of friction (COF). According to this graph, the friction force does not have an influence on the force in the initial forging stage. It is because the workpiece is not in contact with the die insert. After contacting, the COF begins to impact the force. The difference of force is evident when the COF keeps at 0.01, while it is minor between 0.055 and 0.07. As without using strain rate model, the forging force has a big drop for reference group (refers to Table 5-3) compared with Fig. 5-5.

Fig. 5-9 and Fig. 5-10 present the dimensional errors in section ***d*** and ***D*** for the component under the COF of 0.01, 0.055 and 0.07. It shows that reducing COF is an effective way to improve the forming accuracy in section ***d***. The shape of section ***d*** does not display as a "pyramid" when the COF is 0.01. On the contrary, the dimension distribution becomes more even which is helpful for the following forging stage. The increasing COF reduces the forming errors in which peak errors reach more than 0.06 mm at COF of 0.07. In section ***D***, low COF also shows good improvement in forming accuracy. The mean dimension errors are listed in Table 5-10.

Table 5-10: The mean dimension errors under COF of 0.01, 0.05 and 0.07 between die/workpiece.

Coefficient of Friction		0.01	0.055 (standard)	0.07
Mean Error $\bar{e}_D$ (mm)	End of Forging	0.016	0.018	0.019
	Cooling Down	0.017	0.020	0.021
Mean Error $\bar{e}_d$ (mm)	End of Forging	0.019	0.030	0.036
	Cooling Down	0.032	0.051	0.061

The lower COF does not only improve the forming accuracy but also refines the grain flow line in the component. Fig. 5-11 shows the flow line distribution in the head of the component. Although the distribution of grain flow line does not change significantly as increasing of COF, the bending amplitude is increased which is

expressed as distance ***G*** in the figure. According to the experience from industry, the small distance ***G*** brings better mechanical behaviour to resist the tensile stress in the vertical direction. Therefore, to achieve a better grain flow line, the COF should be as low as possible.

In Table 5-11, the estimated fatigue life of die inserts is presented. The good friction condition does improve the tool life in all of the reference elements. It increases the tool life to around 400,000 cycles under COF of 0.01. On the other hand, the low COF also extends the wear life because of reducing the maximum normal load. Also, the wear amount ratio among COF of 0.01, 0.055 and 0.07 stays at 1: 1.53: 1.87, respectively.

Table 5-11: Estimated fatigue life of reference elements under COF of 0.01, 0.055 and 0.07 between die-workpiece.

Tool Life (cycles) / COF / Element	0.01	0.055 (standard)	0.07
1374	310,507	172,066	138,488
1214	32,369,108	759,561	200,827
1215	5,731,785	468,878	253,765
1251	1,756,961	265,302	150,993
1248	401,785	109,137	72,809

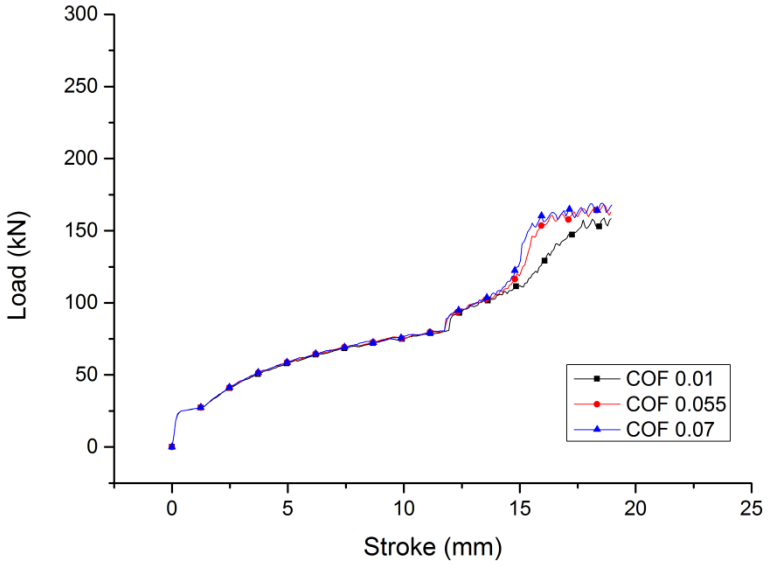

Fig. 5-8: The force-stroke curve under different coefficient of friction between die/workpiece.

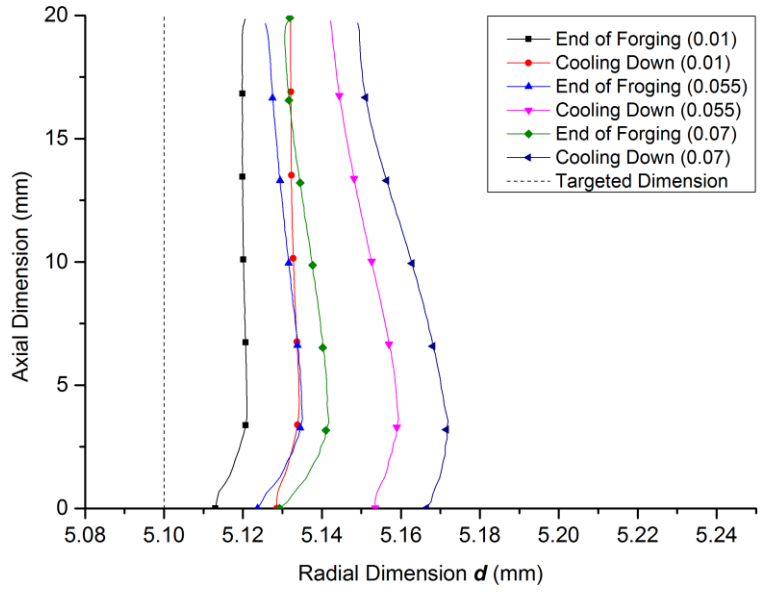

Fig. 5-9: The dimension errors d under COF of 0.01, 0.055 and 0.07 between die/workpiece.

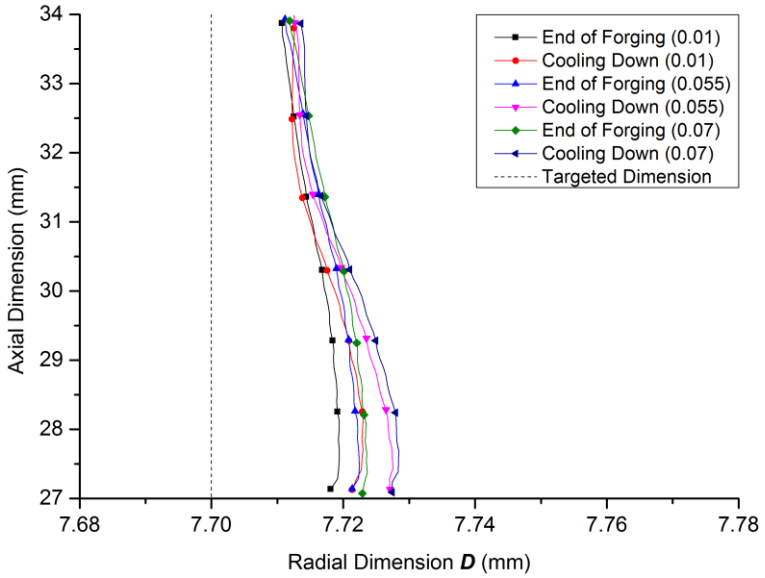

Fig. 5-10: The dimension errors D under COF of 0.01, 0.055 and 0.07 between die/workpiece.

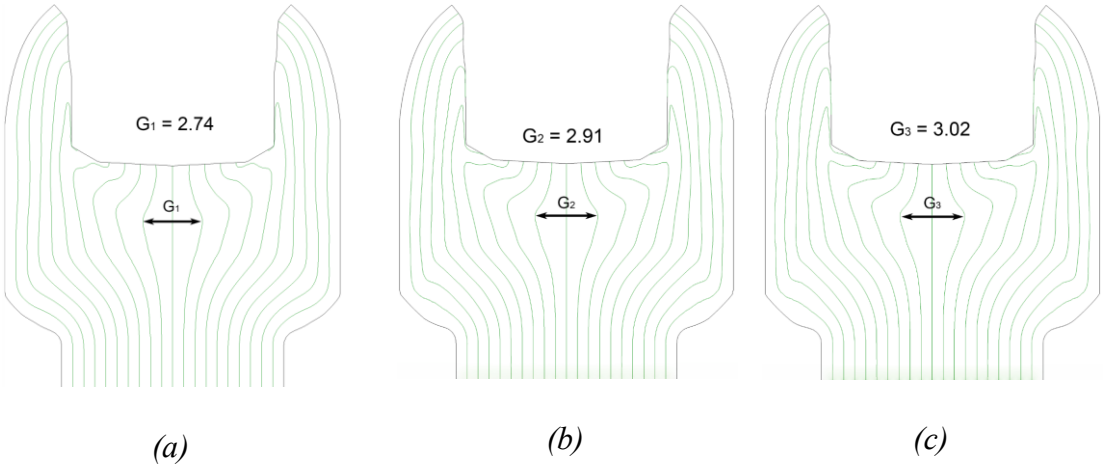

Fig. 5-11: Comparison of flow net in head of component at different coefficients of friction: (a) 0.01, (b) 0.055, (c) 0.07.

5.4.2.2 Friction at Die-Die Interfaces

Fig. 5-12 and Fig. 5-13 represents the influence of friction at die-die interfaces on dimensional errors. The detail of dimensional errors is concluded by mean errors which are listed in Table 5-12. Since splitting of the die insert, the different stress distribution on die inserts causes a slight movement (refers to Fig. 5-14). This movement will weaken the forming accuracy in the horizontal direction. This tends to increase the friction force between die inserts to constrain this movement.

However, the forming errors keeps stable when COF increases. In section ***D***, the high COF even brings slightly larger errors. Therefore, it suggests that the die movement cannot be reduced by increasing the COF between die interfaces.

Table 5-12: The mean dimension errors in COF 0.08, 0.2 and 0.5 between die-die interface.

Coefficient of Friction		0.08	0.2 (standard)	0.5
Mean Error $\bar{e}_D$ (mm)	End of Forging	0.018	0.018	0.019
	Cooling Down	0.020	0.020	0.020
Mean Error $\bar{e}_d$ (mm)	End of Forging	0.030	0.030	0.029
	Cooling Down	0.051	0.051	0.050

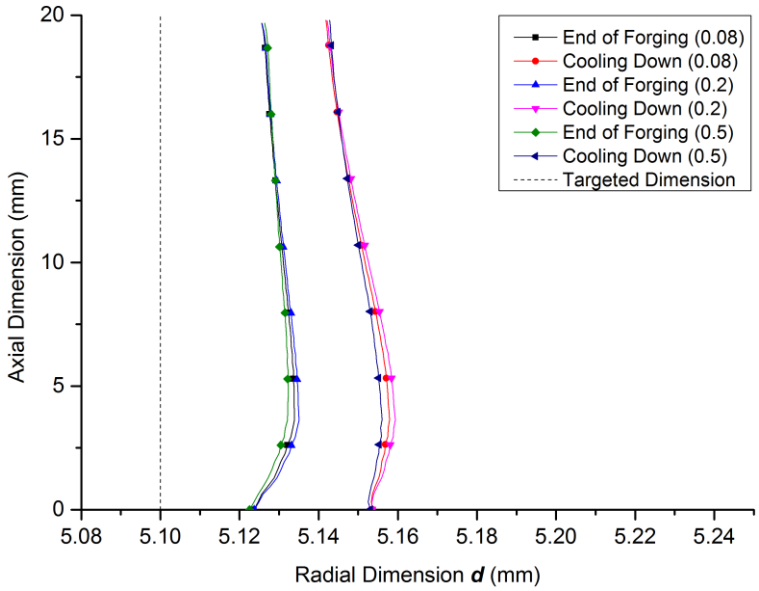

Fig. 5-12: The dimension errors d under coefficient of friction of 0.08, 0.2 and 0.5 between die-die.

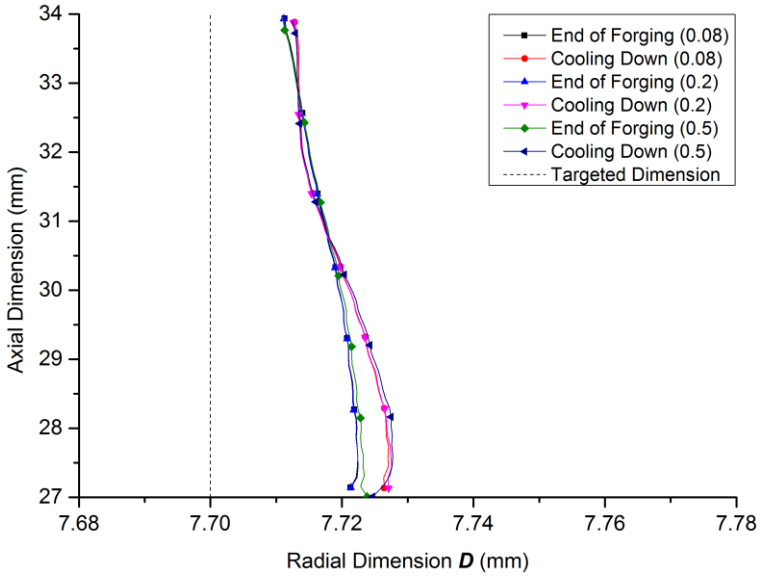

Fig. 5-13: The dimension errors D under coefficient of friction of 0.08, 0.2 and 0.5 between die-die.

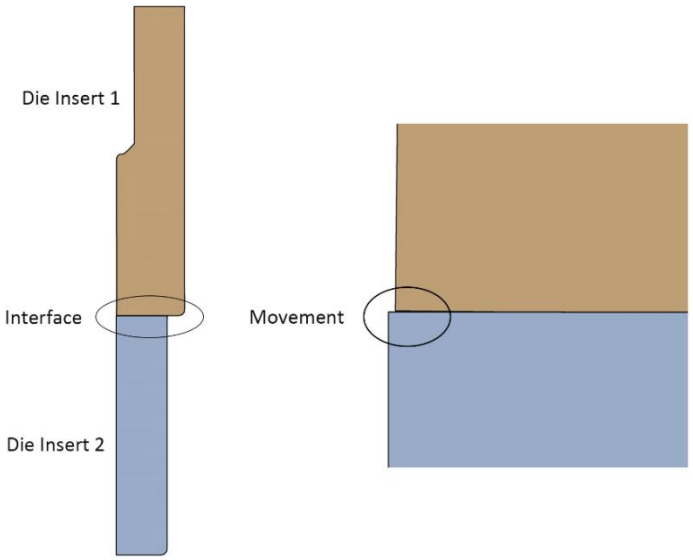

Fig. 5-14: Illustration of the die insert movement during the forging.

5.4.3 Workpiece Geometries and Materials

5.4.3.1 Workpiece Geometries

Fig. 5-15 shows the grain flow line distribution in the head of components with different initial workpiece geometry. It is noticeable that the direction of folding faces to the low surface of the workpiece. Therefore, it can judge the direction of slant for the initial workpiece based on the metallographic analysis in practice.

The increasing degree angle in the end surface bring some effects to the grain flow line. Firstly, the symmetrical grain flow line distribution becomes asymmetrical. It may promote the anisotropy of mechanical properties of the component, which increases the using risk. Secondly, the flow line folds are more and more severe in the component. It is evident when the slant angle reaches to 2 degrees. For the workpiece with 1 degree, the grain flow line is close to the perfect workpiece. It demonstrates that the slant degree within limited ranges is acceptable. It is believed that the intensified fold will affect the tensile strength in practice. Thirdly, the existence of a slant angle in the end surface of the initial workpiece makes it more difficult to get an even component. The unevenness cannot be solved until the component fully fills up the die chamber. However, when the die is fully filled, it brings great stresses which adversely influences the service life.

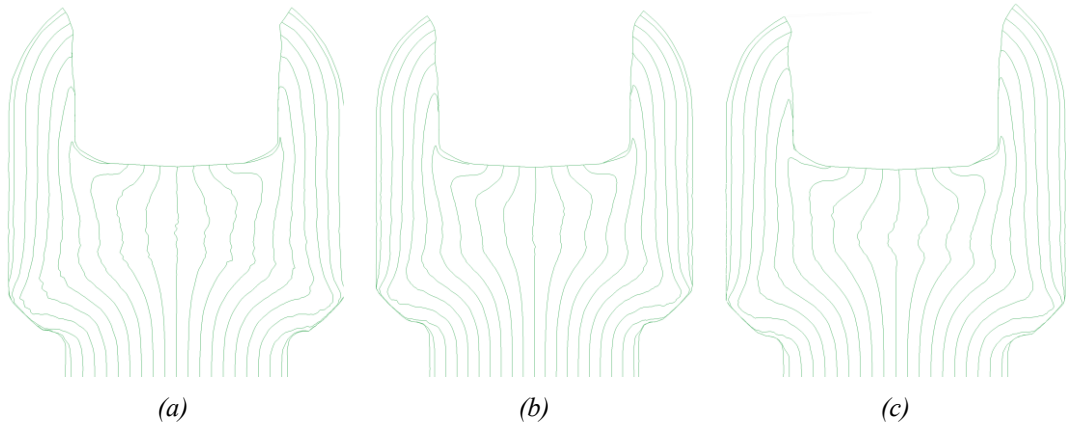

Fig. 5-15: The flow net in the head of component: (a) perfect end surface, (b) 1 degree, (c) 2 degree.

5.4.3.2 Workpiece Materials

Fig. 5-16 and Fig. 5-17 shows the component dimension in section ***d*** and section ***D*** respectively for different workpiece materials. According to results, the workpiece material influences the forming errors significantly. The softest material, pure aluminium, shows the best forming accuracy in mean dimension errors with referring to Table 5-13. By using alloys metal, AISI 4340, the mean errors exceed that of other materials by a substantial degree. Meanwhile, the tougher workpiece material brings plastic deformation to the shrink ring in the current tool design. Therefore, in the next forging cycle, the production dimension could be deteriorated by plastic deformation

in the shrink ring. It suggests that the current tool design is unable to handle this hard material.

Table 5-13: Mean dimension errors for E1CM, AISI 1010 and AISI 4340.

Workpiece Material		Aluminium E1CM	AISI 1010 (standard)	AISI 4340
Mean Error $\bar{e}_D$ (mm)	End of Forging	0.004	0.018	0.027
	Cooling Down	0.008	0.020	0.031
Mean Error $\bar{e}_d$ (mm)	End of Forging	0.007	0.030	0.043
	Cooling Down	0.018	0.051	0.075

Regarding the fatigue life, Table 5-14 presents estimated forging cycles for tools with each workpiece material. From the table, the die inserts with forging aluminium show the longest tool life which profits from the small forging force required. The minimum predicted life is more than 4,000,000 cycles. For the alloys metal, the predicted tool will be cracked after 20,000 cycles. Therefore, to forge tough materials, stronger die inserts material or die configuration should be applied. The high tool stress also influences the tool wear amount. The severe wear will happen in forging alloys metal components. The wear ratio between each die inserts are 1: 4.55: 6.55 (Aluminium E1CM: AISI 1010: AISI 4340).

Table 5-14: Predicted tool life for die inserts with different workpiece materials.

Tool Life (cycles) / Workpiece Material / Element	Aluminium E1CM	AISI 1010 (Standard)	AISI 4340
1374	6,717,987	172,066	38,227
1214	6,341,160	759,561	234,841
1215	5,501,561	468,878	74,607
1251	4,827,949	265,302	62,080
1248	4,078,791	109,137	21,241

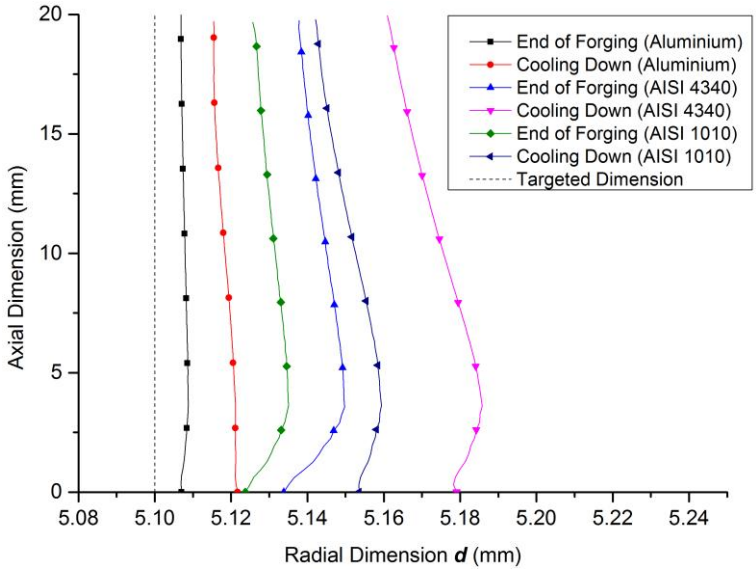

Fig. 5-16: Comparison of forming accuracy in section d for workpiece materials

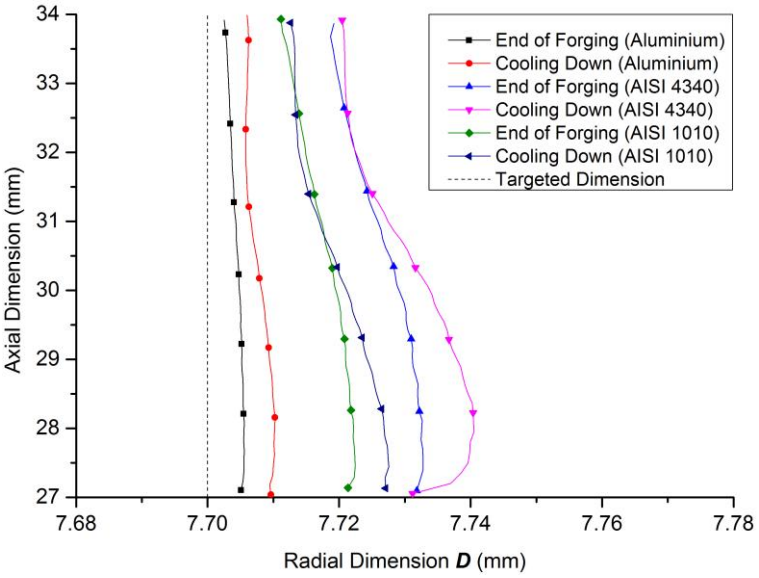

Fig. 5-17: Comparison of forming accuracy in section D for workpiece materials.

5.4.4 Temperature

In this study, the temperature of the component depends on the punch velocity, friction (tool/workpiece) and workpiece materials. Fig. 5-18 shows the temperature distribution at the end of forging under different velocities. Considering the strain rate hardening, the maximum temperature reaches more than 400 ℃ when the punch

speed is 90 mm/s. With reduction of the speed to 30 mm/s, the temperature drops to approximately 300℃. The high-temperature area concentrates on the core of the bolt head because of the large deformation ratio. In the core of the rod, the temperature is low which is near the initial temperature. It reflects the fact that materials in this part barely take part in plastic deformation. In the surface of the rod part, the higher forging speed also brings higher temperature.

Fig. 5-19 shows the temperature distribution difference in components because of workpiece materials. As results, using different workpiece materials impacts the amplitude considerably. The tougher material, AISI 4340, presents the highest forming temperature which is around 430℃. It is much higher than that in aluminium EC1M which only stays at 40℃. For AISI 1010, regardless of strain hardening of the workpiece, the final temperature has a big drop to 280℃.

Change of COF will not change the distribution of the whole part. Fig. 5-20 shows that the temperature in the surface of the billet increases because of the increasing COF. However, the maximum temperature area still keeps at the core of bolt head. The temperature amplitude for each component is at the same level which is around 280℃. It indicates that major thermal energy is contributed by metal deformation but not the friction work.

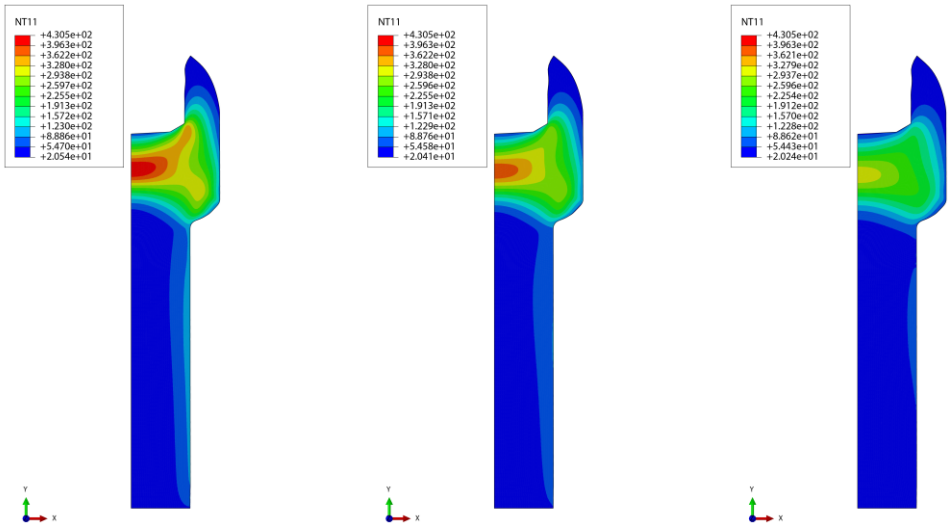

90 mm/s 60 mm/s 30 mm/s

Fig. 5-18: The temperature (centigrade degree) distribution in the end of forging under forging speed of 30 mm/s, 60 mm/s and 90mm/s.

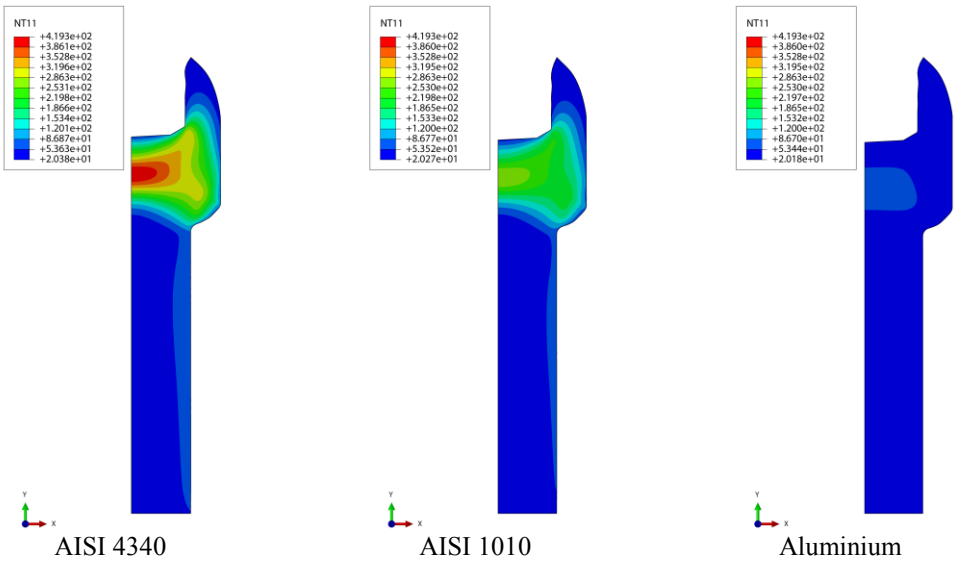

Fig. 5-19: The temperature (centigrade degree) distribution in aluminium, AISI 1010 and AISI 4340.

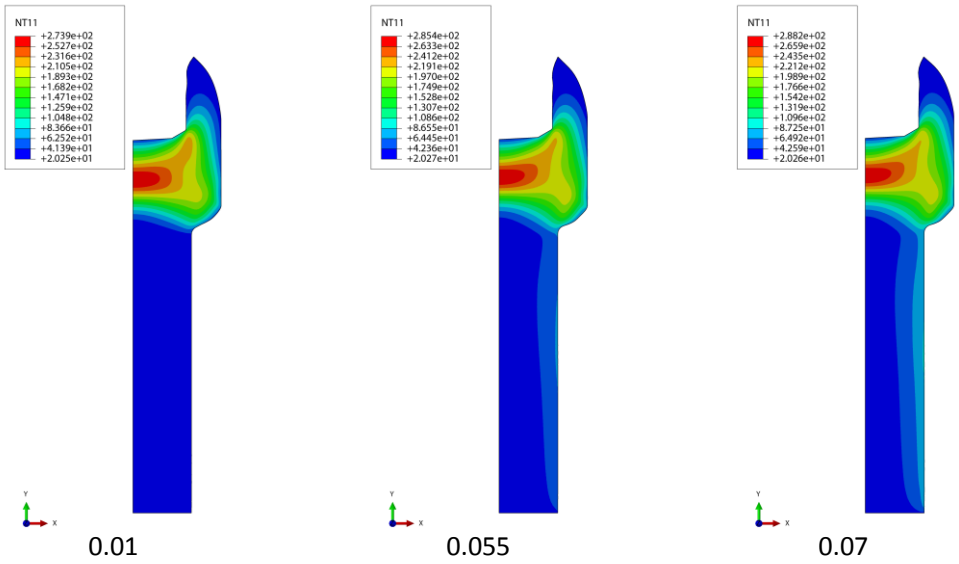

Fig. 5-20: The temperature (centigrade degree) distribution in coefficient of friction 0.01, 0.055 and 0.07 between die/workpiece

5.4.5 Tool Material, Structure and Geometry

5.4.5.1 Tool Material

Fig. 5-21 and Fig. 5-22 show the dimensional errors in section ***d*** and ***D*** for tool materials. From the results, when the shrink ring material is tungsten carbide, the

dimensional errors can be effectively controlled in section ***d*** (refers to Table 5-15). It is because the higher Young's modulus of the tungsten carbide can provide higher pre-stressing when the magnitude of interference is defined. The extra pre-stressing gives the tool configuration more stiffness which in turn reduces the tool deflection. As for the D2 tool steel, it shows similar Young's modulus with H13 tool steel. Therefore, the difference between group A and group D in section ***d*** is mild. However, since the yield stress of D2 is higher than that of H13, the D2 steel can bear more severe pre-stressing which brings more space for interference fit design. It indicates that D2 could be more suitable for shrink ring material when higher pre-stressing is required.

Large forming errors are introduced for die inserts made of D2. It is because the Young's modulus of D2 is lower than tungsten carbide. Moreover, during the process, the die insert yields under large tool stress. It introduces huge dimension errors to the component. Therefore, it is believed that the D2 is unable to replace the tungsten carbide in this study.

Table 5-15: The mean dimension errors in different tool materials (refers to Table 5-1).

Tool material		A (standard)	B	C	D
Mean Error $\bar{e}_D$ (mm)	End of Forging	0.018	0.046	0.016	0.018
	Cooling Down	0.020	0.048	0.017	0.020
Mean Error $\bar{e}_d$ (mm)	End of Forging	0.030	0.097	0.028	0.030
	Cooling Down	0.051	0.116	0.050	0.051

Table 5-16 shows the predicted fatigue tool life. Because the fatigue properties of D2 are unavailable, its tool life is not showed in this study. For other groups, the tool life keeps in the same level when shrink ring material is H13 and D2. However, this value increases more than four times when using tungsten carbide as the shrink ring materials in element 1248. It is because of the higher pre-stressing and stiffness of tungsten carbide. The normal load does not change when using different shrink ring materials. Therefore, the maximum wear amount of group A, C and D should be the same. For group B, because the hardness of D2 tool steel is lower than tungsten

carbide, the wear resistance of D2 is lower than that of tungsten carbide.

Table 5-16: Predicted fatigue life for die inserts with different tool materials (refers to Table 5-1).

Tool Life (cycles) / Tool Material / Element	A	C	D
1374	172,066	2,646,270	164,388
1214	759,561	17,228,421	534,723
1215	468,878	3,056,162	472,439
1251	265,302	631,273	243,058
1248	109,137	477,285	99,876

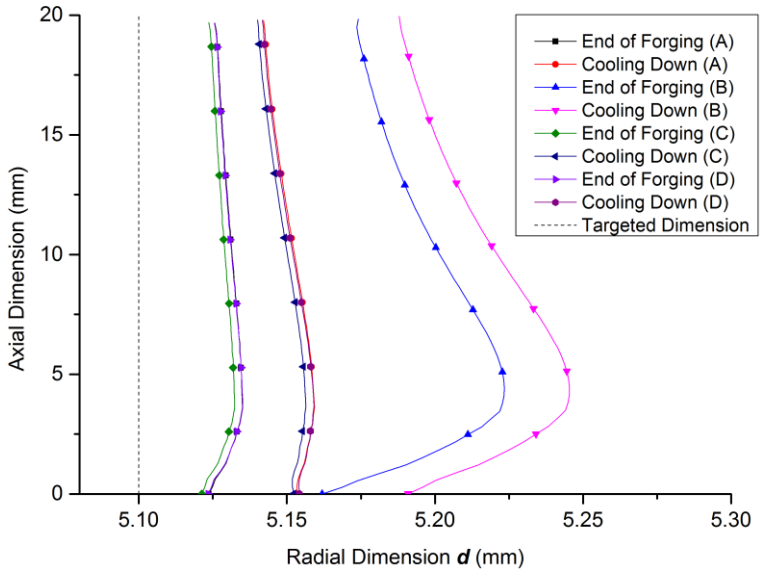

Fig. 5-21: Illustration of dimension errors in section d for tool materials (refers to Table 5-1).

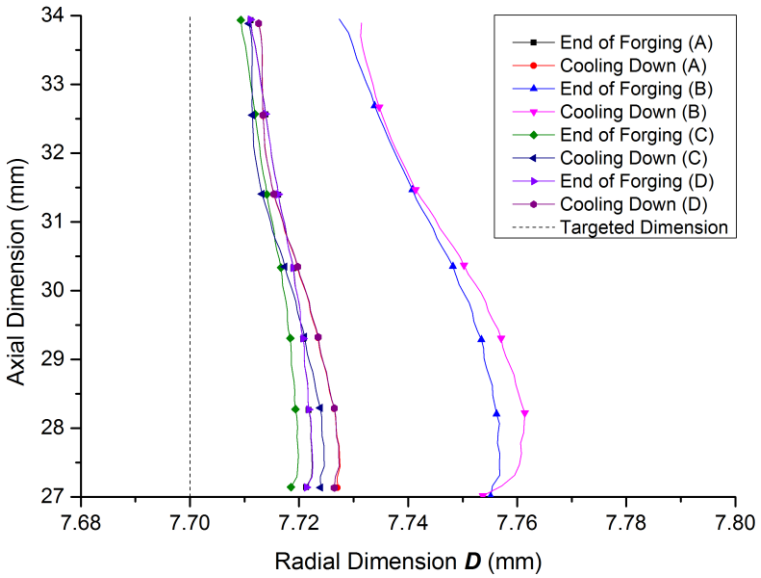

Fig. 5-22: Illustration of dimension errors in section D for tool materials (refers to Table 5-1).

5.4.5.2 Tool Geometry

With using different die insert geometries, the grain flow line in components generate corresponding change. The main change happens in the transition area which is highlighted in Fig. 5-23. As a result, the transition radius $\boldsymbol{R_1}$ shows less influence on grain flow. It makes the group A and group D (refer to Table 5-2) to present similar line distribution. For $\boldsymbol{R_2}$, the increasing radius improves the smothness of grain flow in group B which may improve the maximum tensile strength of the component. In view of transition radius ***SR***, the larger value has an adverse impact which expresses as more winding grain flow line in group C.

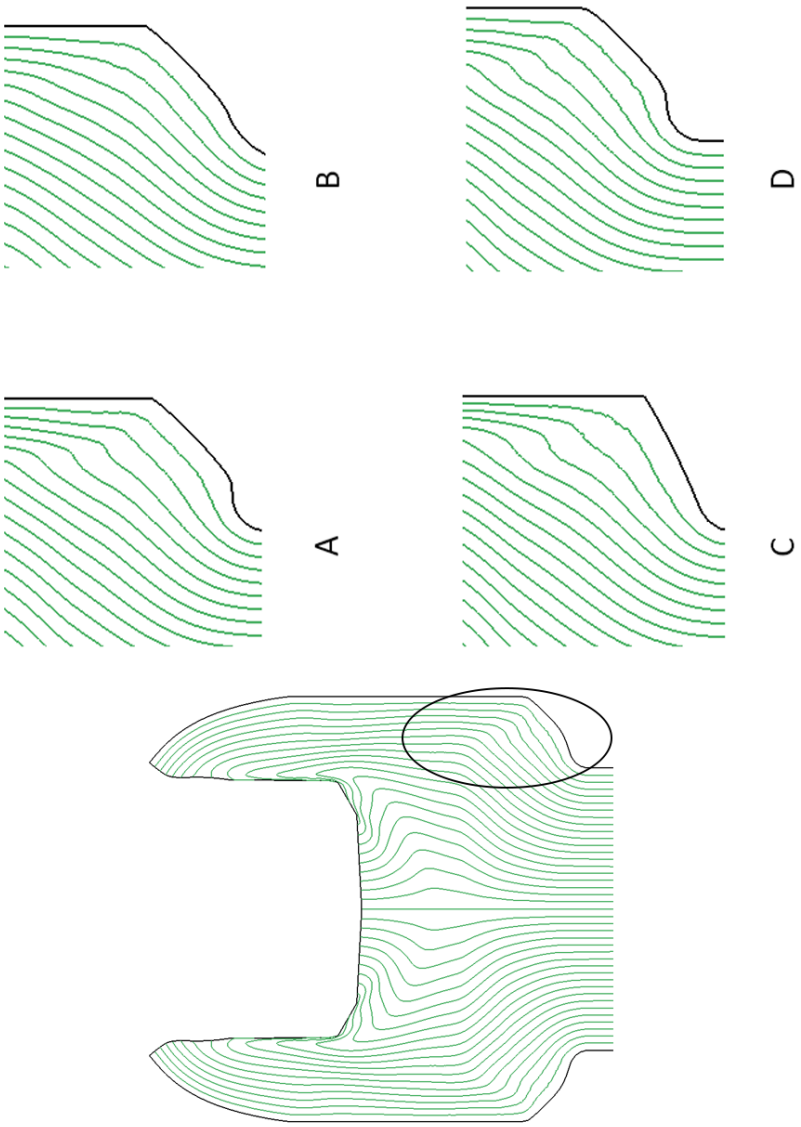

Fig. 5-23: Grain flow line in different die inserts geometries (refer to Table 5-2).

5.4.5.3 Tool Structure

Fig. 5-24 and Fig. 5-25 present the 2D profile of component in section ***D*** and ***d***. The detail value of dimension errors is concluded by mean errors in Table 5-18. From the results, the tool with pre-stressing shows slightly better forming accuracy in section ***D***. It reduces the final mean error from 0.05 mm to 0.049 mm. However, in section ***d***, there is no difference between the FE models with/without pre-stressing in the error distribution.

Table 5-17: The mean dimension errors under different pre-stressing.

Pre-stressing		Without pre-stressing	With pre-stressing
Mean Error $\bar{e}_D$ (mm)	End of Forging	0.017	0.018
	Cooling Down	0.021	0.020
Mean Error $\bar{e}_d$ (mm)	End of Forging	0.030	0.030
	Cooling Down	0.051	0.051

Unlike the forming accuracy, the pre-stressing plays an important role in tool life improvement. The die insert with pre-stressing shows great improvement in all reference elements, as shown in Table 5-18. It improves more than two times of forming cycles in element 1248 than that without pre-stressing reinforce. Therefore, for a good tool design, a suitable pre-stress is necessary. As for the tool wear, using pre-stressing on tools does not reduce the wear amount on die inserts. It is because the maximum normal load in the die inserts for both models are similar which are 59.49 kN and 57.89 kN for the tool with pre-stressing and tool without pre-stressing. Therefore, the wear amount for both tool structures are around 1:1.

Table 5-18: Estimated fatigue life of reference element under different pre-stressing.

Tool Life (cycles) / Tool Structure / Element	Without pre-stressing	With pre-stressing
1374	62,365	172,066
1214	226,832	759,561
1215	177,739	468,878
1251	102,307	265,302
1248	45,051	109,137

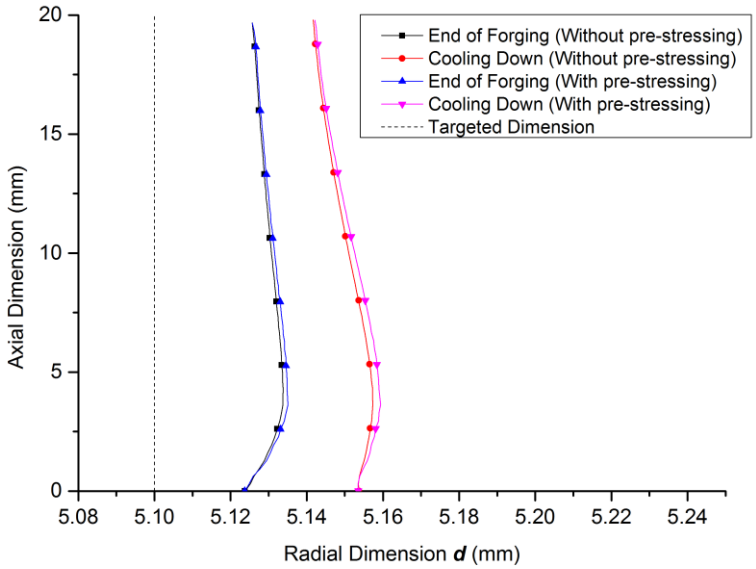

Fig. 5-24: Comparison of dimension error in section d under different pre-stressing.

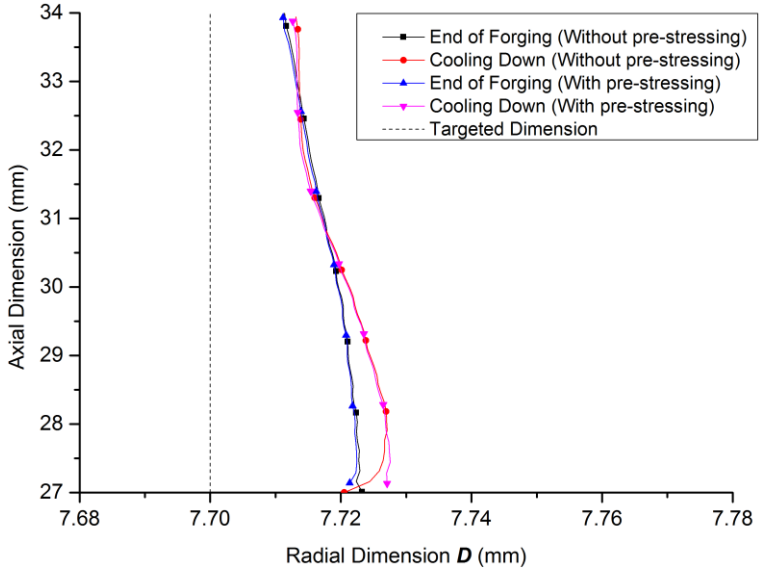

Fig. 5-25: Comparison of dimension errors in section D under different pre-stressing.

5.5 Summary

In this chapter, the influence of process parameters, tool parameters and workpiece parameters on tool life and component quality were investigated by FE simulation. Some conclusions can be drawn from the simulation results.

1) There is no doubt that the high forging speed increases the manufacturing efficiency. However, it brings lower forming accuracy in rod part of the bolt and higher forming temperature. The tool life is also reduced when increasing forging speed. The wear amount of each speed is not obvious in the simulations. It may suggest that the forging speed affects the tool wear slightly.

2) The low COF (workpiece/tool) enhances the metal flow which expresses as mild grain flow line. Meanwhile, the forming accuracy, fatigue life and wear amount also benefit from the low COF (workpiece/tool). However, reduction of COF (workpiece/tool) does not reduce the maximum forging temperature but the workpiece surface temperature is reduced. Increasing COF (die/die) does not constrain the slight movement between die insert.

3) Current tool cannot form the workpiece material with AISI 4340. High forging force introduces large forming errors, low fatigue life and high forging temperature. The wear amount of forging AISI 4340 is sixfold than forging aluminium. Under this condition, it is believed that the tool could fail in a few forging cycles.

4) The uneven end surface of the initial workpiece generates asymmetrical grain flow line distribution. The degree of asymmetry is influenced by the slant angle in the initial workpiece. If the slant angle exceeds a limited range this will affect the practical use of the bolt.

5) Changing the tool geometry shows results of the transition radius $\boldsymbol{R_1}$ that has less influence on grain flow, while the grain flow become more smooth with increasing the transition radius $\boldsymbol{R_2}$. As for $\boldsymbol{SR}$, the larger radius brings more bending flow line in component.

6) D2 is not suitable to be used as die insert material because it yields during the

forming process. However, D2 can replace the H13 as the shrink ring material. It provides high yield strength and similar Young's Modules as H13. Therefore, a tougher interference fit can be introduced. When the shrink ring and die inserts are made of tungsten carbide, the tools shows the best stiffness. It brings better forming accuracy and higher tool life.

7) For the tool structure, the pre-stressing shows less influence on the forming accuracy in section ***d*** and ***D***. This may suggest that increasing pre-stressing cannot improve the forming accuracy. However, in terms of tool life, a suitable pre-stressing is an important factor to ensure long tool life.

Chapter 6

Tool-Design Optimisation

6.1 Introduction

As shown in chapter 5, the tool parameter plays an important role in metal forging, including the tool life and component quality. Therefore, in this chapter, an optimisation was conducted in the tool design, including the die inserts, shrink ring and other parts. The optimisation focused on the tool structure. Through modifying the tool structure, a more stiff and reliable tool was obtained for injection forging. After the optimisation process, the new tools were verified by FE simulations on the forming errors and tool life.

6.2 Tool-Design Optimisation

Previous tool-design includes two die inserts, die insert 1 and die insert 2 (refer to Fig. A-1 (b)). Because of the simple geometry and low tool stress of die insert 2, the optimisation mainly focuses on die insert 1.

6.2.1 Die Inserts

In the forging process, the hoop stress contributes to the tool stress in die inserts. According to the simulations, the hoop stress reaches more than 1000 MPa in most cases at the end of the forging stroke. It is the main reason to cause the vertical crack in die inserts. Therefore, it is important to reduce the hoop stress in this tool optimisation. In the previous simulations, the pre-stressing shows effective influences on reducing the hoop stress. However, the amplitude is limited by the tool material so it cannot achieve satisfactory results. Therefore, it is better to use other methods when the tool materials cannot be changed. In this regards, die splitting in the vertical direction where hoop stress stays at peak value could provide a good inhibiting effect on hoop stresses. The design concept is showed in Fig. 6-1.

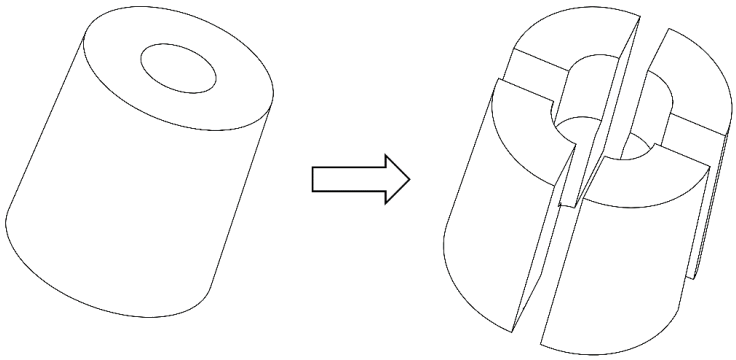

Fig. 6-1: Illustration of die inserts split in the vertical direction.

To prove it, a simple model is developed in ABAQUS. Fig. 6-2 shows the hoop stress in the die insert under 2000 MPa stress before/after optimisation. In the simulations, 2000 MPa load was applied in the die chamber uniformly. The boundary condition for both models is similar. The results show that the benefit from this modification is evident. The maximum hoop stress in the integrated die insert reaches to 1300 MPa, while it is only 200 MPa in separated die insert. Therefore, when splitting the die insert in the vertical direction, the hoop stress can have a considerable drop.

However, this modification also brings some side-effects. Firstly, it makes tool-making more complicated. It cannot just separate the finishing die insert into specified value pieces by wire-electrode cutting (WEC). It is because the WEC causes the finishing surface to be rough and reduces the machining accuracy. Therefore, the WEC needs to be carried out in the early stage of the machining process. After it, each piece needs to be machined carefully to meet high precision level. Therefore, it increases the cost of tool making. Secondly, it increases the risk of slight movement with increasing number of die inserts. It may cause some forming defects e.g. the marks on the component surface. To prevent it, some locating holes must be arranged in the die insert to fix them well in the right position. There is no doubt that it increases the processing difficulty further. Last but not least, if the assembly force cannot hold the separated die inserts together, the gap could grow between the interfaces between die inserts. In this situation, the material can leak through this gap which causes a surface defect and unreliable component size. Hence, the number of dies split should be controlled carefully to reduce the tool-making process. Also, when using this design, the shrink ring material should be

tough enough to hold the die inserts together.

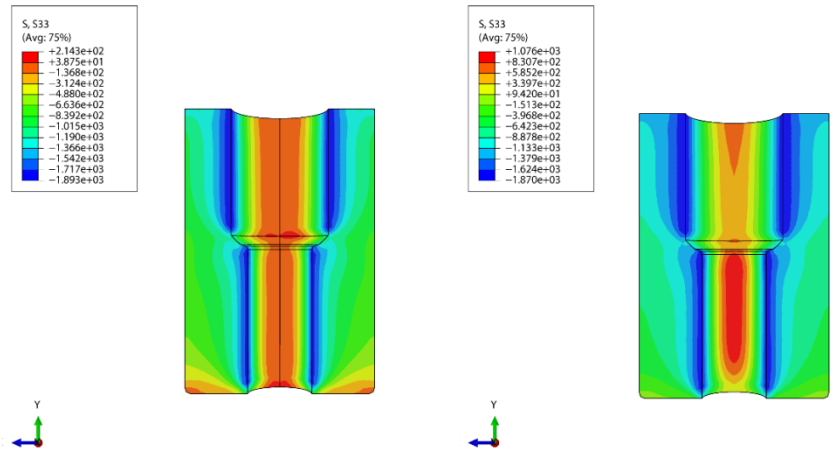

(a) *(b)*

Fig. 6-2: Hoop stress (MPa) distribution in the die inserts: (a) after splitting, (b) before splitting.

An optimisation is proposed for the die inserts shape. In the current tool design, the shape of die inserts is a cylinder which has some hidden limitations. Firstly, the cylinder is hard to assembly in practice production. It is because the mating relationship between the shrink ring and die inserts is an interference fit. Therefore, the industries have to use hot assembly which complicates the assembly process. Secondly, the cylinder shape die inserts may separate from the shrink ring in the ejection process. It is because the ejection force is very large resulting from the workpiece being embedded in the die chamber. This ejection force converts to a corresponding force in the die inserts. When this force is higher than the assembly force from shrink ring, the die inserts may be pushed out from the shrink ring. It is dangerous in high-speed production which may break the forging machine or injure the worker. To prevent these factors, the external shape of die insert is suggested to modify the cone shape. In this design, the assembly can be carried out at room temperature and the die insert is impossible to be ejected.

Moreover, the cone die insert can provide stronger pre-stressing. Fig. 6-3 shows the stresses distribution in die inserts after assembly. The results show that the die inserts with cone shape can intensify the pre-stressing further than traditional die inserts in the same level magnitude of interference. Higher compressive stress is introduced to the hoop direction which is the critical direction for injection forging. Therefore, the

cone shape could be helpful for tool life extension.

As for the material of die inserts, although the tungsten carbide is sensitive to the tensile stress, it is still the best choice because of its outstanding strength and hardness. Perhaps some materials with good ductility may improve the tensile stress resistance. However, the increase of the ductility of die inserts can cause the reduction. In other words, the die deflection could increase which in turns to increase the forming errors. Therefore, it is important to pay attention when changing the die insert materials.

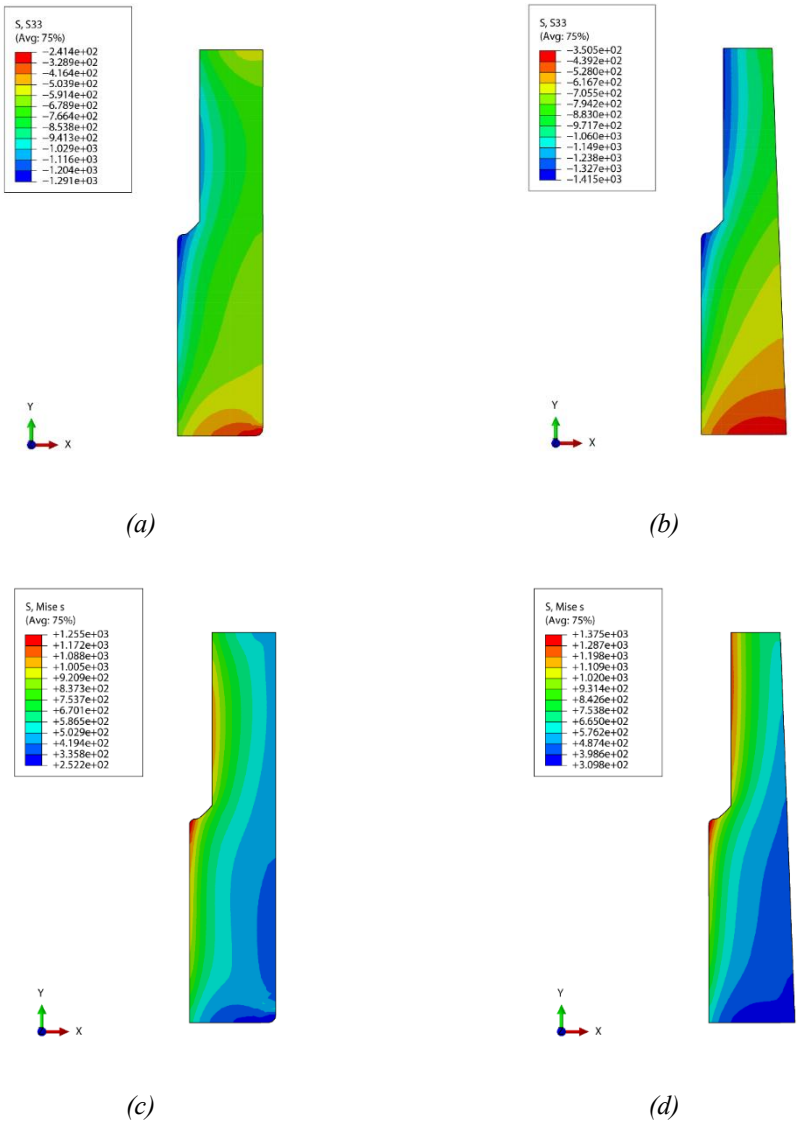

Fig. 6-3: Stress (MPa) distribution in die inserts: (a) Hoop stress cylinder, (b) Hoop stress cone, (c) Effective stress cylinder, (d) Effective stress cone.

6.2.2 Shrink Ring

The current material used for the shrink ring is H13. From the simulations, the shrink ring may yield during the forging of hard material. However, in practice, the yield may not happen. It is because the H13 can reach around 1650 MPa after quenching [171], while the used yield stress in simulation is set as 1300 MPa [99]. Therefore, when using H13 with a lower yield stress, the D2 tool steel is suggested to replace it as results of higher yield stress. However, when using H13 with a high yield stress, the H13 is still an ideal shrink ring material compared to D2 tool steel. It is because the slightly higher Young's modulus of H13 can provide higher stiffness. For the tungsten carbide, it can bring extra high pre-stressing and good tool stiffness when it is used for shrink ring. However, the cost of tungsten carbide and the machining difficulty hamper its application in industries.

Besides the shrink ring material, the configuration of the shrink ring also needs to be considered. The pre-stressing from single shrink ring is limited. It is subjected to the material and structure. Therefore, it is suggested to use a double shrink ring (refer to Fig. 6-4) when higher pre-stressing is required.

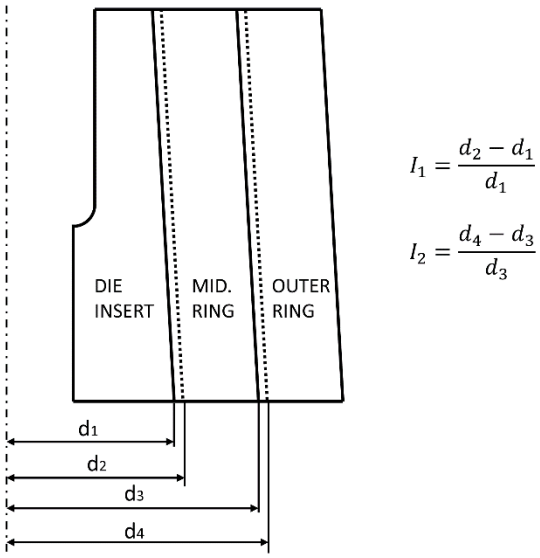

Fig. 6-4: Illustration of tool configuration with double shrink ring

When using the double shrink ring configuration, the magnitude of interference needs to be considered. There are two interference fits, including I_1 (die inserts,

middle shrink ring) and I_2 (die inserts, outer shrink ring). To get the optimisation magnitude of interference for double shrink ring. A series of FE models were conducted in ABAQUS. Both shrink rings were made of D2 tool steel. The results of simulations are showed in Fig. 6-5. According to the simulations, the effective stress in the die insert increases with the amplitude of interference. It brings benefits to the die insert in hoop stress and mean stress which expressed as higher compressive stress. Therefore, it is better to keep the amplitude of interference at a high level for the die insert.

However, the high amplitude of interference also causes two issues. Firstly, it is hard to assemble the tools. Secondly, for the shrink ring, the large amplitude of interference brings positive hoop stress and mean stress, especially for the outer ring. In the highest amplitude of interference, the shrink ring could yield quickly during the forming process. Therefore, the amplitude of interference should keep in a reasonable range. Regarding these issues, the magnitude of interference is set as 0.5%+0.3% (I_1+I_2) for the new tool design.

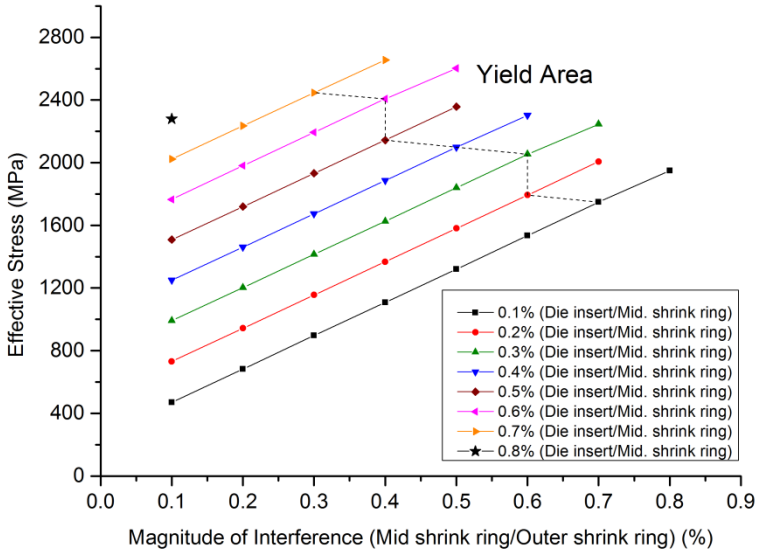

Fig. 6-5: Magnitude of interference for double shrink ring.

Due to applying the cone die insert design, the current shrink ring with two die inserts is unavailable to use because of the assembly problem. In addition, using a shrink ring has some limitations, e.g. stress concentration in the transition positions. It means the amplitude of pre-stressing is limited in this area. In other words, the pre-

stressing could be higher if the stress distribution is even. Hence, it is better to use corresponding values of shrink rings to replace the integrated one. It can make the interference design more flexible.

To reduce the “slight movement” between die inserts, it is suggested that the contact interference between each shrink ring is modified. More specifically, the current contact between shrink rings is in full contact. In order to increase the pressure between shrink rings, the contact method can be changed to local contact. It can resist the pressure from die inserts, and prevent the “slight movement”. Besides this, it also can reduce the movement by introducing the slight interference fit in the vertical direction. In this way, it can increase the holding force between die inserts.

6.2.3 Other Parts

As mentioned in Chapter 4, the air/oil outlet is not covered in current tool design. It brings some problems for production. Firstly, because of the existence of air, it is difficult to assemble each part together. Secondly, due to no air/oil outlet, the lubricant in the die chamber has no space to escape. Therefore, the residual lubricant will block the forming process.

6.3 FE Verification of the Tool Design

Based on the optimisation, a modified geometry model is built in ABAQUS, as shown in Fig. 6-6. By using this model, it intends to examine the new tool structure and analyse the forming errors. The boundary conditions refer to the reference group in chapter 5.

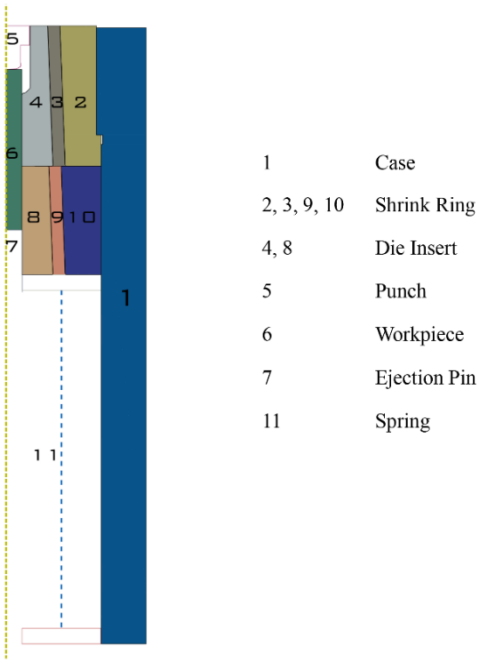

Fig. 6-6: Optimised FE model for Injection Forging.

The dimension errors of the component in section ***d*** and ***D*** are shown in Fig. 6-7 and Fig. 6-8. By using the new tool structure, the forming accuracy in section ***d*** is improved. The mean error reduces to 0.044 mm after cooling down. In section ***D***, the forming errors also have a slight decrease from 0.020 mm to 0.019 mm by using the new tool design.

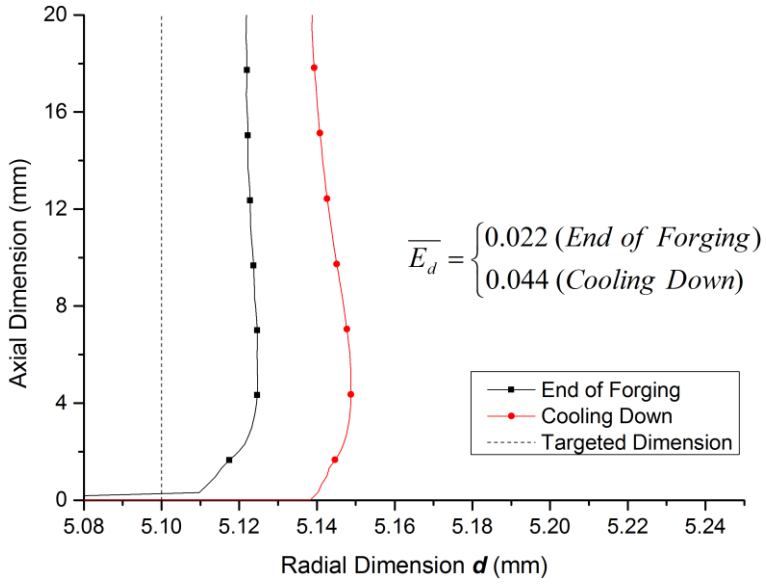

Fig. 6-7: The 2D profile of components in section d.

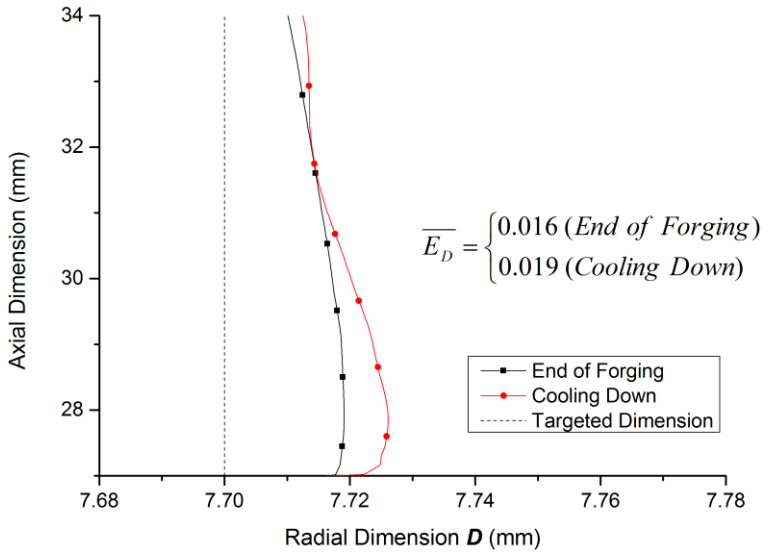

Fig. 6-8: The 2D profile of components in section D.

Table 6-1 shows the predicted fatigue life in a reference element for the die insert. The results show that the tool life has a significant improvement after using the new tool structure. The minimum tool life in 1248 increases by around six times that of the original design.

Table 6-1: Predicted fatigue life of the die insert.

Tool Life (cycles) / Forging Tool / Element	Before optimization	After optimization
1374	172,066	2,808,886
1214	759,561	231,818,660
1215	468,878	6,530,251
1251	265,302	711,789
1248	109,137	664,073

6.4 Summary

In this chapter, the re-designed tool structure was examined by FE simulations. For the tool optimisation, some suggestions have been proposed for the die insert and shrink ring. Firstly, the die split in the vertical direction does release the hoop stress in the die insert significantly. However, it brings some issues such as a complex tool-

making process and more severe slight movement between die inserts. Therefore, it should be applied to this design carefully. Secondly, the higher pre-stressing was introduced by the cone design of die insert and multi shrink rings. After simulation, the optimal amplitude of interference fit between die insert and shrink rings was 0.5%+0.3%.

For the tool material, the die insert still uses tungsten carbide because of its outstanding hardness, strength and toughness, while the D2 tool steel replaces the H13 tool steel as the material for the shrink ring. It is because of its higher yield strength which allows a higher interference fit.

In the FE simulation, the new tool design was analysed in term of tool life and forming accuracy. It showed that the fatigue life in die insert has a big increase which is around 600,000 cycles, while the original design is limited to 100,000 cycles. For the forming accuracy, the dimensional errors were reduced in section ***d***, whereas a slight change took place in section ***D***.

Chapter 7

Conclusions and Recommendations for Future Work

7.1 Conclusions

7.1.1 General Conclusions

The potential of injection forging in fastener production has been investigated in this study which consisted of four main parts: 1) a comparitive study of injection forging and multistep forging based on FE simulations, 2) experimental evaluation of the injection forging concerning the component behaviour and lubricant, 3) FE simulation of the influence of process parameters on tool life and component quality, 4) optimization of tool design. This research presented a method of using injection forging and its limitations, which met the aims and objects in the introduction.

The purpose of a comparison study is to identify merits and drawbacks of injection forging, compared with the conventional multistep forging. Based on the FE simulations, it was found that injection forging required less energy but a higher forming force to form the bolt. Due to the great tool stresses, higher forming errors were introduced in the component which were around two times more than for multistep forging in sections ***D*** and ***d***. In the same section, however, the underlying fold was not an issue for injection forging because of the different metal flow. This metal flow also brought a drawback for injection forging in the grain flow line which was more bending. It may reduce the tensile strength and shear strength of components.

To validate and develop the FE models, many experiments were carried out. The coefficient of friction was obtained by the ring test with ISO 68 forging oil, ISO 100 forging oil and MoS_2 grease. The forging force was monitored and recorded. The component behaviour such as dimensional accuracy, hardness distribution and grain flow line was tested. The results suggested that it was necessary to plan the oil outlet for tools in vertical forging. Because the oil blocked the forming process, the MoS_2 grease showed better forming accuracy. However, considering the better force

reduction and grain flow line, it was assumed that the ISO 68 oil might be more suitable in practice. Meanwhile, the manufacturing trials were carried in industry with different forging speeds. The high speed brought high forging force. It also damaged the ejection pin and the phosphating coating in the workpiece. Therefore, tougher ejection pin material and coating should be used in the high speed forging. Through comparing the results from FE simulations and experiments, the accuracy of FE model was confirmed. Some suggestions, including mesh plan, material model, thermal issues, etc. were proposed for developing FE models.

Based on the developed models, the influence of three groups of parameters, including process parameters (forging speed, friction condition between tool/workpiece and friction condition between tool/tool), workpiece parameters (workpiece material and workpiece geometry) and tool parameters (tool structure, tool materials and tool geometry), on tool life and component quality was investigated. It was found that the improved process parameters, i.e. lower forging speed and COF (tool-workpiece) benefited the tool life and component accuracy. In addition to this, the lower COF (tool-workpiece) could refine the grain flow line in the component. The COF between tool/tool showed less influence on the component accuracy.

The study on the workpiece parameters showed that it was hard to forge the tough material AISI 4340. It introduced great tool stresses which deteriorated tool life and intensified the forming errors. The uneven workpiece end surface caused uneven material flow. It showed as a deflected grain flow line which was hazardous for the production operation.

Research on the tool parameters found that the pre-stressing was important for fatigue life improvement, but showed less effect on wear life, grain flow line and component accuracy. To improve the pre-stressing in die inserts, the shrink ring material H13 could be replaced by tungsten carbide or D2 tool steel. On the other hand, with increasing the transition radius $\boldsymbol{R_2}$, the grain flow line was improved.

To optimise the tool design, some suggestions were proposed for the die inserts, shrink ring and other parts. Based on the FE simulations, the optimised tools were examined with regard to tool life and forming accuracy. It showed that the new tools have improved fatigue life and better forming accuracy.

7.1.2 Contribution to Knowledge and Industries

- Relatively comprehensive FE models have been developed in ABAQUS and DEFORM to simulate the forging force, tool deflection, temperature distribution, springback, grain flow, etc. in automotive fastener production. Based on a series of experiments, the accuracy of FE models is analysed. Through using these models, costly physical experiments can be avoided.

- A procedure of comparing the forging processes in automotive fasteners production has been proposed. It covers the forging force, forming errors, tool stress and grain flow line of the component which are important parameters for fasteners industries. Through analysing these parameters, it reveals the characteristics of injection forging process and traditional forging process.

- For automotive fasteners production, the influence of process parameters, tool parameters and workpiece parameters on tool life and component quality have been systematically studied. It provides a guide for fasteners industries to evaluate each process parameter. Depending on the weight of parameters, some detailed optimisations have been carried out on tool structure. After optimization, the service life of tool has a nearly six times increase.

7.2 Recommendations for Future Work

Based on the research conducted in this study, the following recommendations for future work are given:

1) *Material data*. There are some limitations for the material model used in this study. Firstly, the plastic strain in injection forging is large and reaches around 3.6. For the normal material test, the test range cannot cover it. Therefore, the FE results were not able to show the right value of the stress in the workpiece when the strain exceeds the test range. Secondly, in thermal analysis, the thermal softening of the workpiece material was not covered in this study fully, due to incompleteness of the material data under the condition of thermal loading. Therefore, it makes the force predicted in FE simulation rather higher than that obtained from the experiment. To make the simulation more accurate, a more comprehensive set of the material data will have to be obtained.

2) *Cost model*. The injection forging shortens the forging process, but the tool stresses are more severe. In order to overcome the tool stress, a more sophisticated tool structure may have to be introduced. However, even with higher stiffness, the tool life of injection forging still is a challenge. Therefore, from an economical perspective, it is necessary to introduce a cost model to assess the injection forging and multistep forging when these are considered in industry.

3) *Experiment.* Although a series of experiments have been conducted in this study, some issues were not addressed fully, e.g. the strain sustained in the tool components was not measured in-process, and more workpiece materials and component shapes need to be tested in order to define the process limits of injection forging comprehensively.

4) *FE modelling.* Analysis of the component accuracy on the work was based on single-process forging. However, in practical production, the tools usually experience thousands of forging cycles. Indeed, there are some changes in tools after many forging-cycles, e.g. does the pre-stressing stay at the similar level after the tools have been used? Therefore, in the future, the influences of forging cycles on the tools and products should be considered.

5) *Tool design.* Although some optimised designs have already been proposed for forging tools, there is still a space for improving the tool design further. For example, how to optimise the pre-stressing distribution in the die insert is aspect that could be studied further. Currently, the pre-stressing focused on the shoulder of the die inserts. However, the simulation results show that the maximum effective stress is located at the bottom part of die chamber. Therefore, more pre-stressing should be introduced to this section. There are two concepts, as shown in Fig. 7-1.

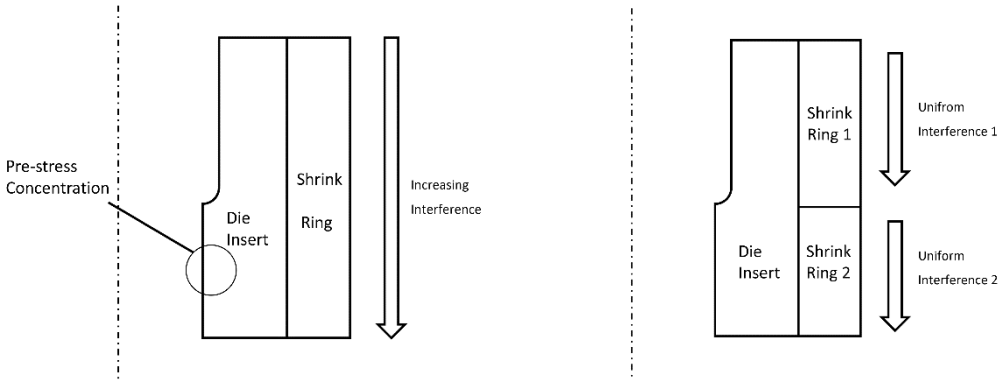

(a) *(b)*

Fig. 7-1: A proposed interference fit design: (a) single shrink ring, (b) multi shrink rings.

The first concept is based on the use of a single shrink ring. In the current design, the interference value is uniform. It could be possible to change the pre-stressing distribution by using a variable interference. In this way, an intensive pre-stressing in the specified area could be obtained. Another approach is based on the use of multistep shrink rings. By using shrink rings with different interferences or different types of materials, the pre-stressing could be achieved to meet the requirements for different reinforcements.

List of References

[1] K. Lange, *Handbook of Metal Forming*. New York: McGraw-Hill, 1985.

[2] K. Lange, "Cost Minimization in Small Quantity Production of Stepped Shafts by Combined NC-Radial Forging and NC-Turning. A New Approach to Flexible Manufacturing Systems," *CIRP Annals - Manufacturing Technology*, vol. 34, no. 2, pp. 549–555, Jan. 1985.

[3] T. Takami, "Production Engineering Strategies and Metalworking at Toyota Motor Corporation," in *11th International Conference on Technology of Plasticity*, 2014, vol. 81, pp. 5–17.

[4] Southern Africa Stainless Steel Development Association, "Cold Forming of Stainless Steels." [Online]. Available: http://sassda.co.za/cold-forming-of-stainless-steels/. [Accessed: 09-Mar-2017].

[5] S. Semiatin, *ASM Handbook, Volume 14A: Metalworking: Bulk Forming*. Ohio: ASM International, 2005.

[6] Y. Yang, "Review of Development of Cold Extrusion Domestic and Abroad," *Metalforming Machinery*, vol. 1, 2001.

[7] J. Nowak, L. Madej, and S. Ziolkiewicz, "Recent Development in Orbital Forging Technology," *International Journal of Metal Forming*, pp. 387–390, 2008.

[8] P. Groche, D. Fritsche, and E. Tekkaya, "Incremental Bulk Metal Forming," *CIRP Annals - Manufacturing Technology*, vol. 56, no. 2, pp. 635–656, 2007.

[9] Li G., J. J.T., W. T. Wu, and S. I. Oh, "Recent Development and Applications of Three-Dimensional Finite Element Modelling in Bulk Forming Process," *Journal of Materials Processing Technology*, vol. 113, no. 1, pp. 40–45, 2001.

[10] Z. Marciniak and K. Shan, "Finite Element Analysis of Orbital Forming Used in Spindle/Inner Ring Assembly," in *Proceeding of the 8th International Conference on Technology of Plasticity*, 2005.

[11] H. Aluminium and D. Gmbh, "Aluminium in Innovative Light-Weight Car Design," *Materials Transactions*, vol. 52, no. 5, pp. 818–824, 2011.

[12] Y. Li, Z. Lin, A. Jiang, and G. Chen, “Use of High Strength Steel Sheet for Lightweight and Crashworthy Car Body,” *Material & Design*, vol. 24, pp. 177–182, 2003.

[13] A. E. Tekkaya, N. Ben Khalifa, G. Grzancic, and R. Hölker, “Forming of Lightweight Metal Components: Need for New Technologies,” in *Proceeding of the 11th International Conference on Technology of Plasticity*, 2014, vol. 81, pp. 28–37.

[14] R. Narayanasamy, K. Baskaran, and D. Muralikrishna, “Some Studies on Stresses and Strains of Aluminium Alloy During Extrusion-Forging at Room Temperature,” *Materials & Design*, vol. 29, no. 8, pp. 1623–1632, Jan. 2008.

[15] R. Narayanasamy, M. Ravi chandran, and N. L. Parthasarathi, “Effect of Annealing on Formability of Aluminium Grade 19000,” *Materials & Design*, vol. 29, no. 8, pp. 1633–1653, Jan. 2008.

[16] D.-C. Chen, S.-K. Syu, C.-H. Wu, and S.-K. Lin, “Investigation into Cold Extrusion of Aluminum Billets Using Three-Dimensional Finite Element Method,” *Journal of Materials Processing Technology*, vol. 192–193, pp. 188–193, Oct. 2007.

[17] F. Ozturk, S. Toros, and H. Pekel, “Evaluation of Tensile Behaviour of 5754 Aluminium–Magnesium Alloy at Cold and Warm Temperatures,” *Materials Science and Technology*, vol. 25, no. 7, pp. 919–924, Jul. 2009.

[18] D. Li and A. Ghosh, “Tensile Deformation Behavior of Aluminum Alloys at Warm Forming Temperatures,” *Materials Science and Engineering: A*, vol. 352, no. 1, pp. 279–286, Jul. 2003.

[19] P. Venugopal, S. Venugopal, and V. Seetharaman, “Influence of Strain Rate and Temperature on the Friction Factor of Commercialy Pure Titanium,” *Journal of Materials Processing Technology*, vol. 22, no. 1, pp. 91–97, 1990.

[20] Q. Zhao, G. Wu, and W. Sha, “Deformation of Titanium Alloy Ti–6Al–4V Under Dynamic Compression,” *Computational Materials Science*, vol. 50, no. 2, pp. 516–526, Dec. 2010.

[21] H. Yang, X. X. Fan, Z. Z. Sun, L. L. Guo, and M. Zhan, “Recent Developments

in Plastic Forming Technology of Titanium Alloys," *Science China Technological Sciences*, vol. 54, no. 2, pp. 490–501, Feb. 2011.

[22] H. W. Wagener and J. Wolf, "Cold forging of MMCs of Aluminium Alloy Matrix," *Journal of Materials Processing Technology*, vol. 37, no. 1, pp. 253–265, Feb. 1993.

[23] J. Skiba, W. Pachla, A. Mazur, and S. Przybysz, "Press for Hydrostatic Extrusion with Back-Pressure and the Properties of Thus Extruded Materials," *Journal of Materials Processing Technology*, vol. 214, no. 1, pp. 67–74, 2014.

[24] S. Suranuntchai, "Finite Element Modeling of Ceramics Particles Reinforced Aluminum Alloy Composites under Forward Extrusion," *Advanced Materials Research*, vol. 548, pp. 17–23, Jul. 2012.

[25] J. Jiang and B. Dodd, "Workability of Aluminium-Based Metal-Matrix Composites in Cold Compression," *Composites*, vol. 26, no. 1, pp. 62–66, 1995.

[26] K. Mori, S. Maki, and Y. Tanaka, "Warm and Hot Stamping of Ultra High Tensile Strength Steel Sheets Using Resistance Heating," *CIRP Annals - Manufacturing Technology*, vol. 54, no. 1, pp. 209–212, 2005.

[27] R. Balendra and Y. Qin, "Injection forging: Engineering and Research," *Journal of Materials Processing Technology*, vol. 145, no. 2, pp. 189–206, Jan. 2004.

[28] R. M. Cogan, "Hydrodynamic Compression Forging," General Electric Company, 1963.

[29] B. Parsons, P. R. Milner, and B. N. Cole, "Study of the Injection Upsetting of Metals," *Journal of Mechanical Engineering Science*, vol. 15, no. 6, pp. 410–421, 1973.

[30] K. Dieterle, "Determination of Operational Limits for the Upsetting of Tubes Blanks," *Industrie Anzeiger*, vol. 97, p. 1653, 1975.

[31] J. C. Hendry and M. T. Watkins, "The Prodcution of Hollow Flanged Components from Bar Stock by Upsetting and Extrusion," National Engineering Laboratory Report 628, 1977.

[32] R. Balendra and Y. Qin, "Material-flow Considerations for the Design of Injection Forging," *Journal of Manufacturing Science and Engineering*, vol.

119, no. 3, pp. 350–357, 1997.

[33] R. Balendra and Y. Qin, “Identification and Classication of Flow-Dependent Defects in the Injection Forging of Solid Billets,” *Journal of Materials Processing Technology*, vol. 106, pp. 199–203, 2000.

[34] Y. Qin and R. Balendra, “Computer-Aided Design of Nett-Forming by Injection Forging of Engineering Components,” *Journal of Materials Processing Technology*, vol. 76, no. 1, pp. 62–68, Apr. 1998.

[35] R. Balendra and Y. Qin, “Pressured-Assisted Injection Forging of Thick-Walled Tubes,” *International Journal of Machine Tools and Manufacture*, vol. 35, no. 11, pp. 1481–1492, 1995.

[36] Y. Qin, Y. Ma, and R. Balendra, “Pressurising Materials and Process Design Considerations of the Pressure-Assisted Injection Forging of Thick-Walled Tubular Components,” *Journal of Materials Processing Technology*, vol. 150, no. 1, pp. 30–39, Jul. 2004.

[37] Y. Qin and R. Balendra, “Optimisation of the Lubrication for the Extrusion of Solid and Tubular Components by Injection Forging,” *Journal of Materials Processing Technology*, vol. 135, pp. 219–227, 2003.

[38] Y. Ma, Y. Qin, and R. Balendra, “Forming of Hollow Gear-Shafts with Pressure-Assisted Injection Forging (PAIF),” *Journal of Materials Processing Technology*, vol. 167, no. 2, pp. 294–301, 2005.

[39] L. M. Alves and P. a. Martins, “Injection Forging of Solid Asymmetric Branched Components,” *Proceedings of the Institution of Mechanical Engineers, Part B: Journal of Engineering Manufacture*, vol. 227, no. 6, pp. 898–907, 2013.

[40] M. Plan, M. Rosochowska, and P. Skakun, “Radial Extrusion of Gear Like Components – Numerical Analysis,” *Technical Gazette*, vol. 20, no. 5, pp. 891–896, 2013.

[41] J. . Choi and Y. Choi, “Precision Forging of Spur Gears with Inside Relief,” *International Journal of Machine Tools and Manufacture*, vol. 39, no. 10, pp. 1575–1588, Oct. 1999.

[42] R. Balendra, “Exit-Geometry for Injection Forming,” in *Proceeding of 4th International Conference on Manufacturing Engineering 1988: Preprints of Paper*, 1988, pp. 11–17.

[43] R. Balendra, “Process Mechanics of Injection Upsetting,” *International Journal of Machine Tool Design and Research*, vol. 85, no. 1, pp. 63–73, 1985.

[44] W. Schatzle, “Transverse Extrusion of a Collar on Solid Steel Bodies,” *Wire*, vol. 34, no. 2, pp. 71–74, 1984.

[45] Y. Qin and R. Balendra, “An Approach for the Forming of Large-Thickness-Flange Components by Injection Forging,” *Journal of Materials Processing Technology*, vol. 145, no. 2, pp. 153–162, Jan. 2004.

[46] S. Petersen, J. Rodrigues, and P. Martins, “Production of Tubular Components by Radial Extrusion—a Finite Element Analysis,” *Journal of Materials Processing Technology*, vol. 45, no. 1–4, pp. 87–92, 1994.

[47] W. Osen, “Variations of the Transverse Impact Extrusion Process,” *Wire*, vol. 35, pp. 109–113, 1985.

[48] B. Andersen and C. B. Andersen, “Radial Extrusion of Tubular Components (Ph.D. Thesis),” University of Strathclyde and Technical University of Denmark, 1991.

[49] M. Arentoft and S. Petersen, “Review of Research into the Injection Forging of Tubular Materials,” *Journal of Materials Processing Technology*, vol. 52, no. 2–4, pp. 460–471, 1995.

[50] W. Osen and K. Lange, “Deformation Pattern, Forces and Process Limits in Combined Radial and Backward Can Extrusion,” *Steel Research International*, vol. 56, no. 4, pp. 221–224, 1985.

[51] B. Lengyel, S. Shahmoradi, and I. Chaudhry, “Cold Extrusion of Flanges on Cylindrical Hollows,” in *Proceedings of the 30th International MATADOR Conference*, 1993, pp. 227–234.

[52] S. Petersen and J. Rodrigues, “Injection Forging of Tubular Materials: a Workability Analysis,” *Journal of Materials Processing Technology*, vol. 65, no. 1–3, pp. 88–93, 1997.

[53] J. Walters, “Troubleshooting Cold Heading Die Failures,” *Wire Journal International*, vol. 1, pp. 62–66, 2004.

[54] J. Domblesky, “Analysis of Die Failures in Cold Heading Using Finite Element Simulation,” *Wire Journal International*, vol. 34, no. 8, pp. 82–88, 2001.

[55] K. Lange, L. Cser, M. Geiger, and J. Kals, “Tool Life and Tool Quality in Bulk Metal Forming,” *CIRP Annals - Manufacturing Technology*, vol. 41, no. 2, pp. 667–675, 1992.

[56] M. Gierzynska, “Effect of the Surface Layer in Increasing the Life of Tools for Plastic Working,” *Journal of Mechanical Working Technology*, vol. 6, no. 2–3, pp. 193–204, 1982.

[57] M. W. Fu, M. S. Yong, and T. Muramatsu, “Die Fatigue Life Design and Assessment via CAE Simulation,” *The International Journal of Advanced Manufacturing Technology*, vol. 35, no. 9–10, pp. 843–851, Nov. 2006.

[58] M. T. Fu MW, Yong MS, Tong KK, “A Methodology for Evaluation of Metal Forming System Design and Performance via CAE Simulation,” *International Journal of Production Research*, vol. 44, no. 6, pp. 1075–1092, 2006.

[59] M. Knoerr, K. Lange, and T. Altan, “Fatigue Failure of Cold Forging Tooling: Causes and Possible Solutions Through Fatigue Analysis,” *Journal of Materials Processing Technology*, vol. 46, no. 1–2, pp. 57–71, 1994.

[60] S. Suresh, *Fatigue of Materials*. Cambridge University Press, 1998.

[61] J. Goodman, *Mechanics Applied to Engineering*. Longmans, Green, 1918.

[62] C. Soderberg, “Factor of Safety and Working Stress,” *ASME Transaction*, vol. 52, no. 2, pp. 13–28, 1930.

[63] W. Gerber, “Bestimmung der Zulassigen Eisen Construction,” *Z. Bayer Arcb. Ing*, vol. 6, pp. 101–110, 1874.

[64] J. Morrow, “Fatigue Properties of Metals,” in *Fatigue Design Handbook*, 1968.

[65] N. E. Dowling, “Mean Stress Effects in Stress-Life and Strain-Life Fatigue,” *SAE Technical Paper*, Apr. 2004.

[66] S. S. Akhtar and a. F. M. Arif, “Fatigue Failure of Extrusion Dies: Effect of

Process Parameters and Design Features on Die Life," *Journal of Failure Analysis and Prevention*, vol. 10, no. 1, pp. 38–49, Nov. 2009.

[67] K. Dehghani and A. Jafari, "Finite Element Stress Analysis of Forging Dies to Improve Their Fatigue Life," *Materials Science-Poland*, vol. 28, no. 1, 2010.

[68] M. a. Saroosh, H.-C. Lee, Y.-T. Im, S.-W. Choi, and D.-L. Lee, "High Cycle Fatigue Life Prediction of Cold Forging Tools Based on Workpiece Material Property," *Journal of Materials Processing Technology*, vol. 191, no. 1–3, pp. 178–181, Aug. 2007.

[69] C. L.F., "A Study of the Effects of Cyclic Thermal Stresses on a Ductile Metal," *ASME*, vol. 76, pp. 931–950, 1954.

[70] M. Jodean, "Cyclic Plastic Strain Energy and Fatigue of Metals," *ASTM International*, pp. 45–87, 1965.

[71] B. Falk, U. Engel, and M. Geiger, "Estimation of Tool Life in Bulk Metal Forming Based on Different Failure Concepts," *Journal of Materials Processing Technology*, vol. 80–81, pp. 602–607, Aug. 1998.

[72] M. Geiger, M. Hänsel, T. Rebhan, M. Hansel, and T. Rebhan, "Improving the Fatigue Resistance of Cold Forging Tools by FE Simulation and Computer Aided Die Shape Optimization," *Proceedings of the Institution of Mechanical Engineers, Part B: Journal of Engineering Manufacture*, vol. 206, no. 2, pp. 143–150, 1992.

[73] Y.-C. Y. Lee and F.-K. F. Chen, "Fatigue Life of Cold-Forging Dies with Various Values of Hardness," *Journal of Materials Processing Technology*, vol. 113, no. 1–3, pp. 539–543, Jun. 2001.

[74] P. Paris and F. Erdogan, "A Critical Analysis of Crack Propagation Laws," *ASME*, pp. 528–534, 1963.

[75] S. Vethe, "Numerical Simulation of Fatigue Crack Growth (Master Thesis)," Norwegian University of Science and Technology, 2012.

[76] J. H. Melson, R. L. West, N. E. Dowling, and J. M. Kennedy, "Fatigue Crack Growth Analysis with Finite Element Methods and a Monte Carlo Simulation," Virginia Tech, 2014.

[77] P. J. G. Schreurs, “Fracture Mechanics (lecture notes),” 2012.

[78] K. Walker, “The Effects of Stress Ratio During Crack Propagation and Fatigue for 2024-T3 and 7075-T6 Aluminum,” in *Effects of Environment and Complex Load History on Fatigue Life*, ASTM International, 1970, pp. 1–14.

[79] R. Forman, V. Kearney, and R. Engle, “Numerical Analysis of Crack Propagation in Cyclic-Loaded Structures,” *Journal of Basic Engineering*, vol. 89, pp. 459–463, 1967.

[80] G. Lee and Y. Im, “Finite-Element Investigation of the Wear and Elastic Deformation of Dies in Metal Forming,” *Journal of materials processing technology*, vol. 90, pp. 123–127, 1999.

[81] M. Sadeghi and T. Dean, “Analysis of Ejection in Precision Forging,” *International Journal of Machine Tools and Manufacture*, vol. 30, no. 4, pp. 509–519, 1990.

[82] J. F. Archard, “Contact and Rubbing of Flat Surface,” *Journal of Applied Physics*, vol. 24, no. 8, p. 981, 1953.

[83] J. H. Kang, I. W. Park, J. S. Jae, and S. S. Kang, “A Study on a Die Wear Model Considering Thermal Softening: (I) Construction of the Wear Model,” *Journal of Materials Processing Technology*, vol. 96, no. 1–3, pp. 53–58, Nov. 1999.

[84] R. . Lee and J. . Jou, “Application of Numerical Simulation for Wear Analysis of Warm Forging Die,” *Journal of Materials Processing Technology*, vol. 140, no. 1–3, pp. 43–48, Sep. 2003.

[85] H. C. Lee, Y. Lee, S. Y. Lee, S. Choi, D. L. Lee, and Y. T. Im, “Tool Life Prediction for the Bolt Forming Process Based on High-Cycle Fatigue and Wear,” *Journal of Materials Processing Technology*, vol. 201, no. 1–3, pp. 348–353, May 2008.

[86] T. Sobis, U. Engel, and M. Geiger, “A Theoretical Study on Wear Simulation in Metal Forming Processes,” *Journal of Materials Processing Technology*, vol. 34, no. 1–4, pp. 233–240, Sep. 1992.

[87] V. Vazquez, D. Hannan, and T. Altan, “Tool Life in Cold Forging – an Example of Design Improvement to Increase Service Life,” *Journal of Materials*

Processing Technology, vol. 98, no. 1, pp. 90–96, Jan. 2000.

[88] N. E. Dowling, *Mechanical Behaviour of Materials: Engineering Methods for Deformation, Fracture, and Fatigue*, 2nd ed. A Wiley-Interscience Publication, 2001.

[89] J. S. Jin, J. C. Xia, X. Y. Wang, and H. Liu, "Failure Analysis of a Die for Cold Precision Forging of Bevel Gears," *Advanced Materials Research*, vol. 44–46, pp. 779–786, 2008.

[90] K. Ohga and K. Kondo, "Research on Precision Die Forging Utilizing Divided Flow (First Report, Theoretical Analysis of Processes Utilizing Flow Relief-Axis and Reliefe-Hole)," in *JSME 25*, 1982, pp. 1828–1835.

[91] K. Kondo and K. Ohga, "Precision Cold Die Forging of a Ring Gear by Divided Flow Method," *International Journal of Machine Tools and Manufacture*, vol. 35, no. 8, pp. 1105–1113, 1995.

[92] Y. Qin and R. Balendra, "FE Simulation for Development of Process Design Considerations-an Industry-Case Study," *International Journal of Manufacutring Science & Production*, vol. 5, pp. 73–77, 2003.

[93] M. Koç and M. a Arslan, "Design and Finite Element Analysis of Innovative Tooling Elements (Stress Pins) to Prolong Die Life and Improve Dimensional Tolerances in Precision Forming Processes," *Journal of Materials Processing Technology*, vol. 142, no. 3, pp. 773–785, Dec. 2003.

[94] K.-D. Hur, Y. Choi, and H.-T. Yeo, "Design for Stiffness Reinforce ment in Backward Extrusion Die," *Journal of Materials Processing Technology*, vol. 130–131, pp. 411–415, Dec. 2002.

[95] P. Skov-Hansen and N. Bay, "Fatigue in Cold-Forging Dies: Tool Life Analysis," *Journal of Materials Processing Technology*, vol. 95, no. 1, pp. 40–48, 1999.

[96] Y. Qin, "Forming-Tool Design Innovation and Intelligent Tool-Structure/System Concepts," *International Journal of Machine Tools and Manufacture*, vol. 46, no. 11, pp. 1253–1260, Sep. 2006.

[97] T. Altan and M. Deshpande, "Selection of Die Materials and Surface Treatments

for Increasing Die Life in Hot and Warm Forging," in *FIA Tech Conference*, 2011, pp. 1–32.

[98] J. Destefani, "Tool materials tackle tough task," *Tooling and Production*, pp. 54–57, 1994.

[99] H. T. Yeo, Y. Choi, and K. D. Hur, "Analysis and Design of the Prestressed Cold Extrusion Die," *The International Journal of Advanced Manufacturing Technology*, vol. 18, no. 1, pp. 54–61, Jul. 2001.

[100] Macsteel, "Soecial Steels Catalogue," *Macsteel*, 2005. [Online]. Available: http://www.macsteel.co.za/products/tool-die-steels. [Accessed: 18-May-2015].

[101] Steelexperss, "A2 Steel Properties," *Steel Express*, 2015. [Online]. Available: http://www.steelexpress.co.uk/toolsteel/A2-Steel-properties.html. [Accessed: 18-May-2015].

[102] Uddeholm, "Calmax," *Uddeholm*, 2015. [Online]. Available: http://www.bohler-uddeholm.co.za/media/calmax_english_04.pdf. [Accessed: 18-May-2015].

[103] P. Brøndsted and P. Skov-Hansen, "Fatigue Properties of High-Strength Materials Used in Cold-Forging Tools," *International Journal of Fatigue*, vol. 20, no. 5. pp. 373–381, 1998.

[104] CB-ceratizit, "CB-Ceratizit Standard Grades Sheet," *CB-ceratizit*, 2015. [Online]. Available: http://www.cbceratizit.com/zh/download/001cbct_grade_comparison_table_CN.pdf. [Accessed: 18-May-2015].

[105] West Yorkshire Steel, "High Speed Steel," *West Yorkshire Steel*, 2015. [Online]. Available: http://www.westyorkssteel.com/tool-steel/high-speed-steel/. [Accessed: 19-May-2015].

[106] O. A. Zeid and O. A. Abu Zeid, "On the Effect of Electrodischarge Machining Parameters on the Fatigue Life of AISI D6 Tool Steel," *Journal of Materials Processing Technology*, vol. 68, no. 1, pp. 27–32, 1997.

[107] Rajurkar, "Surface Damage and Shock Waves in EDM," in *1985 SME Manufacutruing Engineering Transactions and 13 th NAMRC North American*

Manufacturing Research, 1985, pp. 379–385.

[108] K.-K. Choi, W.-J. Nam, and Y.-S. Lee, "Effects of Heat Treatment on the Surface of a Die Steel STD11 Machined by W-EDM," *Journal of Materials Processing Technology*, vol. 201, no. 1–3, pp. 580–584, May 2008.

[109] H. H. Lim, L. C,; Lee, L. C,; Wong, Y. S,; Lu, "Solidification Microstructure of Discharge Machined Surfaces of Tool Steels," *Material Science and Technology*, vol. 7, pp. 239–248, 1991.

[110] H. T. Lee and T. Y. Tai, "Relationship Between EDM Parameters and Surface Crack Formation," *Journal of Materials Processing Technology*, vol. 142, no. 3, pp. 676–683, Dec. 2003.

[111] M. A. E. . Merdan and R. D. Arnell, "The Surface Integrity of a Die Steel After Electrodischarge Machining: I. Structure, Composition and Hardness," *Surface Engineering*, vol. 7, no. 2, pp. 158–164, 1989.

[112] Dorsch. C, "Eliminating the Negative Effects of EDM Through the Strategic Selection of Die Steels," in *Transcations: 16th International Die Casting Congress and Exposition*, 1991, pp. 253–263.

[113] T. Altan and G. Ngaile, *Cold and Hot Forging*. Ohio: ASM International, Metals Park, OH, 2005.

[114] E. L. B. Tohru Arai, Gordon M.Baker, Charles E. Bates, Bruce A. Becherer, Tom Bell, *ASM Metals Handbook, Volume 4: Heat Treating*. ASM International, Metals Park, OH, 1991.

[115] X. L. Ni, G. Q. Zhang, and Y. Zhang, "Research Progress of Cold Working Die Steel," *Materials Science Forum*, vol. 749, pp. 145–150, Mar. 2013.

[116] S. Babu, D. Ribeiro, and R. Shivpuri, "Material and Surface Engineering for Pecision Forging Dies," 1999.

[117] Nikolai Kobasko and N. I. Prokhorenko, "Quenching Cooling Rate Effect on Crack Formation of 45 Steel," *Metallovedenie and Termicheskaya Obrabotka Metallov (in Russian)*, vol. 2, pp. 53–54, 1964.

[118] IQ Technologies Inc, "Summary of Intensive Quenching Processes : Theory and Applications (Company Report)," Akron, 2011.

[119] G. G. Fuentes, “Surface Engineering and Mirco-Manufacutring,” in *Micro-Manufacturing Engineering and Technology*, Y. Qin, Ed. Oxford: Elsevier, 2010, p. 223.

[120] G. H. Farrahi and H. Ghadbeigi, “An Investigation into the Effect of Various Surface Treatments on Fatigue Life of a Tool Steel,” *Journal of Materials Processing Technology*, vol. 174, no. 1–3, pp. 318–324, May 2006.

[121] K. Wagner, R. Völkl, and U. Engel, “Tool Life Enhancement in Cold Forging by Locally Optimized Surfaces,” *Journal of Materials Processing Technology*, vol. 201, no. 1–3, pp. 2–8, May 2008.

[122] C. Suski and C. Oliveira, “The Effect of Nitride and Titanium Carbonitride Coatings on Wearing of Cold Forming Tools,” *Ciência & Tecnologia dos Materiais*, vol. 20, no. 3–4, pp. 2–7, 2008.

[123] T. A. Dr. Tohru Arai and T. Arai, “Carbide Coating Process and Application in Japanese Cold Forging Industry,” *Tool Dynmics TD Center*, 1996. [Online]. Available: http://www.tdcoating.com/literature/t3-03SME1996Feb.html. [Accessed: 15-Apr-2013].

[124] M. Geiger, U. Popp, and U. Engel, “Excimer Laser Micro Texturing of Cold Forging Tool Surfaces-iIfluence on Tool Life,” *CIRP Annals-Manufacturing Technology*, vol. 51, no. l, pp. 231–234, 2002.

[125] F. Smidt, *ASM Handbook Volume 5 Surface Engineering*. Ohio, 1994.

[126] K. Wagner, A. Putz, and U. Engel, “Improvement of Tool Life in Cold Forging by Locally Optimized Surfaces,” *Journal of Materials Processing Technology*, vol. 177, no. 1–3, pp. 206–209, Jul. 2006.

[127] B. Raeymaekers, I. Etsion, and F. E. Talke, “Enhancing Tribological Performance of the Magnetic Tape/Guide Interface by Laser Surface Texturing,” *Tribology Letters*, vol. 27, no. 1, pp. 89–95, Apr. 2007.

[128] Y. S. Lee, J. H. Lee, Y. N. Kwon, and T. Ishikawa, “Effects of Material Properties on Elastic Characteristics of Cold Forged Part,” *Materials Science Forum*, vol. 449–452, pp. 853–856, 2004.

[129] Y. Qin and R. Balendra, “Development of a Methodology of Analysis and

Compensation of Component Form-Errors for High-Precision Forming," in *Proceeding of CAPE*, 2000, pp. 363–372.

[130] E. Doege, G. Silberbach, and F. M. Tools, "Influence of Various Machine Tool Components on Workpiece Quality," *CIRP Annals-Manufacturing Technology*, vol. 39, no. 1, pp. 209–213, 1990.

[131] Y. Lee, J. Lee, Y. Kwon, and T. Ishikawa, "Modeling Approach to Estimate the Elastic Characteristics of Workpiece and Shrink-Fitted Die for Cold Forging," *Journal of Materials Processing Technology*, vol. 147, no. 1, pp. 102–110, Mar. 2004.

[132] K. Kuzman, "Problems of Accuracy Control in Cold Forming," in *Journal of Materials Processing Technology*, 2001, vol. 113, no. 1–3, pp. 10–15.

[133] A. Rosochowski and R. Balendra, "Effect of Secondary Yielding on Nett-Shape Forming," *Journal of materials processing technology*, vol. 58, no. 2–3, pp. 145–152, 1996.

[134] A. Rosochowski and R. Balendra, "Secondary Yielding-Experimental Verification," in *Fifith International Conference on Technology of Plasticity*, 1996, pp. 335–343.

[135] A. Rosochowski and R. Balendra, "Secondary Yielding of Forged Components due to Unloading," *Journal of Materials Processing Technology*, vol. 115, no. 2, pp. 233–239, Sep. 2001.

[136] N. Bay, "The State of the Art in Cold Forging Lubrication," *Journal of Materials Processing Technology*, vol. 46, no. 1–2, pp. 19–40, Oct. 1994.

[137] Y. Qin, R. Balendra, and K. Chodnikiewicz, "Analysis of Temperature and Component Form-Error Variation with the Manufacturing Cycle during the Forward Extrusion of Components," *Journal of Materials Processing Technology*, vol. 145, no. 2, pp. 171–179, Jan. 2004.

[138] R. Balendra, Y. Qin, and X. Lu, "Analysis, Evaluation and Compensation of Component-Errors in the Nett-Forming of Engineering Components," *Journal of Materials Processing Technology*, vol. 106, no. 1–3, pp. 204–211, Oct. 2000.

[139] M. Hillery and S. Griffin, "An Embedded-Strain-Gauge Technique of Stress

Analysis in Rod Drawing," *Journal of Materials Processing Technology*, vol. 47, pp. 1–12, 1994.

[140] Y.-S. Lee, J.-H. Lee, J.-U. Choi, and T. Ishikawa, "Experimental and Analytical Evaluation for Elastic Deformation Behaviors of Cold Forging Tool," *Journal of Materials Processing Technology*, vol. 127, no. 1, pp. 73–82, Sep. 2002.

[141] A. B. Abdullah, S. M. Sapuan, Z. Samad, H. M. T. Khaleed, N. A. Aziz, and N. Tebal, "Quantitative Evaluation of Geometric and Dimensional Error of Cold Forged Auv Propeller Blade Front Hub Blade Rear Hub," *Australian Journal of Basic and Applied Sciences*, vol. 5, no. 9, pp. 1756–1764, 2011.

[142] Y. Qin and R. Balendra, "FE Simulation of the Influence of Die-elasticity on Component Dimensions in Forward Extrusion," *International Journal of Machine Tools and Manufacture*, vol. 37, no. 2, pp. 183–192, 1997.

[143] Y. Lee, J. Lee, and T. Ishikawa, "Analysis of the Elastic Characteristics at Forging Die for the Cold Forged Dimensional Accuracy," *Journal of Materials Processing Technology*, vol. 130–131, pp. 532–539, Dec. 2002.

[144] H. Long, "Quantitative Evaluation of Dimensional Errors of Formed Components in Cold Backward Cup Extrusion," *Journal of Materials Processing Technology*, vol. 177, no. 1–3, pp. 591–595, 2006.

[145] X. Lu and R. Balendra, "Evaluation of FE models for the Calculation of Die-Cavity Compensation," *Journal of materials processing technology*, vol. 58, no. 2–3, pp. 212–216, Mar. 1996.

[146] B. Avitzur, "Flow Characteristics Through Conical Converging Dies," *ASME*, pp. 556–562, 1967.

[147] C. C. Chen, S. I. Oh, and S. Kobayashi, "Ductile Fracture in Axisymmetric Extrusion and Drawing. Part 1. Deformation Mechanics of Extrusion and Drawing metal," *Trans. ASME, J. Eng. Ind.*, vol. 101, no. 1, pp. 23–35, 1979.

[148] H. Long and R. Balendra, "FE Simulation of the Influence of Thermal and Elastic Effects on the Accuracy of Cold-Extruded Components," *Journal of Materials Processing Technology*, vol. 84, no. 1–3, pp. 247–260, Dec. 1998.

[149] T. Wanheim, R. Balendra, and Y. Qin, "Extrusion Die for In-Process

Compensation of Component-Errors due to Die-Elasticity," *Journal of Materials Processing Technology*, vol. 72, no. 2, pp. 177–182, Dec. 1997.

[150] S. M. Ali, "To Study the Influence of Frictional Conditions and Die Land Length on Component Error and Die Deflection in Cold Extrusion by Finite Element Analysis," *Journal of Metallurgical Engineering*, vol. 2, no. 1, pp. 29–38, 2013.

[151] M. Shiraishi, K. Kawasaki, and K. Osakada, "A New Die Structure for Compensation Dimensional Error in Cold Extrusion and Drawing," *Adv. Technol. Plasticity*, vol. 1, pp. 429–434, 1990.

[152] F. Jutte, "Active die for process control in metal forming," *Metal Forming Technology*, vol. 27, pp. 207–210, 1993.

[153] Y. Qin, J. Lin, T. Dean, and R. Balendra, "Intelligent Tools for Ultra High-Precision Forming of Macro- and Mirco-Engineering Components (SMARTOOLS), Internal Report," University of Strathclyde/University of Birmingham, 2003.

[154] S. Sheng and L. Guo, "Preform Design of Axisymmetric Forgings Based on Reverse Simulation Technique of Die Forging Process," *Journal of Materials Processing Technology*, vol. 34, pp. 349–356, 1992.

[155] S. Lee, Y. Lee, C. Park, and D. Yang, "A New Method of Preform Design in Hot Forging by Using Eletric Field Theory," *International Journal of Mechanical Sciences*, vol. 44, no. 4, pp. 773–792, 2002.

[156] X. Zhao, G. Zhao, G. Wang, and T. Wang, "Preform Die Shape Design for Uniformity of Deformation in Forging Based on Preform Sensitivity Analysis," *Journal of Materials Processing Technology*, vol. 128, no. 1–3, pp. 25–32, 2002.

[157] B. Lu, H. Ou, and Z. S. Cui, "Shape Optimisation of Preform Design for Precision Close-Die Forging," *Structural and Multidisciplinary Optimization*, vol. 44, no. 6, pp. 785–796, Jun. 2011.

[158] Z. Zimerman and B. Avitzur, "Metal Flow Through Conical Converging Dies-a Lower Upper Bound Approach Using Generalized Boudaries of the Plastic

Zone," *Journal of Engineering for Industry*, vol. 92, no. 1, pp. 119–129, 1970.

[159] J. Pan, W. Pachla, S. Rosenberry, and B. Avitzur, "The Study of Distorted Grid Patterns for Flow-Through Conical Converging Dies by the Multi-Triangular Velocity Field," *Journal of Engineering for Industry*, vol. 106, pp. 150–160, 1984.

[160] H. Long, "Dimensional Errors of Cold Formed Components Using FE Simulation," *Journal of Materials Processing Technology*, vol. 151, no. 1–3, pp. 355–366, Sep. 2004.

[161] N. Bay, A. Azushima, P. Groche, I. Ishibashi, M. Merklein, M. Morishita, T. Nakamura, S. Schmid, and M. Yoshida, "Environmentally Benign Tribo-Systems for Metal Forming," *CIRP Annals - Manufacturing Technology*, vol. 59, no. 2, pp. 760–780, Jan. 2010.

[162] T. Nakamura, Y. Sumioka, K. Sakoda, S. Miyano, Y. Ishiizumi, I. Ishibashi, and M. Sekizawa, "Lubrication Performance of Environmentally Friendly Lubricants for Forging," in *59th Japanese Joint Conference for the Technology of Plasticity*, 2008, pp. 333–334.

[163] N. Kobatashi, A. Moriyama, and M. Yoshida, "Electrolytical Phosphating Process for Steel Wire Drawing (Technical Report No. 17)," Nihon Parkerizing, 2005.

[164] L. Dubar, C. I. Pruncu, A. Dubois, and M. Dubar, "Effects of Contact Pressure, Plastic Strain and Sliding Velocity on Sticking in Cold Forging of Aluminium Billet," *Procedia Engineering*, vol. 81, no. October, pp. 1842–1847, 2014.

[165] W. Pan and Y. Qin, "FE Analysis of Multi-Cycle Micro-Forming Through Using Closed-Die Upsetting Models and Forward Extrusion Models," *Journal of Materials Processing Technology*, vol. 201, no. 1–3, pp. 220–225, May 2008.

[166] C. Zhang, X. Chu, D. Guines, L. Leotoing, J. Ding, and G. Zhao, "Effects of Temperature and Strain Rate on the Forming Limit Curves of AA5086 Sheet," *Procedia Engineering*, vol. 81, no. October, pp. 772–778, 2014.

[167] M. K. Choi and H. Huh, "Effect of Punch Speed on Amount of Springback in U-bending Process of Auto-body Steel Sheets," *Procedia Engineering*, vol. 81,

no. October, pp. 963–968, 2014.

[168] BS Dassault, *Abaqus 6.13 Manual Example Problem Guide*. 2014.

[169] D. Liu, Z. Liu, and L. Wang, "Simulation of Rolling Process of AZ31 Magnesium Alloy Sheet," *Procedia Engineering*, vol. 81, no. October, pp. 173–178, 2014.

[170] "Tungsten Carbide - An Overview," *AZOM*. [Online]. Available: http://www.azom.com/properties.aspx?ArticleID=1203. [Accessed: 14-Apr-2016].

[171] "MatWeb." [Online]. Available: http://www.matweb.com/index.aspx. [Accessed: 17-Jun-2016].

[172] *Standard Guide for Preparation of Metallographic Specimens*, ASTM E3-11. United States, 2011.

[173] *Metallic Materials - Vickers Hardness Test - Part 4: Tables of Hardness Values*, ISO 6507-4. Switzerland, 2005.

[174] *Metallic Materials - Vickers Hardness Test - Part 1: Test Method*, ISO 6507-1. Switzerland, 2005.

[175] *Standard Method of Macroetch Testing Steel Bars, Billets, Blooms, and Forgings*, ASTM E381. United States, 2001.

[176] X. Chen, R. Balendra, and Y. Qin, "A New Approach for the Optimisation of the Shrink-Fitting of Cold-Forging Dies," *Journal of Materials Processing Technology*, vol. 145, no. 2, pp. 215–223, Jan. 2004.

[177] J. . Lenard, "An Experimental Study of Heat Transfer in Metal-Forming Processes," *CIRP Annals - Manufacturing Technology*, vol. 41, pp. 307–310, 1992.

[178] Whitelaw and J. H, "Convective Heat Transfer," *Thermopedia*, 2011. [Online]. Available: http://www.thermopedia.com/content/660/. [Accessed: 16-Jun-2016].

[179] J. Karnesky, J. Damazo, K. Chow-yee, A. Rusinek, and J. E. Shepherd, "Plastic Deformation due to Reflected Detonation," *International Journal of Solids and Structures*, vol. 50, no. 1, pp. 97–110, 2013.

[180] M. AT and C. MG, “A Method for the Determination of the Coefficient of Friction of Metals under Condition of Bulk Plastic Deformation,” *J Inst Metals*, vol. 93, pp. 38–46, 1964.

[181] T. Barrett, *Fastener Design Manual*. NASA, 1990.

Appendix A. Interference Fit Design and Die Splitting

A simplified FE model, as shown in Fig. A-1(a), was employed in ABAQUS to examine the splitting die and interference fit design. To explore the critical position during forging, the die insert was treated as a single part. No pre-stressing was introduced to avoid its influence on the stress distribution in die inserts. In this model, the constraint to the die was considered as rigidity, so that the edge attached with yellow triangle symbols was fixed in x direction. Other boundary conditions were same as that shown in chapter 3.

Fig. A-2 (a) and Fig. A-3 (a) presents the S22 (axial stresses) and mean principle stresses in die inserts. As results, both maximum axial and mean stresses are tensile stresses. As well known, the tension stress adversely influences the tool service life. It indicates that the initial fatigue crack may grow in these critical positions. Therefore, it is necessary to split the die insert in the position A and B. However, as a feedback from the industry, when splitting the die insert in the position A, it is easy to generate flash in the transition radius of the component (refers to Fig. A-4). It is recommended to use a two die-inserts design instead of a three-inserts design. Based on this recommendation, the die insert is only split in the position B. Fig. A-5 (a) shows the S33 (hoop stresses) in the single die insert design. It indicates that the hoop stresses stay at positive value as well. This brings a highly potential risk of vertical fracture along the stress concentration zone.

According to the previous analysis, a new model was developed. The former single die insert was split into two parts, seen in Fig. A-1 (b). Fig. A-2 (b), Fig. A-3 (b) and Fig. A-5 (b) show the distribution of axial stress, mean stress and hoop stress in the die insert, respectively. As results, the maximum axial stress, mean stress and hoop stress remain stable in the section A. In the section B, the tensile stress concentration is eliminated. It suggests that the die split does not influence the maximum stress in the whole model, while it can release the local stress concentration.

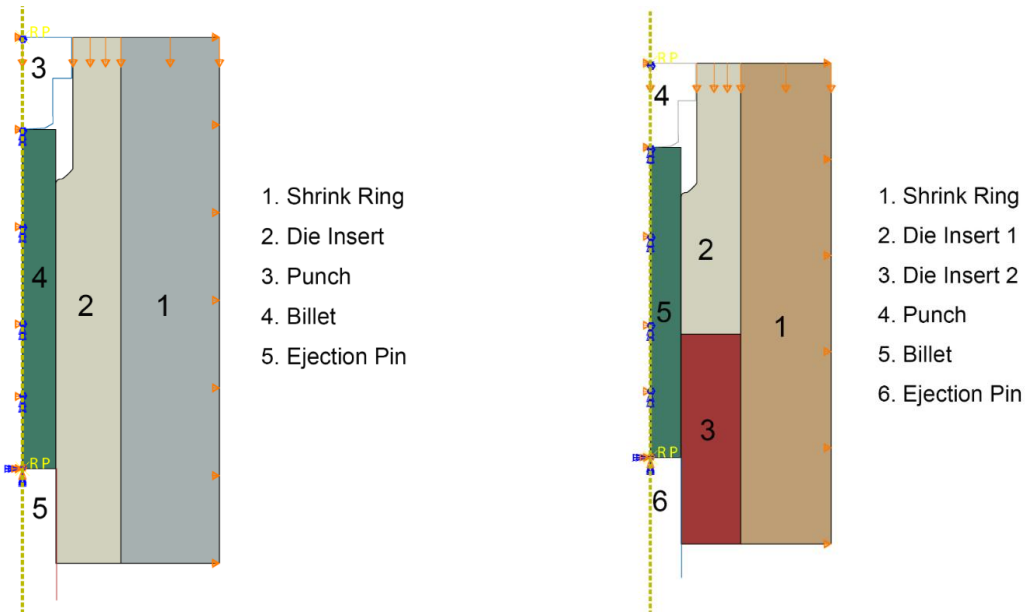

(a) *(b)*

Fig. A-1: FE models in ABAQUS for die split design: (a) before die split, (b) after die split.

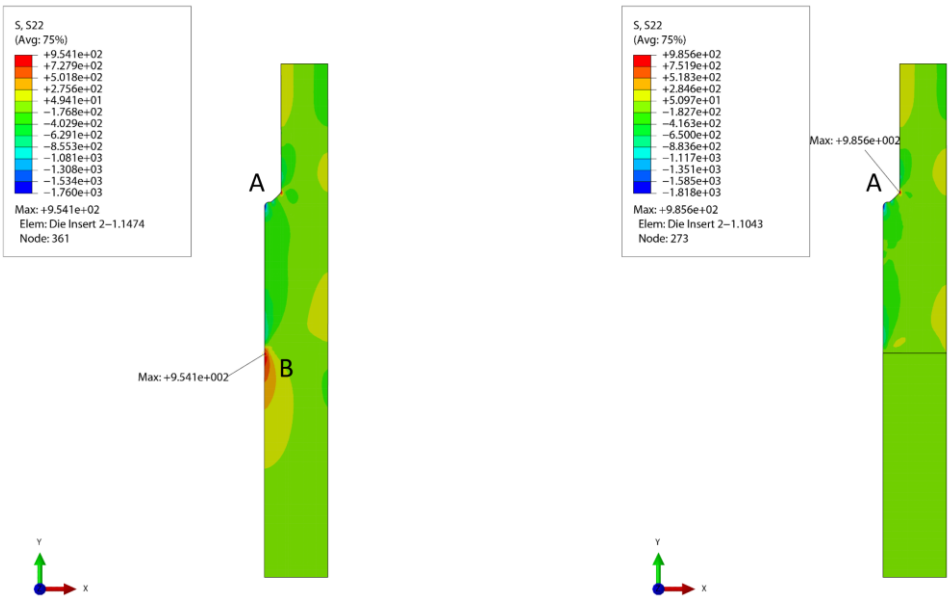

(a) *(b)*

Fig. A-2: The axial stress (MPa) distribution: (a) single die insert, (b) two die inserts.

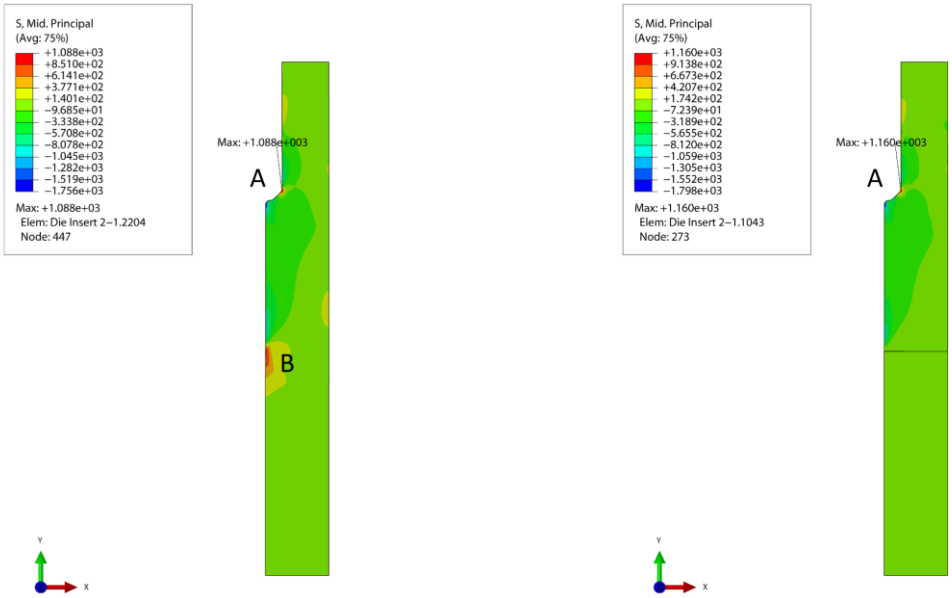

(a) *(b)*

Fig. A-3: The mean stress (MPa) distribution: (a) single die insert, (b) two die inserts.

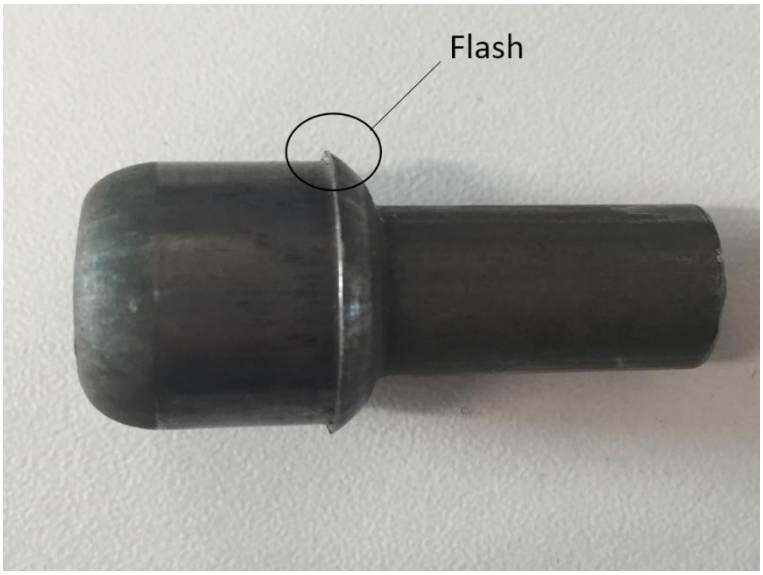

Fig. A-4: Disqualification component with flash near transition radius.

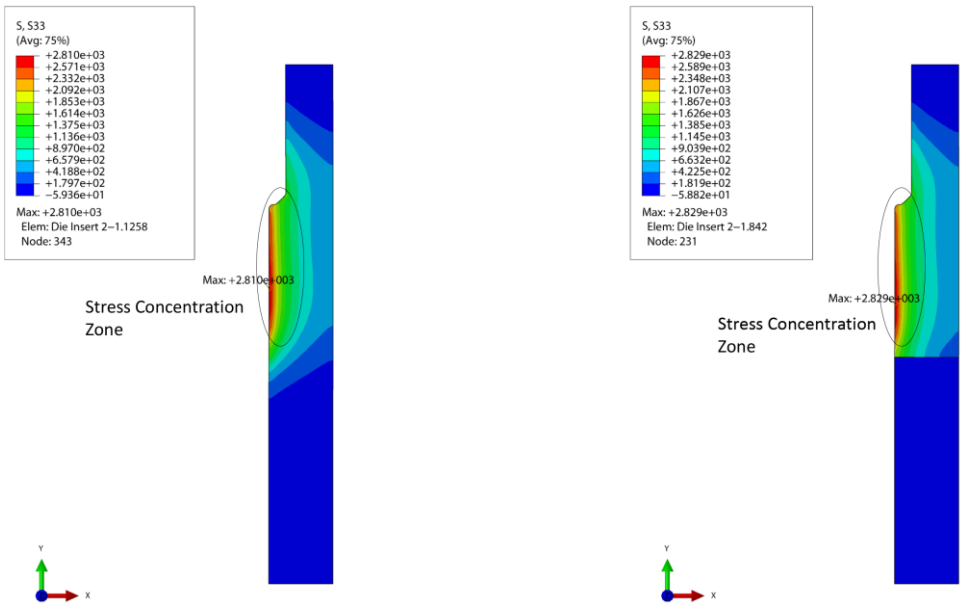

Fig. A-5: The hoop stress (MPa) distribution: (a) single die insert, (b) two die inserts.

To find the optimal interference fit for die inserts, six groups with different amplitudes of interference were used in the simulation, seen in Table A-1. The amplitude of interference I_{amp} is expressed as:

$$I_{amp} = \frac{D_1 - D_2}{D_2} \times 100\%$$

D_1 is the modified external diameter and D_2 is the initial external diameter.

Table A-1: The amplitudes of interference fit used in FE simulations.

Group	A	B	C	D	E	F	G
Amplitude of Interference Fit (%)	0.1	0.2	0.3	0.4	0.5	0.55	0.6

Fig. A-6 shows the changes of maximum axis stresses, hoop stresses and mean stresses in die inserts with the increasing I_{amp}. According to results, the influence of I_{amp} on reducing the hoop stress and mean stress are significant, while it shows a slight effect on the axial stress. For the mean stress, it turns from the tensile stress to the compressive stress which contributes to extending the tool life.

Compared with the hoop stress, the reduction of mean stress is obviously mild. It may be caused by the axis stress. The axis stress does not decrease considerably when the I_{amp} increases. It is because no pre-stressing applies on die insert in the axis direction, which makes the interference fit affect the axis stress slightly. With observing the tendency of the hoop stress in die inserts, it is believed that the hoop stress and mean stress can reduce further with increasing of I_{amp}. However, regarding the yield stress of shrink ring, the I_{amp} cannot increase unlimitedly. From the simulation, when the I_{amp} increases from 0.5% to 0.6%, the shrink ring begins to yield in assembly. After forging, the shrink ring yields when the I_{amp} is 0.5%. Therefore, it suggests that 0.4% is the upper bound of the I_{amp}, and it will be used in the comparison study.

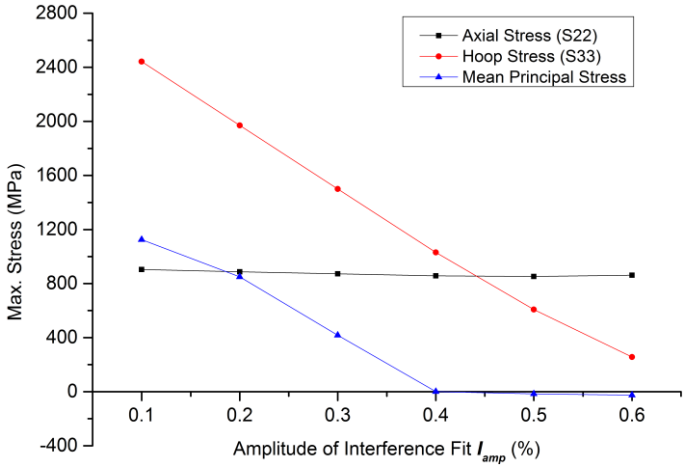

Fig. A-6: The relationship between interference fit and stresses in die insert.

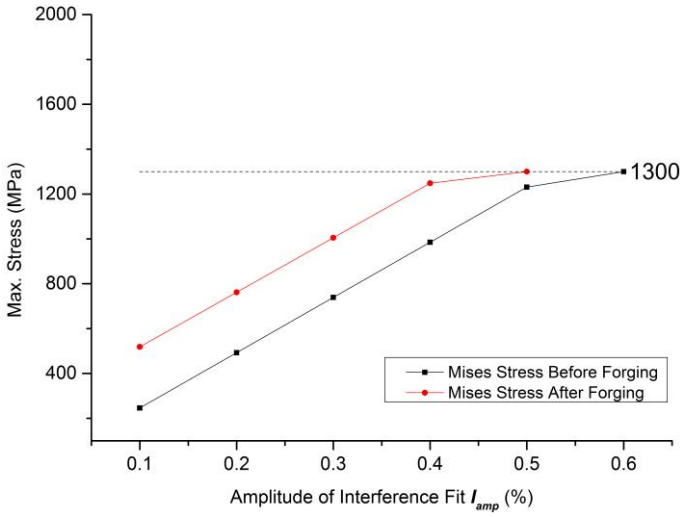

Fig. A-7: The relationship between interference fit and stresses in shrink ring.

Appendix B. Ring Test

The ring test is a widely accepted method for analysing the coefficient of friction (COF) between the workpiece and tools since the 1960s [180]. With comparing the dimensional change of ring size with a calibration curve, it can obtain a magnitude of COF. In this study, the calibration curve was developed by a FE simulation in DEFORM. Three lubricants, ISO 100 forging oil, ISO 68 forging oil and MoS_2 grease, were tested to evaluate the friction condition in forging processes.

The ring size adopted the most widely used ratio 6: 3: 2 which corresponded to out ring diameter, inner ring diameter and height (refer to Fig. B-1). The specimen material was cut from AISI 1010 bars and machined by a CNC machining centre and finally coated with phosphate. Two blocks were fabricated to compress the specimen. The block was made of H13 die steel with heat treatment. The hardness of blocks, therefore, could achieve a high value (54 HRC).

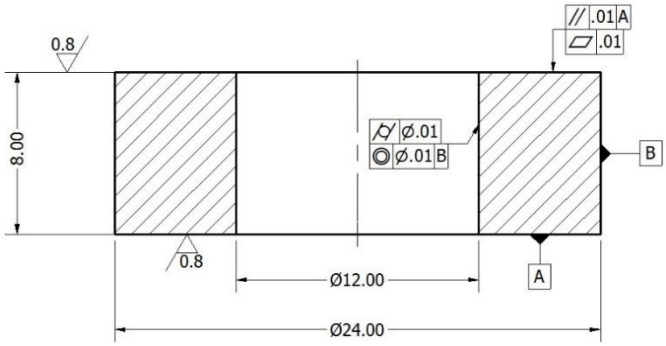

(a)

(b)

Fig. B-1: The ring used in friction test (a) ring dimension (b) specimen.

Before doing the experiment, each ring was measured concerning the internal ring diameter and the height. Then, the block and the ring were washed by alcohol and dried by a blow gun. The ring covering with lubricant was placed on the centre of the block to the greatest extends. Otherwise, the pressure cannot be applied on the specimen surface uniformly when the ring was off-center. The blocks should be set on the centre of work platform either.

In this test, the compression ratio of the ring was around 55%. After one specimen was finished, the dimensional change was measured and recorded. Subsequently, the blocks were washed by alcohol and polished by a sandpaper. It avoided the previous ring test influencing on the following test.

During the test, due to the material structure, dimensional accuracy of the ring, stiffness of machine and lubricant distribution, the material flow on the ring is hard to keep uniform. It caused an irregular shape of ring (refers to Fig. B-2). In this case, the internal diameter was decided by the average of maximum diameter and minimum diameter.

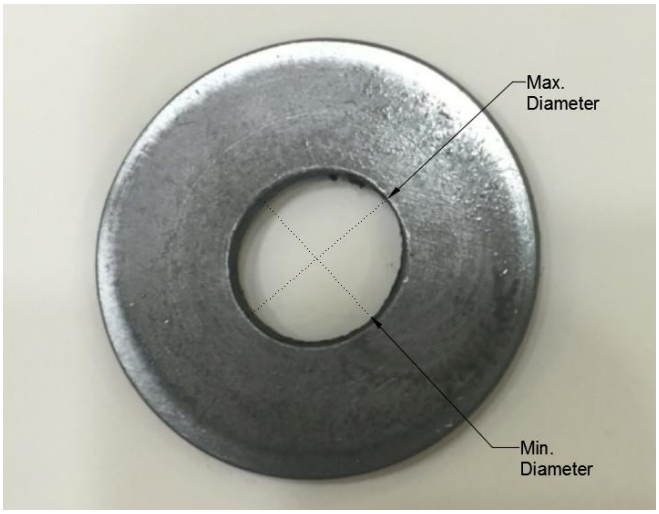

Fig. B-2: Deformed specimen with a maximum diameter and a minimum diameter.

Fig. B-3 shows the simulation model in DEFORM. The calibration curve for ring test was developed by FE simulations which involved three parts, including the workpiece, top platen and bottom platen. Besides the workpiece was regarded as a rigid-plastic body, two platens were set as a rigid body. During the simulation, the movement of top platen was controlled by a constant speed (10 mm/s). The workpiece material was

AISI 1010 which mechanical properties were presented in Table 3-1. In the simulation, the stroke was 4.4 mm that occupied 55% of the component height. To find the influence of COF on the dimensional change, eight groups of COF (refer to Table B-1) were used with Coulomb friction model.

The results were showed in Table B-2. Comparing the results from the FE simulation and the experiment, the magnitude of COF can be limited within a defined range, seen in Fig. B-4. Based on this figure, the COF for ISO 100, ISO 68 and MoS_2 were estimated as 0.055, 0.053 and 0.073, respectively.

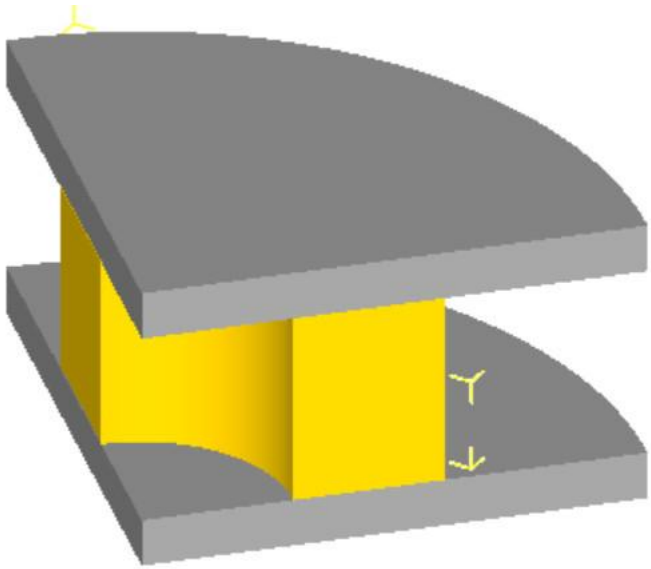

Fig. B-3: Ring test model in DEFORM.

Table B-1: Coefficient of friction used in FE simulation.

Group	A	B	C	D	E	F	G	H
COF	0.05	0.055	0.06	0.065	0.07	0.075	0.08	0.1

Table B-2: Dimension change depends on different lubricants.

Items	Lubricant	Initial height (mm)	Initial internal diameter (mm)	Final height (mm)	Final internal diameter (mm)
1	ISO 100	7.97	11.98	3.57	13.17
2	ISO 100	8.00	11.97	3.59	13.10
3	ISO 100	7.99	12.02	3.36	12.97
4	ISO 68	7.97	12.01	3.65	13.50
5	ISO 68	7.97	12.00	3.57	13.39
6	ISO 68	7.97	11.95	3.55	13.12
7	MoS_2	8.00	11.98	3.51	12.10
8	MoS_2	8.00	11.98	3.54	12.04
9	MoS_2	7.97	12.01	3.51	12.07

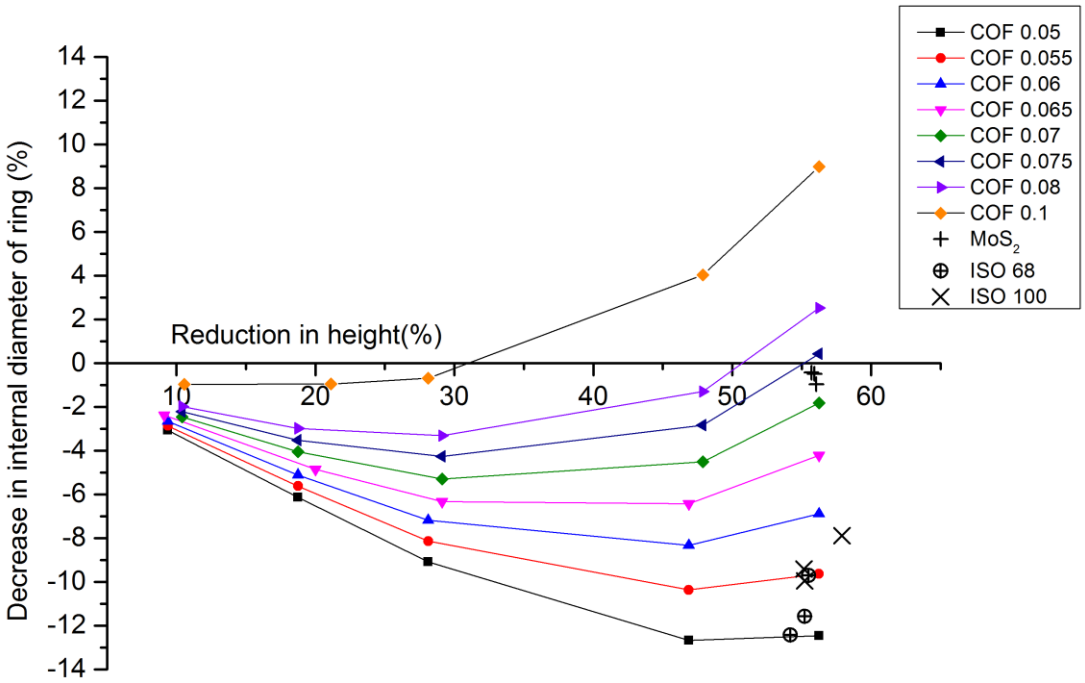

Fig. B-4: Calibration curve for ring test based on FE simulations.

Appendix C. Tool Drawing

Bottom Die: Case

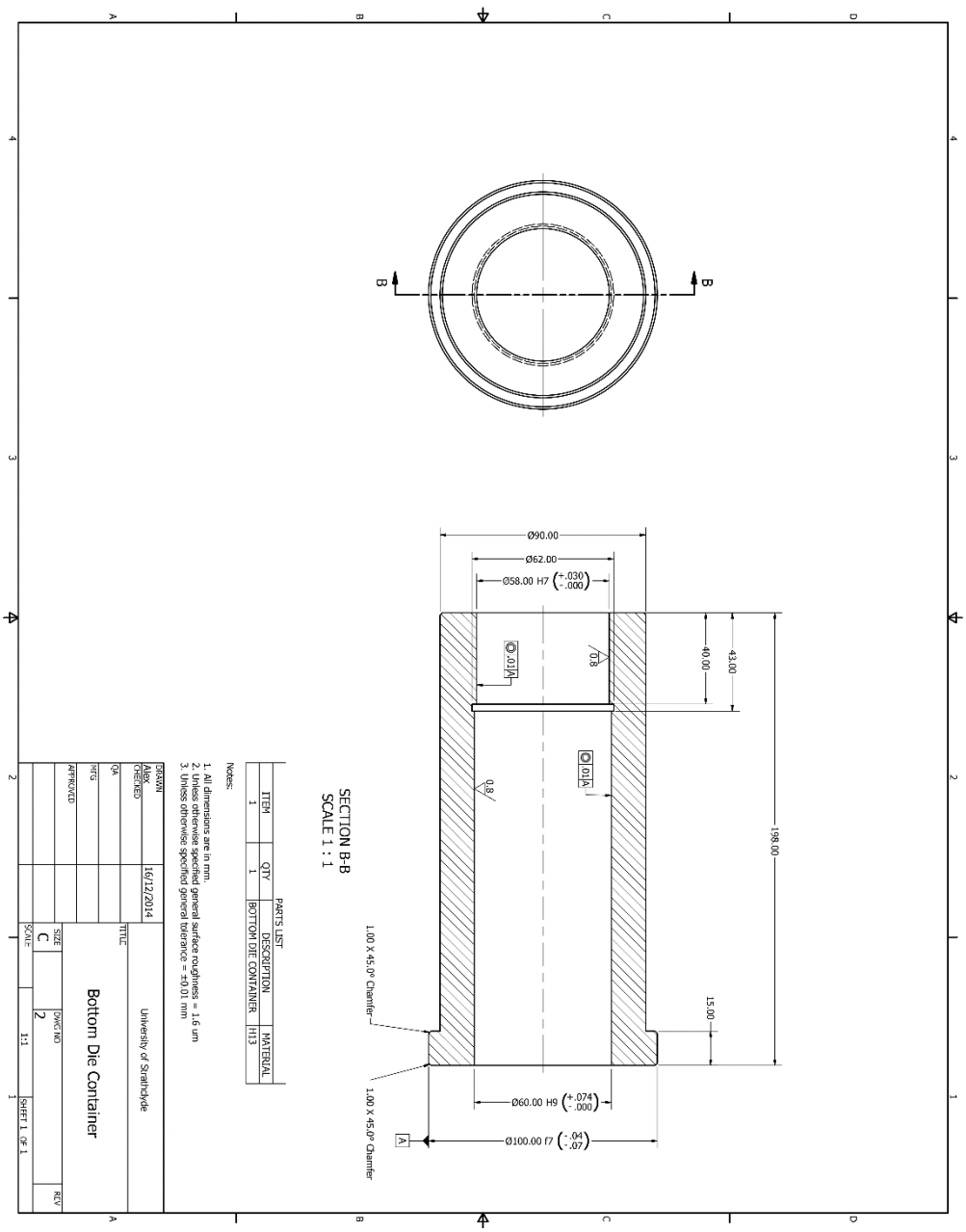

Bottom Die: Shrink Ring

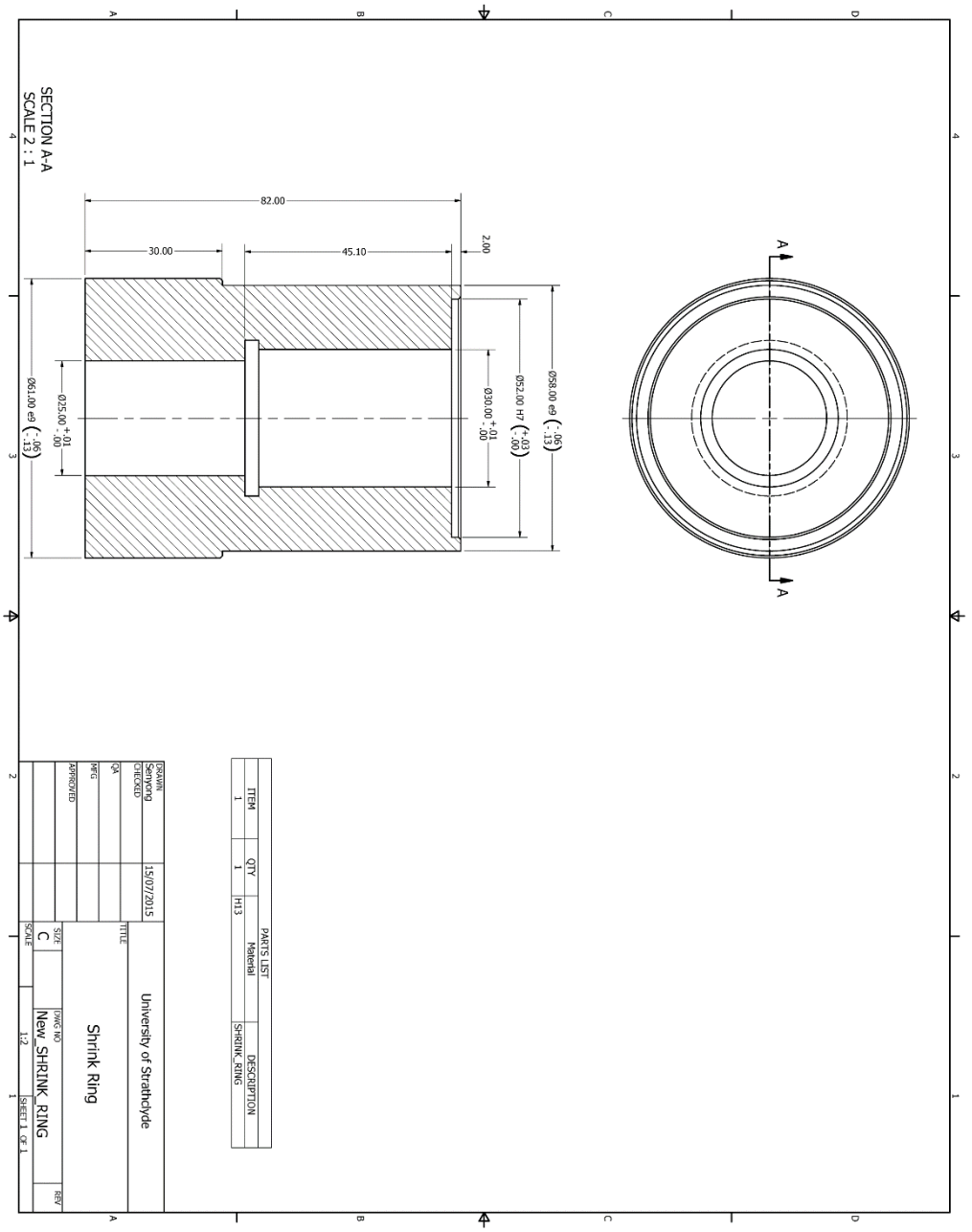

Bottom Die: Die Insert 1

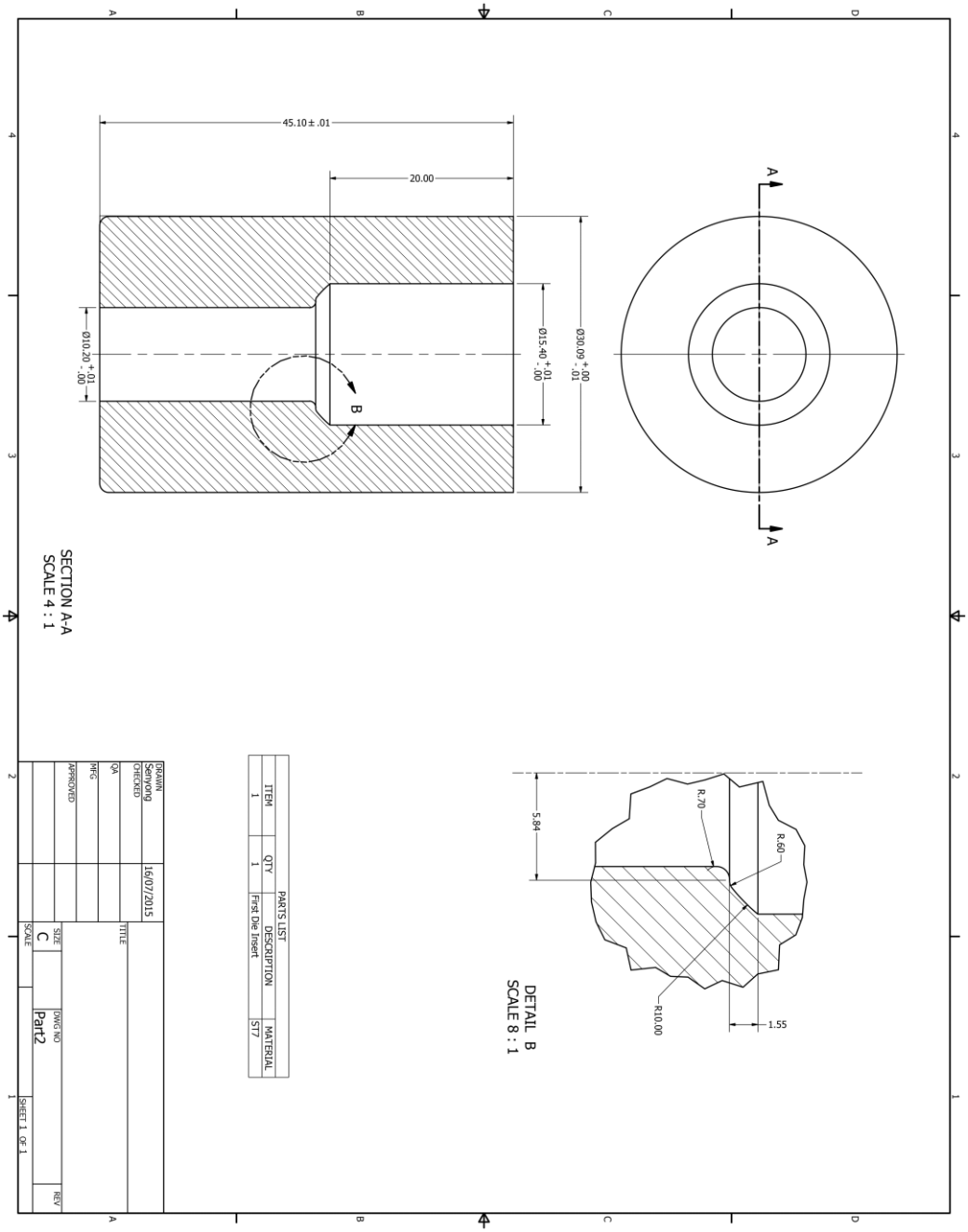

Bottom Die: Die Insert 2

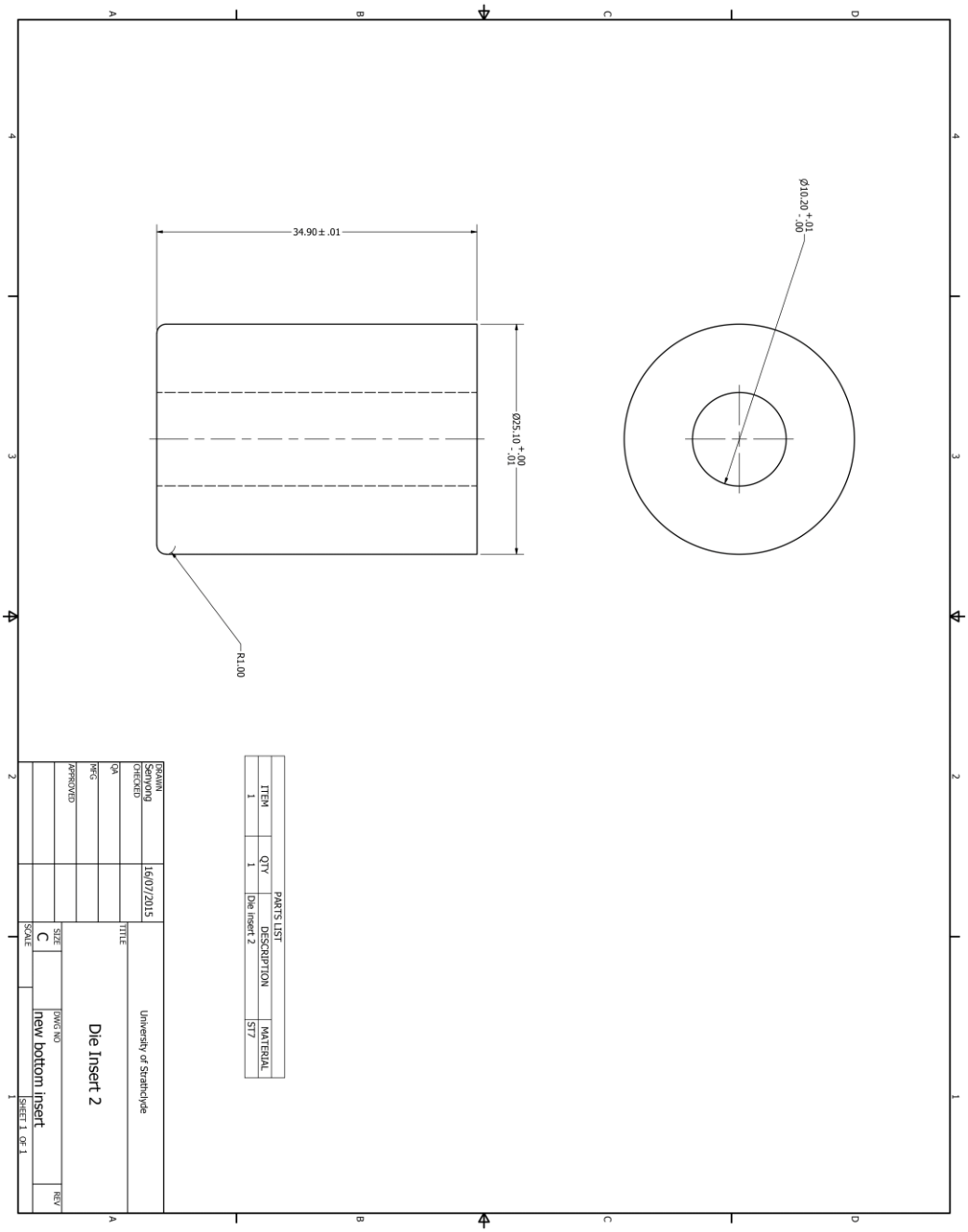

Bottom Die: Spring Fixing Plate

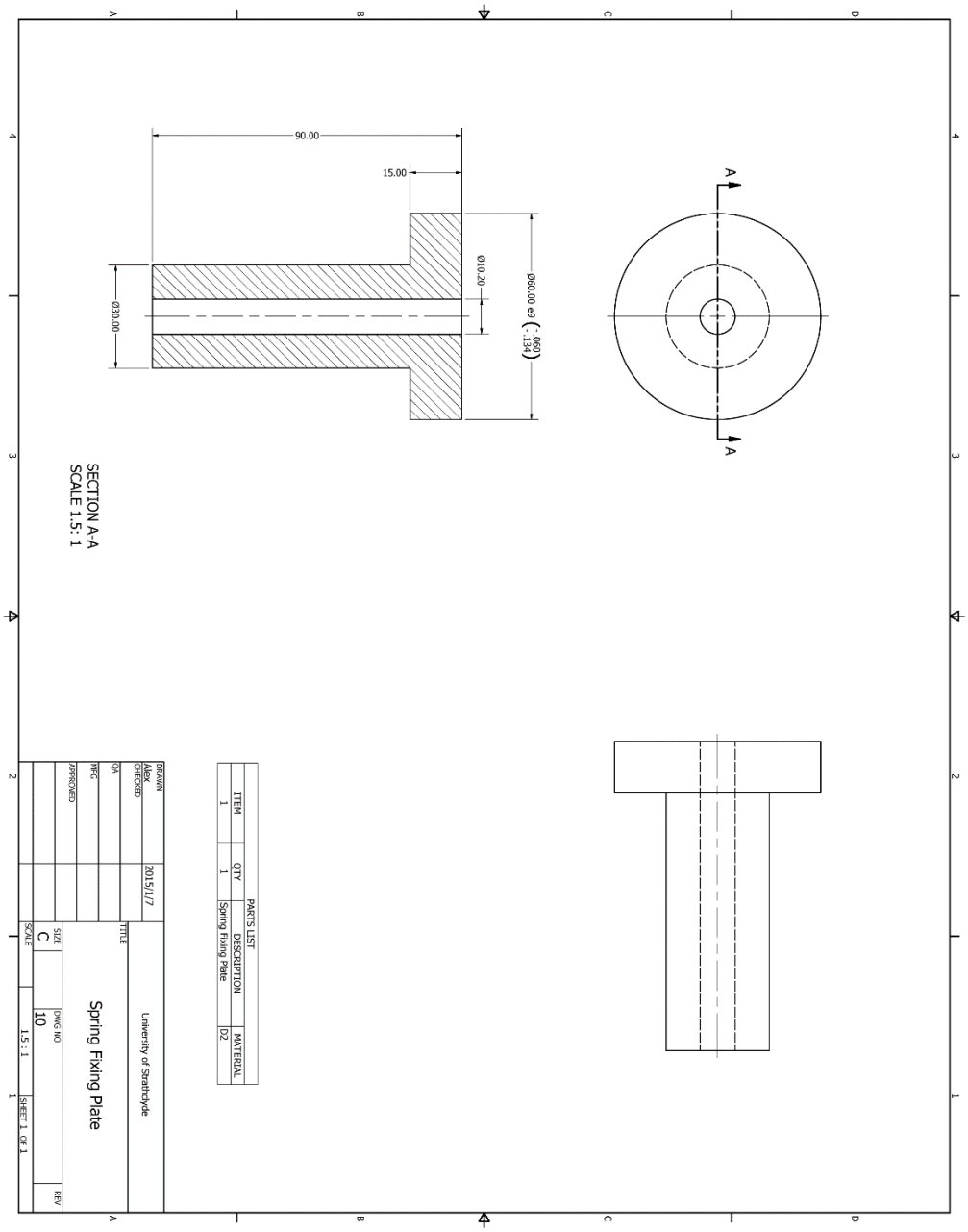

Bottom Die: Base Plate

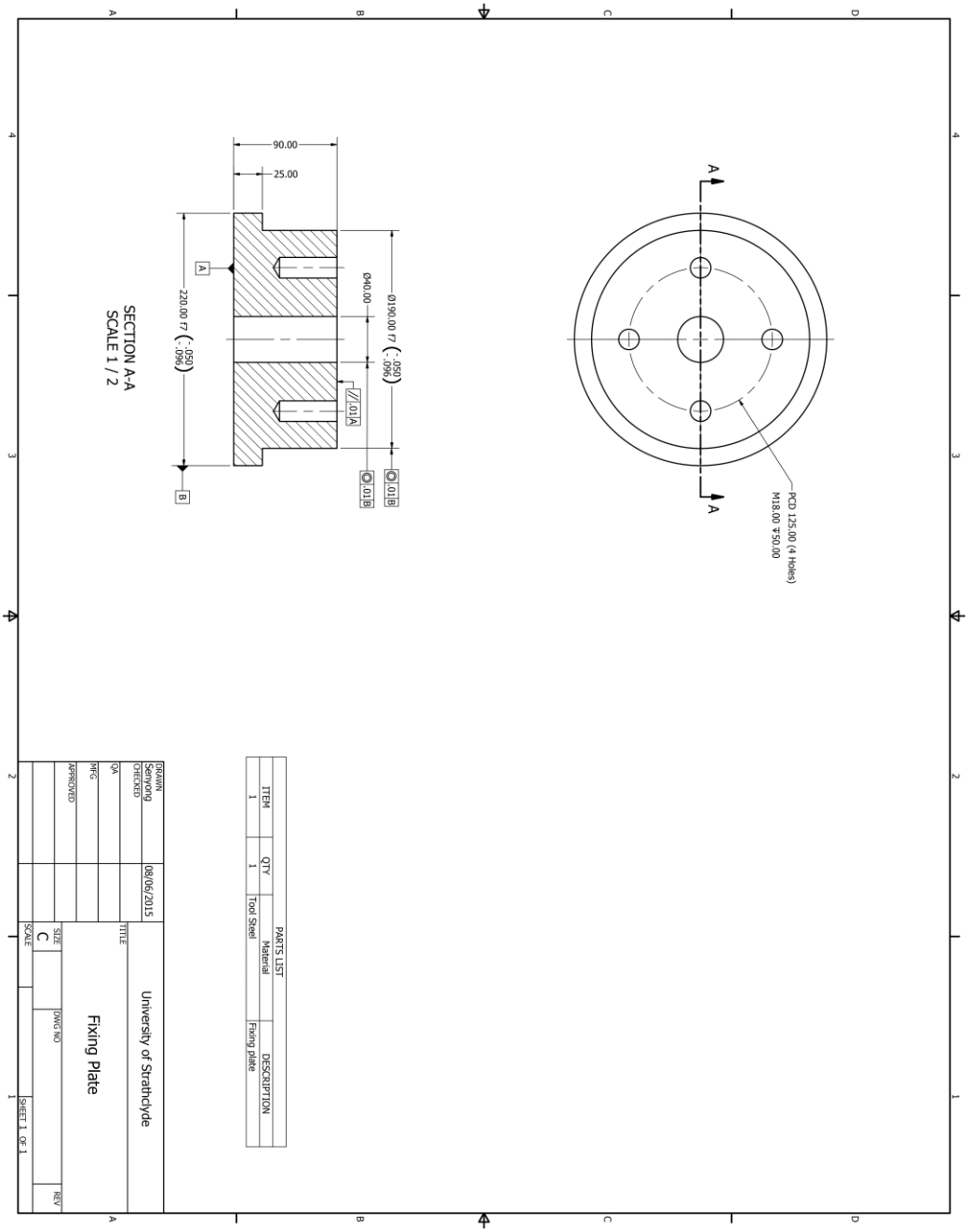

Bottom Die: Fixing Cylinder

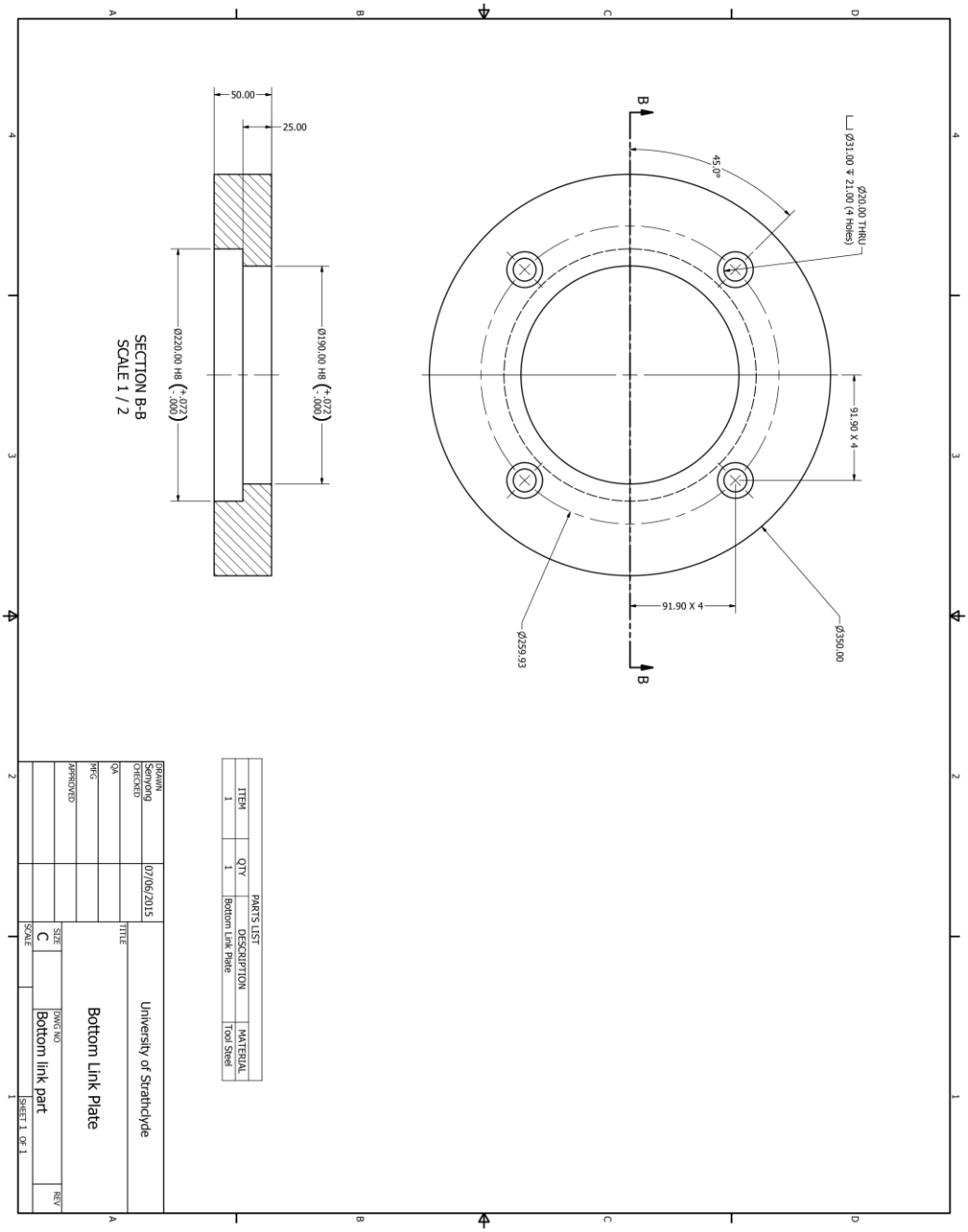

Top Die: Punch

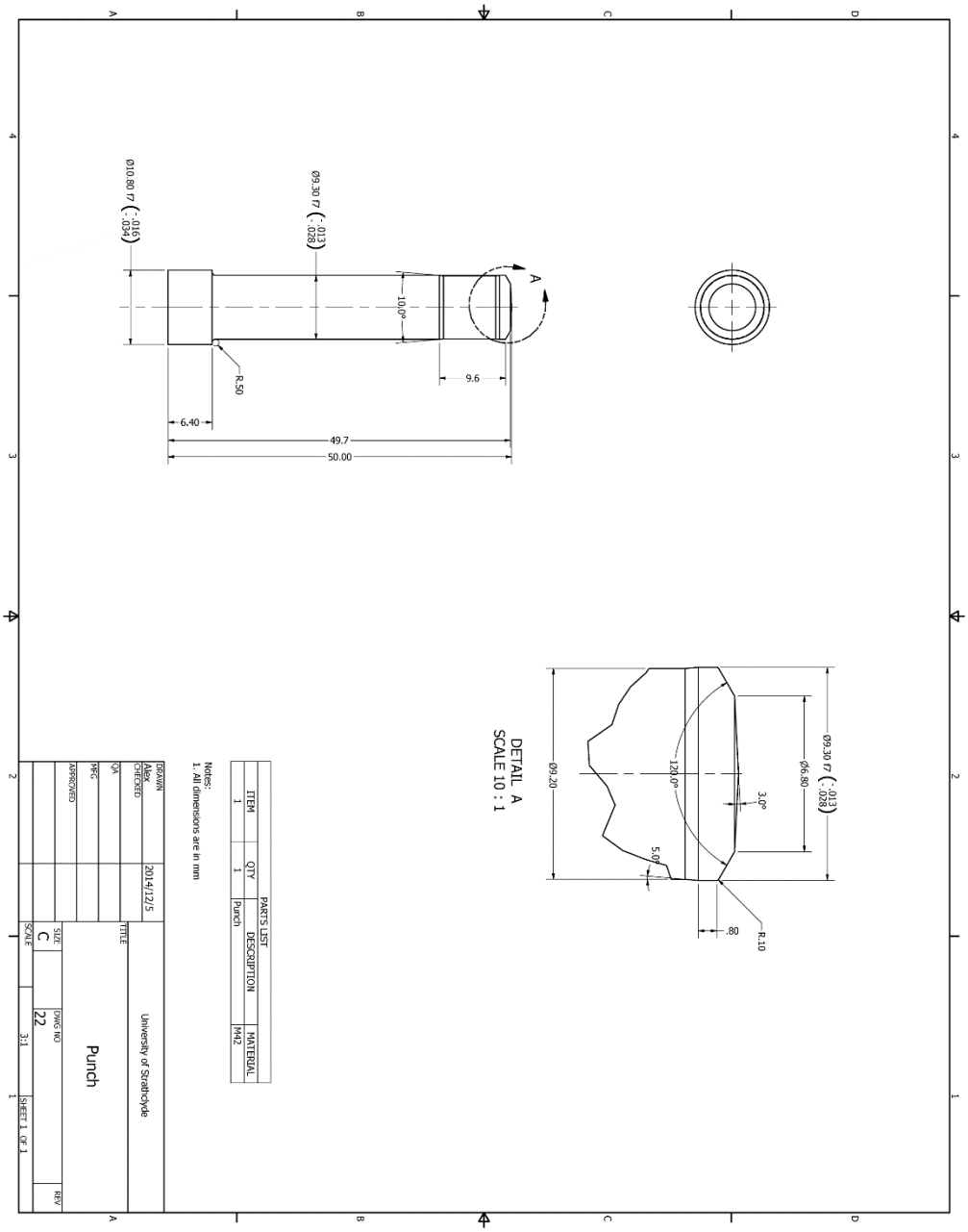

Top Die: Case

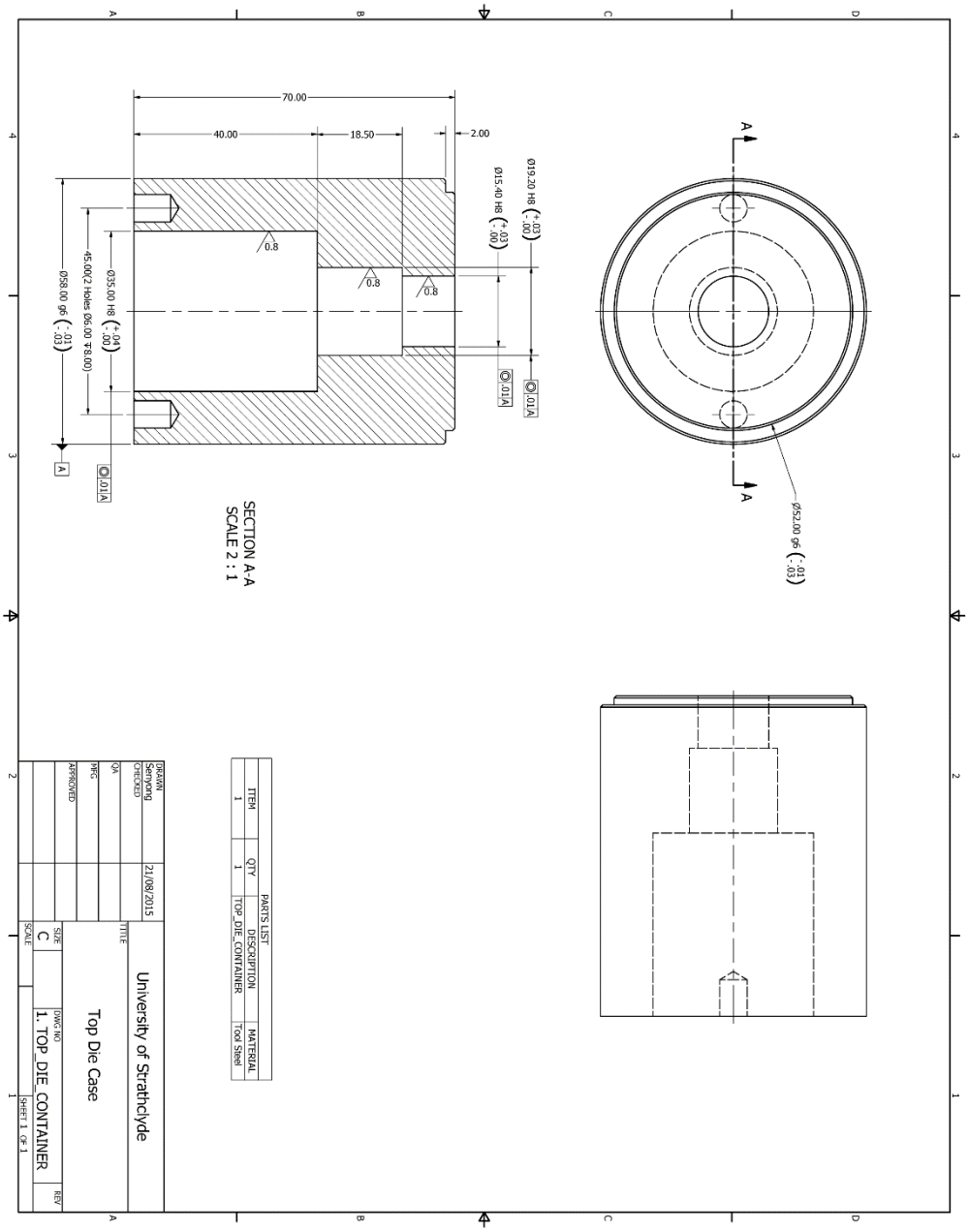
70.00
40.00
18.50
2.00
Ø19.20 H8 (+.03 -.00)
Ø15.40 H8 (+.03 -.00)
0.8
0.8
0.8
Ø58.00 g6 (-.01 -.03)
45.00(2 Holes Ø6.00 ↧8.00)
Ø35.00 H8 (+.04 -.00)
⌖ .01 A
⌖ .01 A
⌖ .01 A
A
A
A
Ø52.00 g6 (-.01 -.03)
SECTION A-A
SCALE 2 : 1
PARTS LIST
ITEM | QTY | DESCRIPTION | MATERIAL
1 | 1 | TOP_DIE_CONTAINER | Tool Steel
DRAWN Sherwyn Chin 21/08/2015
CHK'D
QA
MFG
APPROVED
TITLE
University of Strathclyde
Top Die Case
SIZE C
DWG. NO 1. TOP_DIE_CONTAINER
REV
SCALE
SHEET 1 OF 1

Top Die: Adaptor

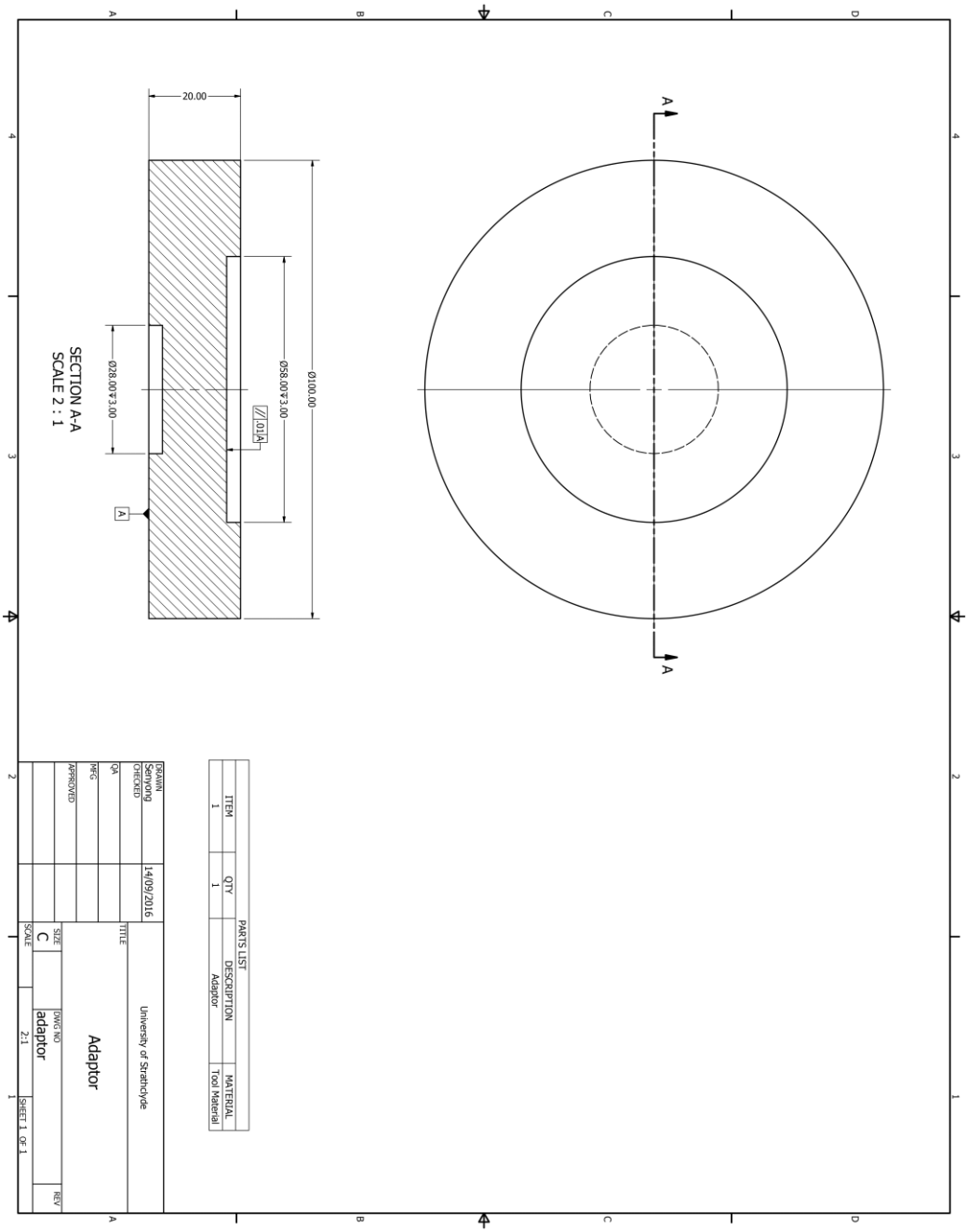

Top Die: Sleeve

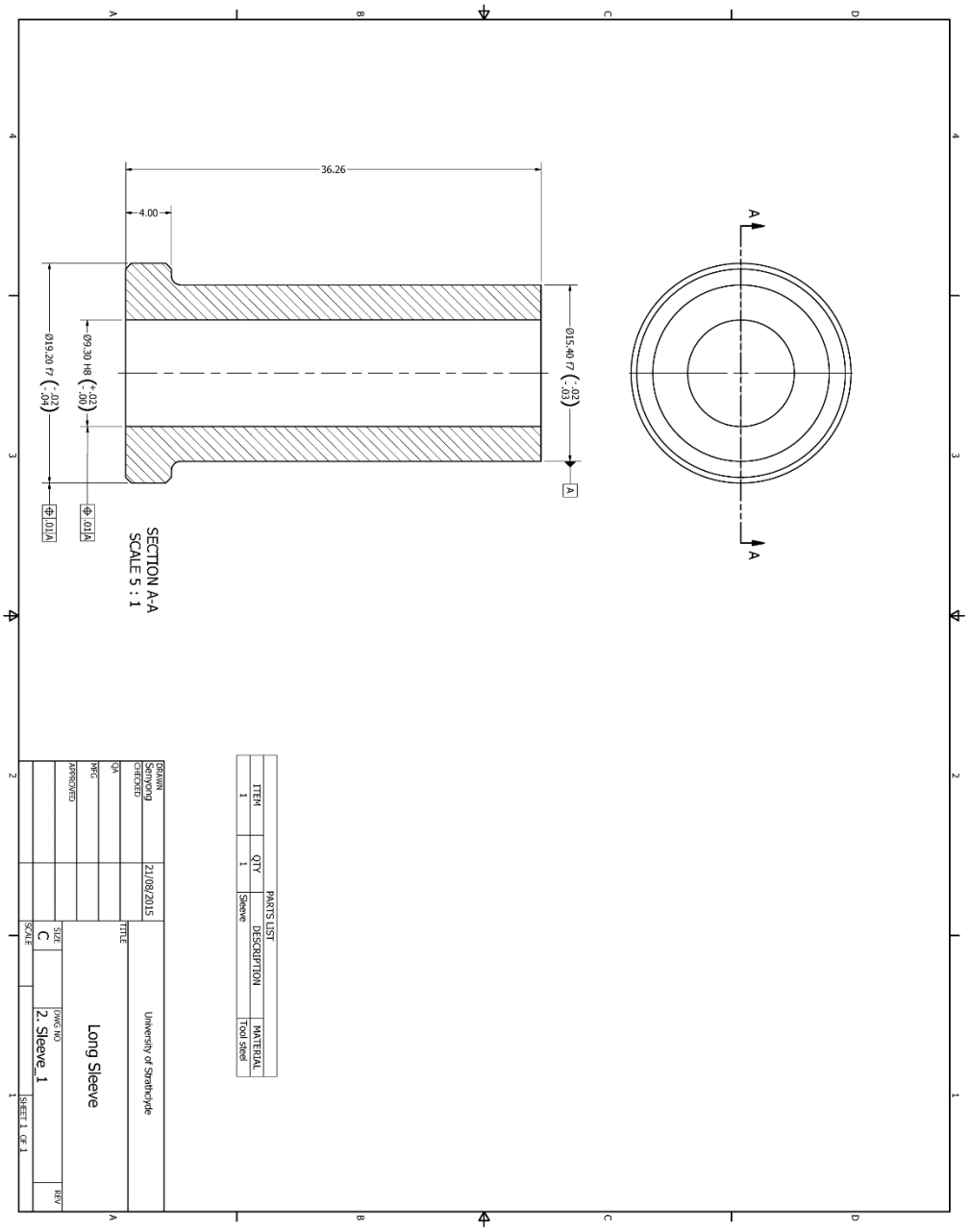

Top Die: Baseplate 1

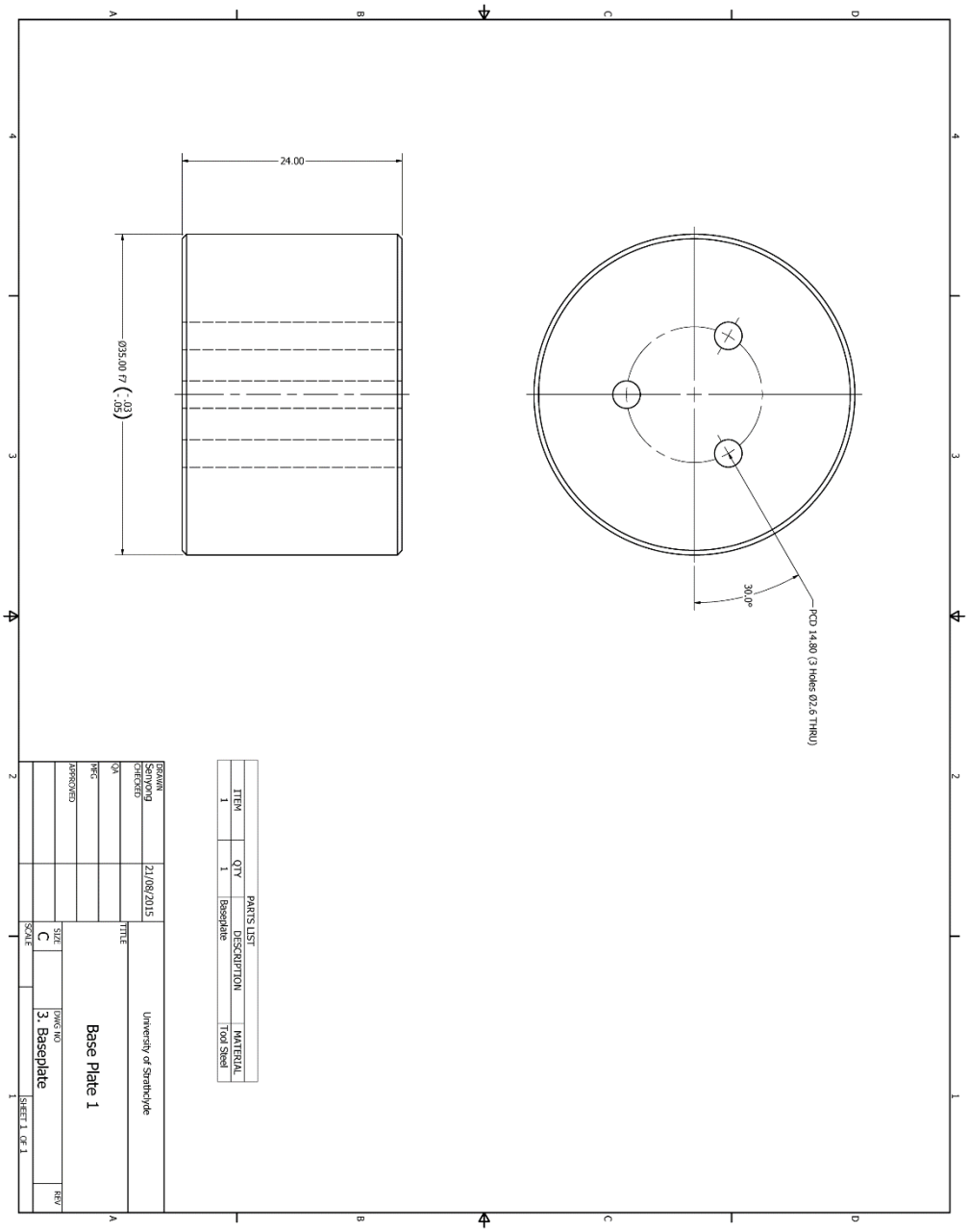

Top Die: Baseplate 2

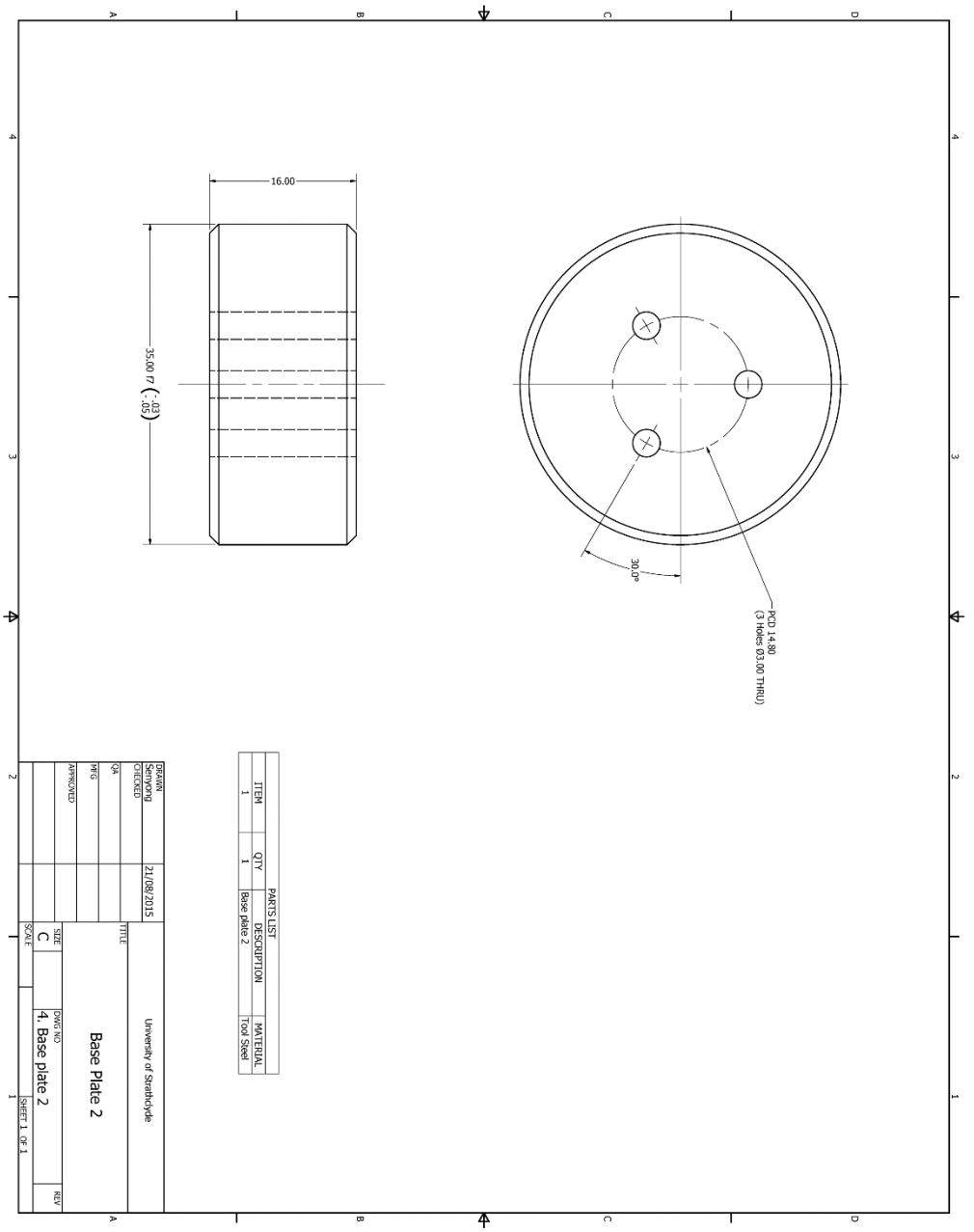

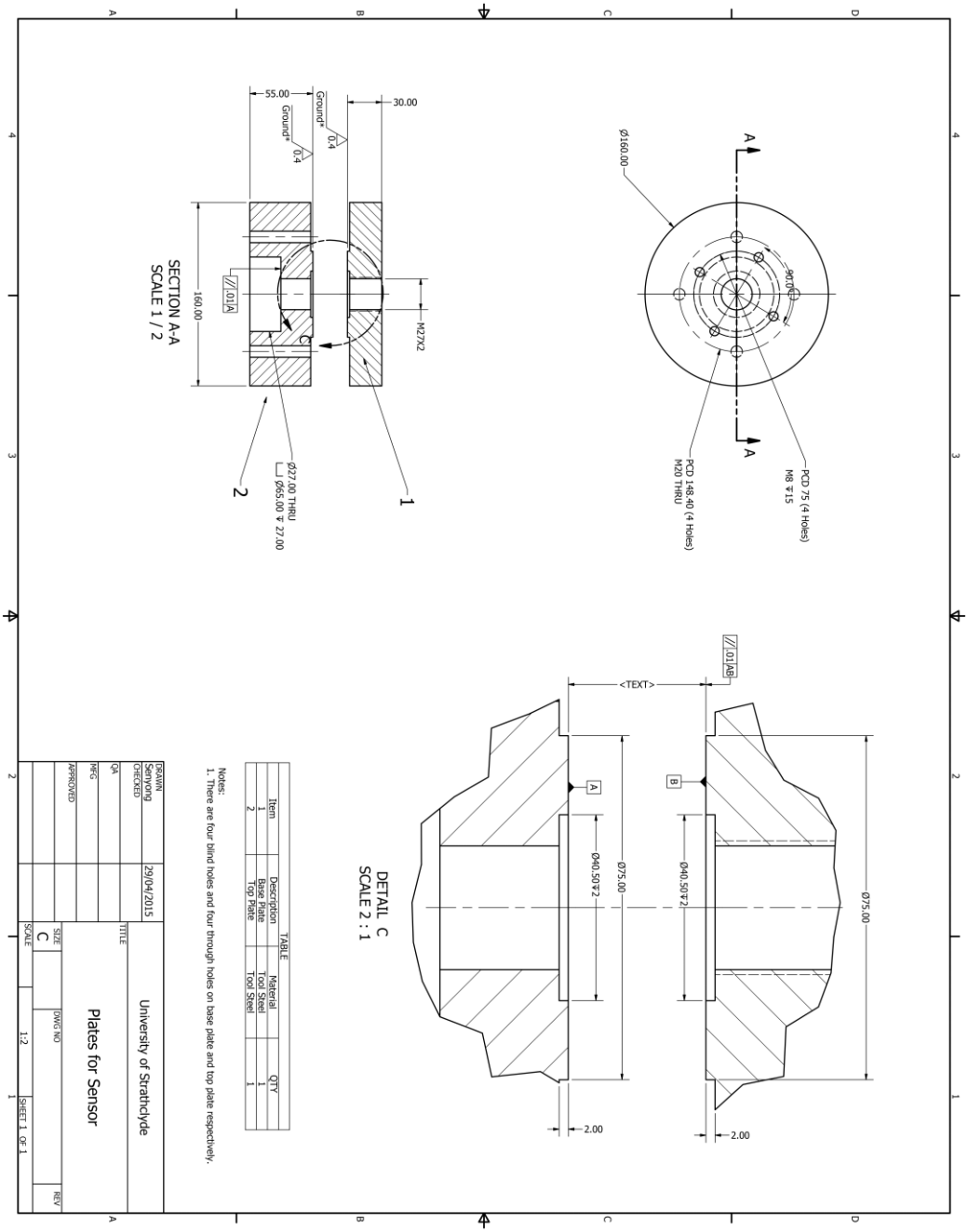
SECTION A-A
SCALE 1 / 2
55.00
30.00
Ground*
0.4
160.00
M27X2
Ø27.00 THRU
⌴ Ø55.00 ↧ 27.00
Ø160.00
90.0°
PCD 148.40 (4 Holes)
M20 THRU
PCD 75 (4 Holes)
M8 ↧15
DETAIL C
SCALE 2 : 1
<TEXT>
Ø40.50↧2
Ø75.00
2.00
Item
Description
Material
QTY
Base Plate
Tool Steel
Top Plate
Notes:
1. There are four blind holes and four through holes on base plate and top plate respectively.
DRAWN
Seryong
29/04/2015
CHECKED
QA
MFG
APPROVED
University of Strathclyde
Plates for Sensor
SIZE
C
SCALE
1:2
SHEET 1 OF 1
DWG NO
REV

Force Measurement Device: Link Plate

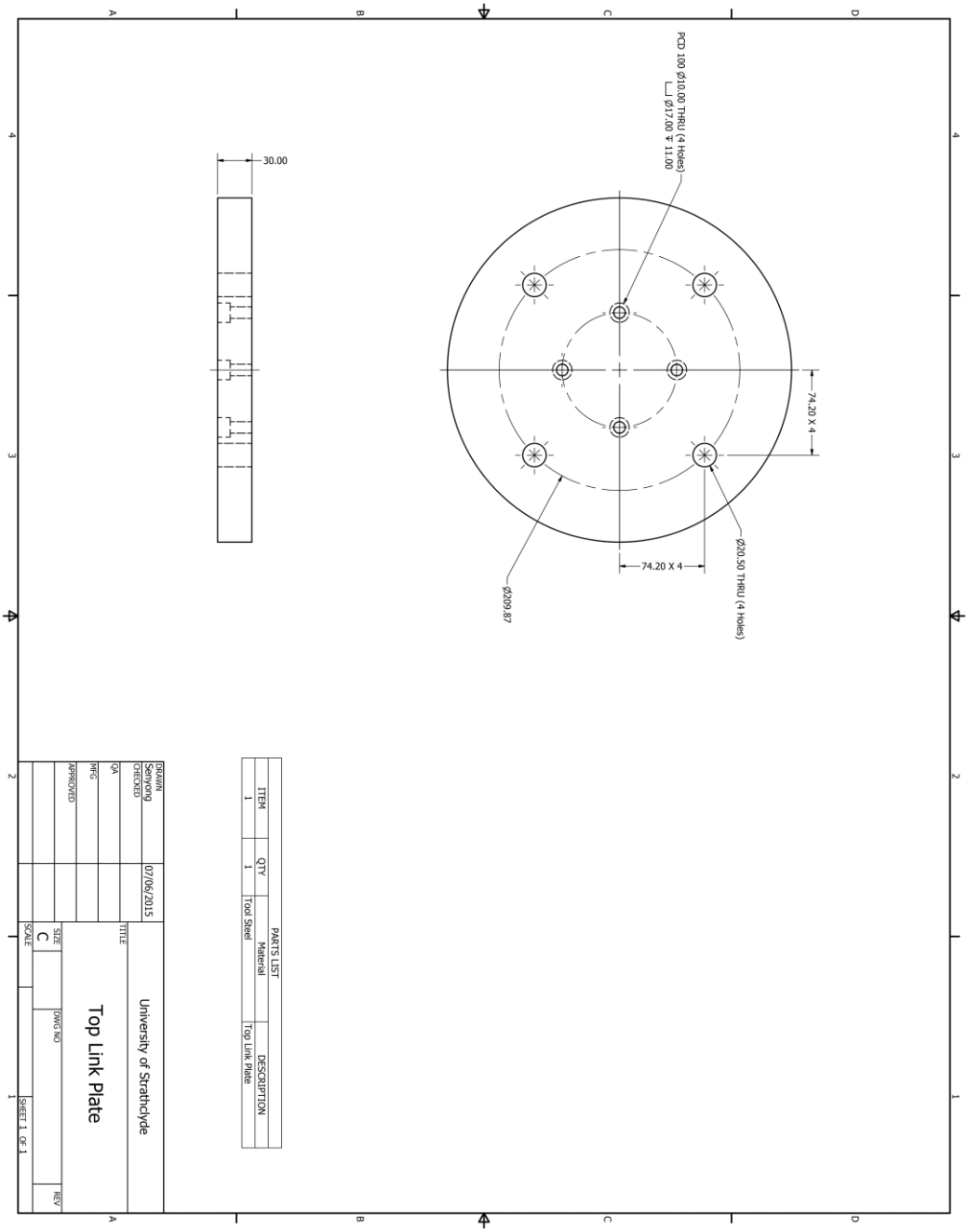

Appendix D. Mechanical Data of 3000 kN Hydraulic Press

Table D-1: Main mechanical data of hydraulic press.

Item	Description		Value
1	Maximum forging force		3,500 kN
2	Maximum ejection force		20 kN
3	Speed	No-load speed	190 mm/sec
		Load speed	Around 7 mm/sec
		Return speed	Around 180 mm/sec
4	Forging Stroke	Open distance	1000 mm
		Close distance	650 mm
		Maximum stroke	350 mm
5	Maximum ejection stroke		60 mm

Fig. D-1: 3000 kN vertical hydraulic press.

Appendix E. Preloading and Calibration of the Load Cell

The preloading was applied to the load cell by the threaded connection in the measurement device (refers to Fig. 4-2). Based on the instruction from Kistler, the maximum pretension of the bolt could withstand 50 % of the load cell range. In this study, the used preloading was 150 kN. According to [181], the preloading calculation formula is showed below:

$$T = KDF$$

where T is applied torque, F is the preload in the bolt, D is bolt diameter, and K is torque coefficient. The torque coefficient depends on the material and lubricants. The commonly assumed value 0.2 [181] was used in this study. The bolt diameter was 27 mm. Therefore, the required torque was 810 N·m. To ensure the preloading, a torque wrench was used, seen in Fig. E-1.

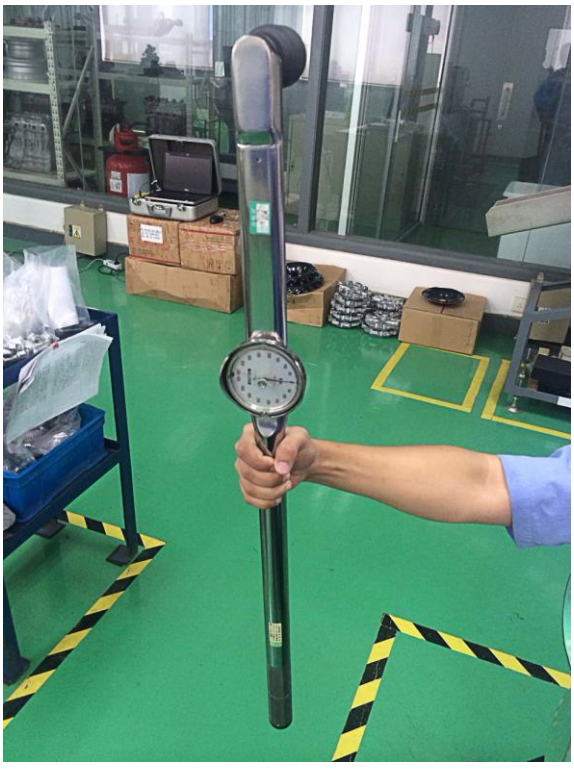

Fig. E-1: Torque wrench for preloading process.

For the calibration of load cell, the results were showed in Table E-1 and Fig. E-2.

Table E-1: The relationship between output voltage and force.

Item	Voltage (V)	Force (kN)
1	0.032	0
2	0.256	10
3	0.362	15
4	0.479	20
5	0.591	25
6	0.703	30
7	0.815	35
8	0.933	40
9	1.045	45
10	1.163	50
11	1.274	55
12	1.392	60
13	1.504	65
14	1.628	70
15	1.740	75
16	1.863	80
17	1.969	85
18	2.093	90
19	2.211	95
20	2.329	100
21	2.446	105
22	2.564	110
23	2.682	115
24	2.800	120
25	2.923	125
26	3.041	130
27	3.159	135
28	3.277	140
29	3.394	145
30	3.518	150
31	3.636	155
32	3.754	160
33	3.877	165
34	3.989	170
35	4.113	175
36	4.231	180
37	4.354	185
38	4.478	190
39	4.602	195
40	4.719	200
41	4.843	205
42	4.967	210

43	5.085	215
44	5.208	220
45	5.332	225
46	5.461	230
47	5.578	235
48	5.715	240
49	5.827	245
50	5.950	250

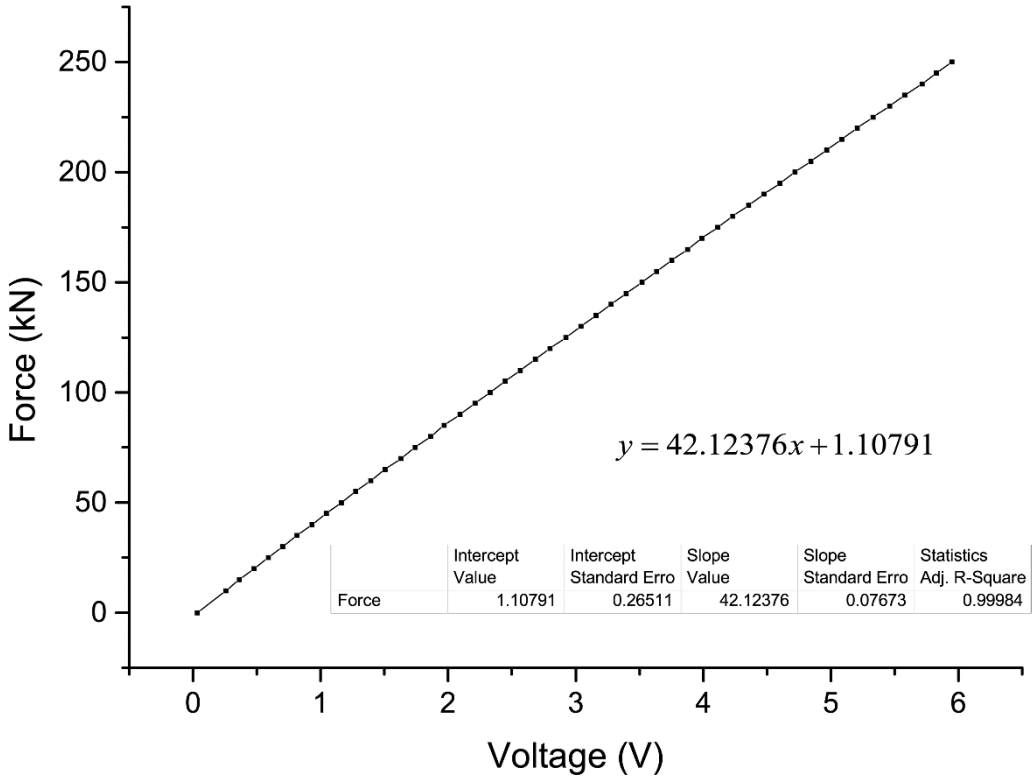

Fig. E-2: The calibration curve of force and voltage.

Appendix F. Specimen Weight

The density of AISI 1010 is regarded as 7.87g/cm^{3,} and the ideal size of the component is 51.60 × 10.10 (height × diameter). So the ideal weight of component is 32.5g

Table F-1: The weight errors of the workpiece before forging.

Item	Weight (g)	Errors (%)
1	32.3	-0.64
2	32.4	-0.55
3	32.3	-0.64
4	32.3	-0.64
5	32.3	-0.64
6	32.3	-0.64
7	32.3	-0.64
8	32.4	-0.55
9	32.3	-0.64
10	32.3	-0.64
Mean weight	32.3g	
Mean absolute errors	0.62%	

Appendix G. Profile of Radii under the Head

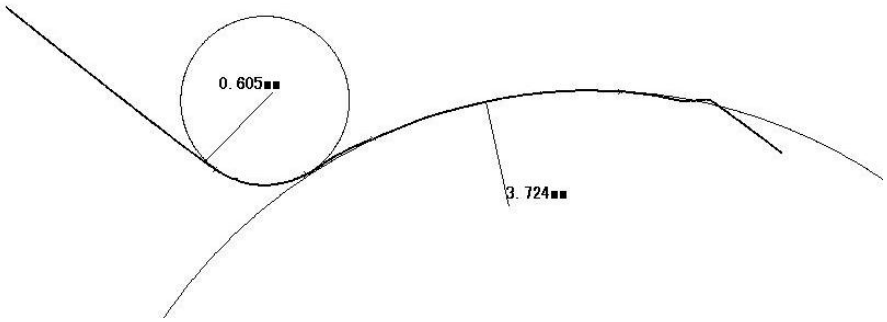

Fig. G-1: The profile of radii under the head for specimen 1 in ISO 100.

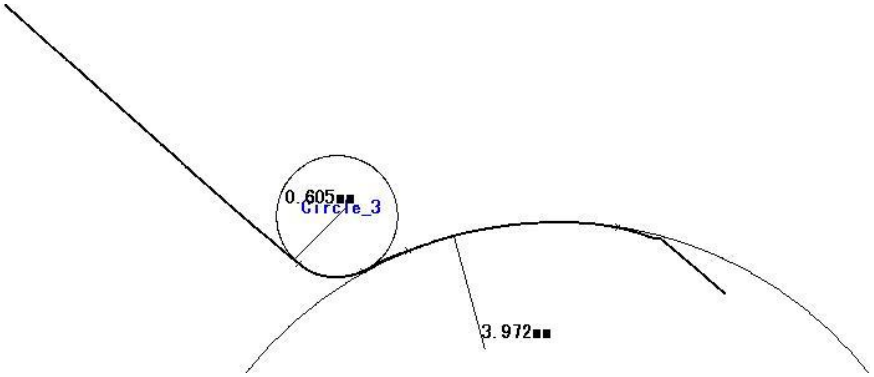

Fig. G-2: The profile of radii under the head for specimen 2 in ISO 100.

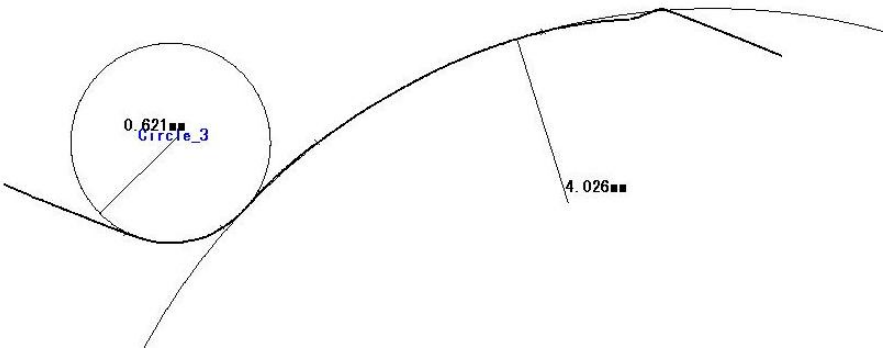

Fig. G-3: The profile of radii under the head for specimen 3 in ISO 100.

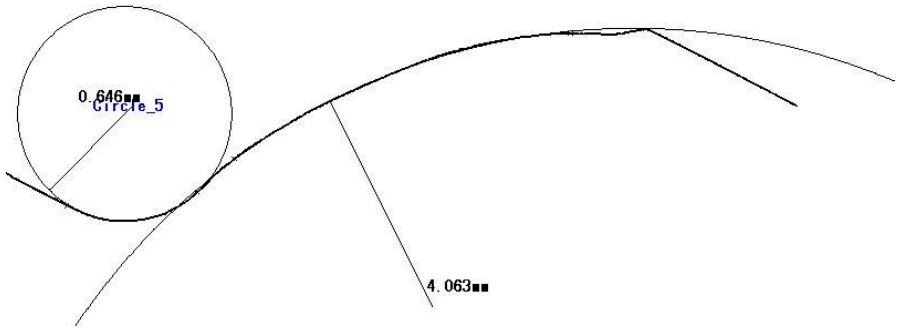

Fig. G-4: The profile of radii under the head for specimen 4 in ISO 100.

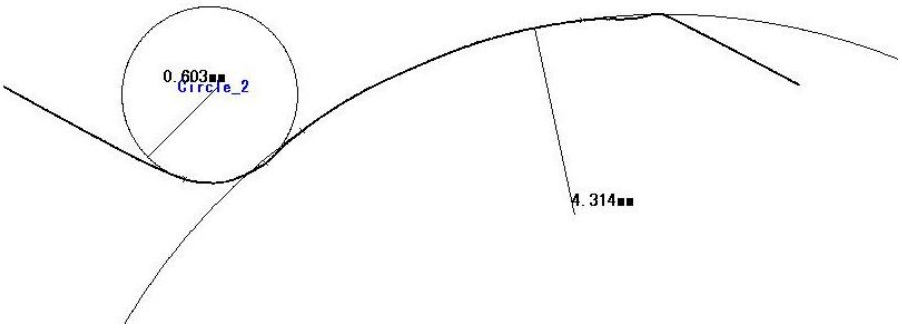

Fig. G-5: The profile of radii under the head for specimen 5 in ISO 100.

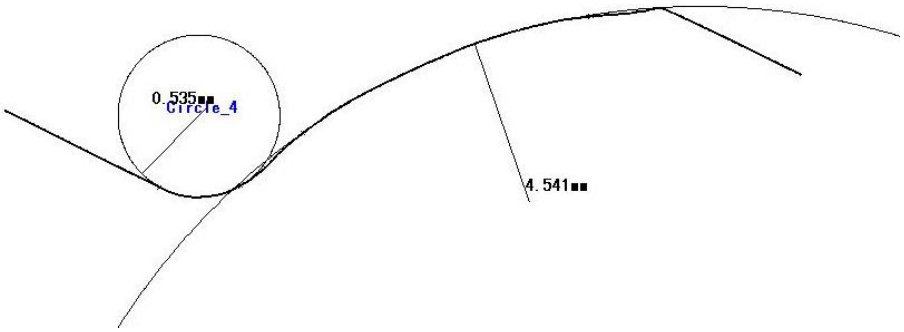

Fig. G-6: The profile of radii under the head for specimen 6 in ISO 100.

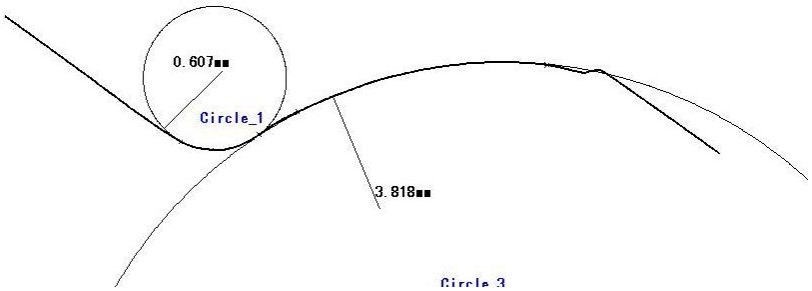

Fig. G-7: The profile of radii under the head for specimen 1 in MoS_2.

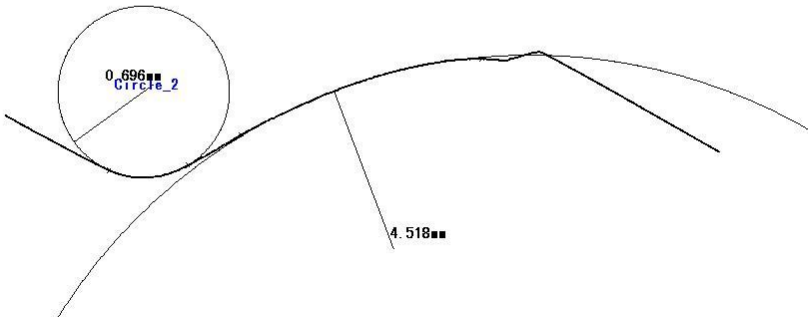

Fig. G-8: The profile of radii under the head for specimen 2 in MoS_2.

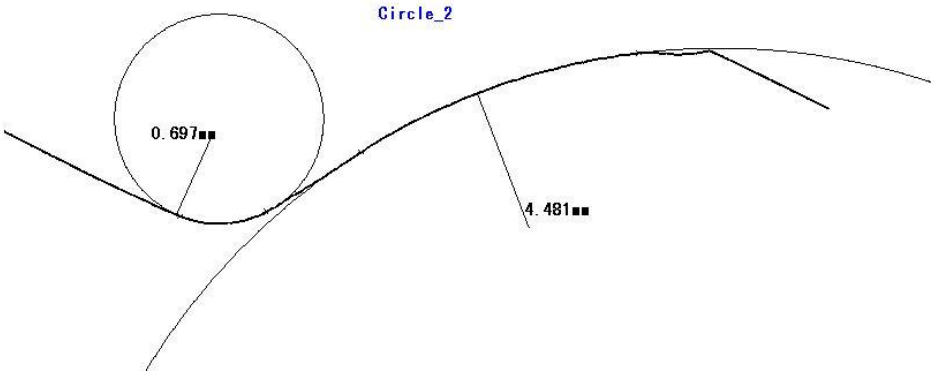

Fig. G-9: The profile of radii under the head for specimen 3 in MoS_2.

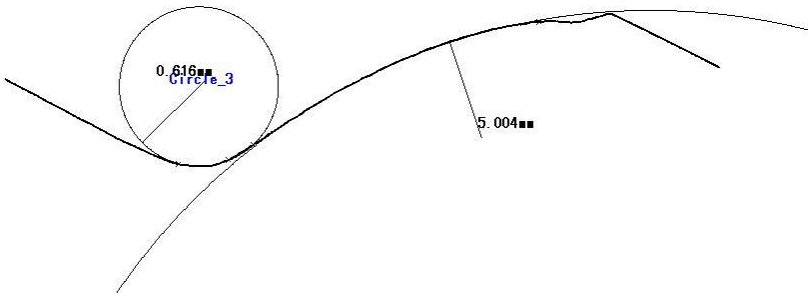

Fig. G-10: The profile of radii under the head for specimen 4 in MoS_2.

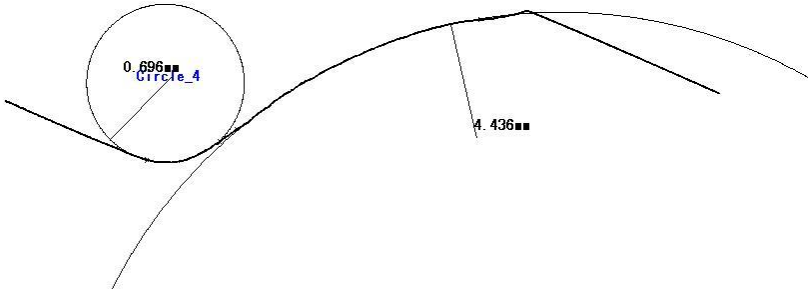

Fig. G-11: The profile of radii under the head for specimen 5 in MoS_2.

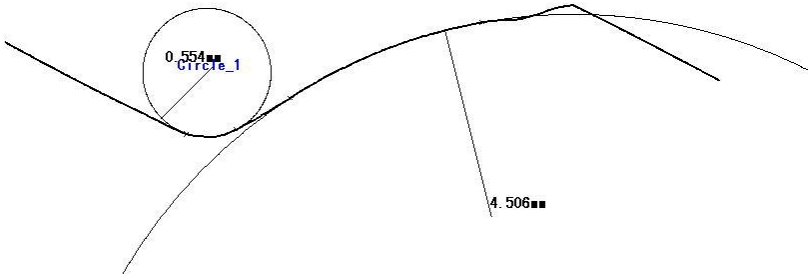

Fig. G-12: The profile of radii under the head for specimen 6 in MoS_2.

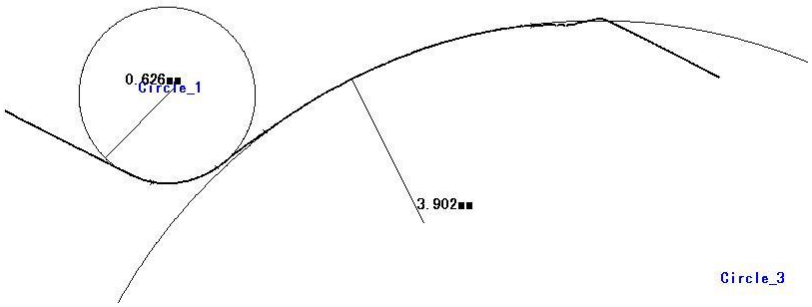

Fig. G-13: The profile of radii under the head for specimen 1 in ISO 68.

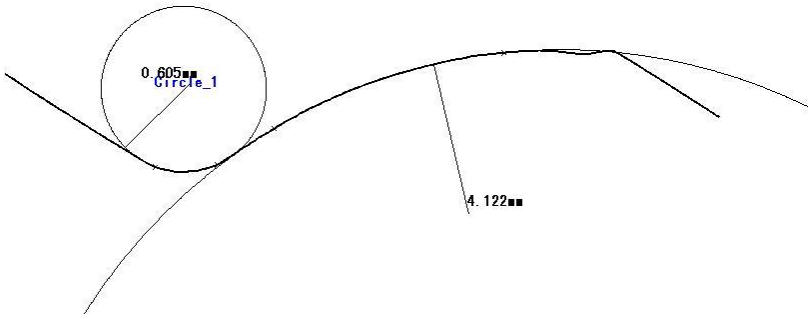

Fig. G-14: The profile of radii under the head for specimen 2 in ISO 68

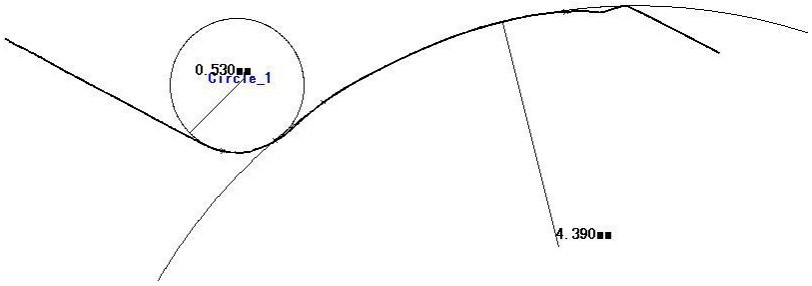

Fig. G-15: The profile of radii under the head for specimen 3 in ISO 68.

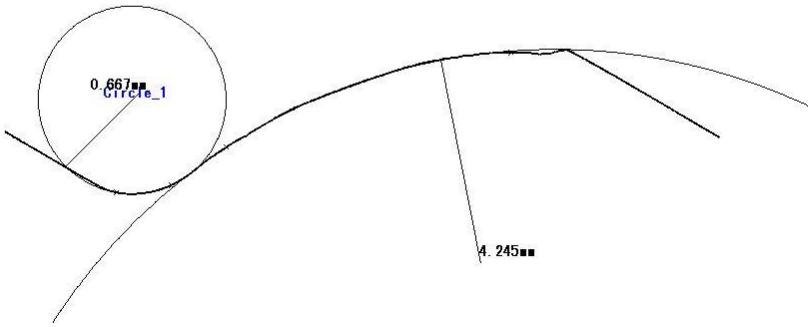

Fig. G-16: The profile of radii under the head for specimen 4 in ISO 68.

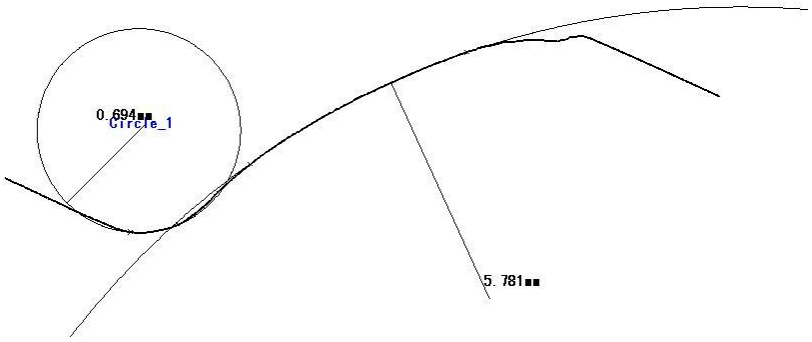

Fig. G-17: The profile of radii under the head for specimen 5 in ISO 68.

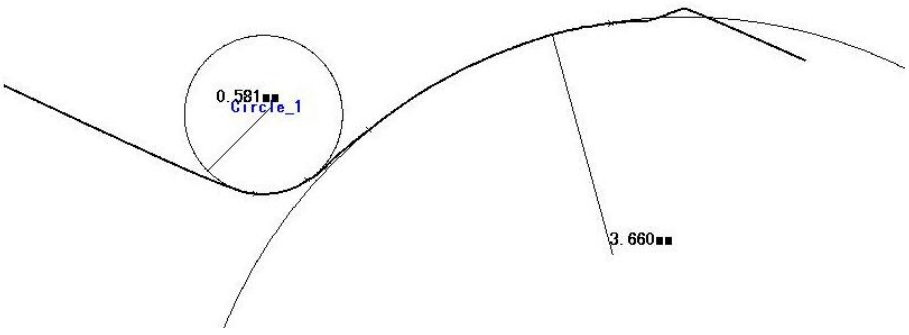

Fig. G-18: The profile of radii under the head for specimen 6 in ISO 68.